# The influence of currents, long waves and wind on gravity–capillary waves

by

Karsten Trulsen

Candidatus Magisterii, Universitetet i Tromsø
1987
Candidatus Scientiarum, Universitetet i Tromsø
1989

Submitted to the Department of Civil and Environmental Engineering
in partial fulfillment of the requirements for the degree of

Doctor of Philosophy

at the

MASSACHUSETTS INSTITUTE OF TECHNOLOGY

June 1995

© Massachusetts Institute of Technology 1995. All rights reserved.

Author .....
Department of Civil and Environmental Engineering
March 16, 1995

Certified by .....
Chiang C. Mei
Professor of Civil and Environmental Engineering
Thesis Supervisor

Accepted by .....
Joseph M. Sussman
Chairman, Departmental Committee on Graduate Studies

# The influence of currents, long waves and wind on gravity–capillary waves

by

Karsten Trulsen

Submitted to the Department of Civil and Environmental Engineering
on March 16, 1995, in partial fulfillment of the
requirements for the degree of
Doctor of Philosophy in Hydrodynamics

## Abstract

We consider various effects of currents, long waves, wind, viscosity and nonlinearity on the evolution of gravity–capillary waves.

In Part I we develop an analytical theory for the modulation and repeated reflection of a wave train by a non-uniform current. The reflection points can be closely spaced. We further include slow time modulation for application to wave packets. Viscous damping is introduced to improve the agreement with experiments.

In part II we consider resonant triads of gravity–capillary waves which are riding on a much longer gravity wave. The long-wave phase is assumed to vary on the same timescale as the slow modulation of the short waves. Viscous damping is weak and is neglected. The resulting dynamics for the three short waves can be represented by a conservative non-autonomous system of only two dimensions. We find that a weak long wave can resonate the natural modulation oscillations of the triad envelope, giving rise to various bifurcations in the Poincaré map. Numerical integration for a stronger long wave reveals that chaos can emerge from these bifurcations. The bifurcation criterion of Chen & Saffman (1979) for collinear Wilton's ripples, is generalized to arbitrary non-collinear triads, and plays an important role as a criterion for the onset of chaotic behavior.

In Part III, we account for the effects of wind and viscosity on the long-time behavior of two second-order resonant gravity–capillary waves in a third-order model. Wave-growth due to wind and viscous damping are balanced at the third order. For weak winds, lower than a certain threshold wind speed, the waves are damped out by viscosity. For slightly stronger winds, we find that a finely tuned gentle wind can balance viscosity and give rise to stable steady progressive Wilton's ripples. For yet stronger winds, our third-order model predicts that the waves will "blow up".

Thesis Supervisor: Chiang C. Mei
Title: Professor of Civil and Environmental Engineering

# The influence of currents, long waves and wind on gravity–capillary waves

by

Karsten Trulsen

Submitted to the Department of Civil and Environmental Engineering
on March 16, 1995, in partial fulfillment of the
requirements for the degree of
Doctor of Philosophy in Hydrodynamics

## Abstract

We consider various effects of currents, long waves, wind, viscosity and nonlinearity on the evolution of gravity–capillary waves.

In Part I we develop an analytical theory for the modulation and repeated reflection of a wave train by a non-uniform current. The reflection points can be closely spaced. We further include slow time modulation for application to wave packets. Viscous damping is introduced to improve the agreement with experiments.

In part II we consider resonant triads of gravity–capillary waves which are riding on a much longer gravity wave. The long-wave phase is assumed to vary on the same timescale as the slow modulation of the short waves. Viscous damping is weak and is neglected. The resulting dynamics for the three short waves can be represented by a conservative non-autonomous system of only two dimensions. We find that a weak long wave can resonate the natural modulation oscillations of the triad envelope, giving rise to various bifurcations in the Poincaré map. Numerical integration for a stronger long wave reveals that chaos can emerge from these bifurcations. The bifurcation criterion of Chen & Saffman (1979) for collinear Wilton's ripples, is generalized to arbitrary non-collinear triads, and plays an important role as a criterion for the onset of chaotic behavior.

In Part III, we account for the effects of wind and viscosity on the long-time behavior of two second-order resonant gravity–capillary waves in a third-order model. Wave-growth due to wind and viscous damping are balanced at the third order. For weak winds, lower than a certain threshold wind speed, the waves are damped out by viscosity. For slightly stronger winds, we find that a finely tuned gentle wind can balance viscosity and give rise to stable steady progressive Wilton's ripples. For yet stronger winds, our third-order model predicts that the waves will "blow up".

Thesis Supervisor: Chiang C. Mei
Title: Professor of Civil and Environmental Engineering

# Acknowledgments

My sincerest gratitude goes to my advisor Chiang C. Mei. He has taught me the genuine satisfaction and excitement that can only be achieved through rigorous scientific research.

Special thanks go to my parents who have always encouraged me to pursue a higher academic education.

Warm regards are extended to my friends at Parsons Laboratory, of whom I will have fond memories.

I thank Prof. Triantaphyllos R. Akylas, Prof. Ole S. Madsen and Prof. Steven H. Strogatz for serving on my thesis committee.

We thank Dr. Norden E. Huang for introducing us to the experimental papers by Badulin, Pokazeyev & Rozenberg (1983) and Pokazeyev & Rozenberg (1983), which initiated the study in Part I.

Financial support is gratefully acknowledged from The Norwegian Research Council for Science and the Humanities (grant NAVF 412.90/024) for a graduate fellowship, and from the U.S. Office of Naval Research (grants N00014–90J–1163 and N00014–92J–1754) and the U.S. National Science Foundation (grant CTS–9115689) for a graduate research and teaching assistantship.

# Contents

**Titlepage** **1**

**Abstract** **2**

**Acknowledgements** **3**

**Table of contents** **4**

**List of figures** **7**

**General introduction** **12**

**Part I: Double reflection of gravity–capillary waves by a non-uniform current — a boundary-layer theory** **17**

Notations for Part I . . . . . 17

I.1 Introduction . . . . . 20

I.1.1 Literature review . . . . . 20

I.1.2 Objectives of the present work . . . . . 22

I.2 Scaling assumptions . . . . . 27

I.3 Approximate equations for the short wave . . . . . 28

I.4 Ray approximation for short waves away from points of reflection . . 30

I.5 Inner solution near a simple turning point . . . . . 34

I.6 Solution near a triple-root turning point . . . . . 40

I.7 Remarks on existing experiments . . . . . 47

I.8 Numerical results for wave packets . . . . . 48

I.8.1 Case 1: Large separation between two reflection points. . . . . 48

I.8.2 Case 2: Moderate separation between two reflection points. . . 52

I.8.3 Case 3: Coalescing reflection points (triple-root turning point). 55

I.9 Conclusions . . . . . 58

I.A Solution near a detuned triple-root turning point . . . . . 60

I.B Solution of the Pearcey equation . . . . . 64

**Part II: Three resonating gravity–capillary waves riding on a long gravity wave** **66**

Notations for Part II . . . . . 66

II.1 Introduction . . . . . 69

II.1.1 Literature review . . . 69
II.1.2 Objectives of the present work . . . 72
II.2 Governing Lagrangian equations . . . 73
II.3 Ordering assumptions and multiple-scale expansions . . . 76
II.4 The long wave . . . 79
II.5 Evolution equations for the short waves . . . 79
II.6 Dynamical system for time evolution . . . 84
II.7 Analytical solution without the long wave . . . 87
II.8 Effects of a weak long wave . . . 93
II.8.1 Non-resonant long wave . . . 96
II.8.2 First-order synchronous modulational resonance $\lambda = 1$ . . . 98
II.8.3 Second-order subharmonic modulational resonance $\lambda = 1/2$ . . . 103
II.8.4 Second-order superharmonic modulational resonance $\lambda = 2$ . . . 106
II.8.5 Third-order subharmonic modulational resonance $\lambda = 1/3$ . . . 109
II.8.6 Third-order superharmonic modulational resonance $\lambda = 3$ . . . 114
II.8.7 Other resonances . . . 115
II.9 Effects of a stronger long-wave disturbance . . . 119
II.10 Conclusion . . . 123
II.A The derivatives of the reference positions . . . 125
II.B Second-order short-wave perturbation equations . . . 125
II.C Phase relations in the Eulerian frame . . . 127
II.D Derivation of the long-wave/short-wave interaction coefficient in Eulerian variables . . . 128
II.E Energy, momentum and action . . . 133
II.F Melnikov analysis for the homoclinic trajectory . . . 134

**Part III: Time evolution of Wilton's ripples forced by wind and damped by viscosity 136**
Notations for Part III . . . 136
III.1 Introduction . . . 140
III.1.1 Literature review . . . 140
III.1.2 Objectives of the present work . . . 145
III.2 Governing equations and steady wind profile . . . 147
III.2.1 The steady wind profile . . . 148
III.3 Scaling assumptions . . . 149
III.3.1 Numerical example — laminar viscosities at 20°C . . . 155
III.4 Multiple-scales perturbation expansions . . . 155
III.4.1 Water flow-field equations and boundary conditions . . . 156
III.4.2 Air flow-field equations and boundary conditions . . . 160
III.5 Evolution equation for a single gravity-capillary wave . . . 163
III.5.1 First-order water interior problem . . . 163
III.5.2 Second-order water interior problem . . . 164
III.5.3 Surface boundary-layer correction in water . . . 166
III.5.4 Third-order water interior problem . . . 167
III.5.5 Summary of the slow evolution equation for a single wave . . . 169

III.6 Evolution equations for Wilton's ripples . . . . . 170
III.6.1 First-order water interior problem . . . . . 170
III.6.2 Second-order water-interior problem . . . . . 170
III.6.3 Surface boundary-layer correction in water . . . . . 172
III.6.4 Third-order water-interior problem . . . . . 173
III.6.5 Summary of the slow evolution equations for Wilton's ripples . 175
III.6.6 Energy and momentum of Wilton's ripples . . . . . 178
III.7 The wave-disturbance in air . . . . . 178
III.7.1 First-order problem in air for a single wave . . . . . 179
III.7.2 Second-order problem in air . . . . . 180
III.7.3 Numerical solution of the Orr–Sommerfeld equation . . . . . 181
III.7.4 Numerical values for linear and nonlinear growth-rates . . . . 183
III.8 Dynamical system for time-evolution . . . . . 186
III.8.1 Second-order behavior . . . . . 188
III.8.2 Third-order behavior . . . . . 191
III.8.3 Fixed points . . . . . 192
III.8.4 The stable steady progressive Wilton's ripple . . . . . 200
III.8.5 Numerical results of phase trajectories . . . . . 200
III.9 Remarks on existing experiments . . . . . 204
III.10 Conclusion . . . . . 207
III.A Energy and momentum of Wilton's ripples . . . . . 209

**Bibliography** **211**

# List of Figures


1 Reproduction of figure 2 in Badulin *et al.* (1983) showing a side view of a non-uniform current flowing from right to left over a sloping bottom. A gravity–capillary wave is propagating from left to right, being shortened down to an extremely short capillary wave which is damped out by viscosity. . . . . 13

2 Reproduction of figure 4 in Janssen (1986) (which was in turn reproduced from Choi (1977)) showing the broadening and downshifting of the frequency spectrum for increasing fetch. . . . . 15

I-1 Geometry of the flow. . . . . 23

I-2 Case 1a. Graphical solution of the dispersion relation and the resulting wave. . . . . 23

I-3 Case 1b. . . . . 24

I-4 Case 2a. . . . . 25

I-5 Case 2b. . . . . 25

I-6 Wavenumber ($m^{-1}$) and wavelength (m) as a function of leftbound current velocity (m/s) for selected frequencies; from left to right: 5, 4, 3, 2, 1.75, 1.5, 1.25 and 1 Hz. The solid lines show gravity–capillary theory, the broken lines show gravity theory without capillarity. . . . 26

I-7 Sketch of the different regions of the wave development. . . . . 32

I-8 Well separated reflection points, frequency 1.9 Hz, current gradient $-0.0075$ $s^{-1}$, no damping. The abscissa shows the position in meters, the ordinate shows normalized amplitude relative to peak unit amplitude at the left edge. . . . . 50

I-9 Well separated reflection points, frequency 1.9 Hz, current gradient $-0.0075$ $s^{-1}$. Waves away from the reflection points are damped. . . 51

I-10 The trajectory of the envelope peak, frequency 1.9 Hz, current gradient $-0.0075$ $s^{-1}$. The abscissa shows the position in meters, the ordinate shows the elapsed time in seconds. . . . . 52

I-11 Double reflection with frequency 1.9 Hz and current gradient $-0.033$ $s^{-1}$. No damping. . . . . 53

I-12 Double reflection with frequency 1.9 Hz and current gradient $-0.033$ $s^{-1}$. Waves away from the reflection points are damped. . . . . 54

I-13 The trajectory of the envelope peak for frequency 1.9 Hz and current gradient $-0.033$ $s^{-1}$. . . . . 55

I-14 The perfect triple-root turning point with current gradient $-0.02\ \mathrm{s}^{-1}$. No damping. . . . . 56
I-15 The perfect triple-root turning point with current gradient $-0.02\ \mathrm{s}^{-1}$. Waves away from the turning point are damped. . . . . 57
I-16 The trajectory of the envelope peak for the perfect triple-root turning point with current gradient $-0.02\ \mathrm{s}^{-1}$. . . . . 58
I-17 Sketch of the surface described by the dispersion relation. . . . . 61
I-18 Projection of the singularity set on the $U\Omega$-plane (solid curves), and the tangent line at the cusp (dashed). . . . . 62
II-1 Geometry of a resonating triad. The angle $v_n$ is between the long wave $\boldsymbol{K}$ and the short wave $\boldsymbol{k}_n$. The angle $u_{nm}$ is between the short waves $\boldsymbol{k}_n$ and $\boldsymbol{k}_m$. The short wave $\boldsymbol{k}_3$ is always the shortest one. . . 80
II-2 The long-wave/short-wave interaction coefficient $\beta_n/KB$ as a function of the angle $v_n/\pi$ and the wavenumber $k_n/k^*$. The zero crossings are indicated by thick contour lines. . . . . 83
II-3 Intersection between two planes. Each axis represents the wave-action of each short wave. The action conservation laws are indicated as planes. The exchange of action between the three resonating waves must happen along the line of intersection. The asymmetry between the two planes is indicated in terms of $j_*$. . . . . 86
II-4 The effective long-wave/short-wave interaction coefficient $\beta/K|B|$ as a function of the angle of incidence $v_1/\pi$ and the wavenumber $k_1/k^*$ in the range (0.1, 5.0) for three selected angles $u_{12} = 30°$, $u_{12} = 45°$ and $u_{12} = 70°$. The zero-crossings are indicated by thick contour lines. 88
II-5 Bifurcation diagram for the location $j_c$ of centers when $j_* = 0$ and $-3 < \Delta/r < 3$. $j = 0$ is a fixed point for all $\Delta/r$. The generalized bifurcation of Chen & Saffman (1979) is seen at $j = 0$ and $\Delta/r = \pm 1$. Solid line $\psi_c = 0$, dashed line $\psi_c = \pi$. . . . . 90
II-6 Diagram for the location $j_c$ of centers when $\Delta = 0$ and $0 \le j_* \le 5$. . 91
II-7 Phase portraits $(j, \psi)$ for the autonomous system. (a) $j_* = 0$, $\Delta/r = 0$; (b) $j_* = 0$, $\Delta/r = 0.5$; (c) $j_* = 0$, $\Delta/r = 1.5$; (d) $j_* = 1$, $\Delta/r = 1.5$. The homoclinic trajectory is drawn as a thick line in (a) and (b). . . 94
II-8 Frequency of envelope oscillation, $2\pi/r\mathcal{T}$, of the autonomous system. Along the first axis, $j$ first increases from 0 to 1 corresponding to $\psi = 0$, then decreases from 1 to 0 corresponding to $\psi = \pi$. (a) $\Delta/r = 0$, (b) $\Delta/r = 0.5$, (c) $\Delta/r = 1$, (d) $\Delta/r = 1.5$ . . . . . 95
II-9 Numerically computed trajectory $(j, \psi)$ (thin line) for $\beta = 0.1$, $r = 0.7$, $j_* = 2$ and $\Delta = 0$. The system evolved from the initial condition $(j, \psi) = (0.6, 0)$ until time $t = 50$. The Poincaré map, sampling every long-wave period $t = 2\pi n$, is indicated by the thick curve. . . . . 99

II-10 Fourier spectrum of $j(t)$ for the trajectory shown in figure 8. The continuous curve is the FFT computed with 8192 samples and time step 0.105. The asterisks are the analytically computed Fourier amplitudes according to our perturbation analysis, with the frequencies adjusted to compensate for slow time modulation. The natural modulation frequency is $\lambda$ and the forcing frequency due to the long wave is unity (1). The expressions for the amplitudes are omitted in the text. 100
II-11 Bifurcation diagram for synchronous modulational resonance. The bifurcation surfaces are shown in the parameter space of $f$, $j_c$ and $\beta$. 104
II-12 Invariant manifolds of the Poincaré map for synchronous modulational resonance. Sketch of the level curves of the Hamiltonian $h(x, y)$ indicating the qualitative behavior of the Poincaré map in regions II and III. . . . . 105
II-13 Bifurcation diagram for subharmonic 1/2 modulational resonance. . 107
II-14 Phase portraits for subharmonic 1/2 modulational resonance. . . . . 108
II-15 Bifurcation diagram for superharmonic 2 modulational resonance. . . 110
II-16 Phase portraits for superharmonic 2 modulational resonance. . . . . 111
II-17 Bifurcation diagram for subharmonic 1/3 modulational resonance. . 112
II-18 Phase portraits for subharmonic 1/3 modulational resonance. . . . . 113
II-19 Bifurcation diagram for superharmonic 3 modulational resonance. . . 116
II-20 Phase portraits for superharmonic 3 modulational resonance. . . . . 117
II-21 Poincaré map for $\beta = 0.1$, $r = 0.7$, $j_* = 0$ and $\Delta = 0.7$, showing the characteristic manifolds of synchronous resonance (a), subharmonic 1/2 resonance (b) and subharmonic 1/3 resonance (c). . . . . 117
II-22 Poincaré map for $\beta = 0.1$, $r = 0.26$, $j_* = 0$ and $\Delta = 0$, showing the characteristic manifolds of subharmonic 1/4 resonance (a), subharmonic 1/5 resonance (b), subharmonic 1/6 resonance (c) and subharmonic 1/7 resonance (d). . . . . 118
II-23 Poincaré map for $r = 0.55$, $j_* = 0$, $\Delta = 0$, $\beta = 0.01$. We see subharmonic 1/2 resonance (a) and subharmonic 1/3 resonance (b). 120
II-24 Poincaré map for $r = 0.55$, $j_* = 0$, $\Delta = 0$, $\beta = 0.1$. . . . . 120
II-25 Poincaré map for $r = 0.55$, $j_* = 0$, $\Delta = 0$, $\beta = 0.2$. . . . . 121
II-26 Poincaré map for $r = 0.55$, $j_* = 0$, $\Delta = 0$, $\beta = 1.2$. . . . . 121
II-27 Poincaré map for $r = 0.55$, $j_* = 0$, $\Delta = 0$, $\beta = 2.0$. . . . . 122
II-28 Poincaré map for $r = 0.55$, $j_* = 0$, $\Delta = 0$, $\beta = 0.1$, showing the tangling of the heteroclinic manifolds of the subharmonic modulational resonance 1/2. . . . . 122
III-1 Comparison of (III.2.19) (- - -) with data used by Gastel *et al.* (1985) (∗). . . . . 150
III-2 Linear-logarithmic wind profile in water and air for $u'_* = 0.1$ m/s. The viscous sublayer depth and height are indicated with dashed lines. The height and speed are normalized by the wavenumber $\bar{k}$ and phase speed $\bar{c}$ of a first-harmonic Wilton's ripple. . . . . 151

III-3 Critical height (—) for Wilton's ripples and viscous sublayer height ($\cdots$) for air friction velocities in the range 0–0.3 m/s. Heights that can be inferred from the data used by Gastel *et al.* (1985) ($*$ and $\diamond$). Scaling heights (- - -) above $z = 0$ corresponding to $\mu = \epsilon^{\frac{1}{2}}$ and $\mu = \epsilon^{\frac{1}{3}}$ for $\epsilon = 0.04$. . . . . 154
III-4 Linear integral coefficients in water. . . . . 176
III-5 Nonlinear integral coefficients in water. . . . . 177
III-6 Our linear growth rates with tangential stress (a) and without tangential stress (c), asymptotic result of Gastel, Janssen & Komen (1985) (b). Air friction velocity $u'_*$: 0.248 m/s ($\cdots$), 0.214 m/s (- - -), 0.170 m/s (- $\cdot$ - $\cdot$), 0.136 m/s (- $\cdots$), 0.050 m/s (— — —), and no wind (solid line). The tangential stress contributes to larger growth for $u'_* > 0.050$ m/s, and stronger damping for $u'_* < 0.050$ m/s. . . . . 184
III-7 Linear coefficients $d_k$, equations (III.6.55) and (III.6.56). . . . . 185
III-8 Nonlinear coefficients $\hat{N}_k^{(2)}$, equation (III.7.27). . . . . 185
III-9 Second-order behavior. Bifurcation diagram showing regions of one and two centers in the parameter plane $(\alpha_{3,0}, E_0)$. Sample phase portraits projected onto the $XY$-plane for parameter values indicated by $\times$. . . . . 190
III-10 Trajectories of second-order system for $u'_* = 0.1$ m/s, $\delta = 0$ ($\alpha_{3,0} = 0.0572$) and $E_0 = 0.01$ (—). The parabola of fixed points indicates the locations of the centers (- - -). . . . . 191
III-11 Wave profiles for the steady-state solutions at the centers for $u'_* = 0.1$ m/s, $\delta = 0$ ($\alpha_{3,0} = 0.0572$) and $E_0 = 0.01$; gravity-like (—), capillary-like ($\cdots$). . . . . 192
III-12 Bifurcation diagram for $\delta = -0.2$. . . . . 195
III-13 Bifurcation diagram for $\delta = -0.1$. . . . . 196
III-14 Bifurcation diagram for $\delta = 0$. . . . . 197
III-15 Bifurcation diagram for $\delta = 0.1$. . . . . 198
III-16 Bifurcation diagram for $\delta = 0.2$. . . . . 199
III-17 Regions of qualitatively different behavior in the parameter plane $(\delta, u'_*)$. (1): The origin is a stable fixed point. (2): There exists a stable non-trivial fixed point and the origin is unstable. (3): The system blows up. In the region where the system blows up, we further distinguish between the regions where volumes in phase-space contract (3a), volumes in phase-space expand (3b and 3c), the first-harmonic wave has positive linear growth-rate and the second-harmonic wave has negative linear growth-rate (3a and 3b), both the first and second-harmonic waves have positive linear growth-rates (3c). . . . . 201
III-18 Wave profiles for the stable steady-state solution for a fixed wind $u'_* = 0.095$ m/s and selected values of detuning $\delta$. . . . . 202
III-19 Two trajectories for $u'_* = 0.08$ m/s, $\delta = 0$. Stable fixed point at the origin $(0, 0, 0)$. Initial conditions $(-0.05, 0, 0.015)$ and $(0.05, 0, 0.015)$. 203

III-20 Two trajectories for $u'_* = 0.1$ m/s, $\delta = 0$. Stable fixed point at $(-0.0076, 0.00079, 0.00094)$. Initial conditions $(-0.05, 0, 0.015)$ and $(0.05, 0, 0.015)$. . . . . 204
III-21 One trajectory for $u'_* = 0.12$ m/s, $\delta = 0$. One initial condition $(0.055, 0, 0.015)$ . . . . . 205
III-22 One trajectory for $u'_* = 0.15$ m/s, $\delta = 0$. One initial condition $(0.03, 0, 0.000001)$. . . . . 206

# General Introduction

Gravity–capillary water-surface waves, or ripples, are waves for which both gravity and surface tension are important as restoring forces. Their wavelengths are typically in the range from 2 mm to 2 dm, which includes the range directly responsible for backscatter of electromagnetic microwaves in the X-band (centimeter range) and the Ka-band (subcentimeter range). The short surface waves often carry information about conditions over much larger scales on or near the water surface. The X and Ka-bands can for example be used to obtain estimates of ocean-surface wind stress, which are valuable for weather prediction. Since short ripples are strongly influenced by capillarity and viscosity, their behavior hence depends indirectly on the water-surface temperature. Short waves are also modulated by longer surface waves and by subsurface currents and internal waves. It is for example possible to observe variations in bottom topography from the modulation of short surface waves, which is brought about indirectly through the variations in oceanic currents induced by the variable bathymetry (Valenzuela, Chen, Garrett & Kaiser 1983). For a review of remote sensing of the ocean surface, see e.g. Phillips (1988). Remote sensing of ripples also has applications for the surveillance of surface and subsurface vessels.

To gain information about larger-scale phenomena on or near the ocean surface from short-wave imagery, it is crucial to understand how larger scale ambient flows like currents, long waves and wind can affect the evolution of the short waves. A proper interpretation of such observations is further complicated by nonlinear wave interactions among the short waves themselves. We shall here focus our attention on three different situations in which ripples are affected by currents, long waves, wind, viscosity and nonlinear interaction. Our research topics are all substantially motivated by recent laboratory and field observations.

Wave-flume experiments on the propagation of short waves against a non-uniform current flowing over sloping bathymetry were performed by Badulin, Pokazeyev & Rozenberg (1983) and Pokazeyev & Rozenberg (1983). They showed that an incident wave train can be drastically shortened, and may be reflected back and forth by the horizontal current gradient induced by the flow over a submerged ridge. With the horizontal current varying from 4 to 30 cm/s, and an incident wave train with central frequency in the range 1.5–11 Hz, the waves could be shortened from 2 dm to 2 mm; a factor of 100! The transmitted waves were strongly attenuated by viscosity, and were completely eradicated without wave breaking.

Figure 1 is a reproduction from Badulin *et al.* (1983) showing the non-uniform current flowing from right to left over the sloping bottom. A gravity–capillary wave can be seen propagating from left to right, being shortened down to an extremely short capillary wave which is damped out by viscosity.

A somewhat similar situation in the ocean was described by Valenzuela *et al.* (1983) whose work was mentioned above, and by Leykin (1987) who reported field measurements on waves in a rip zone due to tidal flow over a submerged ridge. In Leykin's experiment, wind-driven gravity waves propagated against the current flowing over the ridge, and were shortened and reflected by the current gradient. This resulted in a zone of choppy water on top of the ridge, but completely calm water on

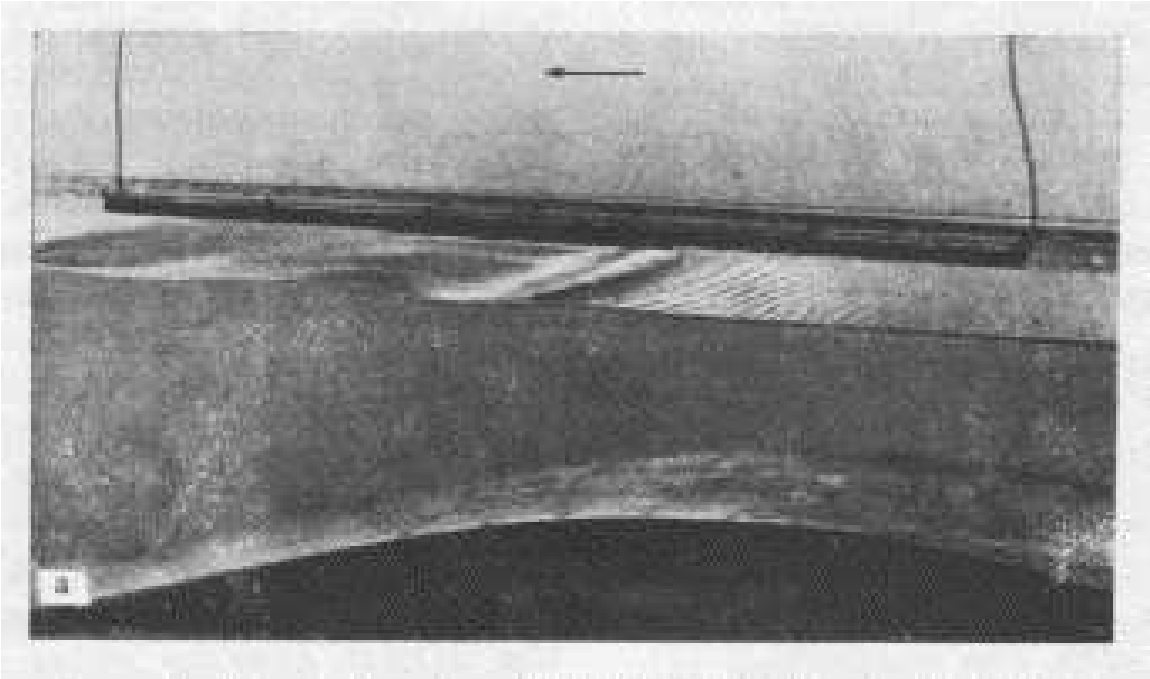

Figure 1: Reproduction of figure 2 in Badulin *et al.* (1983) showing a side view of a non-uniform current flowing from right to left over a sloping bottom. A gravity–capillary wave is propagating from left to right, being shortened down to an extremely short capillary wave which is damped out by viscosity.

the upstream side.

In Part I, we consider the evolution of short waves on a stationary current which varies in strength in the direction of flow. Motivated by the experiments showing that gravity–capillary waves are capable of being reflected multiple times, we derive a theory to explain the amplitude variations of the short waves in regions of multiple reflections. The enhanced role of viscous dissipation in regions with reflection points is clearly demonstrated.

In laboratory experiments, Choi (1977) detected a sudden period-doubling of wind-generated ripples. Brief accounts of these experiments can also be found in Ramamonjiarisoa, Baldy & Choi (1978) and Janssen (1986). A fully turbulent wind with velocity 5 m/s was blown over an initially calm water surface. At 70 cm fetch the first wavelets appeared with a narrow spectral peak at about 16.7 Hz. These initial waves grew according to linear theory up to 100 cm fetch. Then the spectrum broadened up to 150 cm fetch. From 150 to 220 cm fetch there was a definite down-shift in the spectral peak to half its initial value. Figure 2 is a reproduction from Janssen (1986) (which was in turn reproduced from Choi (1977)) showing the broadening and downshifting of the frequency spectrum for increasing fetch. This down-shift has been attributed to second-harmonic resonance by Chen & Saffman (1979) and Janssen (1986).

Field observations of three and four-wave resonant interactions on the sea surface have been reported by Strizhkin & Raletnev (1986). They analyzed photographs taken from a platform at 14 m height. Triad interaction was observed for winds in the range 2.7–18 m/s. Four-wave interaction was also observed, but for a larger threshold wind speed, typically greater than 4–6 m/s. They reported that the detection of resonant triads was often made difficult by the presence of much longer gravity waves. When the long gravity waves were taken into account, the discrepancies in the resonance conditions for frequencies and wavenumbers were reportedly reduced. Unfortunately they did not reproduce any of their photographs or present any further data suitable for comparison with theory.

In Part II, we investigate how the periodic disturbance of a long gravity wave can affect the behavior of a resonating triad of short gravity–capillary waves in a second-order model. The long-wave phase is assumed to vary on the same timescale as the slow nonlinear modulation of the short waves. It is assumed that the damping by viscosity is weak, such that we may neglect viscous damping and forcing mechanisms like wind, within a leading-order approximation. We find that a weak long wave can resonate the natural modulation oscillations of the triad envelope, giving rise to various bifurcations in the Poincaré map. Numerical integration for a stronger long wave reveals that chaos can emerge from these bifurcations. The bifurcation criterion of Chen & Saffman (1979) for collinear Wilton's ripples, is generalized to arbitrary three-dimensional triads, and is found to play an important role as a criterion for the onset of chaotic behavior. Since the periodic disturbance of a triad can cause an otherwise orderly behavior of waves to become chaotic, this may hence be a deterministic path towards understanding the random appearance of the ocean surface.

In recent laboratory experiments by Klinke & Jähne (1992), optical measurements with resolution down to 1/3 mm were taken to study wind-driven gravity–capillary

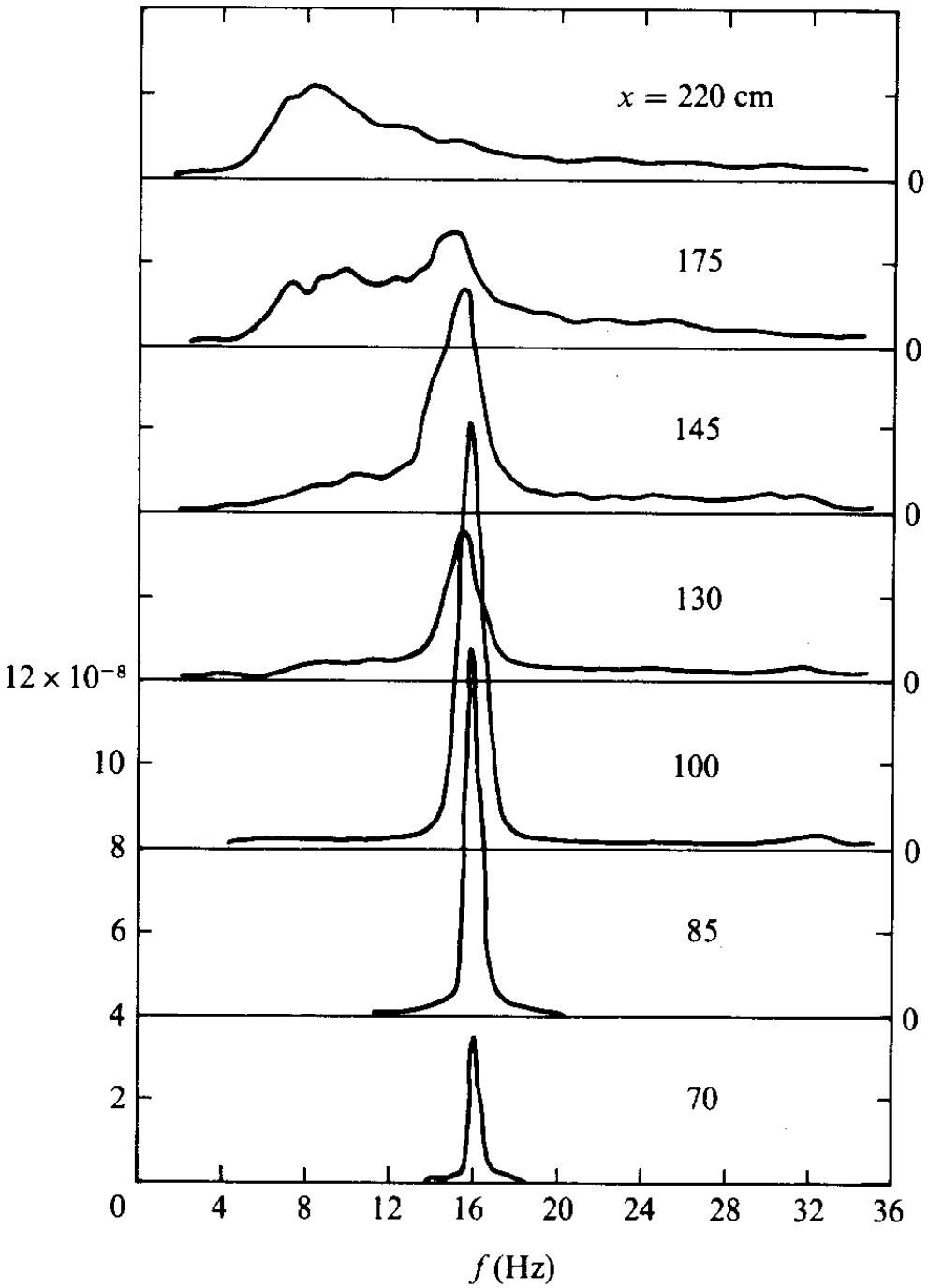


Figure 2: Reproduction of figure 4 in Janssen (1986) (which was in turn reproduced from Choi (1977)) showing the broadening and downshifting of the frequency spectrum for increasing fetch.

waves. Measurements from three different wind-wave facilities were compared in order to deduce laboratory-independent properties of wind-generated waves in the ocean. They found significant energy levels of gravity–capillary waves in the centimeter and subcentimeter range. They also found that the spectrum of wind-generated waves can depend sensitively on the wind-wave experimental facility.

Jurman, Deutsch & McCready (1992) performed experiments on centimeter-range wind-driven surface waves on a shallow and highly viscous fluid (10–100 times more viscous than water. They adjusted the gas flow to be just sufficient to produce measurable waves. They observed that a fundamental wave, corresponding to the highest linear growth rate due to wind, could saturate at a small steepness, while energy was transferred from the fundamental to its second-harmonic which was linearly damped.

In Part III, we account for the effects of wind and viscosity on the long-time behavior of two second-order resonant gravity–capillary waves in a third-order model. Due to the small viscosity of water, we balance wave-growth due to wind and viscous damping at the third order such that the scaling amplitude of the waves can be sufficiently large to be of practical significance. We find that there is a lower threshold wind speed, roughly in agreement with the lower limit given by Strizhkin & Raletnev (1986), above which the waves may be maintained by the wind. We further find that there is a narrow range of wind speeds for which a gentle wind may give rise to a stable steady progressive combination wave of a first and a second-harmonic component. This steady-state wave is found to be rather similar to the classical steady inviscid Wilton's ripples found by Wilton (1915) and Pierson & Fife (1961). For stronger winds, our third-order model predicts "blow-up", i.e. the wave amplitudes grow beyond the validity of our theory. We remark that the "blowing-up" behavior of our model seems to coincide with the broadening of the spectrum that can be seen in figure 2, while our model only accounts for a discrete spectrum.

# Part I: Double reflection of gravity–capillary waves by a non-uniform current — a boundary-layer theory

Notations for Part I

| | |
|---|---|
| $A$ | Leading-order complex amplitude of velocity potential. |
| $A_j$ | Higher-order complex amplitudes of velocity potential. |
| $A_j^{\pm}$ | Branches of amplitudes of velocity potential near turning point. |
| $\mathrm{Ai}(\cdot)$ | Airy function. |
| $a$ | Scale for wave amplitude. |
| $B$ | Leading-order complex amplitude of surface displacement. |
| $B_j$ | Higher-order complex amplitudes of surface displacement. |
| $B^{\pm}$ | Solution branches for amplitude near turning point. |
| $B^{(n)}$ | Complex amplitude of surface displacement of wave $n$. |
| $b(t_2)$ | Time-dependent boundary value of $B$ at $x_2 = x_{ref}$. |
| $b_0, b_1$ | Time-dependent coefficients of the amplitude at turning point. |
| $b_{\pm}$ | Time-dependent boundary values of $B^{\pm}$ at $\tilde{x} = \tilde{x}_{\pm}$. |
| $c$ | Phase velocity. |
| $c_0, c_1$ | Coefficients of amplitude at triple-root turning point. |
| $c_g$ | Intrinsic group velocity. |
| $c_g^{\pm}$ | Solution branches for intrinsic group velocity at turning point. |
| $\boldsymbol{c}_g$ | Intrinsic group velocity vector. |
| c.c. | Complex conjugate terms. |
| $D$ | Scale for current set-down. |
| $E$ | Wave energy. |
| e | 2.71828182845... |
| $f$ | Function representing dispersion relation. |
| $g$ | Gravitational acceleration. |
| $H$ | Scale for water depth. |
| $h$ | Water depth. |
| $h^*$ | Dimensional water depth. |
| h.o.t. | Higher order terms. |

| | |
|---|---|
| i | $\sqrt{-1}$. |
| $K$ | Normalized wavenumber. |
| $K_0$ | Wavenumber at turning point. |
| $K^{\pm}$ | Solution branches for wavenumber near turning point. |
| $K^{(n)}$ | Normalized wavenumber of wave $n$. |
| $k$ | Wavenumber absolute magnitude. |
| $\bar{k}$ | Central wavenumber of incident gravity wave. |
| $\boldsymbol{k}$ | Wavenumber vector. |
| $L$ | Scale for horizontal variation of current. |
| $\mathcal{O}(\cdot)$ | Order of. |
| $P(\cdot)$ | Pearcey function. |
| $P_0$ | Algebraically decaying part of Pearcey function. |
| $P_1$ | Exponentially decaying part of Pearcey function. |
| $R(\tilde{x})$ | Remainder in expansion of wavenumber at turning point. |
| $r$ | Normalized coefficient for wave packet snapshots. |
| $r^*$ | Dimensional coefficient for wave packet. |
| $S$ | Phase function. |
| $T$ | Surface tension between water and air. |
| $\mathcal{T}$ | Normalized reference time for wave packet snapshots. |
| $\mathcal{T}^*$ | Dimensional reference time for wave packet snapshots. |
| $t$ | Time coordinate. |
| $t_2$ | Slow timescale. |
| $t_{ref}$ | Reference time. |
| $U$ | Horizontal current velocity. |
| $U^*$ | Dimensional horizontal current velocity. |
| $U_0$ | $U$ at turning point. |
| $U_1$ | $\partial U/\partial x_2$ at turning point. |
| $U_L$ | Lower limiting current at reflection point. |
| $U_U$ | Upper limiting current at reflection point. |
| $\boldsymbol{U}$ | Current velocity vector. |
| $W$ | Vertical current velocity. |
| $W^*$ | Dimensional vertical current velocity. |
| $X$ | First complex argument of Pearcey function. |
| $x$ | Horizontal coordinate in the upstream direction. |
| $x_0$ | Location of a turning point. |
| $x_2$ | Long horizontal coordinate for current. |
| $x_{ref}$ | Reference horizontal position. |
| $x^*$ | Dimensional horizontal coordinate. |
| $x'$ | Location of the detuned triple-root point. |
| $\tilde{x}$ | Local long horizontal coordinate at turning point. |
| $\hat{\boldsymbol{x}}$ | Unit vector in the horizontal upstream direction. |
| $Y$ | Second (or only) complex argument of Pearcey function. |
| $z$ | Vertical coordinate. |
| $z_1$ | Long vertical coordinate for current. |

| | |
|---|---|
| $z^*$ | Dimensional vertical coordinate. |
| $\hat{\boldsymbol{z}}$ | Unit vector in the vertical direction. |
| $\alpha$ | First coefficient for wavenumber at any turning point. |
| $\alpha_2, \alpha_3$ | Coefficients for wavenumber at triple-root turning point. |
| $\beta$ | Coefficient in expansion for wavenumber at reflection point. |
| $\Gamma$ | Normalized parameter for surface tension. |
| $\Gamma_0$ | The value of $\Gamma$ for a triple-root turning point. |
| $\delta$ | Detuning in frequency. |
| $\epsilon$ | Small ordering parameter. |
| $\zeta$ | Current set-down. |
| $\zeta_0$ | Current set-down at turning point. |
| $\zeta_1$ | Current set-down slope at turning point. |
| $\zeta^*$ | Dimensional current set-down. |
| $\eta$ | Wave surface displacement. |
| $\eta^*$ | Dimensional wave surface displacement. |
| $\nu$ | Kinematic viscosity. |
| $\xi$ | Scaled local horizontal variable at turning point. |
| $\pi$ | 3.1415926535... |
| $\rho$ | Density of water. |
| $\sigma$ | Intrinsic angular frequency. |
| $\sigma_0$ | Intrinsic angular frequency at turning point. |
| $\sigma^{\pm}$ | Solution branches of intrinsic angular frequency at turning point. |
| $\tau$ | Scaled time at turning point. |
| $\phi$ | Wave velocity potential. |
| $\phi^*$ | Dimensional wave velocity potential. |
| $\chi$ | Parameter for viscous damping. |
| $\psi$ | Auxiliary variable for the integration of wave-action. |
| $\Omega$ | Normalized frequency of incident wave train. |
| $\omega$ | Absolute angular frequency. |
| $\omega_0$ | Frequency for triple-root turning point. |
| $\bar{\omega}$ | Central frequency of incident gravity wave. |

# I.1 Introduction

## I.1.1 Literature review

The kinematics of three-dimensional water surface gravity–capillary waves on a current that is non-uniform in the direction of its velocity, was thoroughly investigated by Basovich & Talanov (1977). The conditions for reflection of packets of waves by the inhomogeneous current were determined. They predicted that a short gravity wave with its wavenumber vector directly opposed to the current may be shortened and reflected as a gravity–capillary wave, which may then be further shortened and reflected a second time as a pure capillary wave. They further found that the qualitative behavior of the short waves changes depending on whether the frequency is smaller or greater than a certain characteristic frequency. The double reflection in two dimensions just described can only happen when the frequency is less than this characteristic frequency.

Basovich & Bahanov (1984) further studied the kinematics of gravity–capillary waves which may be refracted and trapped by the variable current field generated by a large-amplitude internal wave. Examples of the rich variety of wave kinematics possible for gravity waves generated at a point source in regions of relatively simple current gradients were given by Trulsen, Dysthe & Trulsen (1990).

On the experimental side, striking examples of wave shortening and double reflection of gravity–capillary waves on an inhomogeneous current were reported by Pokazeyev & Rozenberg (1983) and Badulin, Pokazeyev & Rozenberg (1983). They conducted experiments for short waves on a weak opposing current with speed between 4 and 30 cm/s over a sloping bottom. Wave-packets of three to ten oscillations with central frequencies in the range of 1.5 to 11 Hz were sent toward the opposing current. A drastic shortening of wavelength was found to take place, e.g. from 20 cm down to 2 mm; a factor of 100! The transmitted waves were found to be strongly attenuated. Badulin, Pokazeyev & Rozenberg (1983) specifically focused attention on wave propagation involving reflection, which can happen when the frequency is sufficiently low. They observed that the waves are reflected at two reflection points, accompanied by a drastic reduction of wavelength and amplitude attenuation. Figure 1 shows a photograph of their experiment. In these experiments, the separation between the two reflection points is typically not much greater than a local wavelength.

Yermakov & Salashin (1984) conducted laboratory experiments on transformations of gravity–capillary surface waves on the variable current field of an internal wave. Leykin (1987) described field measurements on waves in a rip zone due to tidal flow over a submerged ridge. Wind driven gravity waves were observed propagating against a current which was weak away from the submerged ridge (0.25 – 0.5 m/s) and strong above the the ridge (2 m/s). The waves were shortened and reflected by the current gradient, resulting in a zone of breaking waves and choppy water. Since no waves could propagate past the ridge, the water was calm on the upstream side. Lai, Long & Huang (1989) did experiments on gravity waves on non-uniform currents and verified the kinematic dispersion relation, but did not investigate reflection of waves.

Modern theories on the dynamics of infinitesimal short gravity waves on longer waves or slowly varying currents were begun by Longuet-Higgins & Stewart (1960), who showed that the short waves become shorter and steeper near the crests and longer and lower near the troughs of the long wave. They introduced the concept of radiation stress for water waves. Longuet-Higgins & Stewart (1961) further discussed the work done by the rate of strain of the ambient current against the radiation stress of the short waves. Bretherton & Garrett (1968) derived the conservation of wave-action for water-waves on a non-uniform current. Phillips (1981) anticipated reflection of gravity–capillary waves by currents or long waves of finite amplitude. Lavrenov (1987) investigated the evolution of a spectrum of gravity waves near a rip, where an oceanic current flows over a submerged ridge. A Hamiltonian account of the evolution of short gravity–capillary waves on two-dimensional long waves was given by Henyey *et al.* (1988).

A review of the interactions between waves and currents was given by Peregrine (1976).

Catastrophe theory provides a convenient framework to describe the behavior at turning points where classical ray theory breaks down. Ordinary reflection points are related to fold catastrophes, because the dispersion relation describes a surface that has a fold at the reflection point. Theories to describe amplitudes of wave trains near reflection points will naturally give rise to Airy functions. Somewhat less common is the type of singularity that arises either in the limit when two reflection points come close together, or near the cusp of a caustic. These singularities are related to cusp catastrophes, due to the local geometry of the dispersion relation. Dynamical theories for the amplitudes of wave trains will then naturally give rise to Pearcey functions, named after Pearcey (1946) who discussed electromagnetic waves near the cusp of a caustic. Stamnes (1986) gave a comprehensive discussion of the use of Pearcey functions in optics. A rigorous discussion of the asymptotic behavior of Pearcey functions was recently given by Paris (1991). For an introduction to catastrophe theory, see for example Saunders (1980).

In this work the singularity described by a cusp catastrophe shall be called a triple-root point since the dispersion relation will have a triple root for the wavenumber. Likewise, we could have called an ordinary reflection point a double-root point, since the dispersion relation will have a double root for the wavenumber.

An asymptotic linear theory uniformly valid near and away from an ordinary reflection point has been given by Smith (1975) for pure gravity waves on a non-uniform current. Smith (1976b) further developed the theory to describe pure gravity waves near triple-root points on a non-uniform current. Thomson & West (1975) gave a linear theory for modulation and reflection of gravity waves by surface currents induced by an internal wave. They showed that the surface waves may be enhanced or depleted in a periodic fashion by the long internal wave. Partial reflection of gravity waves by a non-uniform opposing current was studied by Stiassnie & Dagan (1979). They showed that waves may be partially reflected if the current velocity is close to the critical velocity for which the reflection should have occurred according to the classical theory. Shyu & Phillips (1990) reported a linear analysis of reflection of waves by non-uniform currents or long waves, by extending the work of Smith (1975)

to include capillary effects. They first reduced the free-surface boundary condition to a third-order ordinary differential equation, which was factored and reduced further to a second-order Airy equation near a reflection point. The effects of viscosity were discussed in general terms.

Because wave heights tend to be amplified in the neighborhoods of turning points, it has often been anticipated that nonlinear effects may be important, unless viscous effects dominate. Holliday (1973) predicted that finite-amplitude gravity–capillary waves may propagate beyond the reflection points predicted by linear theory, and not be subject to blocking. However, Holliday's results were later contradicted by various authors (Thomson & West 1975; Smith 1976a). Smith (1976a) discussed the local nonlinear effects on steep gravity waves that are reflected by a non-uniform current, by means of a nonlinear Schrödinger equation. Peregrine & Smith (1979) investigated nonlinear effects on waves near caustics in general, and also anticipated the nonlinear effects near triple-root turning points. They conjectured that nonlinearity may be of great importance near caustics of capillary waves, provided viscous effects do not dominate.

### I.1.2 Objectives of the present work

We get our motivation from the kinematic theory of Basovich & Talanov (1977) and the experimental observation of Badulin, Pokazeyev & Rozenberg (1983) (see figure 1). Our goal is to describe the evolution of a wave packet subject to double reflection, including the situation directly relevant to their experiment where the two reflection points are close together. We further want to assess the importance of viscous damping. Our theory is linear and purely analytical.

The phenomenon of double reflection and reduction of wavelength is best seen from the dispersion relation:

$$(\omega - \boldsymbol{k}\cdot\boldsymbol{U})^2 = gk + \frac{T}{\rho}k^3 \equiv \sigma^2 \tag{I.1.1}$$

Here $\sigma$ is the intrinsic frequency, $\omega$ the absolute frequency, $\boldsymbol{k}$ the wavenumber vector, $k$ its absolute magnitude $|\boldsymbol{k}|$, $\boldsymbol{U}$ the horizontal current velocity vector, $g$ the gravitational acceleration, $T$ the surface tension between water and air, and $\rho$ the density of water. The intrinsic group velocity is $\boldsymbol{c}_g = \partial\sigma/\partial\boldsymbol{k}$, while the absolute group velocity is $\partial\omega/\partial\boldsymbol{k} = \boldsymbol{c}_g - \boldsymbol{U}$. Restricting to the collinear case for simplicity, we shall recapitulate some of the possible scenarios. Throughout the following we shall assume that the current flows from right to left toward increasing depth, see figure I-1. The flow is subcritical, such that the velocity decreases as the depth increases. The following cases can be distinguished.

**Case 1.** $\boldsymbol{k} = -k\hat{\boldsymbol{x}}$, i.e. the wave crests propagate downstream and $\boldsymbol{k}\cdot\boldsymbol{U} > 0$. Two branches exist for the square root in (I.1.1).

**Case 1a.** Positive branch:

$$\sigma = \omega - k|\boldsymbol{U}| = \sqrt{gk + \frac{T}{\rho}k^3} \tag{I.1.2}$$

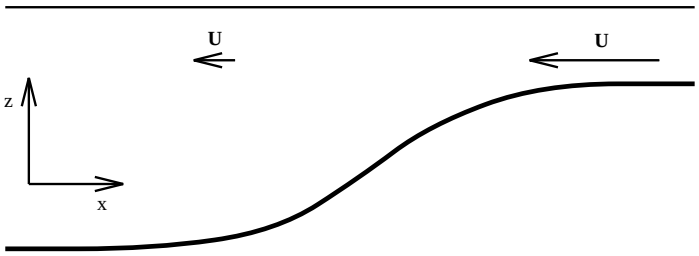


Figure I-1: Geometry of the flow.

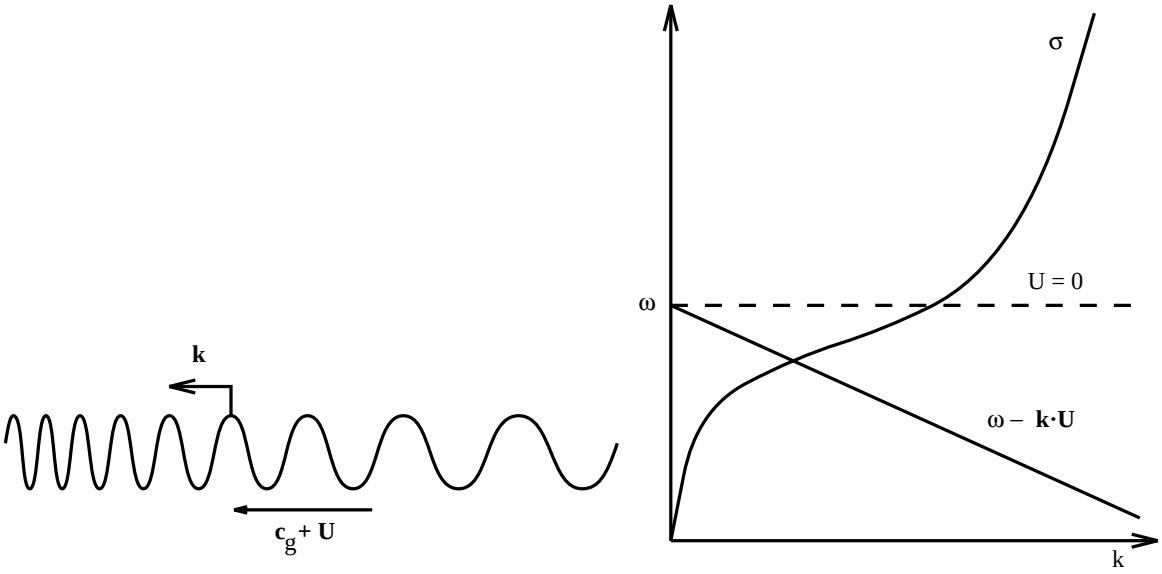


Figure I-2: Case 1a. Graphical solution of the dispersion relation and the resulting wave.

The absolute group velocity vector $\partial\omega/\partial\boldsymbol{k}$ will always point downstream. Hence a long wave will have its energy swept downstream. As the current gets weaker, the wavelength becomes shorter, and will approach the limiting wavelength corresponding to no current. See figure I-2. There can be no reflection.

**Case 1b.** Negative branch:

$$\sigma = \omega - k|\boldsymbol{U}| = -\sqrt{gk + \frac{T}{\rho}k^3} \tag{I.1.3}$$

For a given frequency $\omega$ there is a limiting current $U_L$. For $|\boldsymbol{U}| > U_L$ two waves are possible for the same frequency. For $|\boldsymbol{U}| < U_L$ no waves can exist according to (I.1.3). A gravity–capillary wave will first have its energy swept downstream, and will be shortened. It will then be reflected as a capillary wave with its energy swept upstream, and will be further shortened. This type of wave cannot exist on still water.

**Case 2.** $\boldsymbol{k} = k\hat{\boldsymbol{x}}$, i.e. the wave crests propagate upstream and $\boldsymbol{k} \cdot \boldsymbol{U} < 0$. Only

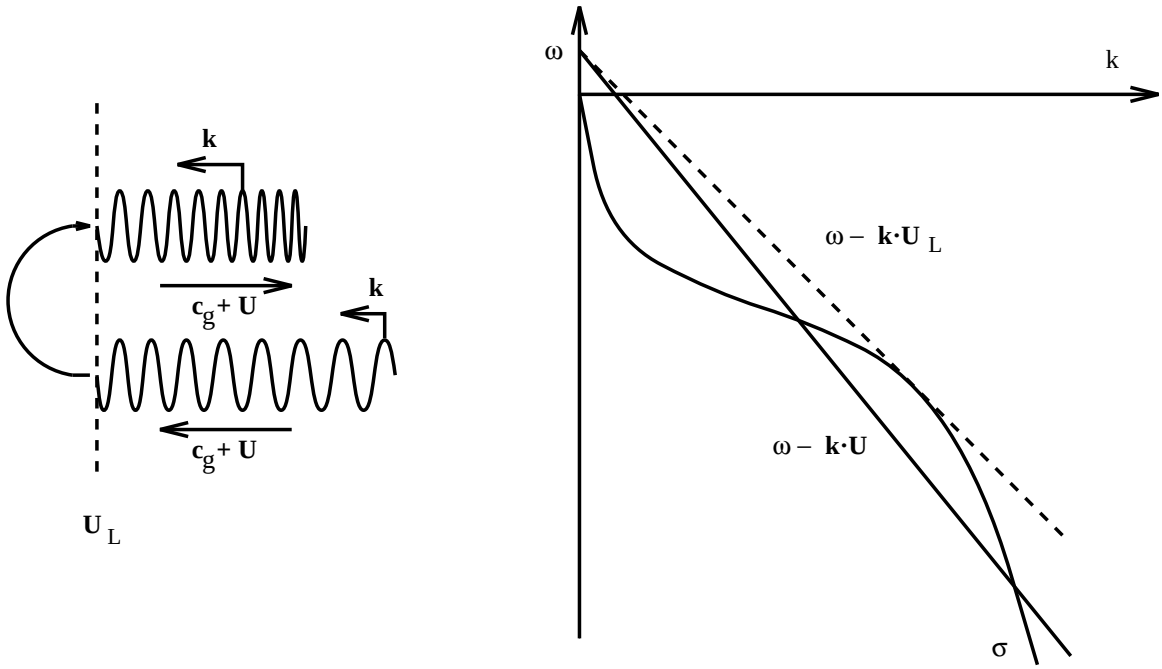


Figure I-3: Case 1b.

the positive branch for the square root can be taken:

$$\omega + k|\boldsymbol{U}| = \sqrt{gk + \frac{T}{\rho}k^3} \tag{I.1.4}$$

Referring to figure I-4 we define $\omega_0$ to be the intersection of the frequency axis and the tangent to the intrinsic frequency curve at the inflection point. There are two subcases.

**Case 2a.** $\omega > \omega_0$. For any $|\boldsymbol{U}|$ there is one and only one solution as shown in figure I-4. Because the absolute group velocity vector $\partial\omega/\partial\boldsymbol{k}$ always points upstream, a long wave with crests propagating upstream will have its energy swept upstream. Since $k$ increases with $|\boldsymbol{U}|$ the wavelength is shortened as the crests advance into a stronger opposing current.

**Case 2b.** $\omega < \omega_0$. For $U_L < |\boldsymbol{U}| < U_U$ three waves are possible for the same frequency as shown in figure I-5. A gravity wave originating downstream with crests propagating upstream, will be reflected twice at two different reflection points where $|\boldsymbol{U}| = U_U$ and $|\boldsymbol{U}| = U_L$. As the crests always propagate upstream, the wave energy is first swept upstream, then downstream, and finally upstream. Throughout this process the continuous shortening of the wavelength can be so drastic that fairly long gravity waves can be transformed into a train of capillary waves which are then damped without any breaking.

In the limiting case of $\omega \to \omega_0$, the two reflection points coalesce. We denote this a triple-root turning point, as discussed earlier in the introduction.

In physical dimensions achievable in the laboratory, solution curves of the dispersion relation for various frequencies and a given non-uniform current, are illustrated

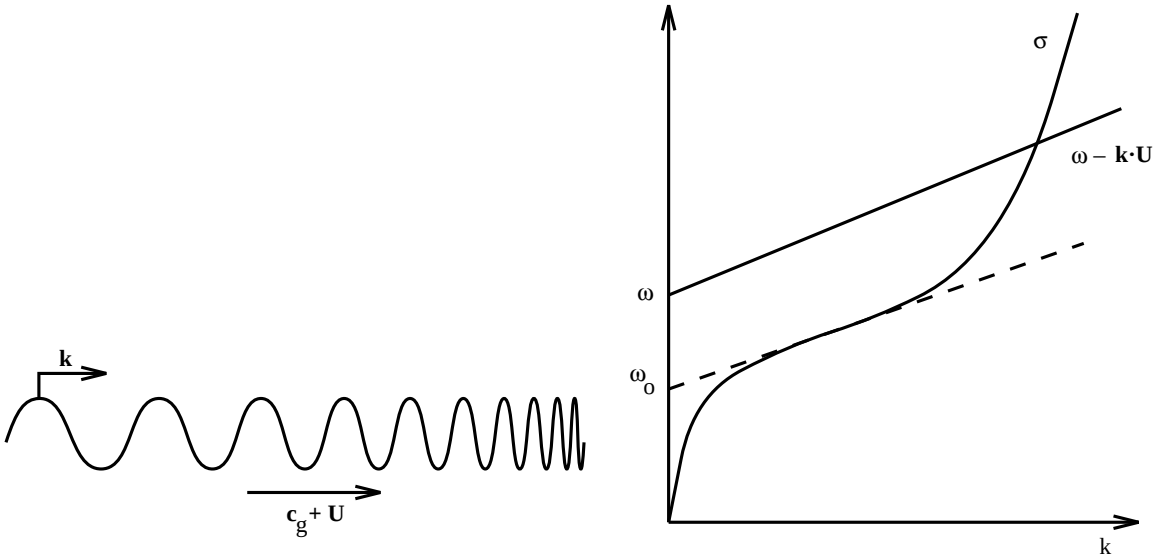


Figure I-4: Case 2a.

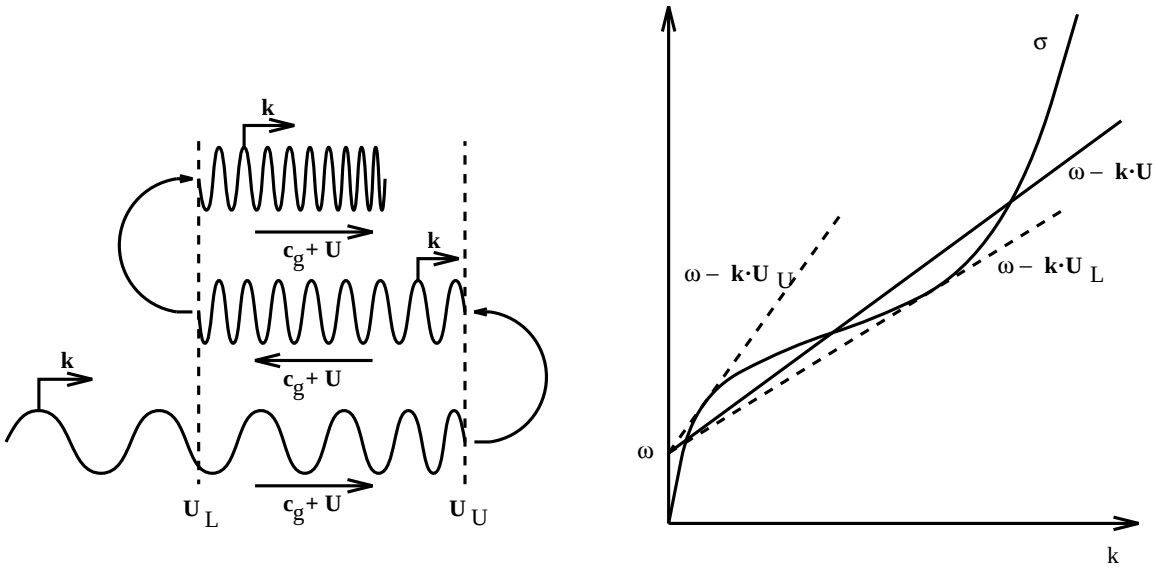


Figure I-5: Case 2b.

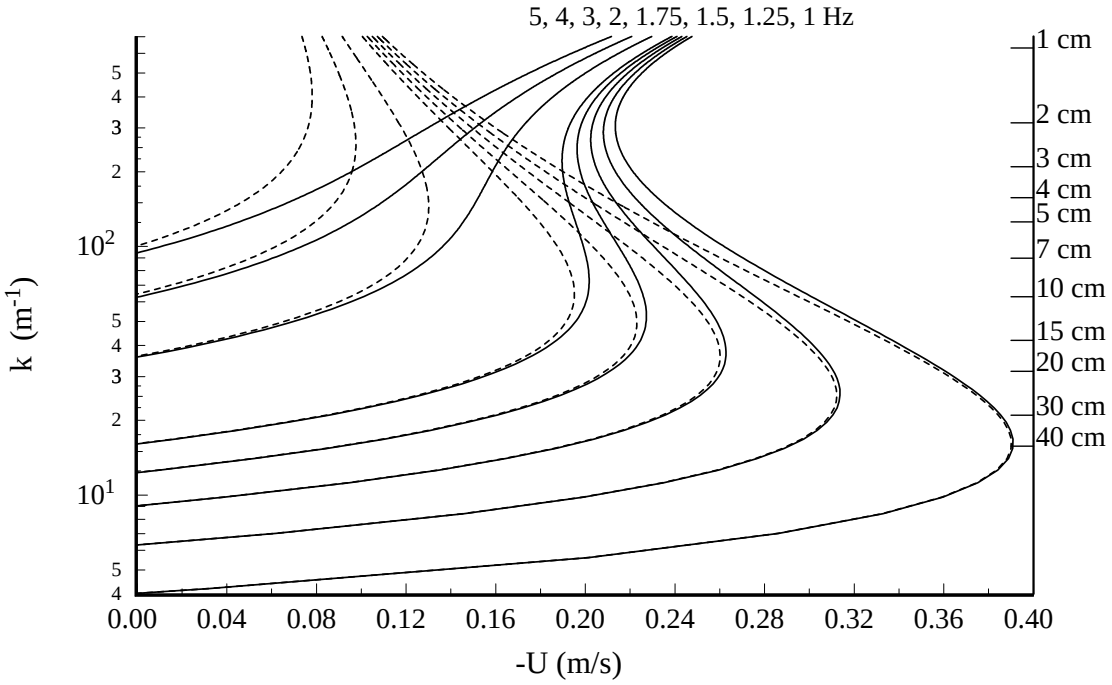


Figure I-6: Wavenumber ($m^{-1}$) and wavelength (m) as a function of leftbound current velocity (m/s) for selected frequencies; from left to right: 5, 4, 3, 2, 1.75, 1.5, 1.25 and 1 Hz. The solid lines show gravity–capillary theory, the broken lines show gravity theory without capillarity.

in figure I-6.

Cases 1a and 2a can both be fully treated by classical ray-theory. Case 1b can be treated by the theory of Shyu & Phillips (1991)[1]. In principle their theory can also be applied to the phenomenon of repeated reflections corresponding to case 2b, provided the reflection points are sufficiently far apart.

We wish to give an alternate theory by a boundary-layer approach, for the double reflection of a packet of gravity–capillary waves corresponding to case 2b for two well-separated reflection points. Our main goal is however to extend the boundary-layer approach to the case where the two reflection points are close together or coalesce to a triple-root turning point. The boundary-layer solution for a triple-root point is developed in section I.6, and is matched to ray-theoretical solutions on each side of the turning point. The case where the two reflection points do not exactly coalesce (a detuned triple-root turning point), is much harder to treat as the mathematical com-

[1]It is being applied by Yiqiang Zhang & O. M. Phillips (private communication 1991) to related problems in gravity waves.

plexity increases enormously. We limit our theoretical development to a derivation of the boundary-layer solution in Appendix I.A. Here the geometry of a cusp-catastrophe is invoked to help identify how the problem can be parameterized.

The results in this part, except for the detuned triple-root turning point, have been published in Trulsen & Mei (1993).

## I.2 Scaling assumptions

Dividing (I.1.1) by $\omega$, we get

$$1 = \sqrt{\frac{gk}{\omega^2} + \frac{Tk^3}{\rho\omega^2}} + \frac{U}{c}, \tag{I.2.1}$$

where $c = \omega/k$ is the phase velocity of the wave. In order to deal with a wide range of wavelengths, we shall require a leading-order balance between all three physical factors: gravity, capillarity and current. Mathematically this is done by formally allowing that $gk/\omega^2$, $(T/\rho)k^3/\omega^2$ and $U/c$ are all $\mathcal{O}(1)$. Since $U/c \sim \sqrt{gD}/c \sim \sqrt{kD}$, where $D$ denotes the scale for the current set-down, it follows that $kD \sim \mathcal{O}(1)$.

In many practical situations, current variations are accompanied by variations in depth. Let the depth and horizontal length scales be $H$ and $L$, respectively, and assume

$$kH \sim \mathcal{O}(\frac{1}{\epsilon}) \qquad \text{and} \qquad \frac{L}{D},\, kL \sim \mathcal{O}(\frac{1}{\epsilon^2}) \tag{I.2.2}$$

where $\epsilon$ defined by

$$\epsilon = (kL)^{-1/2} \tag{I.2.3}$$

is a small parameter. Hence the waves are on deep water, and variations in depth have direct influence only on the current field.

Although the wavenumber varies widely, we shall choose a characteristic wavenumber $\bar{k}$ corresponding to the central frequency $\bar{\omega}$ of the incident gravity wave, i.e. $\bar{k} \equiv \bar{\omega}^2/g$. By this choice the actual ratio between the wave and current length scales is never larger than $1/\bar{k}L = \epsilon^2$.

Let the short wave amplitude be characterized by $a$. The steepness $ka$ is assumed to be so small that nonlinearity is unimportant over the propagation distance of $\mathcal{O}(L)$. From existing theory of slowly varying waves, it is known that nonlinearity is not important over the distance $\mathcal{O}(1/k(ka))$, but will be important over $\mathcal{O}(1/k(ka)^2)$. Therefore we shall assume

$$ka \sim \mathcal{O}(\epsilon^2). \tag{I.2.4}$$

Under these assumptions, it is convenient to employ multiple-scale coordinates. For the waves the dimensional coordinates are $(x, z, t)$, while for the current they are $(x_2 = \epsilon^2 x, z_1 = \epsilon z)$. Explicit expressions for an almost irrotational current over known bathymetry can easily be derived. However, the theory for the short waves is derived below by assuming that the current field is known *a priori*.

## I.3 Approximate equations for the short wave

With $*$ designating physical variables, we let the velocity potential of the wave be $\phi^*$ and the wave-induced free-surface displacement be $\eta^*$. For the current the velocity components are denoted by $(U^*, W^*)$ while the free-surface set-down is $\zeta^*$. The total velocity field is then

$$(U^* + \frac{\partial \phi^*}{\partial x^*})\hat{\boldsymbol{x}} + (W^* + \frac{\partial \phi^*}{\partial z^*})\hat{\boldsymbol{z}},$$

while the total displacement of the free surface is $\zeta^* + \eta^*$. The water depth is $h^*$.

Let $\bar{\omega}$ be the central frequency of the incident gravity wave from deep water, and $\bar{k} = \bar{\omega}^2/g$. We introduce the following normalizations for the current field:

$$x_2 = \epsilon^2 \bar{k} x^*, \quad z_1 = \epsilon \bar{k} z^*, \quad h = \epsilon \bar{k} h^*, \tag{I.3.1}$$

$$\zeta = \bar{k}\zeta^*, \quad U = \sqrt{\frac{\bar{k}}{g}} U^*, \quad W = \frac{1}{\epsilon}\sqrt{\frac{\bar{k}}{g}} W^*. \tag{I.3.2}$$

The following normalized variables are introduced for the short-wave field:

$$x = \bar{k} x^*, \quad z = \bar{k} z^*, \quad t = \bar{\omega} t^*, \quad K = \frac{k^*}{\bar{k}}, \tag{I.3.3}$$

$$\eta = \frac{\bar{k}}{\epsilon^2}\eta^*, \quad \phi = \frac{\bar{k}}{\epsilon^2}\sqrt{\frac{\bar{k}}{g}}\phi^*. \tag{I.3.4}$$

Assuming irrotationality, the dimensionless Laplace equation governing the wave field is

$$\frac{\partial^2 \phi}{\partial x^2} + \frac{\partial^2 \phi}{\partial z^2} = 0 \quad \text{for} \quad -\frac{h}{\epsilon} < z < \zeta + \epsilon^2 \eta. \tag{I.3.5}$$

The boundary condition on the bottom is

$$\frac{\partial \phi}{\partial z} = -\epsilon \frac{\partial \phi}{\partial x}\frac{\partial h}{\partial x_2} \quad \text{at} \quad z = -\frac{h}{\epsilon}. \tag{I.3.6}$$

On the free surface $z = \zeta + \epsilon^2 \eta$, the kinematic condition of the total field reads

$$\epsilon \frac{\partial \eta}{\partial t} + \epsilon \left(U + \epsilon^2 \frac{\partial \phi}{\partial x}\right)\left(\frac{\partial \zeta}{\partial x_2} + \frac{\partial \eta}{\partial x}\right) = W + \epsilon \frac{\partial \phi}{\partial z}, \tag{I.3.7}$$

while the dynamic condition reads

$$\epsilon^2 \frac{\partial \phi}{\partial t} + \zeta + \epsilon^2 \eta + \frac{1}{2}\left[\left(U + \epsilon^2 \frac{\partial \phi}{\partial x}\right)^2 + \left(\epsilon W + \epsilon^2 \frac{\partial \phi}{\partial z}\right)^2\right] = \Gamma \frac{\epsilon^4 \frac{\partial^2 \zeta}{\partial x_2^2} + \epsilon^2 \frac{\partial^2 \eta}{\partial x^2}}{\left[1 + \epsilon^4 \left(\frac{\partial \zeta}{\partial x_2} + \frac{\partial \eta}{\partial x}\right)^2\right]^{3/2}}. \tag{I.3.8}$$

The following dimensionless quantity signifying surface tension has been introduced:

$$\Gamma = \frac{T\bar{k}^3}{\rho\bar{\omega}^2}. \tag{I.3.9}$$

We now Taylor-expand the free-surface conditions about the current set-down $z = \zeta$. Note that the current-related quantities are evaluated at $z_1 = \epsilon\zeta + \epsilon^3\eta$, while wave-related quantities are evaluated at $z = \zeta + \epsilon^2\eta$. Let the current be weakly irrotational, such that

$$\frac{\partial U}{\partial z_1} - \epsilon^2 \frac{\partial W}{\partial x_2} \leq \mathcal{O}(\epsilon^2), \tag{I.3.10}$$

then

$$\begin{aligned} U|_{z_1=\epsilon\zeta+\epsilon^3\eta} &= U|_{z_1=\epsilon\zeta} + \epsilon^3\eta \frac{\partial U}{\partial z_1}\bigg|_{z_1=\epsilon\zeta} + \mathcal{O}(\epsilon^6) \\ &= U|_{z_1=\epsilon\zeta} + \mathcal{O}(\epsilon^5). \end{aligned} \tag{I.3.11}$$

From the kinematic surface condition and the mass conservation equation for the current, we get

$$\begin{aligned} W|_{z_1=\epsilon\zeta+\epsilon^3\eta} &= \left[ W + \epsilon^3\eta \frac{\partial W}{\partial z_1} + \mathcal{O}(\epsilon^6) \right]_{z_1=\epsilon\zeta} \\ &= \left[ \epsilon U \frac{\partial \zeta}{\partial x_2} - \epsilon^3 \eta \frac{\partial U}{\partial x_2} + \mathcal{O}(\epsilon^6) \right]_{z_1=\epsilon\zeta}. \end{aligned} \tag{I.3.12}$$

The wave velocity potential becomes

$$\phi|_{z=\zeta+\epsilon^2\eta} = \left[ \phi + \epsilon^2\eta \frac{\partial \phi}{\partial z} + \mathcal{O}(\epsilon^4) \right]_{z=\zeta}. \tag{I.3.13}$$

Note that in the surface conditions, differentiation must be performed first, before their values are evaluated on the surface. Thus, horizontal and time derivatives of $\phi$ must be taken before expansion about the current set-down.

After Taylor expansion, the kinematic free-surface condition becomes

$$\frac{\partial \eta}{\partial t} + U\frac{\partial \eta}{\partial x} - \frac{\partial \phi}{\partial z} + \epsilon^2 \frac{\partial \zeta}{\partial x_2}\frac{\partial \phi}{\partial x} + \epsilon^2 \frac{\partial U}{\partial x_2}\eta = -\epsilon^2 \frac{\partial \phi}{\partial x}\frac{\partial \eta}{\partial x} + \epsilon^2 \eta \frac{\partial^2 \phi}{\partial z^2} + \mathcal{O}(\epsilon^4) \quad \text{at} \quad z = \zeta. \tag{I.3.14}$$

Similarly, the dynamic free-surface condition is

$$\begin{aligned} &\frac{\partial \phi}{\partial t} + \eta + U\frac{\partial \phi}{\partial x} - \Gamma \frac{\partial^2 \eta}{\partial x^2} + \epsilon^2 U \frac{\partial \zeta}{\partial x_2}\frac{\partial \phi}{\partial z} \\ &= \epsilon^2 \left[ -\eta \frac{\partial^2 \phi}{\partial t \partial z} - U\eta \frac{\partial^2 \phi}{\partial x \partial z} - \frac{1}{2}\left(\frac{\partial \phi}{\partial x}\right)^2 - \frac{1}{2}\left(\frac{\partial \phi}{\partial z}\right)^2 \right] + \mathcal{O}(\epsilon^3) \quad \text{at} \quad z = \zeta. \end{aligned} \tag{I.3.15}$$

In summary, the short wave satisfies (I.3.5) in the fluid, (I.3.6) on the bottom and (I.3.14) and (I.3.15) on the curved surface $z = \zeta(x_2)$. In the sequel we shall seek information regarding the evolution of a slowly varying wave train which is proportional to $\exp\{\mathrm{i}(Kx - t)\}$. The terms linear in $\phi$ or $\eta$ will contain this harmonic while the quadratic terms at $\mathcal{O}(\epsilon^2)$ will give rise to zeroth and second harmonics. Hence the quadratic terms do not affect the first harmonic at order $\mathcal{O}(\epsilon^2)$.

The linear wave solution is expected to attenuate exponentially in $z$, hence the fluid domain is well approximated by $-\infty < z < \zeta$ and the bottom condition may be replaced by

$$\frac{\partial \phi}{\partial z} \to 0 \quad \text{as} \quad z \to -\infty. \tag{I.3.16}$$

# I.4 Ray approximation for short waves away from points of reflection

In this section we present a ray approximation for waves far away from the reflection points. In principle, the results can be inferred from Shyu & Phillips (1990) and Henyey *et al.* (1988). Since the horizontal variation of the current has been assumed to have the characteristic scale $O(\epsilon^2 x)$, it is natural to assume that the resulting modulation of the waves will be on the scales $x_2 = \epsilon^2 x$ and $t_2 = \epsilon^2 t$. First we replace all $x$ and $t$ by $x_2$ and $t_2$ so that

$$\epsilon^4 \frac{\partial^2 \phi}{\partial x_2^2} + \frac{\partial^2 \phi}{\partial z^2} = 0 \quad \text{for} \quad -\infty < z < \zeta, \tag{I.4.1}$$

$$\frac{\partial \phi}{\partial z} = 0 \quad \text{for} \quad z \to -\infty, \tag{I.4.2}$$

$$\epsilon^2 \frac{\partial \eta}{\partial t_2} + \epsilon^2 U \frac{\partial \eta}{\partial x_2} - \frac{\partial \phi}{\partial z} + \epsilon^4 \frac{\partial \zeta}{\partial x_2}\frac{\partial \phi}{\partial x_2} + \epsilon^2 \frac{\partial U}{\partial x_2}\eta = \text{h.o.t.} \quad \text{at} \quad z = \zeta, \tag{I.4.3}$$

$$\epsilon^2 \frac{\partial \phi}{\partial t_2} + \epsilon^2 U \frac{\partial \phi}{\partial x_2} + \eta - \epsilon^4 \Gamma \frac{\partial^2 \eta}{\partial x_2^2} + \epsilon^2 U \frac{\partial \zeta}{\partial x_2}\frac{\partial \phi}{\partial z} = \text{h.o.t.} \quad \text{at} \quad z = \zeta, \tag{I.4.4}$$

where h.o.t. represents higher-order terms.

We now assume WKB-expansions of the form

$$\begin{aligned} \phi &= (A + \epsilon^2 A_2 + \ldots)\exp(\mathrm{i}\epsilon^{-2}S) + \epsilon^2(\text{other harmonics}) + \text{c.c.}, \\ \eta &= (B + \epsilon^2 B_2 + \ldots)\exp(\mathrm{i}\epsilon^{-2}S) + \epsilon^2(\text{other harmonics}) + \text{c.c.}, \end{aligned} \tag{I.4.5}$$

where c.c. denotes complex conjugate and

$$\frac{\partial S}{\partial x_2} = K \quad \text{and} \quad \frac{\partial S}{\partial t_2} = -1. \tag{I.4.6}$$

At the lowest order $\mathcal{O}(1)$, the problem is governed by

$$\frac{\partial^2 A}{\partial z^2} - K^2 A = 0 \quad \text{for} \quad -\infty < z < \zeta, \tag{I.4.7}$$

$$\frac{\partial A}{\partial z} = 0 \quad \text{at} \quad z \to -\infty, \tag{I.4.8}$$

$$-\mathrm{i}B + \mathrm{i}KUB - \frac{\partial A}{\partial z} = 0 \quad \text{at} \quad z = \zeta, \tag{I.4.9}$$

$$-\mathrm{i}A + \mathrm{i}KUA + B + \Gamma K^2 B = 0 \quad \text{at} \quad z = \zeta. \tag{I.4.10}$$

The last two conditions can be combined to

$$\frac{\partial A}{\partial z} - \frac{K(1-KU)^2}{\sigma^2} A = 0, \tag{I.4.11}$$

where

$$\sigma \equiv \sqrt{K + \Gamma K^3} \tag{I.4.12}$$

represents the intrinsic frequency of the wave.

We shall take the solution to be

$$A = -\frac{\mathrm{i}\sigma}{K} B \mathrm{e}^{K(z-\zeta)} \qquad \text{where} \quad B = B(x_2, t_2). \tag{I.4.13}$$

It readily follows that $K(x_2)$ is the solution of the dispersion relation

$$1 - KU = \sqrt{K + \Gamma K^3} \quad \text{or} \quad \Gamma K^3 - U^2 K^2 + (2U+1)K - 1 = 0. \qquad (I.4.14a, b)$$

Equation (I.4.14b) is a cubic equation for $K$ with real coefficients. For a fixed $\Gamma$, $K$ follows one of the curves in figure I-6, which is plotted in physical variables and contrasted with a theory discounting surface tension. Assume that $U(x_2)$ varies monotonically in $x_2$. There are in general three real or one real and two complex conjugate solutions for the wavenumber, $K^{(1)}$, $K^{(2)}$ and $K^{(3)}$. With reference to figure I-7, we divide the physical domain into five parts. In region I there is only one incident long wave ($K^{(1)}$, $B^{(1)}$), while in region III there is only one outgoing short wave ($K^{(3)}$, $B^{(3)}$). In region II there can be three waves. The most general expression for the wave surface displacement in region II is then

$$\eta(x_2, t_2) = \sum_{n=1}^{3} \left\{ B^{(n)}(x_2, t_2) \exp\left( \mathrm{i}\epsilon^{-2} \int^{x_2} K^{(n)} \, \mathrm{d}x_2 \right) + \mathcal{O}(\epsilon^2) \right\} \exp\left( -\mathrm{i}\epsilon^{-2} t_2 \right) + \text{c.c.} \tag{I.4.15}$$

Leaving the neighborhoods of the isolated turning points IV and V to the next section, we first determine the amplitude $B$, the generic symbol for $B^{(1)}$, $B^{(2)}$ and $B^{(3)}$ .

The second-order problem $\mathcal{O}(\epsilon^2)$ is

$$\frac{\partial^2 A_2}{\partial z^2} - K^2 A_2 = -\mathrm{i}\frac{\partial}{\partial x_2}(KA) - \mathrm{i}K\frac{\partial A}{\partial x_2} \quad \text{for} \quad -\infty < z < \zeta, \tag{I.4.16}$$

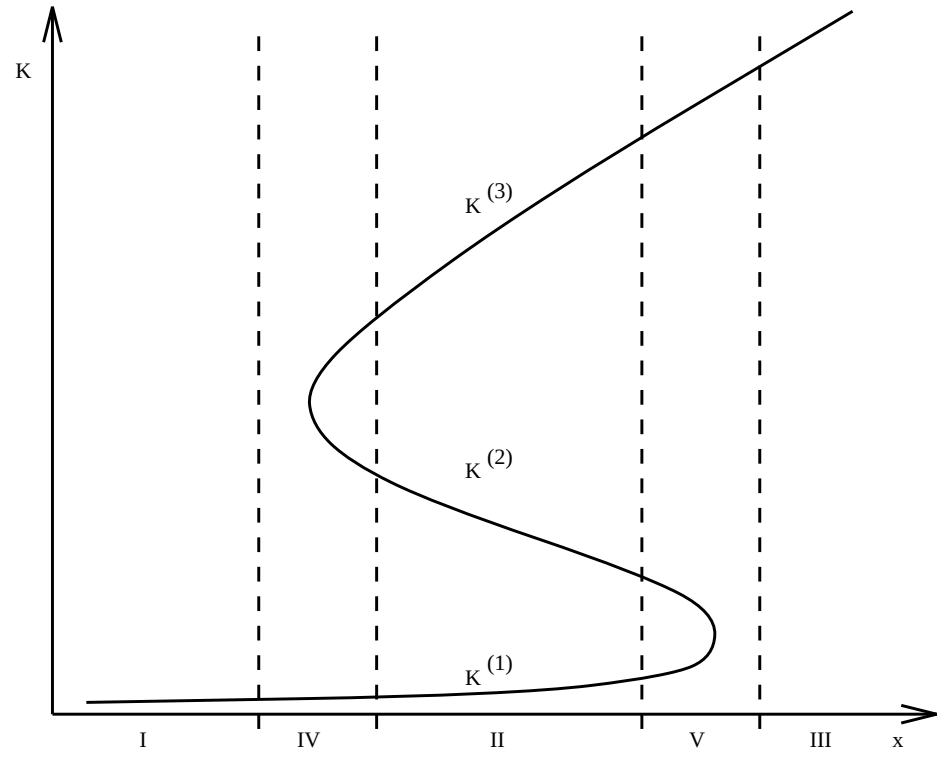


Figure I-7: Sketch of the different regions of the wave development.

$$\frac{\partial A_2}{\partial z} = 0 \quad \text{at} \quad z \to -\infty, \tag{I.4.17}$$

$$\frac{\partial B}{\partial t_2} - \mathrm{i}B_2 + U\frac{\partial B}{\partial x_2} + \mathrm{i}KUB_2 - \frac{\partial A_2}{\partial z} + \mathrm{i}K\frac{\partial \zeta}{\partial x_2}A + \frac{\partial U}{\partial x_2}B = 0 \quad \text{at} \quad z = \zeta, \tag{I.4.18}$$

$$\begin{aligned} &\frac{\partial A}{\partial t_2} - \mathrm{i}A_2 + U\frac{\partial A}{\partial x_2} + \mathrm{i}KUA_2 + B_2 \\ &- \mathrm{i}\Gamma\frac{\partial}{\partial x_2}(KB) - \mathrm{i}\Gamma K\frac{\partial B}{\partial x_2} + \Gamma K^2 B_2 + U\frac{\partial \zeta}{\partial x_2}\frac{\partial A}{\partial z} \;=\; 0 \quad \text{at} \quad z = \zeta. \end{aligned} \tag{I.4.19}$$

The last two equations can be combined by eliminating $B_2$, and the first-order result can further be used to substitute for $A$. The resulting surface condition is

$$\begin{aligned} \frac{\partial A_2}{\partial z} - KA_2 \;=\; & 2\frac{\partial B}{\partial t_2} + U\frac{\partial B}{\partial x_2} + \sigma\frac{\partial \zeta}{\partial x_2}B + \frac{\partial U}{\partial x_2}B \\ & + \frac{KU}{\sigma}\frac{\partial}{\partial x_2}\left(\frac{\sigma}{K}B\right) + \frac{\Gamma K}{\sigma}\frac{\partial}{\partial x_2}(KB) + \frac{\Gamma K^2}{\sigma}\frac{\partial B}{\partial x_2}. \end{aligned} \tag{I.4.20}$$

The problem for $A_2$ is seen to be an inhomogeneous version of the homogeneous problem for $A$. Therefore $A_2$ must satisfy a condition of solvability, which follows

from Green's theorem,

$$\int_{-\infty}^{\zeta} \mathrm{d}z \left[ A\left(\frac{\partial^2 A_2}{\partial z^2} - K^2 A_2\right) - A_2\left(\frac{\partial^2 A}{\partial z^2} - K^2 A\right)\right] = \left[A\frac{\partial A_2}{\partial z} - A_2\frac{\partial A}{\partial z}\right]_{-\infty}^{\zeta}. \quad \text{(I.4.21)}$$

After substituting (I.4.16)–(I.4.20) into this condition, we get the following condition for $B$,

$$\frac{\partial}{\partial x_2}\left\{\left(\frac{\sigma^2}{2K^2} + \frac{\sigma U}{K} + \Gamma K\right) B^2\right\} + \frac{\partial}{\partial t_2}\left\{\frac{\sigma}{K}B^2\right\} = 0. \quad \text{(I.4.22)}$$

Let us introduce the intrinsic group velocity

$$c_g \equiv \frac{\mathrm{d}\sigma}{\mathrm{d}K} = \frac{\sigma}{2K} + \frac{\Gamma K^2}{\sigma}, \quad \text{(I.4.23)}$$

so that we get

$$\frac{\partial}{\partial x_2}\left\{\frac{\sigma}{K}(c_g + U)B^2\right\} + \frac{\partial}{\partial t_2}\left\{\frac{\sigma}{K}B^2\right\} = 0. \quad \text{(I.4.24)}$$

This is the conservation law for wave action

$$\frac{\partial}{\partial x_2}\left\{\frac{E}{\sigma}(c_g + U)\right\} + \frac{\partial}{\partial t_2}\left\{\frac{E}{\sigma}\right\} = 0, \quad \text{(I.4.25)}$$

where $E = \rho\sigma^2 B^2/2K$ is the total energy. This equation has been deduced in similar contexts by Bretherton & Garrett (1968), Henyey *et al.* (1988) and Shyu & Phillips (1990).

As an application, we now seek a solution representing a wave packet. Recall that $c_g$, $U$, $K$ and $\sigma$ are all independent of time. Upon multiplication of equation (I.4.24) by $c_g + U$, and introduction of $\psi = (c_g + U)\sigma B^2/K$, we write

$$\frac{\partial \psi}{\partial t_2} + (c_g + U)\frac{\partial \psi}{\partial x_2} = 0. \quad \text{(I.4.26)}$$

It follows that $\psi$ is constant along the characteristic curve

$$t_2 - t_{ref} = \int_{x_{ref}}^{x_2} \frac{\mathrm{d}x_2}{c_g + U}, \quad \text{(I.4.27)}$$

where $x_{ref}$ and $t_{ref}$ are some reference values for horizontal position and time. Hence the solution for $B$ becomes

$$B(x_2, t_2) = b(t_2 - \int_{x_{ref}}^{x_2} \frac{\mathrm{d}x_2}{c_g + U})\sqrt{\frac{K}{\sigma(c_g + U)}}. \quad \text{(I.4.28)}$$

where $b(t_2)$ is the time-dependent boundary value of $B$ at $x_2 = x_{ref}$,

$$B(x_{ref}, t_2) = b(t_2)\sqrt{\frac{K}{\sigma(c_g + U)}} \quad \text{at} \quad x_2 = x_{ref}. \quad \text{(I.4.29)}$$

Note that the solution breaks down at turning points where $c_g + U = 0$. To further examine its behavior near the turning points, we rewrite the above square root as

$$\left| \frac{1}{\frac{\sigma^2}{2K^2} + \frac{\sigma U}{K} + \Gamma K} \right|^{1/2} = \left| \frac{2K^2}{2\Gamma K^3 - U^2 K^2 + 1} \right|^{1/2}. \tag{I.4.30}$$

Now the dispersion relation (I.4.14b) can be written in the form

$$\Gamma(K - K^{(1)})(K - K^{(2)})(K - K^{(3)}) = 0, \tag{I.4.31}$$

where $K^{(1)} < K^{(2)} < K^{(3)}$ denote the three (real) roots. It is clear that $1/\Gamma = K^{(1)}K^{(2)}K^{(3)}$ and $U^2/\Gamma = K^{(1)} + K^{(2)} + K^{(3)}$. Let us further assume, for illustration, that the wavenumber under consideration is $K = K^{(2)}$, corresponding to $B^{(2)}(x_2)$. We then get from (I.4.30)

$$B^{(2)}(x_2) = b\sqrt{\frac{2K^{(2)}}{\Gamma(K^{(2)} - K^{(1)})(K^{(2)} - K^{(3)})}}. \tag{I.4.32}$$

It is clear that the ray-theoretical solution is valid as long as $K^{(1)} \neq K^{(2)} \neq K^{(3)}$, and breaks down at the points where the dispersion relation has a double root, $K^{(1)} = K^{(2)}$ or $K^{(2)} = K^{(3)}$, or a triple root, $K^{(1)} = K^{(2)} = K^{(3)}$. The asymptotic behavior of the amplitude near such points will depend on the multiplicity of the roots, as discussed separately in subsequent sections.

## I.5 Inner solution near a simple turning point

In this section we shall rederive the theory of Shyu & Phillips (1990) by matched asymptotics for an isolated turning point and apply the results to the case with two well separated turning points.

Let us consider the neighborhood of a simple turning point at $x_2 = x_0$ where there is a double root for the wavenumber, $K = K_0$. Thus two solution branches $B^+$ and $B^-$, with their respective wavenumbers $K^+$ and $K^-$, converge to $K_0$ at the turning point. In the following, we shall let indices $-$ and $+$ denote the longer and shorter waves, respectively, such that $K^- < K^+$. With this general convention, the theory is equally valid in both regions IV and V in figure I-7.

Let us shift the origin by $\tilde{x} = x_2 - x_0$, and expand the current field in local expansions. We begin by noting that the current set-down can be expanded as

$$\zeta(x_2) = \zeta_0 + \tilde{x}\zeta_1 + \mathcal{O}(\tilde{x}^2), \tag{I.5.1}$$

where $\zeta_0 \equiv \zeta$ and $\zeta_1 \equiv \partial\zeta/\partial x_2$, both evaluated at $x_2 = x_0$. The surface horizontal current can then be expanded as

$$U(x_2) = U_0 + \tilde{x}\frac{\partial U}{\partial x_2} + \epsilon\tilde{x}\zeta_1\frac{\partial U}{\partial z_1} + \mathcal{O}(\tilde{x}^2), \tag{I.5.2}$$

where the terms on the right-hand side are evaluated at $z_1 = \epsilon\zeta_0$ and $x_2 = x_0$. Due to the assumption that the current has weak vorticity

$$\frac{\partial U}{\partial z_1} - \epsilon^2 \frac{\partial W}{\partial x_2} \leq \mathcal{O}(\epsilon^2), \tag{I.5.3}$$

we have $\partial U/\partial z_1 = \mathcal{O}(\epsilon^2)$. If we define $U_1 \equiv \partial U/\partial x_2$ at $x_2 = x_0, z_1 = \epsilon\zeta_0$, the expansion for the surface horizontal current is

$$U(x_2) = U_0 + \tilde{x}U_1 + \mathcal{O}(\tilde{x}^2, \epsilon^3\tilde{x}). \tag{I.5.4}$$

Suppose that the wavenumber behaves as $K = K_0 + R(\tilde{x})$ for small $\tilde{x}$, where $R(\tilde{x}) = o(1)$. Substituting these expansions into the dispersion relation (I.4.14b), and expanding for small $\tilde{x}$, we get

$$R^2(3\Gamma K_0 - U_0^2) + R^3\Gamma + 2U_1K_0\sigma_0\tilde{x} = \mathcal{O}(\tilde{x}R), \tag{I.5.5}$$

where $\sigma_0 \equiv \sqrt{K_0 + \Gamma K_0^3}$, and use has been made of the fact that $c_g \equiv d\sigma/dK = -U$ at $\tilde{x} = 0$. Clearly, the leading asymptotic behavior for small $\tilde{x}$ is $R \sim \tilde{x}^{1/2}$. Consequently, the wavenumber can be expanded in half powers of $\tilde{x}$,

$$K \sim K_0 + \alpha\tilde{x}^{1/2} + \beta\tilde{x}, \tag{I.5.6}$$

where

$$\alpha = \left(-\frac{2U_1K_0\sigma_0}{3\Gamma K_0 - U_0^2}\right)^{1/2} \qquad \text{and} \qquad \beta = \frac{U_1(5K_0^2U_0\Gamma - 2K_0\Gamma - 2K_0U_0^3 + U_0^2)}{(3K_0\Gamma - U_0^2)^2}. \tag{I.5.7}$$

Substitution of expansions (I.5.4) and (I.5.6) for $U$ and $K$ into (I.4.28) gives the inner approximation of the outer (ray) solution near the turning point

$$\begin{aligned} B^{\pm}(\tilde{x}, t_2) &= b_{\pm}(t_2 - \int_{\tilde{x}_{\pm}}^{\tilde{x}} \frac{\mathrm{d}\tilde{x}}{c_g^{\pm} + U}) \sqrt{\frac{K^{\pm}}{\sigma^{\pm}(c_g^{\pm} + U)}} \\ &\sim b_{\pm}(t_2 - \int_{\tilde{x}_{\pm}}^{\tilde{x}} \frac{\mathrm{d}\tilde{x}}{c_g^{\pm} + U}) \left( \left| -\frac{\alpha}{2\sigma_0 U_1} \right|^{\frac{1}{2}} |\tilde{x}|^{-\frac{1}{4}} + \mathcal{O}(\tilde{x}^{\frac{1}{4}}) \right) \end{aligned} \tag{I.5.8}$$

where $b_-$ and $b_+$ are the complex amplitudes of the incident and reflected waves, respectively, on the incidence side of the reflection point, and $\tilde{x}_{\pm}$ are the starting points for the time and phase integrals.

The evanescent modes on the opposite side of the reflection point are exponentially attenuated in $\tilde{x}$, and need not be taken into account for the present purposes.

From the inhomogeneous Laplace equation at order $\mathcal{O}(\epsilon^2)$, (I.4.16), the dominant behavior at this order can be seen to be

$$A_2^{\pm} \sim B_2^{\pm} \sim \mathcal{O}(\tilde{x}^{-5/4}). \tag{I.5.9}$$

Therefore the surface displacement on the incidence side of the singularity can be expanded as

$$\eta(\tilde{x},t_2) = B^- \exp\left(\mathrm{i}\epsilon^{-2}(\int_{\tilde{x}_-}^{\tilde{x}} K^- \,\mathrm{d}\tilde{x} - t_2)\right) + B^+ \exp\left(\mathrm{i}\epsilon^{-2}(\int_{\tilde{x}_+}^{\tilde{x}} K^+ \,\mathrm{d}\tilde{x} - t_2)\right) + \mathcal{O}(\epsilon^2)$$

$$\sim \left|-\frac{\alpha}{2\sigma_0 U_1}\right|^{\frac{1}{2}} |\tilde{x}|^{-\frac{1}{4}} \left\{ b_-(t_2 - \int_{\tilde{x}_-}^{\tilde{x}} \frac{\mathrm{d}\tilde{x}}{c_g^- + U}) \exp\left(\mathrm{i}\epsilon^{-2}(\int_{\tilde{x}_-}^{0} K^- \,\mathrm{d}\tilde{x} + K_0\tilde{x} - \frac{2}{3}|\alpha\tilde{x}^{\frac{3}{2}}|)\right) \right.$$

$$\left. + b_+(t_2 - \int_{\tilde{x}_+}^{\tilde{x}} \frac{\mathrm{d}\tilde{x}}{c_g^+ + U}) \exp\left(\mathrm{i}\epsilon^{-2}(\int_{\tilde{x}_+}^{0} K^+ \,\mathrm{d}\tilde{x} + K_0\tilde{x} + \frac{2}{3}|\alpha\tilde{x}^{\frac{3}{2}}|)\right)\right\}$$

$$\exp(-\mathrm{i}\epsilon^{-2}t_2) \tag{I.5.10}$$

Higher powers of $\tilde{x}$ from $B^\pm$ will give contributions of $\mathcal{O}(\tilde{x}^{1/4})$, while the $\mathcal{O}(\epsilon^2)$ terms will give contributions of $\mathcal{O}(\epsilon^2\tilde{x}^{-5/4})$. Hence this one-term asymptotic expansion for the amplitude of the outer solution is valid for $\epsilon^2 \ll |\tilde{x}| \ll 1$.

We now examine the neighborhood of the singularity, which is the inner region. Let us expand the velocity potential at the surface about the current set-down, which is at the constant height $\zeta_0$,

$$\phi|_{z=\zeta} = \left[\phi + \tilde{x}\zeta_1\frac{\partial\phi}{\partial z} + \mathcal{O}(\tilde{x}^2)\right]_{z=\zeta_0}. \tag{I.5.11}$$

Once again, horizontal derivatives of $\phi$ must be taken before the expansion, which should not be differentiated with respect to $\tilde{x}$. The kinematic and dynamic surface conditions (I.3.14) and (I.3.15) become

$$\frac{\partial\eta}{\partial t} + U_0\frac{\partial\eta}{\partial x} + \tilde{x}U_1\frac{\partial\eta}{\partial x} - \frac{\partial\phi}{\partial z} - \tilde{x}\zeta_1\frac{\partial^2\phi}{\partial z^2} = \mathcal{O}(\epsilon^2,\tilde{x}^2), \tag{I.5.12}$$

$$\frac{\partial\phi}{\partial t} + \tilde{x}\zeta_1\frac{\partial^2\phi}{\partial t\partial z} + U_0\frac{\partial\phi}{\partial x} + \tilde{x}U_0\zeta_1\frac{\partial^2\phi}{\partial x\partial z} + \tilde{x}U_1\frac{\partial\phi}{\partial x} + \eta - \Gamma\frac{\partial^2\eta}{\partial x^2} = \mathcal{O}(\epsilon^2,\tilde{x}^2). \tag{I.5.13}$$

In the neighborhood of a simple turning point (the inner region), we expect the spatial dependence of the amplitude to be governed by an Airy differential equation of the form

$$\epsilon^4\frac{\partial^2 B}{\partial\tilde{x}^2} - c\tilde{x}B = 0. \tag{I.5.14}$$

The boundary layer thickness must then be $\tilde{x} = \mathcal{O}(\epsilon^{4/3})$. The local characteristic timescale for this inner region is the time for energy to pass through at the propagation speed $c_g + U \sim \tilde{x}^{1/2}$, is

$$t_2 \sim \int_0^{\epsilon^{4/3}} \frac{\mathrm{d}\tilde{x}}{c_g + U} \sim \mathcal{O}(\epsilon^{2/3}). \tag{I.5.15}$$

If transients are important in this inner region, the space and time coordinates for the inner problem must be renormalized by

$$\xi = \epsilon^{-4/3}\tilde{x} \qquad \text{and} \qquad \tau = \epsilon^{-2/3}t_2 \tag{I.5.16}$$

which is adopted here for the sake of generality. The governing equations (I.3.5)–(I.3.8) can be rewritten as follows

$$\epsilon^{\frac{4}{3}}\frac{\partial^2\phi}{\partial\xi^2}+\frac{\partial^2\phi}{\partial z^2}=0 \quad \text{for} \quad -\infty<z<\zeta_0, \tag{I.5.17}$$

$$\frac{\partial\phi}{\partial z}=0 \quad \text{for} \quad z\to-\infty, \tag{I.5.18}$$

$$\epsilon^{\frac{4}{3}}\frac{\partial\eta}{\partial\tau}+\epsilon^{\frac{2}{3}}U_0\frac{\partial\eta}{\partial\xi}+\epsilon^2\xi U_1\frac{\partial\eta}{\partial\xi}-\frac{\partial\phi}{\partial z}-\epsilon^{\frac{4}{3}}\xi\zeta_1\frac{\partial^2\phi}{\partial z^2}=\text{h.o.t.} \quad \text{at} \quad z=\zeta_0, \tag{I.5.19}$$

$$\begin{aligned}\epsilon^{\frac{4}{3}}\frac{\partial\phi}{\partial\tau}+\epsilon^{\frac{8}{3}}\xi\zeta_1\frac{\partial^2\phi}{\partial\tau\partial z}+\epsilon^{\frac{2}{3}}U_0\frac{\partial\phi}{\partial\xi}+\epsilon^2\xi U_0\zeta_1\frac{\partial^2\phi}{\partial\xi\partial z}\\ +\epsilon^2\xi U_1\frac{\partial\phi}{\partial\xi}+\eta-\epsilon^{\frac{4}{3}}\Gamma\frac{\partial^2\eta}{\partial\xi^2}=\text{h.o.t.} \quad \text{at} \quad z=\zeta_0.\end{aligned} \tag{I.5.20}$$

Higher powers in $\xi$ have been incorporated in h.o.t.

Let us assume a solution of the WKB-type

$$\begin{aligned}\phi &= (A+\epsilon^{\frac{2}{3}}A_1+\epsilon^{\frac{4}{3}}A_2+\ldots)\exp\{\mathrm{i}(\epsilon^{-\frac{2}{3}}K_0\xi-\epsilon^{-\frac{4}{3}}\tau)\}+\text{c.c.},\\ \eta &= (B+\epsilon^{\frac{2}{3}}B_1+\epsilon^{\frac{4}{3}}B_2+\ldots)\exp\{\mathrm{i}(\epsilon^{-\frac{2}{3}}K_0\xi-\epsilon^{-\frac{4}{3}}\tau)\}+\text{c.c.}\end{aligned} \tag{I.5.21}$$

The lowest-order problem $\mathcal{O}(1)$ is governed by

$$\frac{\partial^2A}{\partial z^2}-K_0^2A=0 \quad \text{for} \quad -\infty<z<\zeta_0, \tag{I.5.22}$$

$$\frac{\partial A}{\partial z}\to 0 \quad \text{at} \quad z\to-\infty, \tag{I.5.23}$$

$$-\mathrm{i}B+\mathrm{i}K_0U_0B-\frac{\partial A}{\partial z}=0 \quad \text{at} \quad z=\zeta_0, \tag{I.5.24}$$

$$-\mathrm{i}A+\mathrm{i}K_0U_0A+B+\Gamma K_0^2B=0 \quad \text{at} \quad z=\zeta_0. \tag{I.5.25}$$

We shall take as the solution

$$A=-\frac{\mathrm{i}\sigma_0}{K_0}B\mathrm{e}^{K_0(z-\zeta_0)} \qquad \text{with} \qquad B=B(\xi,\tau) \tag{I.5.26}$$

subject to the dispersion relation

$$1-K_0U_0=\sqrt{K_0+\Gamma K_0^3}. \tag{I.5.27}$$

The problem at order $\mathcal{O}(\epsilon^{2/3})$ is

$$\frac{\partial^2A_1}{\partial z^2}-K_0^2A_1=-2\mathrm{i}K_0\frac{\partial A}{\partial\xi} \quad \text{for} \quad -\infty<z<\zeta_0, \tag{I.5.28}$$

$$\frac{\partial A_1}{\partial z} = 0 \quad \text{at} \quad z \to -\infty, \tag{I.5.29}$$

$$-\mathrm{i}B_1 + U_0\frac{\partial B}{\partial \xi} + \mathrm{i}K_0U_0B_1 - \frac{\partial A_1}{\partial z} = 0 \quad \text{at} \quad z = \zeta_0, \tag{I.5.30}$$

$$-\mathrm{i}A_1 + U_0\frac{\partial A}{\partial \xi} + \mathrm{i}K_0U_0A_1 + B_1 - 2\mathrm{i}\Gamma K_0\frac{\partial B}{\partial \xi} + \Gamma K_0^2 B_1 = 0 \quad \text{at} \quad z = \zeta_0. \tag{I.5.31}$$

The last two equations can be combined by eliminating $B_1$, and the lowest-order result can further be used to substitute for $A$. The resulting surface condition is

$$\frac{\partial A_1}{\partial z} - K_0 A_1 = -\frac{\sigma_0}{K_0}\frac{\partial B}{\partial \xi}. \tag{I.5.32}$$

In obtaining the last result, use has been made of the fact that at the reflection point, $c_g + U_0 = 0$.

The problem for $A_1$ is seen to be an inhomogeneous version of the homogeneous problem for $A$. However, it is readily seen that the solvability condition is identically satisfied. We must therefore go to the next order to find a governing equation for $A$. Particular solutions for $A_1$ and $B_1$ can be found as

$$A_1 = -\frac{\sigma_0}{K_0}\frac{\partial B}{\partial \xi}(z-\zeta_0)\mathrm{e}^{K_0(z-\zeta_0)} \tag{I.5.33}$$

and

$$B_1 = -\mathrm{i}(\frac{1}{K_0} + \frac{U_0}{\sigma_0})\frac{\partial B}{\partial \xi}. \tag{I.5.34}$$

The problem at order $\mathcal{O}(\epsilon^{4/3})$ is

$$\frac{\partial^2 A_2}{\partial z^2} - K_0^2 A_2 = -\frac{\partial^2 A}{\partial \xi^2} - 2\mathrm{i}K_0\frac{\partial A_1}{\partial \xi} \quad \text{for} \quad -\infty < z < \zeta_0, \tag{I.5.35}$$

$$\frac{\partial A_2}{\partial z} = 0 \quad \text{at} \quad z \to -\infty, \tag{I.5.36}$$

$$\frac{\partial B}{\partial \tau} - \mathrm{i}B_2 + U_0\frac{\partial B_1}{\partial \xi} + \mathrm{i}K_0U_0B_2 + \mathrm{i}\xi K_0U_1B - \frac{\partial A_2}{\partial z} - \xi\zeta_1\frac{\partial^2 A}{\partial z^2} = 0 \quad \text{at} \quad z = \zeta_0, \tag{I.5.37}$$

$$\begin{aligned}\frac{\partial A}{\partial \tau} - \mathrm{i}A_2 - \mathrm{i}\xi\zeta_1\frac{\partial A}{\partial z} + U_0\frac{\partial A_1}{\partial \xi} + \mathrm{i}K_0U_0A_2 + \mathrm{i}\xi K_0U_0\zeta_1\frac{\partial A}{\partial z} \\ + \mathrm{i}\xi K_0U_1A + B_2 - \Gamma\frac{\partial^2 B}{\partial \xi^2} - 2\mathrm{i}\Gamma K_0\frac{\partial B_1}{\partial \xi} + \Gamma K_0^2 B_2 \;=\; 0 \quad \text{at} \quad z = \zeta_0.\end{aligned} \tag{I.5.38}$$

The last two equations can be combined by eliminating $B_2$, and the previous lower-order results can further be used to substitute for $A_1$, $B_1$ and $A$. The resulting surface condition is

$$\frac{\partial A_2}{\partial z} - K_0 A_2 = 2\frac{\partial B}{\partial \tau} - \frac{\mathrm{i}}{\sigma_0}\left[3\Gamma K_0 - U_0^2\right]\frac{\partial^2 B}{\partial \xi^2} + 2\mathrm{i}K_0U_1\xi B. \tag{I.5.39}$$

Both the dispersion relation (I.5.27) and the identity $c_g + U_0 = 0$ have been used.

The solvability condition for $A_2$ requires that the right-hand side of (I.5.39) vanishes, hence $B$ must satisfy the following Schrödinger equation,

$$-\mathrm{i}\frac{\partial B}{\partial \tau} - \frac{3\Gamma K_0 - U_0^2}{2\sigma_0}\frac{\partial^2 B}{\partial \xi^2} + K_0 U_1 \xi B = 0. \tag{I.5.40}$$

Equation (I.5.40) applies to problems where transients are important in the boundary layer.

For a slowly modulated incident wave packet, described near the end of section I.4, the timescale of interest is $t_2 = \mathcal{O}(1)$ which is much longer than that of the characteristic time of the inner region defined by (I.5.16b). It is seen that if the modulation timescale is $t_2$ in (I.5.40), the inner region is approximately quasi-stationary. Consequently, (I.5.40) reduces to the ordinary Airy differential equation

$$\frac{\partial^2 B}{\partial \xi^2} + \alpha^2 \xi B = 0, \tag{I.5.41}$$

where the coefficient $\alpha$ is defined by (I.5.7).

The wave amplitude near the reflection point is

$$B(\xi, t_2) = b_0(t_2)\,\mathrm{Ai}(-\alpha^{\frac{2}{3}}\xi). \tag{I.5.42}$$

where $b_0(t_2)$ remains to be found. As $\alpha^{2/3}\xi \sim \infty$, or far away from the reflection point on the incidence side, the asymptotic behavior is

$$B \sim b_0(t_2)\left[\pi^{-\frac{1}{2}}|\alpha|^{-\frac{1}{6}}|\xi|^{-\frac{1}{4}}\sin\left(\frac{2}{3}|\alpha\xi^{\frac{3}{2}}| + \frac{\pi}{4}\right) + \mathcal{O}(\xi^{-\frac{7}{4}})\right], \tag{I.5.43}$$

and from (I.5.34),

$$B_1 \sim \mathcal{O}(\xi^{\frac{1}{4}}). \tag{I.5.44}$$

The corresponding asymptotic behavior of the surface displacement, here expressed in terms of $\tilde{x}$, is

$$\eta(\tilde{x}, t_2) \sim b_0(t_2)\pi^{-\frac{1}{2}}|\alpha|^{-\frac{1}{6}}\epsilon^{\frac{1}{3}}|\tilde{x}|^{-\frac{1}{4}}\sin\left(\frac{2}{3}\epsilon^{-2}|\alpha\tilde{x}^{\frac{3}{2}}| + \frac{\pi}{4}\right)\exp\left(\mathrm{i}\epsilon^{-2}[K_0\tilde{x} - t_2]\right). \tag{I.5.45}$$

This is the outer expansion of the inner solution.

Higher powers of $\tilde{x}$ from $B$ give contributions of $\mathcal{O}(\epsilon^{7/3}\tilde{x}^{-7/4})$, while terms from $B_1$ give contributions of $\mathcal{O}(\epsilon^{1/3}\tilde{x}^{1/4})$. Therefore, this one-term asymptotic expansion is valid in the region $\epsilon^{4/3} \ll |\tilde{x}| \ll 1$.

Both asymptotic expansions (I.5.10) and (I.5.45) have a common region of validity, $\epsilon^{4/3} \ll |\tilde{x}| \ll 1$. The relationship between the coefficients can now be found by asymptotic matching. The time dependent coefficients of the ray solution, (I.5.10), are most easily evaluated at the time when the ray reaches the reflection point. Hence the time integrals in (I.5.10) are to be evaluated with the upper limit set to $\tilde{x} = 0$.

This can be done because the errors introduced in the time and phase integrals are smaller than the accuracy of the asymptotic result. The results of matching are then,

$$b_+(t_2 - \int_{\tilde{x}_+}^0 \frac{\mathrm{d}\tilde{x}}{c_g^+ + U}) = -\mathrm{i}b_-(t_2 - \int_{\tilde{x}_-}^0 \frac{\mathrm{d}\tilde{x}}{c_g^- + U})\mathrm{e}^{\mathrm{i}\epsilon^{-2}\left[\int_{\tilde{x}_-}^0 K^-\,\mathrm{d}\tilde{x} - \int_{\tilde{x}_+}^0 K^+\,\mathrm{d}\tilde{x}\right]}, \qquad \text{(I.5.46)}$$

and

$$b_0(t_2) = b_-(t_2 - \int_{\tilde{x}_-}^0 \frac{\mathrm{d}\tilde{x}}{c_g^- + U})\epsilon^{-\frac{1}{3}} \left|\frac{2\pi}{\sigma_0 U_1}\right|^{\frac{1}{2}} |\alpha|^{\frac{2}{3}} \exp\left(\mathrm{i}\epsilon^{-2}\int_{\tilde{x}_-}^0 K^-\,\mathrm{d}\tilde{x} - \frac{\pi\mathrm{i}}{4}\right). \qquad \text{(I.5.47)}$$

Both the inner and outer solutions are therefore determined. The theory is equally valid in either of regions IV and V in figure I-7, by a proper choice of solution branches of the dispersion relation.

To summarize, the amplitude far from the reflection point is given by (I.5.10) while the solution at the reflection point is given by (I.5.42). A solution uniformly valid to the leading order with $O(\epsilon^{2/3})$ error can be obtained by adding the inner and outer solutions and subtracting the common asymptotic part in (I.5.45).

Numerical examples are discussed in section I.8.

We remark that the accuracy of the results in the inner regions can be improved by including $\epsilon^{2/3}(A_1, B_1)$. We also notice that if corrections at order $\mathcal{O}(\epsilon^{2/3})$ are included, the inner region can not be approximated as stationary unless the modulation time of the incoming wave packet is slower than $t_2$. On the other hand, by keeping just the leading order in the outer ray approximation, the error is $O(\epsilon^2)$ which is relatively small.

## I.6 Solution near a triple-root turning point

As shown in figure I-6, for a sufficiently low wave frequency, there are two simple reflection points (double-roots of (I.4.14b)). For a sufficiently high frequency, there are no reflection points. Therefore, a triple-root point exists for some intermediate wave frequency, $\omega_0$, where the two reflection points coalesce. We now assume the incident wave frequency to be precisely the critical frequency $\bar{\omega} = \omega_0$.

From (I.4.14a,b), the following three conditions must be satisfied simultaneously at the perfect triple-root point: The dispersion relation

$$\Gamma_0 K_0^3 - U_0^2 K_0^2 + (2U_0 + 1)K_0 - 1 = 0, \qquad \text{(I.6.1)}$$

the condition for a reflection point $\mathrm{d}\sigma/\mathrm{d}K = -U$

$$3\Gamma_0 K_0^2 - 2U_0^2 K_0 + 2U_0 + 1 = 0, \qquad \text{(I.6.2)}$$

and the condition for a triple-root $\mathrm{d}^2\sigma/\mathrm{d}K^2 = 0$

$$3\Gamma_0 K_0 - U_0^2 = 0. \qquad \text{(I.6.3)}$$

We have denoted the critical solution at the triple-root point by subscript $(\,)_0$. The solution to (I.6.1)–(I.6.3) is

$$K_0 = 3 + 2\sqrt{3}, \quad \Gamma_0 = -5 + \frac{26}{9}\sqrt{3}, \quad U_0 = -2 + \sqrt{3} \quad \text{and} \quad \sigma_0 = 1 + \sqrt{3}. \tag{I.6.4}$$

Recall that the dimensionless quantities (in capital letters $K_0$, $U_0$, $\Gamma_0$) are related to the dimensional quantities (in small letters $k_0$, $u_0$, $\omega_0$) by $\Gamma_0 = T\omega_0^4/(\rho g^3)$, $K_0 = gk_0/\omega_0^2$ and $U = \omega_0 u_0/g$. For typical values $g = 9.8\,\mathrm{m/s^2}$ and $T/\rho = 7.3 \times 10^{-5}\,\mathrm{m^3/s^2}$, the triple-root point occurs when the absolute frequency is 2.4 Hz, the wavelength is 4.4 cm and the current velocity is $-18$ cm/s.

Let us define the local, slow horizontal coordinate as $\tilde{x} = x_2 - x_0$, where $x_0$ is the location of the triple-root turning point. Let the current field be expanded as in section I.5,

$$\begin{aligned} \zeta &= \zeta_0 + \tilde{x}\zeta_1 + \mathcal{O}(\tilde{x}^2), \\ U &= U_0 + \tilde{x}U_1 + \mathcal{O}(\tilde{x}^2, \epsilon^3\tilde{x}). \end{aligned} \tag{I.6.5}$$

To find the asymptotic behavior of the wavenumber, we substitute the surface current expansion (I.6.5) and the following expansion for the wavenumber,

$$K = K_0 + R(\tilde{x}, \epsilon), \tag{I.6.6}$$

into the dispersion relation (I.4.14b). The resulting expressions can then be simplified by using the exact solution (I.6.4).

The equation governing the leading behavior of the wavenumber is

$$R^3\Gamma_0 + 2U_1K_0\sigma_0\tilde{x} = \mathcal{O}(\tilde{x}R), \tag{I.6.7}$$

which suggests an asymptotic expansion in powers of $\tilde{x}^{1/3}$. We then assume

$$K \sim K_0 + \alpha\tilde{x}^{\frac{1}{3}} + \alpha_2\tilde{x}^{\frac{2}{3}} + \alpha_3\tilde{x}, \tag{I.6.8}$$

and determine

$$\alpha = \left(-\frac{2K_0\sigma_0U_1}{\Gamma_0}\right)^{\frac{1}{3}} = [-(4770 + 2754\sqrt{3})U_1]^{\frac{1}{3}}, \tag{I.6.9}$$

$$\alpha_2 = \frac{-21 + 13\sqrt{3}}{18}\alpha^2, \qquad \alpha_3 = \frac{33 - 19\sqrt{3}}{18}\alpha^3. \tag{I.6.10}$$

This expansion is asymptotically valid for $|\tilde{x}| \ll 1$.

Substitution of the expansions for $U$ and $K$ into the ray solution (I.4.28), gives the behavior for small $\tilde{x}$, i.e. the inner expansion of the outer ray approximation

$$B^{(\pm)}(\tilde{x}, t_2) = b_\pm(t_2 - \int_{\tilde{x}_\pm}^{\tilde{x}} \frac{\mathrm{d}\tilde{x}}{c_g + U})\sqrt{\frac{K}{\sigma(c_g + U)}} \;\sim$$

$$b_\pm(t_2 - \int_{\tilde{x}_\pm}^{\tilde{x}} \frac{\mathrm{d}\tilde{x}}{c_g + U}) \left\{ \sqrt{6}(7+4\sqrt{3})\alpha^{-1}|\tilde{x}|^{-\frac{1}{3}} + \frac{\sqrt{2}(5+3\sqrt{3})}{12}\,\mathrm{sign}(\tilde{x}) + \mathcal{O}(\tilde{x}^{\frac{1}{3}}) \right\}. \tag{I.6.11}$$

Similar to before, we let indices $-$ and $+$ denote the longer incident wave from $\tilde{x} < 0$ and the shorter transmitted wave to $\tilde{x} > 0$, respectively. We also let $\tilde{x}_\pm$ be the starting points for the time and phase integrals on either side.

From the inhomogeneous Laplace equation at order $\mathcal{O}(\epsilon^2)$, (I.4.16), the dominant $\tilde{x}$-behavior of $B_2^\pm$ near $\tilde{x} = 0$ is

$$A_2^\pm \sim B_2^\pm \sim \mathcal{O}(\tilde{x}^{-4/3}). \tag{I.6.12}$$

Therefore, the surface displacement on either side of the singularity can be expanded as

$$\begin{aligned} \eta^{(\pm)}(\tilde{x}, t_2) \;&=\; (B^{(\pm)} + \epsilon^2 B_2^{(\pm)} + \ldots) \exp\left\{ \mathrm{i}\epsilon^{-2} \left[ \int_{\tilde{x}_\pm}^{\tilde{x}} K\,\mathrm{d}\tilde{x} - t_2 \right] \right\} + \text{c.c.} \\ &\sim\; b_\pm(t_2 - \int_{\tilde{x}_\pm}^{\tilde{x}} \frac{\mathrm{d}\tilde{x}}{c_g + U}) \left\{ \sqrt{6}(7+4\sqrt{3})\alpha^{-1}|\tilde{x}|^{-\frac{1}{3}} + \frac{\sqrt{2}(5+3\sqrt{3})}{12}\,\mathrm{sign}(\tilde{x}) \right\} \\ &\qquad \exp\left\{ \mathrm{i}\epsilon^{-2} \left[ \int_{\tilde{x}_\pm}^{0} K\,\mathrm{d}\tilde{x} + K_0\tilde{x} + \frac{3}{4}\alpha\tilde{x}^{\frac{4}{3}} - t_2 \right] \right\} + \text{c.c.} \end{aligned} \tag{I.6.13}$$

In this outer approximation, the singularity is more severe than for a simple reflection point. Moreover, the second term of the expansion (I.6.13) is non-vanishing as $\tilde{x} \to 0$. Therefore, a satisfactory theory for the triple-root turning point will require at least a two-term expansion, so that the truncation error is asymptotically vanishing.

In this case of a perfect triple root, it can be shown that the two-term inner expansion of the outer ray approximation is valid for $\epsilon^{3/2} \ll |\tilde{x}| \ll 1$. The one-term expansion is valid for a much larger region $\epsilon^2 \ll |\tilde{x}| \ll 1$.

We next proceed to find the inner solution in the neighborhood of the triple turning point, $\tilde{x} = 0$. An envelope equation is anticipated of the form

$$\epsilon^6 \frac{\partial^3 B}{\partial \tilde{x}^3} + c\tilde{x}B = 0, \tag{I.6.14}$$

the corresponding boundary-layer thickness is $\tilde{x} = \mathcal{O}(\epsilon^{3/2})$. Asymptotic evaluation of the energy propagation speed for the ray solution now gives $c_g + U \sim \tilde{x}^{2/3}$. Therefore, a characteristic time for energy to propagate through the inner region is

$$t_2 \sim \int_0^{\epsilon^{3/2}} \frac{\mathrm{d}\tilde{x}}{c_g + U} \sim \mathcal{O}(\epsilon^{1/2}). \tag{I.6.15}$$

If transients are allowed in the inner region, the following boundary-layer coordinates are appropriate

$$\xi = \epsilon^{-3/2}\tilde{x} \qquad \text{and} \qquad \tau = \epsilon^{-1/2}t_2. \tag{I.6.16}$$

The governing equations (I.3.5)–(I.3.8) can be rewritten as follows

$$\epsilon\frac{\partial^2\phi}{\partial\xi^2}+\frac{\partial^2\phi}{\partial z^2}=0 \quad \text{for} \quad -\infty<z<\zeta_0, \tag{I.6.17}$$

$$\frac{\partial\phi}{\partial z}=0 \quad \text{for} \quad z\to-\infty, \tag{I.6.18}$$

$$\epsilon^{\frac{3}{2}}\frac{\partial\eta}{\partial\tau}+\epsilon^{\frac{1}{2}}U_0\frac{\partial\eta}{\partial\xi}+\epsilon^2U_1\xi\frac{\partial\eta}{\partial\xi}-\frac{\partial\phi}{\partial z}-\epsilon^{\frac{3}{2}}\zeta_1\xi\frac{\partial^2\phi}{\partial z^2}=\text{h.o.t.} \quad \text{at} \quad z=\zeta_0, \tag{I.6.19}$$

$$\begin{aligned}&\epsilon^{\frac{3}{2}}\frac{\partial\phi}{\partial\tau}+\epsilon^3\zeta_1\xi\frac{\partial^2\phi}{\partial\tau\partial z}+\eta+\epsilon^{\frac{1}{2}}U_0\frac{\partial\phi}{\partial\xi}+\epsilon^2U_0\zeta_1\xi\frac{\partial^2\phi}{\partial\xi\partial z}\\&+\epsilon^2U_1\xi\frac{\partial\phi}{\partial\xi}-\epsilon\Gamma_0\frac{\partial^2\eta}{\partial\xi^2} \;=\; \text{h.o.t.} \quad \text{at} \quad z=\zeta_0.\end{aligned} \tag{I.6.20}$$

The following WKB expansions are assumed:

$$\left.\begin{aligned}\phi &= (A+\epsilon^{\frac{1}{2}}A_1+\epsilon A_2+\epsilon^{\frac{3}{2}}A_3+\ldots)\exp\{\mathrm{i}(\epsilon^{-\frac{1}{2}}K_0\xi-\epsilon^{-\frac{3}{2}}\tau)\}+\text{c.c.}\\ \eta &= (B+\epsilon^{\frac{1}{2}}B_1+\epsilon B_2+\epsilon^{\frac{3}{2}}B_3+\ldots)\exp\{\mathrm{i}(\epsilon^{-\frac{1}{2}}K_0\xi-\epsilon^{-\frac{3}{2}}\tau)\}+\text{c.c.}\end{aligned}\right\} \tag{I.6.21}$$

The problems at orders $\mathcal{O}(1)$ and $\mathcal{O}(\epsilon^{1/2})$ are identical to the case of a simple reflection point, and therefore the solutions (I.5.26), (I.5.33) and (I.5.34) still hold.

The order $\mathcal{O}(\epsilon)$ problem is

$$\frac{\partial^2A_2}{\partial z^2}-K_0^2A_2=-\frac{\partial^2A}{\partial\xi^2}-2\mathrm{i}K_0\frac{\partial A_1}{\partial\xi} \quad \text{for} \quad -\infty<z<\zeta_0, \tag{I.6.22}$$

$$\frac{\partial A_2}{\partial z}=0 \quad \text{at} \quad z\to-\infty, \tag{I.6.23}$$

$$-\mathrm{i}\sigma_0B_2+U_0\frac{\partial B_1}{\partial\xi}-\frac{\partial A_2}{\partial z}=0 \quad \text{at} \quad z=\zeta_0, \tag{I.6.24}$$

$$-\mathrm{i}\sigma_0A_2+U_0\frac{\partial A_1}{\partial\xi}+B_2-\Gamma_0\frac{\partial^2B}{\partial\xi^2}-2\mathrm{i}\Gamma_0K_0\frac{\partial B_1}{\partial\xi}+\Gamma_0K_0^2B_2=0 \quad \text{at} \quad z=\zeta_0. \tag{I.6.25}$$

The last two equations can be combined to eliminate $B_2$, and the lower-order results can further be used to eliminate $A$, $A_1$ and $B_1$. After we make use of the exact values of $K_0$, $\Gamma_0$, $U_0$ and $\sigma_0$, we arrive at the following surface condition

$$\frac{\partial A_2}{\partial z}-K_0A_2=0. \tag{I.6.26}$$

The solvability condition can again be shown to be identically satisfied. The particular solution at this order can be summarized as

$$A_2=\frac{\mathrm{i}\sigma_0}{2K_0}(z-\zeta_0)^2\frac{\partial^2B}{\partial\xi^2}\mathrm{e}^{K_0(z-\zeta_0)}, \tag{I.6.27}$$

$$B_2 = -\left(\frac{U_0}{K_0\sigma_0} + \frac{U_0^2}{\sigma_0^2}\right)\frac{\partial^2 B}{\partial \xi^2}. \tag{I.6.28}$$

The problem at order $\mathcal{O}(\epsilon^{3/2})$ is

$$\frac{\partial^2 A_3}{\partial z^2} - K_0^2 A_3 = -\frac{\partial^2 A_1}{\partial \xi^2} - 2\mathrm{i}K_0\frac{\partial A_2}{\partial \xi} \quad \text{for} \quad -\infty < z < \zeta_0, \tag{I.6.29}$$

$$\frac{\partial A_3}{\partial z} = 0 \quad \text{at} \quad z \to -\infty, \tag{I.6.30}$$

$$\frac{\partial B}{\partial \tau} - \mathrm{i}\sigma_0 B_3 + U_0\frac{\partial B_2}{\partial \xi} + \mathrm{i}K_0 U_1 \xi B - \frac{\partial A_3}{\partial z} - \zeta_1 \xi \frac{\partial^2 A}{\partial z^2} = 0 \quad \text{at} \quad z = \zeta_0, \tag{I.6.31}$$

$$\begin{aligned}\frac{\partial A}{\partial \tau} - \mathrm{i}\sigma_0 A_3 + U_0\frac{\partial A_2}{\partial \xi} + B_3 - \Gamma_0\frac{\partial^2 B_1}{\partial \xi^2} - 2\mathrm{i}\Gamma_0 K_0\frac{\partial B_2}{\partial \xi} \\ + \Gamma_0 K_0^2 B_3 + \mathrm{i}K_0 U_1 \xi A - \mathrm{i}\sigma_0\zeta_1\xi\frac{\partial A}{\partial z} = 0 \quad \text{at} \quad z = \zeta_0.\end{aligned} \tag{I.6.32}$$

If the last two equations are combined to eliminate $B_3$, and the lower-order results are used to eliminate $A$, $A_1$, $A_2$, $B_1$ and $B_2$, we get the surface condition

$$\frac{\partial A_3}{\partial z} - K_0 A_3 = 2\frac{\partial B}{\partial \tau} - \frac{\Gamma_0}{\sigma_0}\frac{\partial^3 B}{\partial \xi^3} + 2\mathrm{i}K_0 U_1 \xi B. \tag{I.6.33}$$

The solvability condition gives the following third-order partial differential equation governing the complex envelope $B$,

$$\frac{\partial B}{\partial \tau} - \frac{\Gamma_0}{2\sigma_0}\frac{\partial^3 B}{\partial \xi^3} + \mathrm{i}K_0 U_1 \xi B = 0. \tag{I.6.34}$$

Employing the theory of averaged Lagrangian and including nonlinearities, Peregrine & Smith (1979) deduced formally a similar equation with a cubic nonlinearity. However, they did not work out the coefficients explicitly, and hence did not examine the physical implications in detail.

For a slowly modulated incident wave packet, described near the end of section I.4, the timescale of interest is $t_2 = \mathcal{O}(1)$ which is much longer than that of the characteristic time of the inner region defined by (I.6.16b). It is seen that if the modulation timescale is $t_2$ or slower in (I.6.34), the inner region is approximately stationary. Consequently, the stationary limit of equation (I.6.34) reduces to the following Pearcey differential equation for the amplitude $B$,

$$\frac{\partial^3 B}{\partial \xi^3} - \frac{2\mathrm{i}K_0\sigma_0 U_1}{\Gamma_0}\xi B = 0. \tag{I.6.35}$$

The solution of this equation is a special case of the Pearcey function. With reference

to appendix I.B, the solution which is bounded as $\xi \to \pm\infty$ is

$$B(\xi, t_2) = b_0(t_2)P(Y), \tag{I.6.36}$$

where $P(Y)$ denotes the Pearcey function defined by (I.B.5) in the appendix. Here, $Y$ is the complex argument

$$Y = \sqrt{2}\alpha^{\frac{3}{4}}\mathrm{e}^{-\frac{\pi\mathrm{i}}{8}}\xi, \tag{I.6.37}$$

and $\alpha$ is the coefficient in the wavenumber expansion (I.6.9). For the sake of convenience, we give in appendix I.B approximations for large $\xi$, which can be found in Paris (1991).

The solutions for $B_1$ and $B_2$ are now given by

$$\begin{aligned} B_1 &= -\mathrm{i}\left[\frac{1}{K_0} + \frac{U_0}{\sigma_0}\right]\frac{\partial B}{\partial \xi} + \text{homogeneous solution} \\ &= \mathrm{i}b_0(t_2)\left[\frac{1}{K_0} + \frac{U_0}{\sigma_0}\right]\sqrt{2}\alpha^{\frac{3}{4}}\mathrm{e}^{-\frac{\pi\mathrm{i}}{8}}\frac{\partial P(Y)}{\partial Y} + b_1(t_2)P(Y) \end{aligned} \tag{I.6.38}$$

and

$$B_2(\xi, t_2) \sim \frac{\partial^2 P(Y)}{\partial Y^2} \sim \mathcal{O}(\xi^{\frac{1}{3}}), \tag{I.6.39}$$

confer (I.5.34) and (I.6.28). To simplify the notation, we shall recombine the arbitrary complex constants as follows,

$$c_0 = b_0 + \epsilon^{\frac{1}{2}}b_1 \qquad \text{and} \qquad c_1 = -\mathrm{i}b_0\left[\frac{1}{K_0} + \frac{U_0}{\sigma_0}\right]\sqrt{2}\alpha^{\frac{3}{4}}\mathrm{e}^{-\frac{\pi\mathrm{i}}{8}}, \tag{I.6.40}$$

which must be determined by asymptotic matching. Afterward, the surface displacement $\eta$ becomes

$$\begin{aligned} \eta(\xi, t_2) &= [B + \epsilon^{\frac{1}{2}}B_1 + \epsilon B_2 + \ldots]\mathrm{e}^{\mathrm{i}\epsilon^{-\frac{1}{2}}K_0\xi - \mathrm{i}t} + \text{c.c.} \\ &\sim \left[c_0(t_2)P(Y) + \epsilon^{\frac{1}{2}}c_1(t_2)\frac{\partial P(Y)}{\partial Y} + \mathcal{O}(\epsilon\xi^{\frac{1}{3}})\right]\mathrm{e}^{\mathrm{i}\epsilon^{-\frac{1}{2}}K_0\xi - \mathrm{i}t} + \text{c.c.} \end{aligned} \tag{I.6.41}$$

We now need the large-argument expansion ($\xi \to \pm\infty$) of the inner surface displacement approximation. With reference to appendix I.B, we note that for $|\arg Y| < 3\pi/8$, the Pearcey function takes the form

$$P(Y) = P_0(Y) + P_1(Y), \tag{I.6.42}$$

where $P_0$ is algebraically decaying in $\xi$ and $P_1$ is exponentially decaying in $\xi$. Hence for purposes of asymptotic matching, we need only consider $P_0$, whose large $\xi$ expansion is

$$P_0(Y) \sim \sqrt{\frac{\pi}{3}}\mathrm{e}^{-\frac{\pi\mathrm{i}}{8}}\exp\left(\frac{3}{4}\mathrm{i}\alpha\xi^{\frac{4}{3}}\right)\left\{\alpha^{-\frac{1}{4}}|\xi|^{-\frac{1}{3}} + \mathcal{O}(\xi^{-\frac{5}{3}})\right\}. \tag{I.6.43}$$

Correspondingly, the asymptotic behavior for $\eta$, here expressed in terms of the

outer variable $\tilde{x}$, is

$$\eta(\tilde{x},t_2) \sim \left[c_0(t_2)\sqrt{\frac{\pi\epsilon}{3}}\mathrm{e}^{-\frac{\pi\mathrm{i}}{8}}\alpha^{-\frac{1}{4}}|\tilde{x}|^{-\frac{1}{3}} + c_1(t_2)\sqrt{\frac{\pi\epsilon}{6}}\mathrm{i}\,\mathrm{sign}(\tilde{x}) + \mathcal{O}(\epsilon^{\frac{1}{2}}\tilde{x}^{\frac{1}{3}})\right] \exp\left\{\mathrm{i}\epsilon^{-2}(K_0\tilde{x} + \frac{3}{4}\alpha\tilde{x}^{\frac{4}{3}})\right\}. \quad \text{(I.6.44)}$$

When this outer expansion of the inner solution is compared with the inner expansion of the outer solution (I.6.13), it is clear that both the amplitude and the phase match to two significant terms.

From (I.6.43) we see that higher-order terms from $B$ are $\mathcal{O}(\epsilon^{5/2}\tilde{x}^{-5/3})$, higher-order terms from $B_1$ are $\mathcal{O}(\epsilon^{5/2}\tilde{x}^{-4/3})$, while terms from $B_2$ are $\mathcal{O}(\epsilon^{1/2}\tilde{x}^{1/3})$. From this it follows that the one-term asymptotic form is valid for $\epsilon^{\frac{3}{2}} \ll |\tilde{x}| \ll 1$, and the two term asymptotic form is valid for $\epsilon^{\frac{6}{5}} \ll |\tilde{x}| \ll 1$.

The inner and outer solutions have an overlapping region of validity for their respective asymptotic expansions. The matching region for a one-term match is $\epsilon^{\frac{3}{2}} \ll |\tilde{x}| \ll 1$, and for a two-term match $\epsilon^{\frac{6}{5}} \ll |\tilde{x}| \ll 1$. Higher-order asymptotic matching is seen to give a smaller matching region, as is usually expected.

Similarly to the case of a simple reflection-point, we fix the time-dependent coefficients of the ray solution, (I.6.13), at the time when the ray reaches the triple-root point. We can do this because the relative error introduced is small, less than the accuracy of the asymptotic match. Hence the time and phase integrals in equation (I.6.13) are to be evaluated with the upper limit set to $\tilde{x} = 0$. Asymptotic matching now gives $c_0(t_2)$, $c_1(t_2)$ and $b_+(t_2)$ in terms of the incident wave $b_-(t_2)$ as follows

$$c_0(t_2) = b_-(t_2 - \int_{\tilde{x}_-}^0 \frac{\mathrm{d}\tilde{x}}{c_g+U})\frac{\sqrt{2}(21+12\sqrt{3})}{\sqrt{\pi\epsilon}}\alpha^{-\frac{3}{4}}\exp\left\{\mathrm{i}\epsilon^{-2}\int_{\tilde{x}_-}^0 K\,\mathrm{d}\tilde{x} + \frac{\pi\mathrm{i}}{8}\right\}, \quad \text{(I.6.45)}$$

$$c_1(t_2) = b_-(t_2 - \int_{\tilde{x}_-}^0 \frac{\mathrm{d}\tilde{x}}{c_g+U})\frac{9+5\sqrt{3}}{6\sqrt{\pi\epsilon}}\exp\left\{\mathrm{i}\epsilon^{-2}\int_{\tilde{x}_-}^0 K\,\mathrm{d}\tilde{x} - \frac{\pi\mathrm{i}}{2}\right\} \quad \text{(I.6.46)}$$

and

$$b_+(t_2 - \int_{\tilde{x}_+}^0 \frac{\mathrm{d}\tilde{x}}{c_g+U}) = b_-(t_2 - \int_{\tilde{x}_-}^0 \frac{\mathrm{d}\tilde{x}}{c_g+U})\exp\left\{\mathrm{i}\epsilon^{-2}\int_{\tilde{x}_-}^{\tilde{x}_+} K\,\mathrm{d}\tilde{x}\right\}. \quad \text{(I.6.47)}$$

We note that both coefficients for the inner solution have the same order in $\epsilon$, this indicates that the matching is consistent with respect to the ordering parameter.

In summary, the outer solutions in regions I and III, depicted in figure I-7, are still given by (I.6.13), and the inner solution which can now be thought of as covering all of regions II, IV and V, is given by (I.6.41) where the coefficients are given by (I.6.45)–(I.6.47).

Numerical results will be presented in section I.8.

For a successful asymptotic matching, we need to consider a minimum of two terms in the inner approximation (I.6.21). The relative difference between consecutive terms in (I.6.21) is only $\mathcal{O}(\epsilon^{\frac{1}{2}})$. Therefore, the approximation that the inner region is

stationary requires that the modulation time of the incoming wave packet is strictly slower than $t_2$. To reduce the truncation error at and near the triple-root turning point, it would be desirable to include one more term, $A_2, B_2 \propto P''(Y)$. This is a very lengthy task. On the other hand, keeping the leading-order term in the outer approximation implies a much smaller error of $\mathcal{O}(\epsilon^2)$.

If the triple-root conditions are not exactly met, a theory that accounts for slight detuning is needed. This theory is less attractive since the mathematical complexity increases enormously. In Appendix I.A we present a derivation of the inner solution only, which turns out to be given in terms of the general Pearcey function of two parameters.

## I.7 Remarks on existing experiments

Pokazeyev & Rozenberg (1983) performed experiments for wave packets on co-flowing and counter-flowing currents over a sloping bottom in a wave tank. The wave packets typically contained 3 to 10 oscillations with the central frequency 2–11 Hz. The adverse current varied from 0.04 m/s at the deep end to 0.2 m/s at the shallow end of a slope of length 0.8 m. From figure (5.c) in their paper, the current varied linearly with distance along the tank. Most of the cases discussed in their paper are for frequencies too high (greater than 2.4 Hz) for double reflection. Detailed time series records were not reported; amplitude plots were presented as if the wave trains were uniform. Only one case, with frequency 2 Hz, corresponds to double reflection. However, for this frequency only one or two amplitude measurements were recorded between the two reflection points, which are separated by 6 cm, as can be estimated from figure I-6. This lack of information precludes a meaningful comparison with our theory.

In a subsequent paper, Badulin, Pokazeyev & Rozenberg (1983) performed wave packet experiments for lower frequencies 1.5–3 Hz with a view to observing double reflection. The current velocity varied over the range 0.04–0.25 m/s, but now over a slope of length 1.6 m. Amplitude data were presented schematically as a continuous function of the horizontal distance for one frequency only (2 Hz). According to their description, the data were recorded for every 2.5 cm. For the given current gradient, the distance between the reflection points is about 12 cm, which implies that there were 4 or 5 measurements in this region. However, without the knowledge of the time and positions of the measurements in the relatively narrow region where modulation is strong, a comparison with our theory cannot be made.

The parameter $\epsilon = (\bar{k}L)^{-1/2}$ can be estimated for the two experiments as follows: For the two slope lengths 0.8 m and 1.6 m, the current gradient can be estimated at $\partial U/\partial x = 0.2\ \mathrm{s}^{-1}$, $0.1\ \mathrm{s}^{-1}$. Defining the long length scale of the current by

$$\frac{1}{L} = \frac{1}{U_{\mathrm{ave}}}\frac{\partial U}{\partial x}, \tag{I.7.1}$$

where $U_{\mathrm{ave}}$ is the average current over the slope, we estimate $L = 0.6$ m and 1.2 m, respectively. It follows from (I.2.3) that for $\omega/2\pi = 2$ Hz, $\epsilon = 0.32$ and 0.23,

respectively.

Viscous damping is also important in these experiments. Pokazeyev & Rozenberg (1983) measured the amplitude attenuation rates in still water and uniform currents, and found the actual damping rate to be 2–3 times that of a semi-theoretical model combining viscous dissipation in the interior of the fluid, boundary layer dissipation and losses near the free surface which was assumed to behave as an inextensible film.

For pure gravity waves on a non-uniform current Lai, Long & Huang (1989) performed similar experiments by focusing attention on the kinematics only. They confirmed the dispersion relation and the implied reflection, but no measurements on amplitude modulation were reported.

Clearly, a meaningful comparison between experiments and theory awaits more detailed measurements of amplitude and proper accounts of damping, detuning and possibly nonlinearity.

## I.8 Numerical results for wave packets

We now describe the time evolution of wave packets with two different central frequencies, one lower than and one equal to the frequency for the perfect triple-root turning point.

For $\omega/2\pi = 1.9$ Hz, far lower than the triple-root frequency (2.4 Hz), there are two reflection points. The distance between them depends on the current gradient, which is chosen to be a constant small enough so that the reflection points are sufficiently far apart to be treated independently of each other.

In all the plots, the peak amplitude at the left edge of the figure is normalized to unity. The locations of the turning points are indicated by vertical lines. In order to suggest possible experiments, the abscissas are labelled by the position in meters.

### I.8.1 Case 1: Large separation between reflection points.

Referring to figures I-8 and I-9, which cover the entire horizontal extent of the sloping bottom, the current velocity at the left edge is $-0.19$ m/s and at the right edge $-0.22$ m/s. We assume the current gradient to be constant $\partial U/\partial x = -0.0075$ s$^{-1}$ over a slope of 4 m length. The length $L$ of normalization should be about $L = 27$ m, calculated according to (I.7.1). This gives the dimensionless parameters $\epsilon = 0.050$ and $\Gamma = 0.0016$. Recall that the dimensionless parameter $\epsilon$ was defined as the ratio of the wavelength of a pure gravity wave of the given frequency on still water, to the current length scale $L$. Since the wavelength in the zone of reflections is always shorter than that of the pure gravity wave, the local ratio between the short and long scales is never larger than the one given above. The boundary condition at the left edge of each snapshot is (in non-dimensional variables)

$$\eta(t_2) = \exp\{-r(t_2 - \mathcal{T})^2 - \mathrm{i}\epsilon^{-2}(t_2 - \mathcal{T})\}, \tag{I.8.1}$$

where $r = 0.5$. Starting with $\mathcal{T} = 0$, the time interval between each snapshot is $\Delta\mathcal{T} = 1.2$. Alternatively, in physical coordinates,

$$\eta(t^*) = \exp\{-r^*(t^* - \mathcal{T}^*)^2 - \mathrm{i}\omega(t^* - \mathcal{T}^*)\}, \tag{I.8.2}$$

where $r^* \approx 4.5 \cdot 10^{-4}$ s$^{-2}$ and $\mathcal{T}^*$ increases in steps of about 40 s.

To estimate crudely the effect of viscous damping, we introduce in the ray solutions the theoretical value accounting for internal dissipation only. Specifically, we use the model of Shyu & Phillips (1991),

$$\frac{\partial}{\partial t_2}\left(\frac{E}{\sigma}\right) + \frac{\partial}{\partial x_2}\left((c_g + U)\frac{E}{\sigma}\right) = -\chi K^2 \frac{E}{\sigma}, \tag{I.8.3}$$

where $\chi = 4\epsilon^{-2}\nu\omega^3/g^2$ is a dimensionless parameter. In the present case, this parameter is $\chi = 0.028$.

We first show the development without damping in figure I-8. The drastic reduction of wavelength after the second reflection is evident. In figure I-9 damping is introduced for the ray solutions away from the reflection points. Since the distance between the reflection points is large, the short gravity wave reflected from the first reflection point is completely damped out before it reaches the second reflection point.

Corresponding to figures I-8 and I-9, we plot in figure I-10 the trajectory of the envelope peak as a function of time, according to the characteristic curve for the ray solution given by equation (I.4.27). We have labelled the abscissa in meters in accordance with the other figures, while the ordinate shows the elapsed time in seconds. It is evident that despite the reduction of wavelength the speed of the envelope remains relatively unchanged.

If the characteristic time for viscous damping is calculated at the two reflection points as $\tau = 1/(\nu k^2)$, we find $\tau \approx 250$ s at the (first) gravity reflection point and $\tau \approx 18$ s at the (second) capillary reflection point. We now calculate the characteristic time, according to the ray theory, for the center of the wave packet to propagate through the inner regions. This is done by measuring on figure I-10 the time it takes to pass through the inner region corresponding to setting the inner variable $\xi = \mathcal{O}(1)$. Let $U_0$ and $k_0$ be the local values for the current and wavenumber at the reflection point. Then $L_0 = U_0/(\partial U/\partial x)$ and $\epsilon_0 = 1/\sqrt{k_0 L_0}$ are the local values for the long length scale and the ordering parameter. According to (I.5.16), the thickness of the inner region should then be $\Delta x = 1/(\epsilon_0^{2/3} k_0) = k_0^{-2/3} L_0^{1/3}$. The characteristic times of propagation through the inner regions should therefore be 55 s at the gravity reflection point and 35 s at the capillary reflection point. Hence damping in the inner region of the gravity reflection point should be negligible as assumed, but considerable at the capillary reflection point. In this case, however, the capillary wave is completely damped out before it even reaches the capillary reflection point, the error by not accounting for dissipation in the second boundary layer is immaterial.

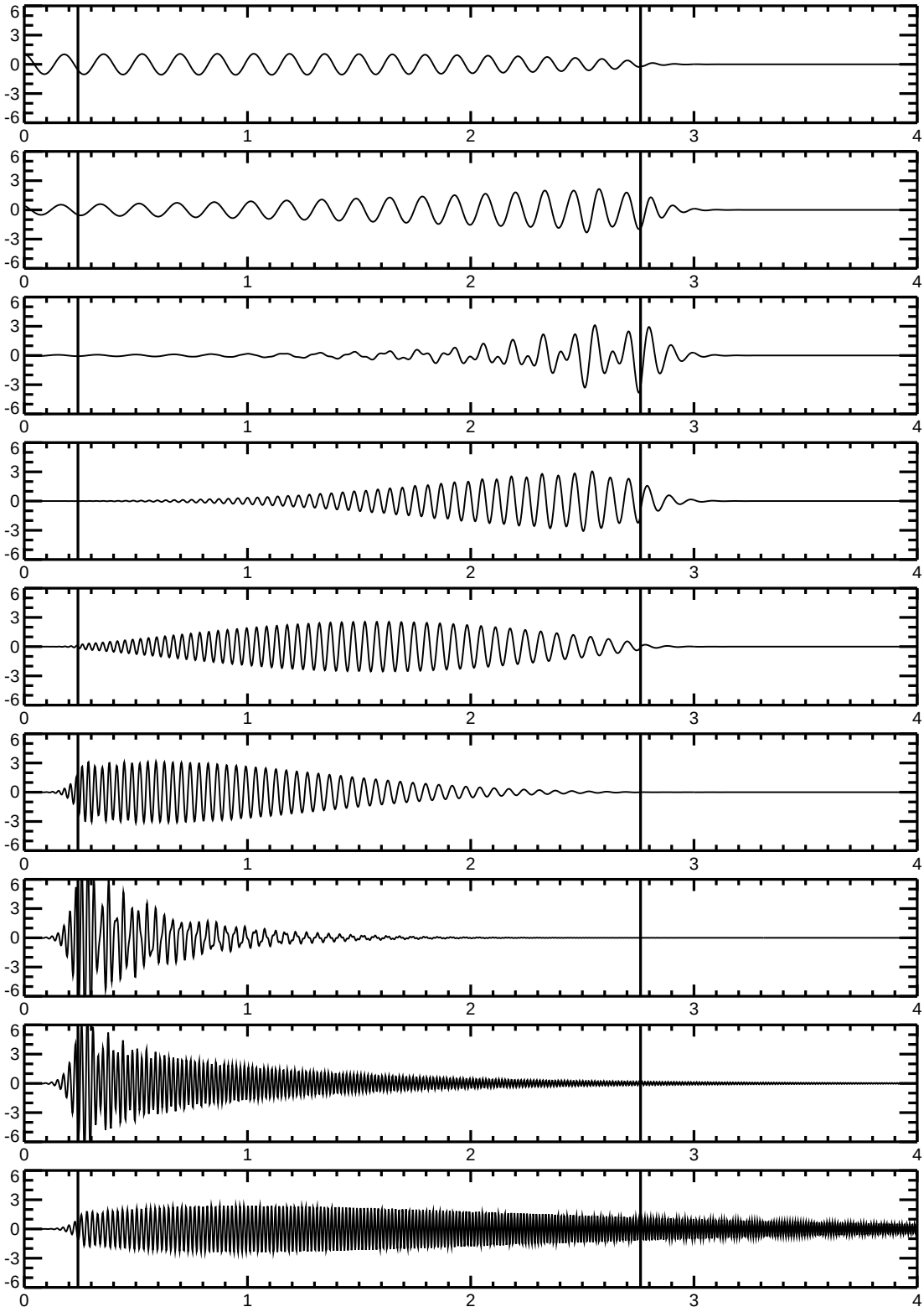


Figure I-8: Well separated reflection points, frequency 1.9 Hz, current gradient $-0.0075$ s$^{-1}$, no damping. The abscissa shows the position in meters, the ordinate shows normalized amplitude relative to peak unit amplitude at the left edge.

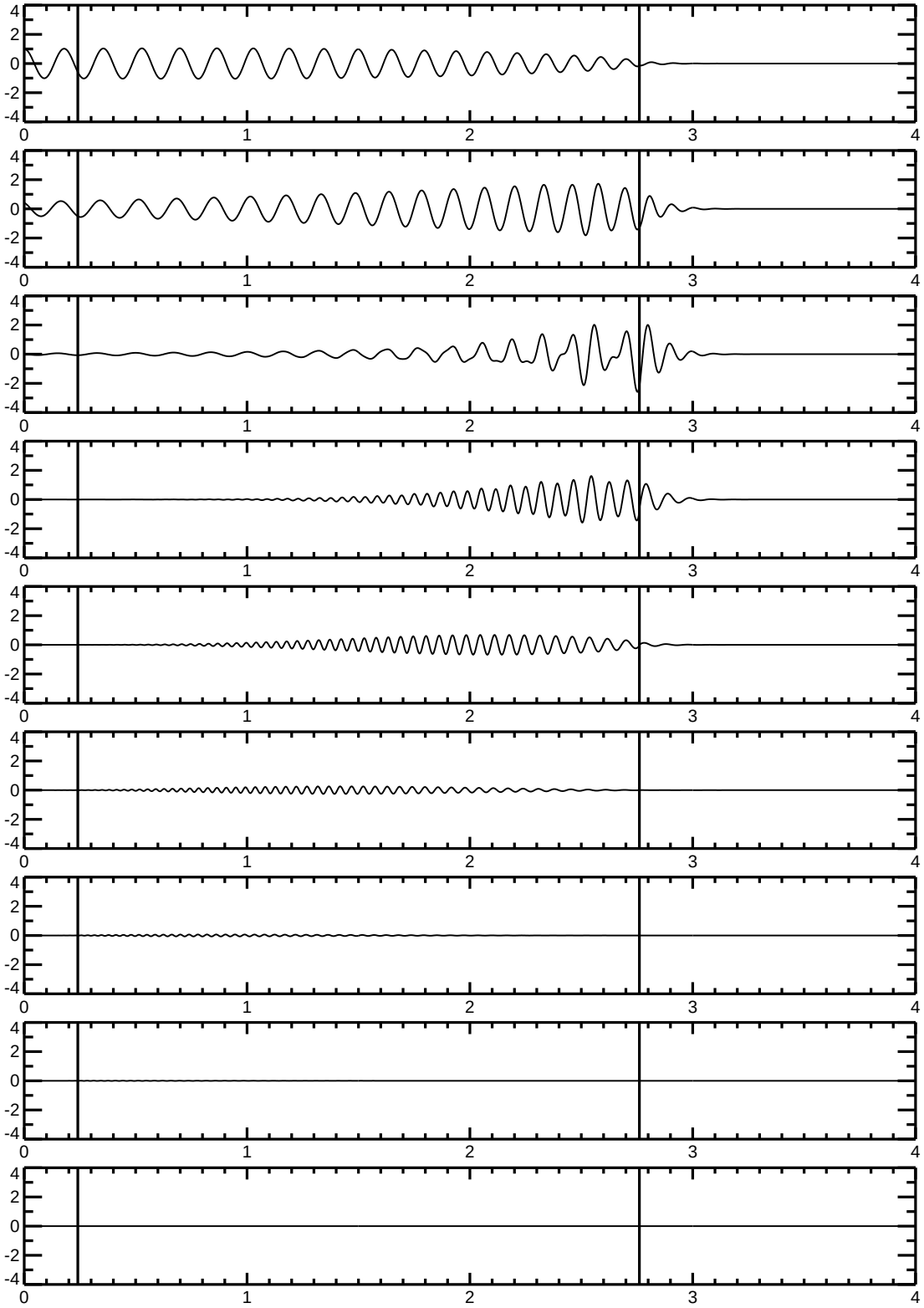


Figure I-9: Well separated reflection points, frequency 1.9 Hz, current gradient $-0.0075$ s$^{-1}$. Waves away from the reflection points are damped.

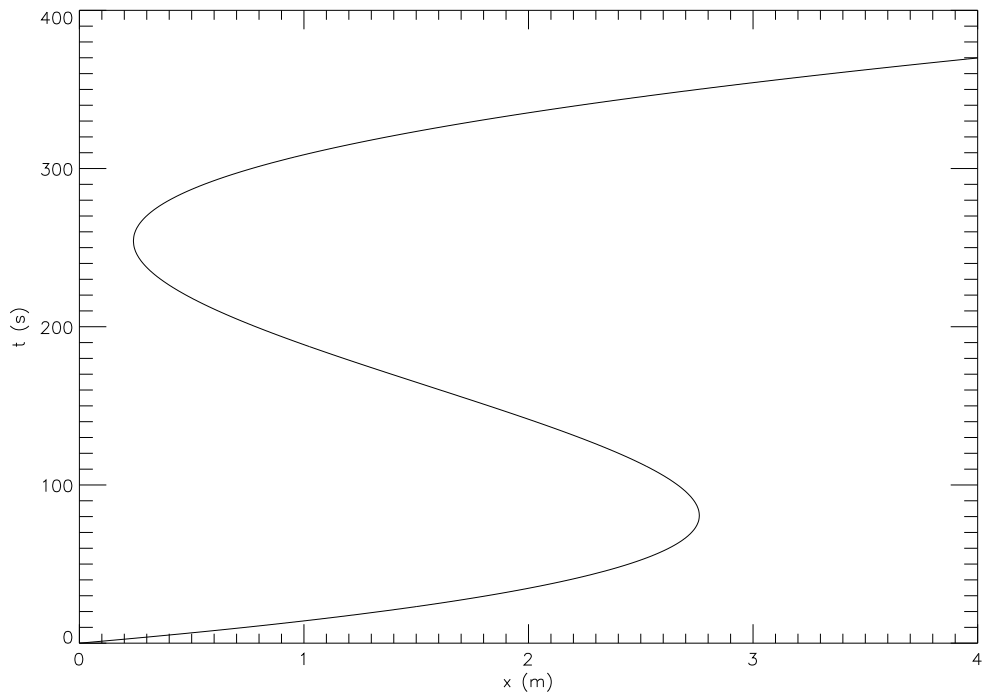


Figure I-10: The trajectory of the envelope peak, frequency 1.9 Hz, current gradient $-0.0075$ s$^{-1}$. The abscissa shows the position in meters, the ordinate shows the elapsed time in seconds.

### I.8.2 Case 2: Moderate separation between two reflection points.

In figures I-11–I-13 we keep the frequency 1.9 Hz and the horizontal length of the slope at 4 m, but change the current velocity at the left edge to $-0.13$ m/s and at the right edge to $-0.26$ m/s. The current gradient is now $-0.033$ s$^{-1}$. This gives the dimensionless parameters $\epsilon = 0.11$ and $\Gamma = 0.0016$. The boundary condition at the left edge of each snapshot is given by equations (I.8.1) and (I.8.2), where $r = 0.15$. Starting with $\mathcal{T} = 0$, the time interval between each consecutive snapshot is $\Delta\mathcal{T} = 1.6$. In physical variables, $r^* \approx 3.1 \cdot 10^{-3}$ s$^{-2}$ and the time interval between each snapshot is approximately 11 s.

Damping is added to the ray solutions in the same way as in case 1, which gives the same damping parameter $\chi$. Because of the reduced separation, the wave packet goes through the second reflection point before it is damped out, as is apparent from figure I-12.

We also trace the peak of the envelope as a function of time in figure I-13. After the first reflection, the envelope slows down considerably before being reflected the second time. We note that the characteristic times for viscous damping at the two reflection points are the same as in the previous case. However the times for propagation through the reflection point boundary layers are now 20 s and 12 s, respectively. The effect of damping is now negligible at the (first) gravity reflection point, while it is significant but not of dominating importance at the capillary reflection point.

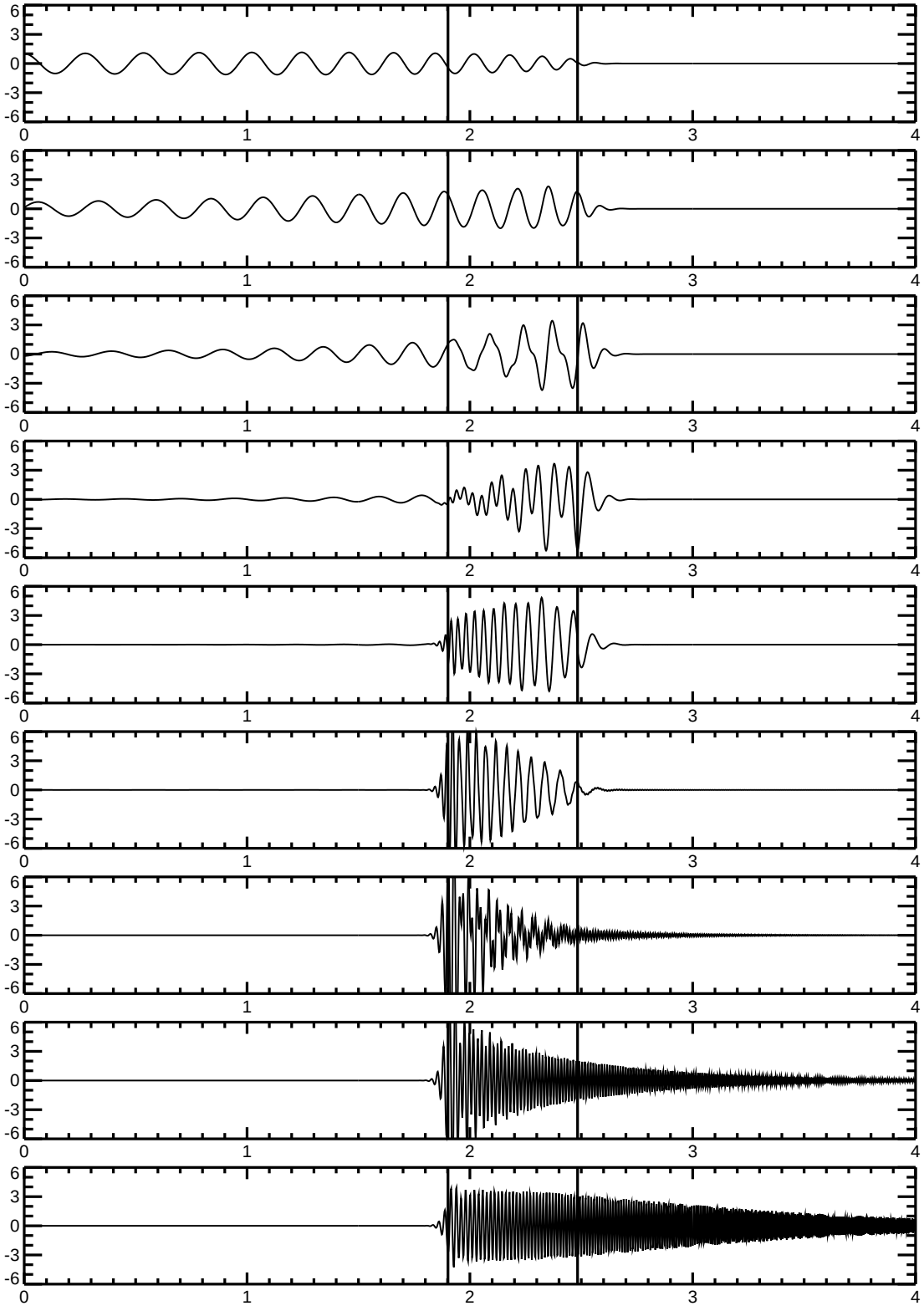


Figure I-11: Double reflection with frequency 1.9 Hz and current gradient $-0.033\ \mathrm{s}^{-1}$. No damping.

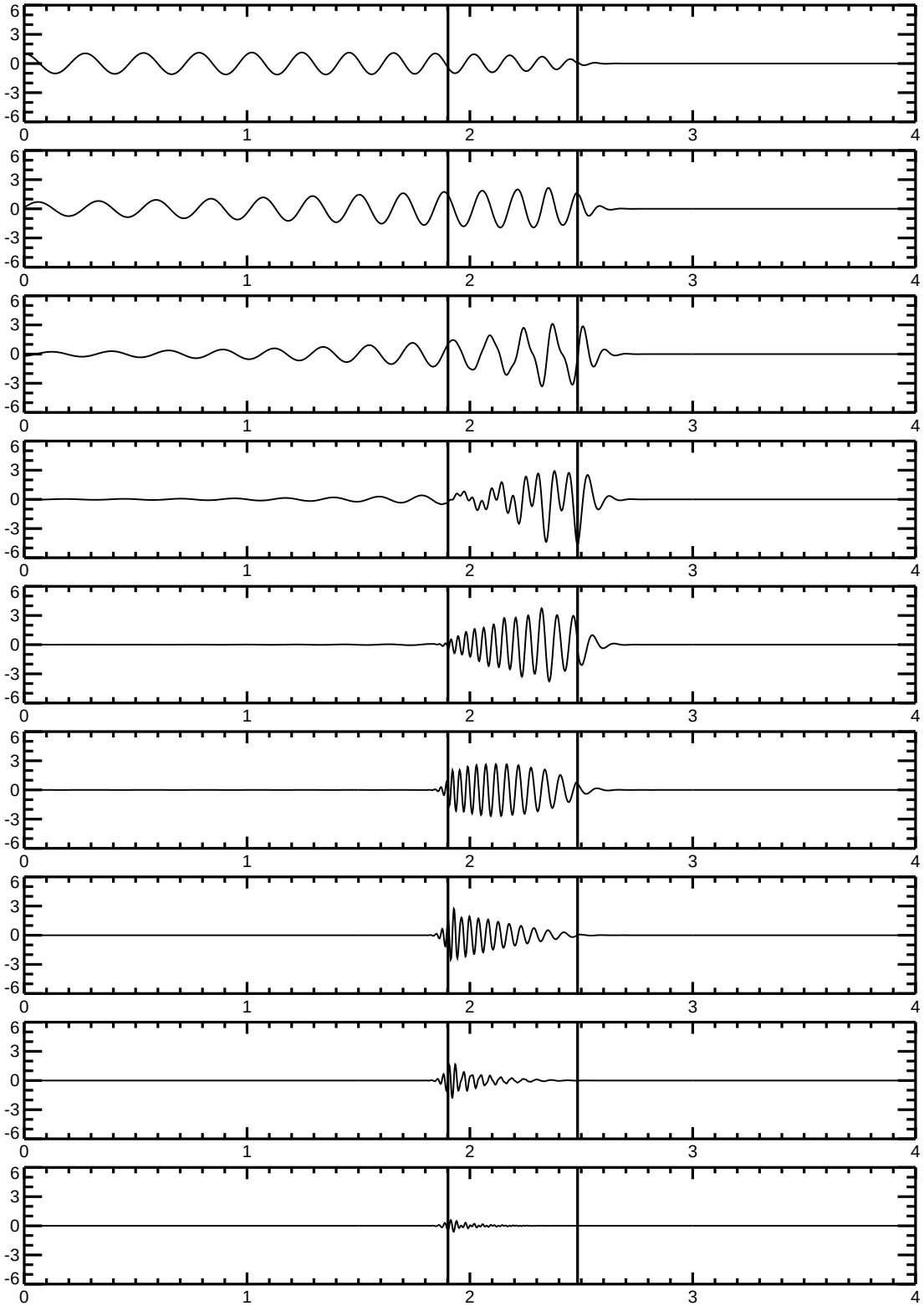


Figure I-12: Double reflection with frequency 1.9 Hz and current gradient $-0.033\ \mathrm{s}^{-1}$. Waves away from the reflection points are damped.

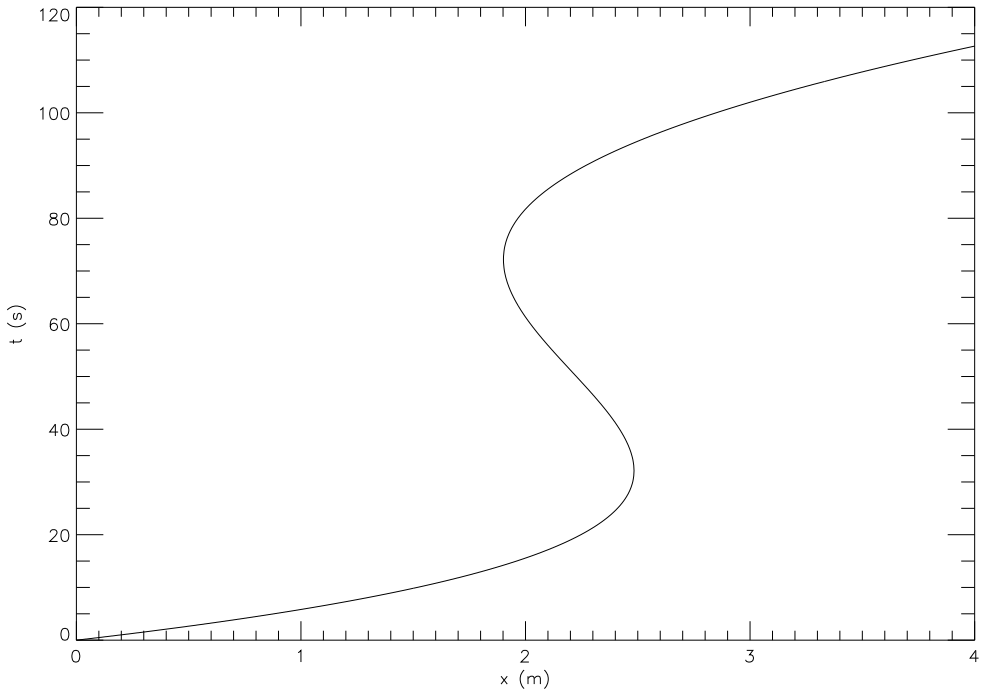

Figure I-13: The trajectory of the envelope peak for frequency 1.9 Hz and current gradient $-0.033$ s$^{-1}$.

### I.8.3 Case 3: Coalescing reflection points (triple-root turning point).

In this example, a wave packet with the perfect triple-root turning point frequency (about 2.35 Hz) is considered, as shown in figure I-14, here without viscous damping. We have used a linear current flowing from right to left, with the current velocity at the left edge being $-0.15$ m/s and at the right edge $-0.21$ m/s. The horizontal length across the figure is 3 m. The current gradient is $-0.02$ s$^{-1}$, and the long length scale should be about $L = 9$ m. This gives the dimensionless parameters $\epsilon = 0.071$ and $\Gamma = 0.0037$. The boundary condition at the left edge for consecutive snapshots is given by equations (I.8.1)–(I.8.2), where $r = 0.08$. It is important to notice that since $r \ll 1$, we are satisfying the condition that the modulation time of the incoming wave packet is slower than $t_2$, and therefore the quasi-stationary theory of section I.6 is valid. Starting with $\mathcal{T} = -2.8$, the time interval between consecutive snapshots is $\Delta\mathcal{T} = 1.4$. In physical coordinates, this corresponds to $r^* \approx 4.4 \cdot 10^{-4}$ s$^{-2}$ and the time between consecutive snapshots is approximately 19 s.

As in the case of double reflection, the long incident gravity wave and the short transmitted capillary wave have speeds comparable to each other. However, it takes a considerable time for the wave packet to go through the turning point. The trajectory of the peak of the wave packet shown in figure I-16 shows that the wave packet comes almost to a standstill near the turning point. In physical units, the time spent in the inner region can be estimated at about 36 s, by using the inner scaling law (I.6.16) as before.

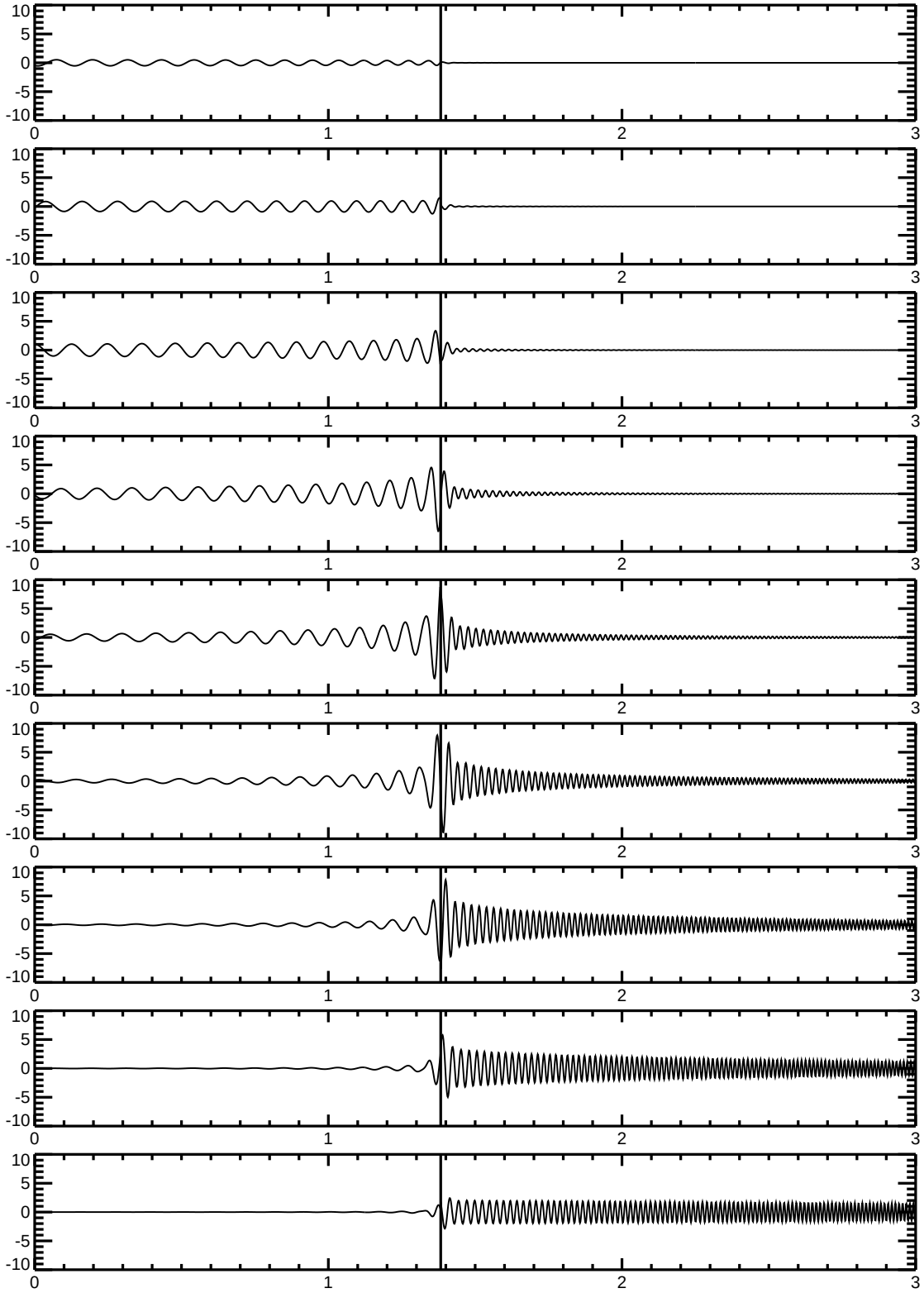


Figure I-14: The perfect triple-root turning point with current gradient $-0.02$ s$^{-1}$. No damping.

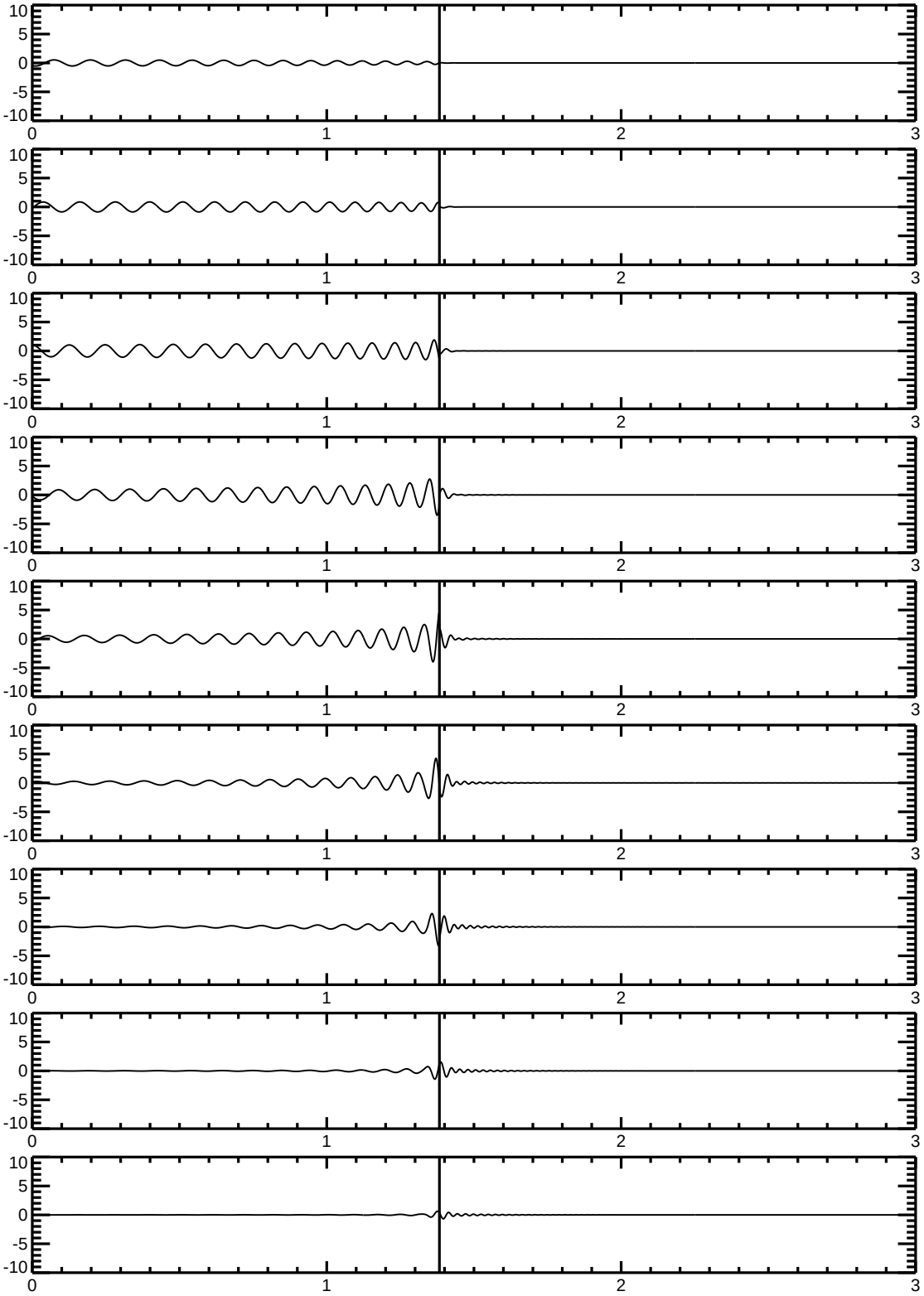


Figure I-15: The perfect triple-root turning point with current gradient $-0.02$ s$^{-1}$. Waves away from the turning point are damped.

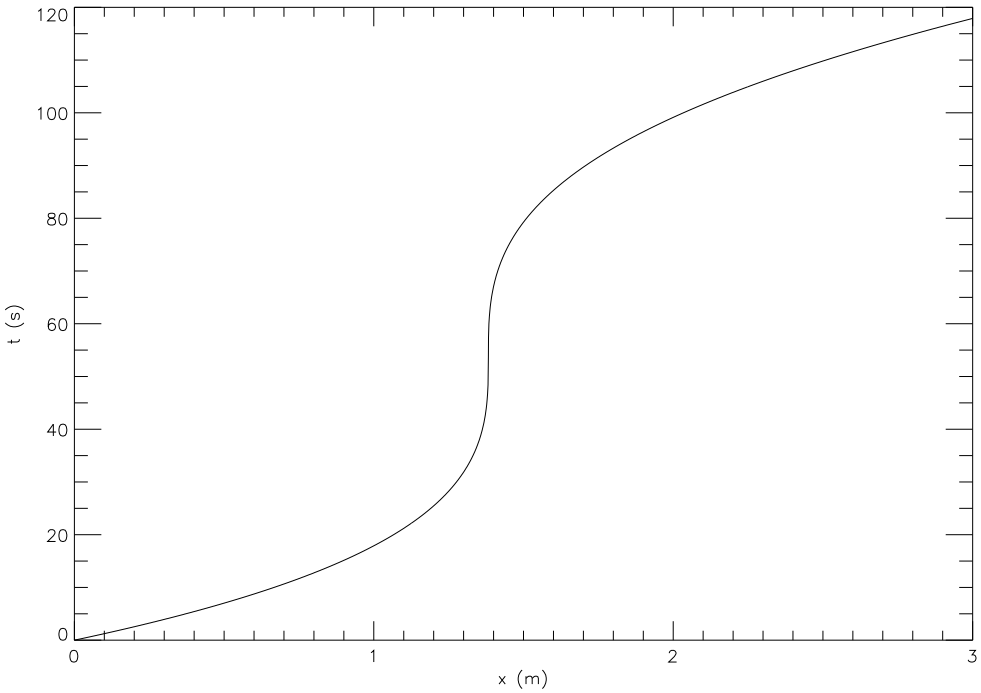

Figure I-16: The trajectory of the envelope peak for the perfect triple-root turning point with current gradient $-0.02$ s$^{-1}$.

The characteristic time for viscous damping at the triple-root point can be estimated at about 48 s. In this case, viscous damping effects should be considerable in the boundary layer. However the theory for damping is difficult here since the region is small and the spatial variation of the wavelength is fast. With these reservations, we present in figure I-15 the results with damping imposed only to waves away from the turning point. Even with this partial account of dissipation, waves are effectively annihilated near the triple-root point.

# I.9 Conclusions

We have developed a linearized theory of waves propagating on an opposing current of increasing strength. Attention is focused on the effect of capillarity which makes it possible for repeated reflection. This process enhances the role of dissipation by viscosity, which can damp out the waves completely without breaking. For a wave train of a given frequency, an increase of the current gradient narrows the region between the two reflection points. It is found that as the region gets narrower the wave packet remains relatively longer within that region.

For comparison with future experiments, it may be desirable to include higher order terms to allow moderate values of $\epsilon$. In addition, nonlinear and viscous effects deserve future attention. The role of nonlinearity may be treated by pursuing further the physical implications of the cubic Schrödinger equations derived in form by Peregrine & Smith (1979). Since the zone of a simple reflection point or a triple-root

turning point is a thin boundary layer where the wavelength varies relatively rapidly, the treatment of viscosity is not trivial. In view of the present study, the effects of viscosity may also be of overwhelming importance.

# I.A Solution near a detuned triple-root turning point

When the conditions for the existence of a triple root for the wavenumber are not exactly satisfied, a theory that accounts for slight detuning is called for. We limit our discussion to a derivation of the inner solution, and show how the first and second parameters of the Pearcey function naturally relate to detuning and horizontal position, respectively.

It is most natural to fix the normalization frequency at the perfect triple-root frequency $\bar{\omega} = \omega_0$. The normalized frequency $\Omega = \omega/\omega_0$ should therefore be close to unity. The dispersion relation (I.4.14) now generalizes to

$$\Omega - KU = \sqrt{K + \Gamma_0 K^3} \quad \text{or} \quad \Gamma_0 K^3 - U^2 K^2 + (2\Omega U + 1)K - \Omega^2 = 0. \quad (I.A.1a, b)$$

Here

$$\Gamma_0 = T\omega_0^4/(\rho g^3) = -5 + \frac{26}{9}\sqrt{3} \tag{I.A.2}$$

as in section I.6, but $U$, $\Omega$ and $K$ are now free variables.

Let us introduce the function $f(U, \Omega, K)$ to represent the left-hand side of (I.A.1b)

$$f(U, \Omega, K) = \Gamma_0 K^3 - U^2 K^2 + (2\Omega U + 1)K - \Omega^2. \tag{I.A.3}$$

The dispersion relation can now be represented as the surface defined by

$$f(U, \Omega, K) = 0, \tag{I.A.4}$$

and is sketched in figure I-17. This sketch should be compared to figure I-6, which is drawn in dimensional units. The surface is seen to describe a cusp catastrophe. The singularity set of the surface, which is the locus of multiple-root points for the wavenumber, is defined by the condition

$$\frac{\partial f}{\partial K} = 0. \tag{I.A.5}$$

On the singularity set, the total differential of $f$ reduces to

$$\mathrm{d}f = \frac{\partial f}{\partial U}\mathrm{d}U + \frac{\partial f}{\partial \Omega}\mathrm{d}\Omega. \tag{I.A.6}$$

From these three relationships, we get

$$\left.\frac{\mathrm{d}\Omega}{\mathrm{d}U}\right|_{f=\frac{\partial f}{\partial K}=0} = -\frac{\partial f/\partial U}{\partial f/\partial \Omega} = K, \tag{I.A.7}$$

which is a differential equation that describes the projection of the singularity set on the $U\Omega$-plane. See figure I-18. Corresponding to the two possible reflection points, there are two curves emanating from the perfect triple-root point ($U = U_0, \Omega = 1$),

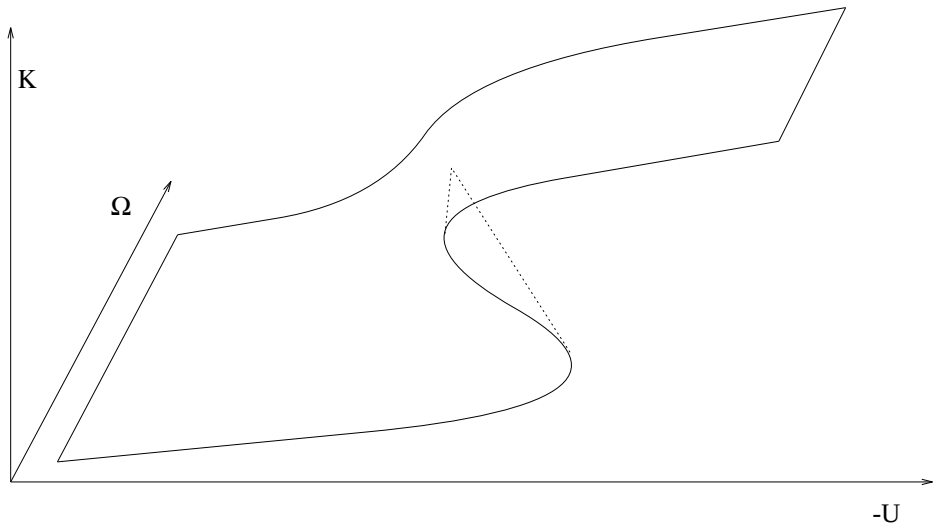


Figure I-17: Sketch of the surface described by the dispersion relation.

and thus forming a cusp in the $U\Omega$-plane. At the cusp, both of these curves are tangent to the straight line $\Omega - 1 = K_0(U - U_0)$, along which it is most natural to parameterize the detuning. The values of $U_0$ and $K_0$ are given in section I.6.

We shall allow for a small detuning in frequency of the form

$$\Omega = 1 + \epsilon\delta, \tag{I.A.8}$$

where $\epsilon \ll 1$ is the usual ordering parameter and $\delta$ is a detuning parameter assumed to be of order unity. The corresponding detuning for the current must then be

$$U = U_0 + \frac{\epsilon\delta}{K_0}. \tag{I.A.9}$$

The last condition implies that the local expansions are to be carried out around the point $x_2 = x'$ (the "detuned triple-root point") where

$$U(x') = U_0 + \frac{\epsilon\delta}{K_0} \qquad \text{at} \qquad z_1 = \epsilon\zeta(x'). \tag{I.A.10}$$

The boundary layer coordinates that were used in section I.6 may also be used here,

$$\xi = \epsilon^{-3/2}\tilde{x} \qquad \text{and} \qquad \tau = \epsilon^{-1/2}t_2, \tag{I.A.11}$$

where $\tilde{x} = x_2 - x'$ is a local horizontal coordinate. The governing equations (I.4.1)–(I.4.4) can now be rewritten as follows

$$\epsilon\frac{\partial^2\phi}{\partial\xi^2} + \frac{\partial^2\phi}{\partial z^2} = 0 \quad \text{for} \quad -\infty < z < \zeta_0, \tag{I.A.12}$$

$$\frac{\partial\phi}{\partial z} = 0 \quad \text{for} \quad z \to -\infty, \tag{I.A.13}$$

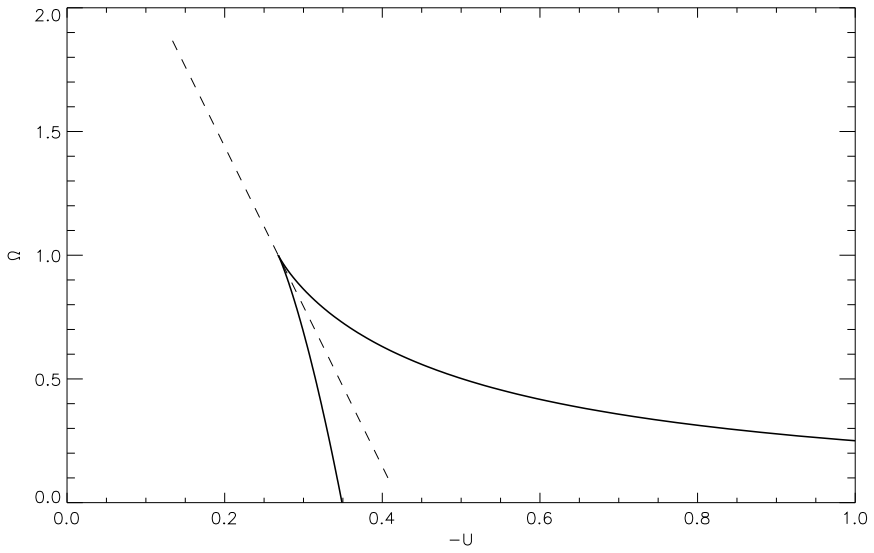


Figure I-18: Projection of the singularity set on the $U\Omega$-plane (solid curves), and the tangent line at the cusp (dashed).

$$\epsilon^{\frac{3}{2}}\frac{\partial\eta}{\partial\tau}+\epsilon^{\frac{5}{2}}\delta\frac{\partial\eta}{\partial\tau}+\epsilon^{\frac{1}{2}}U_0\frac{\partial\eta}{\partial\xi}+\epsilon^{\frac{3}{2}}\frac{\delta}{K_0}\frac{\partial\eta}{\partial\xi}+\epsilon^2U_1\xi\frac{\partial\eta}{\partial\xi}-\frac{\partial\phi}{\partial z}$$
$$-\epsilon^{\frac{3}{2}}\zeta_1\xi\frac{\partial^2\phi}{\partial z^2}\;=\;\text{h.o.t.}\quad\text{at}\quad z=\zeta_0, \tag{I.A.14}$$
$$\epsilon^{\frac{3}{2}}\frac{\partial\phi}{\partial\tau}+\epsilon^3\zeta_1\xi\frac{\partial^2\phi}{\partial\tau\partial z}+\epsilon^{\frac{5}{2}}\delta\frac{\partial\phi}{\partial\tau}+\eta+\epsilon^{\frac{1}{2}}U_0\frac{\partial\phi}{\partial\xi}+\epsilon^2U_0\zeta_1\xi\frac{\partial^2\phi}{\partial\xi\partial z}+\epsilon^{\frac{3}{2}}\frac{\delta}{K_0}\frac{\partial\phi}{\partial\xi}$$
$$+\epsilon^2U_1\xi\frac{\partial\phi}{\partial\xi}-\epsilon\Gamma_0\frac{\partial^2\eta}{\partial\xi^2}\;=\;\text{h.o.t.}\quad\text{at}\quad z=\zeta_0. \tag{I.A.15}$$

Here, the three current field quantities

$$U_1=\frac{\partial U}{\partial x_2}(x'),\quad \zeta_0=\zeta(x')\quad\text{and}\quad\zeta_1=\frac{\partial\zeta}{\partial x_2}(x') \tag{I.A.16}$$

have been evaluated at the detuned triple-root point.

The following WKB expansions are assumed, similar to section I.6,

$$\phi\;=\;(A+\epsilon^{\frac{1}{2}}A_1+\epsilon A_2+\epsilon^{\frac{3}{2}}A_3+\ldots)\exp\{\mathrm{i}(\epsilon^{-\frac{1}{2}}K_0\xi-\epsilon^{-\frac{3}{2}}\tau)\}+\text{c.c.}, \tag{I.A.17}$$
$$\eta\;=\;(B+\epsilon^{\frac{1}{2}}B_1+\epsilon B_2+\epsilon^{\frac{3}{2}}B_3+\ldots)\exp\{\mathrm{i}(\epsilon^{-\frac{1}{2}}K_0\xi-\epsilon^{-\frac{3}{2}}\tau)\}+\text{c.c.} \tag{I.A.18}$$

The problems at orders $\mathcal{O}(1)$ and $\mathcal{O}(\epsilon^{1/2})$ are identical to both the case of a simple reflection point and the case of a perfect triple-root point, and therefore the solutions (I.5.26), (I.5.33) and (I.5.34) still hold.

At order $\mathcal{O}(\epsilon)$, the effects of the detuning should in principle show up for the first time since it has been scaled at this order. However, these effects cancel exactly out

at this order because the detuning has been parameterized along the line of symmetry of the cusp, according to equations (I.A.8) and (I.A.9), and illustrated in figure I-18. The order $\mathcal{O}(\epsilon)$ problem is therefore identical to (I.6.22)–(I.6.25), and we use the solutions (I.6.27) and (I.6.28).

The problem at order $\mathcal{O}(\epsilon^{3/2})$ is

$$\frac{\partial^2 A_3}{\partial z^2} - K_0^2 A_3 = -\frac{\partial^2 A_1}{\partial \xi^2} - 2\mathrm{i}K_0 \frac{\partial A_2}{\partial \xi} \quad \text{for} \quad -\infty < z < \zeta_0 \tag{I.A.19}$$

$$\frac{\partial A_3}{\partial z} = 0 \quad \text{for} \quad z \to -\infty \tag{I.A.20}$$

$$\frac{\partial B}{\partial \tau} - \mathrm{i}\sigma_0 B_3 + U_0 \frac{\partial B_2}{\partial \xi} + \frac{\delta}{K_0}\frac{\partial B}{\partial \xi} + \mathrm{i}K_0 U_1 \xi B - \frac{\partial A_3}{\partial z} - \zeta_1 \xi \frac{\partial^2 A}{\partial z^2} = 0 \quad \text{at} \quad z = \zeta_0 \tag{I.A.21}$$

$$\begin{aligned} \frac{\partial A}{\partial \tau} - \mathrm{i}\sigma_0 A_3 + \frac{\delta}{K_0}\frac{\partial A}{\partial \xi} + U_0 \frac{\partial A_2}{\partial \xi} + B_3 - \Gamma_0 \frac{\partial^2 B_1}{\partial \xi^2} - 2\mathrm{i}\Gamma_0 K_0 \frac{\partial B_2}{\partial \xi} \\ + \Gamma_0 K_0^2 B_3 + \mathrm{i}K_0 U_1 \xi A - \mathrm{i}\sigma_0 \zeta_1 \xi \frac{\partial A}{\partial z} = 0 \quad \text{at} \quad z = \zeta_0 \end{aligned} \tag{I.A.22}$$

If the last two equations are combined to eliminate $B_3$, and the lower-order results are used to eliminate $A$, $A_1$, $A_2$, $B_1$ and $B_2$, we get the surface condition

$$\frac{\partial A_3}{\partial z} - K_0 A_3 = 2\frac{\partial B}{\partial \tau} - \frac{\Gamma_0}{\sigma_0}\frac{\partial^3 B}{\partial \xi^3} + 2\frac{\delta}{K_0}\frac{\partial B}{\partial \xi} + 2\mathrm{i}K_0 U_1 \xi B. \tag{I.A.23}$$

The solvability condition gives the following third-order partial differential equation governing the complex envelope $B$,

$$\frac{\partial B}{\partial \tau} - \frac{\Gamma_0}{2\sigma_0}\frac{\partial^3 B}{\partial \xi^3} + \frac{\delta}{K_0}\frac{\partial B}{\partial \xi} + \mathrm{i}K_0 U_1 \xi B = 0. \tag{I.A.24}$$

As before, if the characteristic time for the incident wave packet is $t_2 = \mathcal{O}(1)$ or longer, the inner region $\tilde{x} = \mathcal{O}(\epsilon^{3/2})$ can be considered quasi-stationary. The stationary limit of equation (I.A.24) reduces to the following Pearcey differential equation for the amplitude $B$,

$$\frac{\partial^3 B}{\partial \xi^3} - \frac{2\sigma_0 \delta}{\Gamma_0 K_0}\frac{\partial B}{\partial \xi} - \frac{2\mathrm{i}K_0 \sigma_0 U_1}{\Gamma_0}\xi B = 0. \tag{I.A.25}$$

The solution of this equation is the Pearcey function with two parameters. In Appendix I.B we summarize an integral form of the solution, appropriate for obtaining asymptotic expansions for large and small $\xi$. With reference to Appendix I.B, the solution which is bounded as $\xi \to \pm\infty$ is

$$B(\xi, t_2) = b_0(t_2) P(X, Y). \tag{I.A.26}$$

Here, $X$ and $Y$ are the complex arguments

$$X = \frac{2\sigma_0\delta}{\Gamma_0 K_0}\alpha^{-\frac{3}{2}}\mathrm{e}^{\frac{\pi\mathrm{i}}{4}} \qquad \text{and} \qquad Y = \sqrt{2}\alpha^{\frac{3}{4}}\mathrm{e}^{-\frac{\pi\mathrm{i}}{8}}\xi, \tag{I.A.27}$$

and $\alpha$ is the coefficient in the wavenumber expansion, corresponding to (I.6.9). It is now evident that for this problem, the first parameter of the Pearcey function measures detuning, while the second parameter measures the horizontal position.

# I.B Solution of the Pearcey equation

Consider equations (I.6.35) and (I.A.25)

$$\frac{\mathrm{d}^3B}{\mathrm{d}\xi^3} - \frac{2\sigma_0\delta}{\Gamma_0 K_0}\frac{\mathrm{d}B}{\mathrm{d}\xi} - \frac{2\mathrm{i}K_0\sigma_0 U_1}{\Gamma_0}\xi B = 0. \tag{I.B.1}$$

subject to the boundary conditions that $B$ is bounded as $\xi \to \pm\infty$. The independent variable $\xi$ is restricted to real values only.

Let us introduce the coefficient of the wavenumber expansion (I.6.9)

$$\alpha = \left(-\frac{2K_0\sigma_0 U_1}{\Gamma_0}\right)^{1/3}, \tag{I.B.2}$$

and do the substitutions

$$X = \frac{2\sigma_0\delta}{\Gamma_0 K_0}\alpha^{-\frac{3}{2}}\mathrm{e}^{\frac{\pi\mathrm{i}}{4}} \qquad \text{and} \qquad Y = \sqrt{2}\alpha^{\frac{3}{4}}\mathrm{e}^{-\frac{\pi\mathrm{i}}{8}}\xi. \tag{I.B.3}$$

Equation (I.B.1) then becomes

$$\frac{\mathrm{d}^3B}{\mathrm{d}Y^3} - \frac{1}{2}X\frac{\mathrm{d}B}{\mathrm{d}Y} - \frac{1}{4}YB = 0. \tag{I.B.4}$$

The solution of (I.B.4) is the Pearcey-function (after Pearcey (1945)) of the two parameters $X$ and $Y$

$$P(X,Y) = \int_{-\infty}^{\infty} \mathrm{e}^{-t^4 - Xt^2 + \mathrm{i}Yt}\,\mathrm{d}t, \tag{I.B.5}$$

which has been discussed by Stamnes (1986) and Paris (1991). The integral above corresponds to Paris' equation (2.2) (scaled by a factor of $\exp(\pi\mathrm{i}/8)$).

In the following, we limit the discussion to $X = 0$, which is appropriate for the perfect triple-root turning point. We may then introduce the simplified notation

$$P(Y) \equiv P(0,Y). \tag{I.B.6}$$

For $\xi > 0$, we have $\arg Y = -\pi/8$. From (2.11) in Paris (1991), we get

$$P(Y) \sim P_0 + P_1 \quad \text{for} \quad |\arg Y| < \frac{3\pi}{8}. \tag{I.B.7}$$

where $P_m$ is the contribution from the saddle point at $t_m = 4^{-\frac{1}{3}} \exp\{\frac{\mathrm{i}}{3}(\frac{\pi}{2} + \arg Y) + \frac{2\pi \mathrm{i} m}{3}\}$.

For large $Y$, the general expression for $P_m$ is (see Paris' equation (2.14))

$$\begin{aligned} P_m(Y) &\sim \sqrt{\frac{\pi}{3}} 2^{\frac{1}{6}} \exp\left\{ \frac{3}{4^{\frac{4}{3}}} Y^{\frac{4}{3}} \mathrm{e}^{\frac{2\pi \mathrm{i}(1+m)}{3}} \right\} \cdot \\ &\quad \left\{ Y^{-\frac{1}{3}} \mathrm{e}^{-\frac{\pi \mathrm{i}}{6} - \frac{2\pi \mathrm{i} m}{3}} - \frac{7}{36} 4^{\frac{1}{3}} Y^{-\frac{5}{3}} \mathrm{e}^{\frac{\pi \mathrm{i}}{6} + \frac{2\pi \mathrm{i} m}{3}} + \mathcal{O}(Y^{-\frac{7}{3}}) \right\}. \end{aligned} \tag{I.B.8}$$

For ease of reference, we shall display the first two terms of the derivative,

$$\begin{aligned} \frac{\partial P_m(Y)}{\partial Y} &\sim \sqrt{\frac{\pi}{3}} 2^{\frac{1}{6}} \exp\left\{ \frac{3}{4^{\frac{4}{3}}} Y^{\frac{4}{3}} \mathrm{e}^{\frac{2\pi \mathrm{i}}{3} + \frac{2\pi \mathrm{i} m}{3}} \right\} \cdot \\ &\quad \left\{ 4^{-\frac{1}{3}} \mathrm{e}^{\frac{\pi \mathrm{i}}{2}} - \frac{7}{36} Y^{-\frac{4}{3}} \mathrm{e}^{-\frac{\pi \mathrm{i}}{6} - \frac{2\pi \mathrm{i} m}{3}} + \mathcal{O}(Y^{-2}) \right\}. \end{aligned} \tag{I.B.9}$$

Since $\xi$ is real, $P_0$ represents an algebraically damped oscillation, while $P_1$ is exponentially damped. Hence for purposes of asymptotic matching, only $P_0$ is needed.

# Part II: Three resonating gravity–capillary waves riding on a long gravity wave

Notations for Part II

| | |
|---|---|
| $A$ | Amplitude of short wave. |
| $A_n$ | Section II.8 only: Coefficients of modulation equations. |
| $A_n$ | Amplitudes of three short resonating waves. |
| $A'_n$ | Normalized amplitudes of three short waves. |
| $\bar{A}_n$ | Amplitudes of three detuned short waves. |
| $a$ | Horizontal reference coordinate in $X$-direction. |
| $a_1, a_2$ | Long horizontal reference coordinates. |
| $\boldsymbol{a}$ | Horizontal reference coordinate vector. |
| $B$ | Amplitude of long wave. |
| $b$ | Horizontal reference coordinate in $Y$-direction. |
| $b_1, b_2$ | Long horizontal reference coordinates. |
| $C_1, C_2$ | Coefficients of modulation equation. |
| $c$ | Vertical reference coordinate. |
| $c_1, c_2$ | Long vertical reference coordinates. |
| $\boldsymbol{c}_{g,1}, \boldsymbol{c}_{g,2}, \boldsymbol{c}_{g,3}$ | Group velocity vectors of the short waves. |
| c.c. | Complex conjugate terms. |
| $E$ | Energy of short waves. |
| e | 2.71828182845... |
| $f$ | Detuning in modulation frequency. |
| $g$ | Acceleration due to gravity. |
| $H$ | Hamiltonian. |
| $I_n$ | Wave actions of the short waves. |
| i | $\sqrt{-1}$. |
| $J$ | Wave action of the shortest wave. |
| $J(a, b, c, t)$ | Jacobian. |
| $J_1, J_2$ | Conserved combinations of wave actions of the short waves. |
| $J_m$ | The minimum of $J_1$ and $J_2$. |
| $J_{(-1)}$ | Jacobian due to long wave. |
| $J_{(1)}, J_{(2)}$ | Jacobians due to short waves. |

| | |
|---|---|
| $j$ | Dynamical variable measuring amplitude of shortest wave. |
| $j_c$ | Value of $j$ at a center. |
| $j_*$ | Parameter for the difference in wave action between the two longer resonating waves. |
| $K$ | Wavenumber of long wave. |
| $\boldsymbol{K}$ | Wavenumber vector of long wave. |
| $\mathrm{K}(\cdot)$ | Elliptic integral of the first kind. |
| $k$ | Wavenumber of short wave. |
| $k_n$ | Wavenumbers of three short waves. |
| $\boldsymbol{k}_n$ | Wavenumber vectors of three short waves. |
| $\boldsymbol{k}'_n$ | Detuned wavenumber vectors of three short waves. |
| $k_{a,n}, k_{b,n}$ | Wavenumber components of short waves. |
| $k^*$ | Characteristic dimensional wavenumber. |
| $\boldsymbol{M}$ | Horizontal momentum vector of short waves. |
| $P$ | Initial condition for $p_1$. |
| $p$ | Pressure. |
| $p_n, p_{nm}$ | Amplitudes of free oscillation of $j$, order $n$, harmonic $m$. |
| $p_{\mathrm{atm}}$ | Atmospheric pressure. |
| $q_n, q_{nm}$ | Amplitudes of forced oscillation of $j$, order $n$, harmonic $m$. |
| $r$ | Parameter for the maximum amplitude of the shortest wave. |
| $r_n, r_{nm}$ | Amplitudes of free oscillation of $\psi$, order $n$, harmonic $m$. |
| $S_n$ | Bifurcation surfaces in parameter space. |
| $\mathcal{S}$ | Simplifying notation, function of $j_c$. |
| $s_n, s_{nm}$ | Amplitudes of forced oscillation of $\psi$, order $n$, harmonic $m$. |
| $T$ | Surface tension between water and air. |
| $\mathcal{T}$ | Period of modulation oscillation. |
| $t$ | Time. |
| $t_1, t_2$ | Slow timescales. |
| $u$ | Velocity component in $X$-direction. |
| $u_{nm}$ | Angle of incidence between $\boldsymbol{k}_n$ and $\boldsymbol{k}_m$. |
| $v$ | Velocity component in $Y$-direction. |
| $v_1, v_2, v_3$ | Angles between the long wave and three short waves. |
| $v_n^*$ | Angle of incidence for which $\beta_n = 0$. |
| $\boldsymbol{v}$ | Total velocity vector. |
| $w$ | Velocity component in $Z$-direction. |
| $X$ | Horizontal Lagrangian position in long-wave direction. |
| $\boldsymbol{X}$ | Horizontal Lagrangian position vector. |
| $x$ | Horizontal Lagrangian displacement component. |
| $x_{-1}$ | Horizontal displacement of long wave. |
| $x_{-10}$ | Horizontal slow drift of long wave. |
| $x_1, x_2$ | Horizontal displacements of short wave. |
| $x_{10}, x_{20}$ | Horizontal slow drift of short waves. |
| $Y$ | Horizontal Lagrangian position transverse to long-wave direction. |
| $y$ | Horizontal Lagrangian displacement component. |
| $y_1, y_2$ | Horizontal displacements of short wave. |

| | |
|---|---|
| $y_{10}, y_{20}$ | Horizontal slow drift of short waves. |
| $Z$ | Vertical Lagrangian position. |
| $z$ | Vertical Lagrangian displacement. |
| $z_{-1}$ | Vertical displacement of long wave. |
| $z_{-10}$ | Vertical slow drift of long wave. |
| $z_1, z_2$ | Vertical displacement of short wave. |
| $z_{10}, z_{20}$ | Vertical slow drift of short waves. |
| $\alpha$ | Combined nonlinear interaction coefficient. |
| $\alpha'$ | Normalized combined nonlinear interaction coefficient. |
| $\alpha_n$ | Nonlinear interaction coefficients. |
| $\beta$ | Total long-wave forcing. |
| $\beta_n$ | Long-wave/short-wave interaction coefficients. |
| $\beta'_n$ | Normalized long-wave/short-wave interaction coefficients. |
| $\gamma$ | $T/\rho$. |
| $\Delta$ | Total detuning. |
| $\Delta'_n$ | Normalized detuning of the short waves. |
| $\boldsymbol{\delta}_n$ | Detuning vector of short-wave wavenumbers. |
| $\epsilon$ | Small ordering parameter for short-wave and long-wave slope. |
| $\zeta$ | Surface elevation. |
| $\theta_n$ | Phases of three short waves. |
| $\lambda$ | Frequency of modulation oscillation at a center. |
| $\mu$ | Small ordering parameter for modulation resonance. |
| $\nu$ | Kinematic viscosity. |
| $\pi$ | 3.1415926535... |
| $\rho$ | Density of water. |
| $\tau$ | Slow modulation timescale. |
| $\phi$ | Phase of long wave. |
| $\psi$ | Total short-wave phase. |
| $\psi_c$ | Value of $\psi$ at a center. |
| $\Omega$ | Angular frequency of long wave. |
| $\Omega_X, \Omega_Y, \Omega_Z$ | Vorticity vector components. |
| $\omega$ | Angular frequency of short wave. |
| $\omega_1, \omega_2, \omega_3$ | Angular frequencies of three short waves. |
| $\omega^*$ | Characteristic dimensional angular frequency. |

# II.1 Introduction

## II.1.1 Literature review

The theoretical study of resonant interactions between gravity–capillary waves was initiated by Harrison (1909) and Wilton (1915), who found that a progressive wave can resonantly excite its $n$th harmonic through nonlinear interactions. When this happens, the classical Stokes wave solution for a steady progressive wave train breaks down. Wilton (1915) solved the steady progressive waves resulting from exact second-harmonic resonance. The resulting waves are now known as steady Wilton's ripples. Pierson & Fife (1961) considered the same problem, but allowed for slight detuning from exact resonance.

Extending the seminal work by Phillips (1960), who showed that pure gravity waves can resonate one another in quartets at the third order in wave steepness, McGoldrick (1965) showed that gravity–capillary waves can interact in triplets at the second order. Wilton's ripples constitute the special case when two of the waves are equal. McGoldrick (1965) derived the nonlinear evolution equations under the assumption that the wave envelopes are uniform in space and subject to temporal modulation only, and found the analytical solution for waves modulated in amplitude, but not in phase. Simmons (1969) generalized the evolution equations to account for modulation of both amplitude and phase, in both time and space. Limiting to time evolution only, Simmons solved the quadratic evolution equations for three different waves in perfect resonance. McGoldrick (1970b) pointed out that the steady solutions of Wilton (1915) are indeed limiting cases of the general triad interaction theory, corresponding to special initial conditions. Case & Chiu (1977) considered three-wave interaction where each wave consists of two components propagating in opposite directions. They found no coupling at the second order between the oppositely propagating waves. A general account of the Hamiltonian formulation of a resonating triad, and of several resonating triads that have one wave in common, was given by Meiss & Watson (1978).

Hasselmann (1967) derived a general criterion for the stability of a monochromatic wave subject to infinitesimal perturbations in a resonating triad. It was shown that a wave is stable to such perturbations if and only if it is one of the two longer waves of the triad. Wilton's ripples constitute an exception to this rule.

Bifurcation of steady wave trains subject to harmonic resonance was studied by Chen & Saffman (1979). They showed that steady Wilton's ripples are associated with a period-doubling bifurcation, through which a pure steady second-harmonic wave can become a steady combination wave of the first and second harmonics. It was later shown independently by Reeder & Shinbrot (1981a) and Ma (1982) that the same bifurcation can also occur for the special case of triad resonance in three dimensions when the two longer waves have the same amplitude and the wavenumber vectors form an isosceles triangle. A rigorous analysis of the bifurcations of Wilton's ripples was given by Reeder & Shinbrot (1981b) and Jones & Toland (1986). Janssen (1986) further discussed period doubling of weakly nonlinear gravity–capillary waves

forced by wind.[2]

Jones (1992) derived cubic nonlinear equations to investigate the slow time and space evolution of Wilton's ripples, which he only solved for certain special cases. Christodoulides & Dias (1994) considered cubically nonlinear steady Wilton's ripples on the interface between two fluids of different densities. They let each wave consist of two components propagating in opposite directions, and found that the oppositely propagating waves are coupled at the cubic nonlinear order. They also found that new and interesting bifurcations arise when the density ratio is varied.

The simultaneous evolution in time and space of the conservative three-wave equations has been solved analytically, see Kaup (1981) and references cited therein.

On the experimental side, collinear Wilton's ripples were verified by McGoldrick (1970a). Banerjee & Korpel (1982) studied triads where the wavenumber vectors form an isosceles triangle. Recent experiments on more general configurations of triads have been described in a series of papers by Henderson & Hammack (1987), Perlin, Henderson & Hammack (1990) and Perlin & Hammack (1991), and surveyed by Henderson & Hammack (1993). They showed how the stability criterion of Hasselmann (1967) together with ubiquitous noise in their experiments are important in the selection process that determines which discrete triads will eventually emerge. Experiments on steep Wilton's ripples and higher-order harmonic resonances were performed by Perlin & Ting (1992). They compared their measured wave profiles with fully nonlinear theories and found good agreement. Strizhkin & Raletnev (1986) observed resonant triads in the ocean when the wind speed was in the range from 2.7 to 18 m/s. They reported that the detection of the resonant triads was often made difficult due to the presence of long gravity waves.

Modern theories on how short waves evolve on a long wave were begun by Longuet-Higgins & Stewart (1960), who considered a linear short wave on top of a weakly nonlinear long wave. They discussed how the former steepens near the crests, and flattens near the troughs of the latter. Most of the existing works are concerned with the linear evolution of a single train of gravity or gravity–capillary waves, over a relatively short time or distance which is comparable with a long-wave period or wavelength. Phillips (1981) studied the evolution of a short linear gravity–capillary wave on a prescribed long wave, in an orthogonal coordinate system moving with the long-wave surface. Longuet-Higgins (1987) considered the effects of a steep long wave, which was calculated numerically, on a linear short gravity wave. The linear evolution of gravity–capillary waves on steep gravity waves was considered by Grimshaw (1988) by using non-orthogonal coordinates in an Eulerian formalism. Long-wave/short-wave interaction treated by a Zhakharov spectral formulation was presented by Craik (1988). A general Hamiltonian account of the linear evolution of short waves on a two dimensional long wave was given by Henyey *et al.* (1988). Shyu & Phillips (1990) investigated the possibility of blocking of short gravity and capillary waves by the variable orbital velocity of a long wave. So far the short wave is linear.

Benney (1976) described a special case of long-wave/short-wave interaction in which two short waves and one long wave resonate in a triad.

[2]Non-conservative triad interaction is considered in Part III.

The nonlinear evolution of a short gravity wave on a long gravity wave was investigated by Zhang & Melville (1990) by using an orthogonal coordinate system defined by the long wave. Subsequently, Zhang & Melville (1992) used this theory to investigate the evolution of a narrow-banded wave train on top of a long wave. Naciri & Mei (1992) used a Lagrangian formulation through which a short gravity wave is described relative to the long-wave particle displacement. They let the long wave be a rotational Gerstner wave of finite slope. In these papers, it was found that the long wave excites the short wave parametrically and enlarges the domain of Benjamin–Feir instability in the parametric space. Naciri & Mei (1992) further found that the post-instability evolution is chaotic, therefore suggesting that the irregular appearance of the sea surface need not be solely due to the turbulent eddies in wind, but is inherent in the deterministic nonlinear mechanics of the water surface.

Short waves riding on long waves can also be modulated indirectly by the long-wave induced modulation of the wind, which will give rise to a periodic wind-forcing of the short waves. This problem was recently discussed by Troitskaya (1994).

Woodruff & Messiter (1994) derived a theory for dispersive short capillary waves riding on a long gravity wave of finite steepness. In a general discussion of a short gravity wave riding on top of a long gravity wave (on page 163), they state the following two facts: If dispersion due to gravitation and advection due to the long wave balance at leading order, then the long-wave slope must be small. If on the other hand the long wave has finite slope, then the short wave must be non-dispersive to leading order because advection due to the long wave must dominate over dispersion due to gravitation. However, Woodruff & Messiter then claim (on page 181) that since Naciri & Mei (1992) describe a short gravity wave that is dispersive to leading order while riding on a long wave of finite steepness, Naciri & Mei (1992) may not be fully self-consistent.

The first two statements are both easily shown to be correct in a horizontally inertial reference system, which is what Woodruff & Messiter (1994) used. However, their claim that Naciri & Mei (1992) is not self-consistent reveals that they did not fully take into account the Lagrangian formulation employed by Naciri & Mei (1992).

The Lagrangian formulation employed by Naciri & Mei (1992) causes the short wave to be described in a horizontally accelerated reference system such that the short wave does not appear to be advected by the long wave. Hence the short wave may be dispersive to leading order in the Lagrangian frame, although it may at the same time be non-dispersive to leading order when the results are translated to a horizontally inertial frame. The Lagrangian dispersion relation (4.8) in Naciri & Mei (1992),

$$\sigma^2 = gk,$$

shows that the short wave is dispersive to leading order in the Lagrangian system. Here $\sigma$ is the intrinsic frequency of the short wave, $g$ is the acceleration due to gravity and $k$ is the wavenumber of the short wave. The corresponding dispersion relation in

a horizontally stationary Eulerian frame is given in their equation (5.33),

$$\frac{\omega}{\sigma} = 1 + \frac{1}{\epsilon}\frac{\sigma}{\Omega} KB \frac{1+K^2B^2}{1-KB\cos\phi} \frac{-2KB + (1+K^2B^2)\cos\phi}{(1-2KB\cos\phi + K^2B^2)^2} + O(\epsilon).$$

Here $\omega$ is the absolute frequency of the short wave, $\epsilon \ll 1$ is a small ordering parameter, while the frequency, wavenumber, amplitude and phase of the long wave are given by $\Omega$, $K$, $B$ and $\phi$, respectively. The first and second terms on the right-hand side of this equation represent dispersion and Doppler-shift, respectively. The fact that the second term is a non-dispersive Doppler-shift, is easier to see from equation (II.5.44) in Naciri's (1992) thesis,

$$\omega = \sigma + \frac{1}{\epsilon} k\Omega B \frac{1+K^2B^2}{1-KB\cos\phi} \frac{-2KB + (1+K^2B^2)\cos\phi}{(1-2KB\cos\phi + K^2B^2)^2} + O(\epsilon).$$

Clearly, the Doppler-shift dominates over dispersive effects by a factor $\epsilon^{-1} \gg 1$, and hence the short wave is indeed non-dispersive to leading order in the stationary coordinate system. Hence Naciri & Mei (1992) remains self-consistent.

### II.1.2 Objectives of the present work

In nature, gravity–capillary waves often appear in short-crested form. Our purpose here is to study the evolution of three resonating gravity–capillary waves propagating in different directions on a long gravity wave. This is important both for a fuller understanding of the sea-surface dynamics and to facilitate interpretation of remote sensing data.

For a meaningful theoretical analysis it is important to assess the role of viscous damping. Let us first show that for a fresh and clean water surface without the effects of aging or contamination, viscous damping occurs over a timescale much longer than the time for quadratic interaction. At 20°C the following values for surface tension, density, gravitational acceleration and viscosity can be taken:

$$T = 7.28\times10^{-2}\,\mathrm{N/m}, \quad \rho = 9.98\times10^{2}\,\mathrm{kg/m^3}, \quad g = 9.80\,\mathrm{m/s^2}, \quad \nu = 1.00\times10^{-6}\mathrm{m^2/s}.$$

We define the characteristic wavenumber and frequency by equating the gravity and capillary terms in the dispersion relation, which corresponds to the minimum phase velocity, i.e.

$$k^* = \sqrt{\frac{\rho g}{T}} = 367\,\mathrm{m^{-1}}, \quad \omega^* = \sqrt{2gk^*} = 84.8\,\mathrm{s^{-1}}. \tag{II.1.1}$$

These correspond to wavelength 1.7 cm and frequency 13 Hz. For a clean water surface, the ratio of a wave period to the damping time is

$$\frac{1}{\omega^*} 2\nu (k^*)^2 = 0.0032.$$

The ratio of a wave period to the timescale of resonant interaction is comparable to the wave steepness. If we let the steepness be of the order $\epsilon = \mathcal{O}(0.05)$–$\mathcal{O}(0.1)$,

then internal viscous damping is clearly unimportant for a time range compatible with quadratic nonlinear interaction. However, it is equally clear that viscous effects cannot be neglected for a cubically nonlinear theory. If on the other hand, contamination is so strong that the surface behaves as an inextensible film, the non-dimensional characteristic damping rate can be found to be

$$\frac{1}{\omega^*}\frac{k^*}{2}\sqrt{\frac{\nu\omega^*}{2}} = 0.014.$$

Viscosity would then be much more important in the study of the long-time behavior.

Based on these estimates, we shall here consider inviscid triad interaction up to quadratic nonlinear order, with the effect of the long wave balanced at the second order. In Part III, we consider second-harmonic resonance subject to viscous effects and wind forcing at the third order, while also including cubic nonlinear interactions.

Assuming that the amplitude of the long wave is much greater than the typical wavelength of the short waves, we employ in section II.2 the Lagrangian description (as in Naciri & Mei (1992)) in order to simplify the consideration of the free surface. Multiple-scales perturbation expansions are introduced in section II.3. The long wave is briefly summarized in section II.4. Equations are then deduced in section II.5 for the envelopes of the interacting short waves on top of a uniform long wave, in the framework of potential theory. In section II.6 we limit our discussion to slow time evolution only, but allow for detuning from exact resonance. To facilitate the discussion of the influence of the long wave, we summarize the analytical solution for a resonant triad without the long wave in section II.7, allowing for imperfect resonance. As a result, we generalize the bifurcation criterion of Chen & Saffman (1979), Reeder & Shinbrot (1981a) and Ma (1982) to arbitrary three-wave configurations. For a weak long wave, approximate analysis is then pursued in section II.8 to reveal bifurcations due to modulational resonance, by which the natural envelope oscillations of the triad are resonated by the long wave. Confirmation of the analytical results by direct numerical integration of the evolution equations, is also shown. Finally, in section II.9 numerical results for a relatively strong long wave are presented. Details of the approach to Hamiltonian chaos are shown.

This work is currently being published in Trulsen & Mei (1995). A similar discussion of modulational resonance as that presented in section II.8, but applied to resonance of surface waves in a current over a wavy bottom, has been published in Sammarco, Mei & Trulsen (1994).

## II.2 Governing Lagrangian equations

To analyze the short waves with wavelengths much shorter than the amplitude of the long wave, one may use non-orthogonal curvilinear coordinates as in Grimshaw (1988), orthogonal curvilinear coordinates defined by the long wave as in Zhang & Melville (1990) or Lagrangian coordinates as in Naciri & Mei (1992). Here we adopt the last approach and first summarize the Lagrangian equations governing irrotational

deep water waves on the surface of an inviscid, incompressible fluid.

Let the instantaneous horizontal and vertical position of a fluid particle, $(X, Y, Z)$, be parameterized by the reference coordinates $(a, b, c)$ and time $t$. We sometimes use the boldface vector notation $\boldsymbol{X} = (X, Y)$ and $\boldsymbol{a} = (a, b)$ to denote the horizontal position and coordinates. The fluid velocity is expressed by

$$\boldsymbol{v} = (u, v, w) = \left(\frac{\partial X}{\partial t}, \frac{\partial Y}{\partial t}, \frac{\partial Z}{\partial t}\right). \tag{II.2.1}$$

Continuity of an incompressible fluid requires that the following Jacobian is independent of time:

$$\frac{\partial(X, Y, Z)}{\partial(a, b, c)} = J(a, b, c). \tag{II.2.2}$$

The vorticity components are assumed to be zero,

$$\Omega_X = \frac{\partial w}{\partial Y} - \frac{\partial v}{\partial Z}, \quad \Omega_Y = \frac{\partial u}{\partial Z} - \frac{\partial w}{\partial X}, \quad \Omega_Z = \frac{\partial v}{\partial X} - \frac{\partial u}{\partial Y}. \qquad (II.2.3a, b, c)$$

For deep water waves, irrotationality in the two horizontal directions implies irrotationality in the vertical direction. This follows from the vector identity $\nabla \cdot \nabla \times \boldsymbol{v} = 0$. If $\Omega_X = \Omega_Y = 0$, then $\Omega_Z$ is independent of $Z$. Since the fluid velocity $\boldsymbol{v}$ vanishes at great depth ($Z \to -\infty$), it follows that $\Omega_Z$ vanishes identically everywhere. As a result, (II.2.2) and (II.2.3a,b) are sufficient to determine the three unknowns $X, Y, Z$.

The two horizontal components of the vorticity vector can be expressed in Lagrangian form as

$$\Omega_X = \frac{\partial a}{\partial Y}\frac{\partial^2 Z}{\partial a \partial t} + \frac{\partial b}{\partial Y}\frac{\partial^2 Z}{\partial b \partial t} + \frac{\partial c}{\partial Y}\frac{\partial^2 Z}{\partial c \partial t} - \frac{\partial a}{\partial Z}\frac{\partial^2 Y}{\partial a \partial t} - \frac{\partial b}{\partial Z}\frac{\partial^2 Y}{\partial b \partial t} - \frac{\partial c}{\partial Z}\frac{\partial^2 Y}{\partial c \partial t}, \tag{II.2.4}$$

$$\Omega_Y = \frac{\partial a}{\partial Z}\frac{\partial^2 X}{\partial a \partial t} + \frac{\partial b}{\partial Z}\frac{\partial^2 X}{\partial b \partial t} + \frac{\partial c}{\partial Z}\frac{\partial^2 X}{\partial c \partial t} - \frac{\partial a}{\partial X}\frac{\partial^2 Z}{\partial a \partial t} - \frac{\partial b}{\partial X}\frac{\partial^2 Z}{\partial b \partial t} - \frac{\partial c}{\partial X}\frac{\partial^2 Z}{\partial c \partial t}. \tag{II.2.5}$$

The derivatives of $a, b, c$ can be expressed in terms of derivatives of the particle positions, as summarized in Appendix II.A.

Conservation of momentum requires

$$\frac{\partial^2 X}{\partial t^2} = -\frac{1}{\rho}\frac{\partial p}{\partial X}, \qquad \frac{\partial^2 Y}{\partial t^2} = -\frac{1}{\rho}\frac{\partial p}{\partial Y}, \qquad \frac{\partial^2 Z}{\partial t^2} = -\frac{1}{\rho}\frac{\partial p}{\partial Z} - g, \qquad (II.2.6a, b, c)$$

where $p$ is the water pressure, $\rho$ the water density and $g$ the acceleration due to gravity. By combining (II.2.6a,b,c), we get

$$\frac{\partial X}{\partial a}\frac{\partial^2 X}{\partial t^2} + \frac{\partial Y}{\partial a}\frac{\partial^2 Y}{\partial t^2} + \frac{\partial Z}{\partial a}\left(\frac{\partial^2 Z}{\partial t^2} + g\right) = -\frac{1}{\rho}\frac{\partial p}{\partial a} \tag{II.2.7}$$

and

$$\frac{\partial X}{\partial b}\frac{\partial^2 X}{\partial t^2} + \frac{\partial Y}{\partial b}\frac{\partial^2 Y}{\partial t^2} + \frac{\partial Z}{\partial b}\left(\frac{\partial^2 Z}{\partial t^2} + g\right) = -\frac{1}{\rho}\frac{\partial p}{\partial b}. \tag{II.2.8}$$

In the Lagrangian description, the kinematic condition for the free surface is simply that the free surface is at $c = 0$. The vertical displacement of the free surface is given by $\zeta = Z(a, b, 0, t)$. The dynamic surface boundary condition is that the atmospheric pressure $p_{\rm atm}$ is constant, hence

$$\frac{\partial p_{\rm atm}}{\partial a} = \frac{\partial p_{\rm atm}}{\partial b} = 0 \quad \text{at} \quad c = 0. \tag{II.2.9}$$

With surface tension, the water pressure at the free surface is

$$p = p_{\rm atm} + T\nabla_{\boldsymbol{X}} \cdot \frac{(-\nabla_{\boldsymbol{X}}\zeta, 1)}{\sqrt{1 + |\nabla_{\boldsymbol{X}}\zeta|^2}}. \tag{II.2.10}$$

Here $T$ the surface tension between water and air and $\nabla_{\boldsymbol{X}} = (\partial/\partial X, \partial/\partial Y)$. In the following, we will set $\gamma = T/\rho$. Using the definition of $\zeta$, we may now write

$$\frac{\partial \zeta}{\partial X} = \frac{\partial a}{\partial X}\frac{\partial Z}{\partial a} + \frac{\partial b}{\partial X}\frac{\partial Z}{\partial b} \qquad \text{at} \quad c = 0, \tag{II.2.11}$$

and similarly for the other derivatives.

Following Naciri & Mei (1992), it is convenient to introduce the Lagrangian displacements $(x, y, z)$ relative to the reference coordinates $(a, b, c)$ as follows:

$$X = a + x(a, b, c, t), \qquad Y = b + y(a, b, c, t), \qquad Z = c + z(a, b, c, t). \tag{II.2.12}$$

The resulting governing equations for the Lagrangian displacements are summarized in the following. For later analysis it is sufficient to display quadratic terms only. The continuity condition requires that the following expression is independent of time:

$$\frac{\partial x}{\partial a} + \frac{\partial y}{\partial b} + \frac{\partial z}{\partial c} - \frac{\partial x}{\partial b}\frac{\partial y}{\partial a} + \frac{\partial x}{\partial a}\frac{\partial y}{\partial b} - \frac{\partial x}{\partial c}\frac{\partial z}{\partial a} - \frac{\partial y}{\partial c}\frac{\partial z}{\partial b} + \frac{\partial x}{\partial a}\frac{\partial z}{\partial c} + \frac{\partial y}{\partial b}\frac{\partial z}{\partial c} \tag{II.2.13}$$

Irrotationality, $x$-component:

$$\begin{aligned} &-\frac{\partial^2 y}{\partial c \partial t} + \frac{\partial^2 z}{\partial b \partial t} + \frac{\partial x}{\partial c}\frac{\partial^2 y}{\partial a \partial t} + \frac{\partial^2 y}{\partial b \partial t}\frac{\partial y}{\partial c} - \frac{\partial x}{\partial a}\frac{\partial^2 y}{\partial c \partial t} - \frac{\partial y}{\partial b}\frac{\partial^2 y}{\partial c \partial t} \\ &\quad - \frac{\partial x}{\partial b}\frac{\partial^2 z}{\partial a \partial t} + \frac{\partial x}{\partial a}\frac{\partial^2 z}{\partial b \partial t} + \frac{\partial^2 z}{\partial b \partial t}\frac{\partial z}{\partial c} - \frac{\partial z}{\partial b}\frac{\partial^2 z}{\partial c \partial t} = 0 \end{aligned} \tag{II.2.14}$$

Irrotationality, $y$-component:

$$\begin{aligned} &\frac{\partial^2 x}{\partial c \partial t} - \frac{\partial^2 z}{\partial a \partial t} - \frac{\partial^2 x}{\partial a \partial t}\frac{\partial x}{\partial c} + \frac{\partial x}{\partial a}\frac{\partial^2 x}{\partial c \partial t} + \frac{\partial^2 x}{\partial c \partial t}\frac{\partial y}{\partial b} - \frac{\partial^2 x}{\partial b \partial t}\frac{\partial y}{\partial c} \\ &\quad - \frac{\partial y}{\partial b}\frac{\partial^2 z}{\partial a \partial t} + \frac{\partial y}{\partial a}\frac{\partial^2 z}{\partial b \partial t} - \frac{\partial^2 z}{\partial a \partial t}\frac{\partial z}{\partial c} + \frac{\partial z}{\partial a}\frac{\partial^2 z}{\partial c \partial t} = 0 \end{aligned} \tag{II.2.15}$$

Free surface condition, $a$-component:

$$\frac{\partial^2 x}{\partial t^2}+g\frac{\partial z}{\partial a}+\frac{\partial x}{\partial a}\frac{\partial^2 x}{\partial t^2}+\frac{\partial y}{\partial a}\frac{\partial^2 y}{\partial t^2}+\frac{\partial z}{\partial a}\frac{\partial^2 z}{\partial t^2}+\gamma\left(-\frac{\partial^3 z}{\partial a\partial b^2}-\frac{\partial^3 z}{\partial a^3}\right.$$
$$+\frac{\partial^3 x}{\partial a\partial b^2}\frac{\partial z}{\partial a}+\frac{\partial^3 x}{\partial a^3}\frac{\partial z}{\partial a}+2\frac{\partial^2 x}{\partial a\partial b}\frac{\partial^2 z}{\partial a\partial b}+3\frac{\partial^2 y}{\partial a^2}\frac{\partial^2 z}{\partial a\partial b}+\frac{\partial^2 y}{\partial b^2}\frac{\partial^2 z}{\partial a\partial b}$$
$$+2\frac{\partial y}{\partial b}\frac{\partial^3 z}{\partial a\partial b^2}+3\frac{\partial^2 x}{\partial a^2}\frac{\partial^2 z}{\partial a^2}+\frac{\partial^2 x}{\partial b^2}\frac{\partial^2 z}{\partial a^2}+2\frac{\partial x}{\partial b}\frac{\partial^3 z}{\partial a^2\partial b}+2\frac{\partial y}{\partial a}\frac{\partial^3 z}{\partial a^2\partial b}$$
$$\left.+2\frac{\partial x}{\partial a}\frac{\partial^3 z}{\partial a^3}+\frac{\partial^3 y}{\partial a\partial b^2}\frac{\partial z}{\partial b}+\frac{\partial^3 y}{\partial a^3}\frac{\partial z}{\partial b}+2\frac{\partial^2 y}{\partial a\partial b}\frac{\partial^2 z}{\partial b^2}\right)=0 \qquad \text{(II.2.16)}$$

Free surface condition, $b$-component:

$$\frac{\partial^2 y}{\partial t^2}+g\frac{\partial z}{\partial b}+\frac{\partial x}{\partial b}\frac{\partial^2 x}{\partial t^2}+\frac{\partial y}{\partial b}\frac{\partial^2 y}{\partial t^2}+\frac{\partial z}{\partial b}\frac{\partial^2 z}{\partial t^2}+\gamma\left(-\frac{\partial^3 z}{\partial a^2\partial b}-\frac{\partial^3 z}{\partial b^3}\right.$$
$$+\frac{\partial^3 x}{\partial a^2\partial b}\frac{\partial z}{\partial a}+\frac{\partial^3 x}{\partial b^3}\frac{\partial z}{\partial a}+\frac{\partial^2 x}{\partial a^2}\frac{\partial^2 z}{\partial a\partial b}+3\frac{\partial^2 x}{\partial b^2}\frac{\partial^2 z}{\partial a\partial b}+2\frac{\partial^2 y}{\partial a\partial b}\frac{\partial^2 z}{\partial a\partial b}$$
$$+2\frac{\partial x}{\partial b}\frac{\partial^3 z}{\partial a\partial b^2}+2\frac{\partial y}{\partial a}\frac{\partial^3 z}{\partial a\partial b^2}+2\frac{\partial^2 x}{\partial a\partial b}\frac{\partial^2 z}{\partial a^2}+2\frac{\partial x}{\partial a}\frac{\partial^3 z}{\partial a^2\partial b}+\frac{\partial^3 y}{\partial a^2\partial b}\frac{\partial z}{\partial b}$$
$$\left.+\frac{\partial^3 y}{\partial b^3}\frac{\partial z}{\partial b}+\frac{\partial^2 y}{\partial a^2}\frac{\partial^2 z}{\partial b^2}+3\frac{\partial^2 y}{\partial b^2}\frac{\partial^2 z}{\partial b^2}+2\frac{\partial y}{\partial b}\frac{\partial^3 z}{\partial b^3}\right)=0 \qquad \text{(II.2.17)}$$

## II.3 Ordering assumptions and multiple-scale expansions

We shall assume that the water depth is much greater than the length of the long wave and that both short and long waves have small steepnesses. Let the physical wavenumber, frequency and amplitude of the short wave be denoted by $k, \omega, A$, respectively, and the corresponding quantities for the long wave by $K, \Omega, B$. The following ordering assumptions are assumed with a view to yielding simple and interesting asymptotic results:

$$kA=\mathcal{O}(\epsilon), \qquad KB=\mathcal{O}(\epsilon), \qquad \frac{K}{k}=\mathcal{O}(\epsilon^2), \qquad \frac{\Omega}{\omega}=\mathcal{O}(\epsilon), \qquad \text{(II.3.1)}$$

where $\epsilon \ll 1$. The last two are dictated by the anticipated dispersion relations

$$\Omega^2=gK \quad \text{and} \quad \omega^2=gk+\gamma k^3. \qquad (II.3.2a,b)$$

Under these scaling assumptions,

$$\Omega B=\mathcal{O}(\omega/k) \quad \text{and} \quad kB=\mathcal{O}(1/\epsilon), \qquad \text{(II.3.3)}$$

meaning, respectively, that the orbital velocity of the long wave is comparable in order of magnitude to the phase and group velocities of the short waves, and that the short-wave wavelength is much smaller than the long-wave amplitude.

We shall assume that the long wave is unidirectional in the $x$-direction, while the short waves propagate in different horizontal directions as long as they are in resonance. As a consequence, the long wave will have only $x$ and $z$ components, which are independent of the coordinate $b$.

We let the basic reference lengthscales and timescales be defined by $k^{-1}$ and $\omega^{-1}$ of the short wave. In view of the scale contrast between short and long waves and the anticipated growth due to resonance, we introduce a cascade of slow coordinates

$$(a_j, b_j, c_j, t_j) = \epsilon^j (a, b, c, t) \quad \text{for} \quad j = 1, 2, 3, \ldots . \tag{II.3.4}$$

From (II.3.1) the amplitudes of the short and long waves are $\mathcal{O}(\epsilon/k)$ and $\mathcal{O}(1/\epsilon k)$ respectively. To the leading order the particle displacement field can therefore be decomposed into long-wave components $x_{-1}$ and $z_{-1}$ at $\mathcal{O}(\epsilon^{-1})$, and short-wave components $x_1, y_1$ and $z_1$ at $\mathcal{O}(\epsilon)$. The lowest order at which the short waves can influence the long wave is $\mathcal{O}(KB(kA)^2)$. On the other hand, triad resonance of short waves is known to reach maturity at $\mathcal{O}(kA)^2$ over the timescale $t_1 = \mathcal{O}(1)$. Self-modulation of the long wave will occur by nonlinear interaction at the third order over much longer timescales and lengthscales described by $a_3, c_3, t_2$ . The short waves will be modulated by both nonlinear self-interaction and by the long wave. Since the short-wave steepness is $kA = \mathcal{O}(\epsilon)$, self-interaction must be described by coordinates $a_1, b_1, c_1, t_1$ . Modulation of the short waves by the long wave will of course be over the scales of the long wave.

We shall here only examine the effect of a long wave on the second-order interactions of the short waves, over the timescale of triad resonance $t_1$. Hence the long wave will not be affected by the short waves and can be described by a linearized theory. Thus we expand the short-wave displacements to the second order, while we only need the long-wave displacement to the leading order. The resulting expansions, with both long and short-wave contributions, are

$$\left.\begin{array}{rcccl} x &=& \epsilon^{-1} x_{-1} &+& \epsilon x_1 + \epsilon^2 x_2 \\ y &=& & & \epsilon y_1 + \epsilon^2 y_2 \\ z &=& \epsilon^{-1} z_{-1} &+& \epsilon z_1 + \epsilon^2 z_2 \end{array}\right\} \tag{II.3.5}$$

The long-wave contributions at $\mathcal{O}(\epsilon^{-1})$ depend on $a_2, c_2, t_1$. The short-wave contributions at $\mathcal{O}(\epsilon)$ and $\mathcal{O}(\epsilon^2)$ depend on $a, b, a_1, b_1, c, c_1, t, t_1$.

In the following, it is convenient to decompose the Jacobian as

$$J = 1 + \epsilon(J_{(-1)} + J_{(1)}) + \epsilon^2 J_{(2)} + \ldots , \tag{II.3.6}$$

where $J_{(-1)}$ is the leading-order contribution due to the long wave, $J_{(1)}$ is the leading-order contribution due to the short waves, and $J_{(2)}$ is the second-order contribution due to the short waves.

The first-order equations for the long wave are the following:

Continuity:

$$\frac{\partial x_{-1}}{\partial a_2} + \frac{\partial z_{-1}}{\partial c_2} = J_{(-1)}. \tag{II.3.7}$$

Irrotationality, $y$-component:

$$\frac{\partial^2 x_{-1}}{\partial c_2 \partial t_1} - \frac{\partial^2 z_{-1}}{\partial a_2 \partial t_1} = 0. \tag{II.3.8}$$

Free surface condition, $a$-component:

$$\frac{\partial^2 x_{-1}}{\partial {t_1}^2} + g\,\frac{\partial z_{-1}}{\partial a_2} = 0. \tag{II.3.9}$$

Here $J_{(-1)}$ is of course independent of time.

The first and second-order equations for the short waves, corresponding to $n = 1$ and $n = 2$, respectively, are as follows:
Continuity:

$$\frac{\partial x_n}{\partial a} + \frac{\partial y_n}{\partial b} + \frac{\partial z_n}{\partial c} = \mathcal{E}_n. \tag{II.3.10}$$

Irrotationality, $x$-component:

$$\frac{\partial^2 y_n}{\partial c \partial t} - \frac{\partial^2 z_n}{\partial b \partial t} = \mathcal{F}_n. \tag{II.3.11}$$

Irrotationality, $y$-component:

$$\frac{\partial^2 x_n}{\partial c \partial t} - \frac{\partial^2 z_n}{\partial a \partial t} = \mathcal{G}_n. \tag{II.3.12}$$

Free surface condition, $a$-component:

$$\frac{\partial^2 x_n}{\partial t^2} + g\,\frac{\partial z_n}{\partial a} - \gamma\left(\frac{\partial^3 z_n}{\partial a \partial b^2} + \frac{\partial^3 z_n}{\partial a^3}\right) = \mathcal{H}_n. \tag{II.3.13}$$

Free surface condition, $b$-component:

$$\frac{\partial^2 y_n}{\partial t^2} + g\,\frac{\partial z_n}{\partial b} - \gamma\left(\frac{\partial^3 z_n}{\partial a^2 \partial b} + \frac{\partial^3 z_n}{\partial b^3}\right) = \mathcal{I}_n. \tag{II.3.14}$$

The leading-order short-wave problem has $\mathcal{E}_1 = J_{(1)}$, which is independent of time. Furthermore, $\mathcal{F}_1 = \mathcal{G}_1 = \mathcal{H}_1 = \mathcal{I}_1 = 0$. The lengthy right-hand-side expressions of the second-order problem, $\mathcal{E}_2$, $\mathcal{F}_2$, $\mathcal{G}_2$, $\mathcal{H}_2$ and $\mathcal{I}_2$ are given in Appendix II.B.

## II.4 The long wave

The leading-order long-wave equations are satisfied by the basic linear wave solution

$$x_{-1} = x_{-10} + \frac{\mathrm{i}}{2} B \mathrm{e}^{\mathrm{i}(Ka_2 - \Omega t_1) + Kc_2} + \text{c.c.}, \tag{II.4.1}$$

$$z_{-1} = z_{-10} + \frac{1}{2} B \mathrm{e}^{\mathrm{i}(Ka_2 - \Omega t_1) + Kc_2} + \text{c.c.}, \tag{II.4.2}$$

where $B$ is the long-wave amplitude. The slow drift due to the long wave $(x_{-10}, z_{-10})$ is assumed to be independent of the fast scales of the long-wave phase, $a_2$ and $t_1$.

Without loss of generality, we take the initial condition for the slow drift to be $x_{-10} = z_{-10} = 0$ at $t = 0$. Upon substitution of (II.4.1)–(II.4.2) into the continuity condition (II.3.7), we extract the following equation for the slow drift from the zeroth harmonic problem

$$\frac{\partial z_{-10}}{\partial c_2} = J_{(-1)}. \tag{II.4.3}$$

Since the Jacobian is independent of time, and $z_{-10}$ vanishes at initial time, it follows that $z_{-10} = 0$ and $J_{(-1)} = 0$. The horizontal component $x_{-10}$ remains undetermined, but is not needed in the following analysis.

The contribution from the first harmonic of the surface condition (II.3.9) gives the anticipated dispersion relation

$$\Omega^2 = gK. \tag{II.4.4}$$

## II.5 Evolution equations for the short waves

Let us begin with three trains of short waves with amplitudes $A_n$ for $n = 1, 2, 3$. The leading-order sum of the short waves is given by

$$x_1 = x_{10} + \frac{\mathrm{i}}{2} \sum_{n=1}^{3} \frac{k_{a,n}}{k_n} A_n \mathrm{e}^{\mathrm{i}\theta_n + k_n c} + \text{c.c.}, \tag{II.5.1}$$

$$y_1 = y_{10} + \frac{\mathrm{i}}{2} \sum_{n=1}^{3} \frac{k_{b,n}}{k_n} A_n \mathrm{e}^{\mathrm{i}\theta_n + k_n c} + \text{c.c.}, \tag{II.5.2}$$

$$z_1 = z_{10} + \frac{1}{2} \sum_{n=1}^{3} A_n \mathrm{e}^{\mathrm{i}\theta_n + k_n c} + \text{c.c.}. \tag{II.5.3}$$

The wavenumber vector of the $n$th wave is $\boldsymbol{k}_n = (k_{a,n}, k_{b,n})$ with $k_n = |\boldsymbol{k}_n|$, while the phase is $\theta_n = k_{a,n} a + k_{b,n} b - \omega_n t$. Each amplitude $A_n(a_1, b_1, c_1, t_1)$ depends on the slow coordinates only. The slow drift due to the short waves $(x_{10}, y_{10}, z_{10})$ is assumed to be independent of the fast scales of the short-wave phase, $a, b$ and $t$.

Without loss of generality, we take the initial condition for the slow drift that $x_{10} = y_{10} = z_{10} = 0$ at $t = 0$. Upon substitution of (II.5.1)–(II.5.3) into the leading-order continuity condition (II.3.10), we extract the following equation for the slow

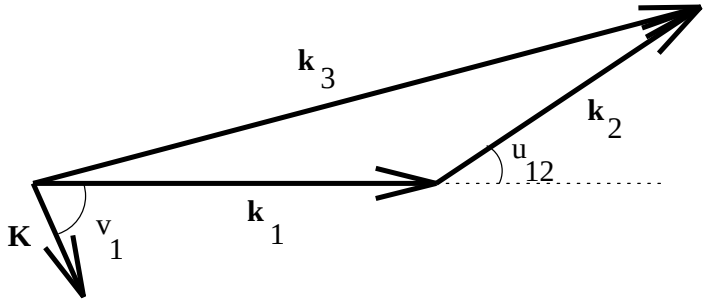


Figure II-1: Geometry of a resonating triad. The angle $v_n$ is between the long wave $\boldsymbol{K}$ and the short wave $\boldsymbol{k}_n$. The angle $u_{nm}$ is between the short waves $\boldsymbol{k}_n$ and $\boldsymbol{k}_m$. The short wave $\boldsymbol{k}_3$ is always the shortest one.

drift from the zeroth harmonic problem

$$\frac{\partial z_{10}}{\partial c} = J_{(1)}. \tag{II.5.4}$$

Since the Jacobian is independent of time, and $z_{10}$ vanishes at initial time, it follows that $z_{10} = 0$ and $J_{(1)} = 0$.

Upon substitution of (II.5.1)–(II.5.3) into the leading-order equations (II.3.10)–(II.3.14), we get the dispersion relation for each short wave from the first-harmonic problem

$$\omega_n^2 = gk_n + \gamma k_n^3. \tag{II.5.5}$$

Note that a Doppler shift is not apparent in the Lagrangian dispersion relation. This is because the Lagrangian coordinates for the short waves are referred to a fluid particle which moves with the long wave. In Appendix II.C we show that by transformation to a stationary Eulerian coordinate system, we can show that the Lagrangian dispersion relation (II.5.5) implies the anticipated Doppler shift due to the long wave.

The evolution equations for three resonant short waves are found at the second order. First, the following resonance conditions must be satisfied

$$\left.\begin{array}{l} \boldsymbol{k}_3 = \boldsymbol{k}_1 + \boldsymbol{k}_2 \\ \omega_3 = \omega_1 + \omega_2 \end{array}\right\} \Rightarrow \theta_3 = \theta_1 + \theta_2, \tag{II.5.6}$$

where each individual wave satisfies the dispersion relation (II.5.5).

Figure II-1 shows a typical geometry of a resonating triad, with wavenumber vectors $\boldsymbol{k}_1$, $\boldsymbol{k}_2$ and $\boldsymbol{k}_3$. The angle between vectors $\boldsymbol{k}_1$ and $\boldsymbol{k}_2$ is denoted by $u_{12}$, as indicated in the figure. This angle is always less than 90° (see the footnote in McGoldrick (1965, p. 309)). We shall therefore denote $\boldsymbol{k}_3$ the shortest wave, and $\boldsymbol{k}_1$ and $\boldsymbol{k}_2$ as the two longer waves.

The second-order solution is assumed to be of the form

$$x_2 \;=\; x_{20} + \frac{\mathrm{i}}{2}\sum_{n=1}^{3}\frac{k_{a,n}}{k_n}\left(x_{21,n}\mathrm{e}^{\mathrm{i}\theta_n} + x_{22,n}\mathrm{e}^{2\mathrm{i}\theta_n}\right) + \text{c.c.}, \tag{II.5.7}$$

$$y_2 = y_{20} + \frac{\mathrm{i}}{2}\sum_{n=1}^{3}\frac{k_{b,n}}{k_n}\left(y_{21,n}\mathrm{e}^{\mathrm{i}\theta_n} + y_{22,n}\mathrm{e}^{2\mathrm{i}\theta_n}\right) + \text{c.c.}, \tag{II.5.8}$$

$$z_2 = z_{20} + \frac{1}{2}\sum_{n=1}^{3}\left(z_{21,n}\mathrm{e}^{\mathrm{i}\theta_n} + z_{22,n}\mathrm{e}^{2\mathrm{i}\theta_n}\right) + \text{c.c.}. \tag{II.5.9}$$

The zeroth harmonics $(x_{20}, y_{20}, z_{20})$ are corrections to the leading-order slow drift, while $(x_{21,n}, y_{21,n}, z_{21,n})$ and $(x_{22,n}, y_{22,n}, z_{22,n})$ are the slowly varying amplitudes of the first and second harmonics, each of which depends on the scales $(a_1, b_1, c, c_1, t_1)$. We only need to consider the first-harmonic displacements. The problem then becomes

$$\frac{\partial z_{21,n}}{\partial c} - \frac{k_{a,n}^2}{k_n}x_{21,n} - \frac{k_{b,n}^2}{k_n}y_{21,n} = E_n, \tag{II.5.10}$$

$$\frac{\partial y_{21,n}}{\partial c} - k_n z_{21,n} = F_n, \tag{II.5.11}$$

$$\frac{\partial x_{21,n}}{\partial c} - k_n z_{21,n} = G_n, \tag{II.5.12}$$

$$z_{21,n} - x_{21,n} = H_n, \qquad z_{21,n} - y_{21,n} = I_n \qquad \text{at} \quad c = 0. \tag{II.5.13}$$

By using MACSYMA, the lengthy expressions $E_n$, $F_n$, $G_n$, $H_n$ and $I_n$ have been obtained, but they are too long to be reproduced here. The above inhomogeneous differential system possesses non-trivial homogeneous solutions, and must be subjected to the following solvability condition for each $n$:

$$\int_{-\infty}^{0}\mathrm{e}^{k_n c}(k_n^2 E_n - k_{a,n}^2 G_n - k_{b,n}^2 F_n)\,\mathrm{d}c = k_{a,n}^2 H_n + k_{b,n}^2 I_n \qquad \text{for} \quad n = 1, 2, 3. \tag{II.5.14}$$

As results of solvability, the evolution equations for the envelopes of the three resonating short waves riding on the long wave are obtained:

$$\frac{\partial A_1}{\partial t_1} + \boldsymbol{c}_{g,1}\cdot\nabla_{\boldsymbol{a}_1}A_1 + \mathrm{i}\beta_1 A_1\cos\phi + \mathrm{i}\alpha_1 A_2^* A_3 = 0, \tag{II.5.15}$$

$$\frac{\partial A_2}{\partial t_1} + \boldsymbol{c}_{g,2}\cdot\nabla_{\boldsymbol{a}_1}A_2 + \mathrm{i}\beta_2 A_2\cos\phi + \mathrm{i}\alpha_2 A_1^* A_3 = 0, \tag{II.5.16}$$

$$\frac{\partial A_3}{\partial t_1} + \boldsymbol{c}_{g,3}\cdot\nabla_{\boldsymbol{a}_1}A_3 + \mathrm{i}\beta_3 A_3\cos\phi + \mathrm{i}\alpha_3 A_1 A_2 = 0. \tag{II.5.17}$$

Here, $\boldsymbol{c}_{g,n}$ is the group velocity

$$\boldsymbol{c}_{g,n} = \frac{g + 3\gamma k_n^2}{2\omega_n}\frac{\boldsymbol{k}_n}{k_n}, \tag{II.5.18}$$

and $\nabla_{\boldsymbol{a}_1} = (\partial/\partial a_1, \partial/\partial b_1)$ is a horizontal gradient operator. The coefficients for nonlinear interaction between short waves are

$$\alpha_n = \frac{k_n}{\omega_n}\alpha, \qquad n = 1, 2, 3, \tag{II.5.19}$$

where

$$16k_1k_2k_3\alpha \equiv g(k_3-k_2-k_1)(k_3-k_2+k_1)(k_3+k_2-k_1)(k_3+k_2+k_1)+ \\ \gamma\left\{(k_1+k_2+k_3)^2\left[k_1^3(k_1-k_2-k_3)+k_2^3(k_2-k_1-k_3)+k_3^3(k_3-k_1-k_2)\right]\right. \\ \left.+4k_1k_2k_3\left[k_1^2(k_2+k_3)+k_2^2(k_1+k_3)+k_3^2(k_1+k_2)\right]\right\}. \qquad \text{(II.5.20)}$$

It can be shown that our nonlinear coefficients are equal to those of McGoldrick (1965) (after correcting a typographical error), Simmons (1969) and Case & Chiu (1977), all derived in the Eulerian frame. The fact that these coefficients are the same in both the Lagrangian and Eulerian descriptions, implies that the second-order nonlinear dynamics is not affected by the transformation of coordinates.

The long-wave phase is

$$\phi = Ka_2 - \Omega t_1 + \arg B, \qquad \text{(II.5.21)}$$

and the long-wave/short-wave interaction coefficients are

$$\beta_n = \left\{\frac{3\omega_n^2K-2k_n\Omega^2}{2\omega_n}\cos^2 v_n - \frac{\Omega^2k_n}{2\omega_n}\right\}|B| \qquad \text{(II.5.22)}$$

$$= K|B|\frac{k_n}{2\omega_n}\left(3\gamma k_n^2\cos^2 v_n - g\sin^2 v_n\right). \qquad \text{(II.5.23)}$$

Here, the angle between the long and the short wavenumber vectors $\boldsymbol{K}$ and $\boldsymbol{k}_n$ is denoted by $v_n$ (see figure II-1).

The first term in (II.5.22) is due to the effectively horizontally accelerated coordinate system inherent in the Lagrangian description of the short waves. This term does not appear in a stationary Eulerian description, e.g. Grimshaw (1988). Except for Naciri & Mei (1992), we are not aware that this kind of interaction term has been considered in previous works on long-wave/short-wave interaction. We show in Appendix II.D that this term does occur in a horizontally accelerated Eulerian coordinate system such that the short waves appear to propagate in a stationary medium. The presence of this interaction term can therefore be considered complementary to the fact that the Lagrangian dispersion relation for the short waves does not have a Doppler shift.

The last term in (II.5.22) accounts for the vertical acceleration of the long-wave surface, and gives a modification to the effective gravitational acceleration felt by the short waves as they ride on top of the long wave. In some works on long-wave/short-wave interaction, e.g. Grimshaw (1988), this modification is accounted for in the dispersion relation for the short wave, and does not appear as part of the interaction coefficient between the long and the short waves.

It is important to note that under the assumed scale ratios, the Lagrangian spatial gradients involve only $a_1, b_1$, but not $a_2, b_2$ . Within the domain defined by $\mathcal{O}(\omega t_1) = 1$ and $\mathcal{O}(ka_1, kb_1) = 1$, the spatial dependence of the long wave is only of parametric significance; only the time dependence matters. Thus the direct effect of the long wave is that of a time periodic, but spatially uniform flow.

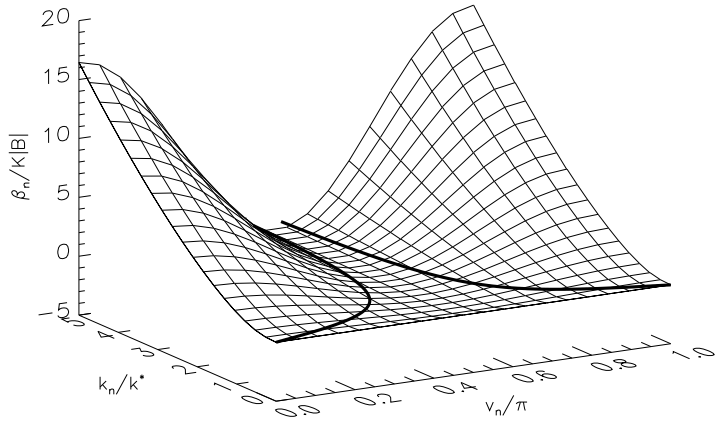


Figure II-2: The long-wave/short-wave interaction coefficient $\beta_n/KB$ as a function of the angle $v_n/\pi$ and the wavenumber $k_n/k^*$. The zero crossings are indicated by thick contour lines.

Each of the coefficients $\beta_n$ is strictly positive if the short and the long waves are collinear, and strictly negative if they are orthogonal. A typical $\beta_n$ vanishes for some intermediate angle of incidence $v_n^*$ independent of the long wave,

$$\tan^2 v_n^* = \frac{3\gamma k_n^2}{g}. \tag{II.5.24}$$

However, all three waves in a resonating triad cannot satisfy (II.5.24) simultaneously, since $v_n^*$ depends on $k_n$. Figure II-2 shows the variation of $\beta_n$ as a function of the short-wave wavenumber $k_n$ and the angle $v_n$ between the short wave and the long wave. The zero crossings of $\beta_n$ are plotted as thick contour curves on the surface.

We remark that in the absence of nonlinear interactions, our coefficients $\beta_n$ can only affect the phase and not the amplitude of a single linear short wave. In a resonating triad, however, the phases of any two waves will affect the amplitude of the third wave through the nonlinear interaction terms. Our long-wave/short-wave interaction coefficients are therefore sufficient to describe both amplitude and phase modulation of the waves in a triad.

We show in Appendix II.E that the density of energy and momentum of the short waves are

$$E = \frac{\rho}{2}\sum_{n=1}^{3}\omega_n\frac{\omega_n}{k_n}|A_n|^2 \quad \text{and} \quad \boldsymbol{M} = \frac{\rho}{2}\sum_{n=1}^{3}\boldsymbol{k}_n\frac{\omega_n}{k_n}|A_n|^2, \tag{II.5.25}$$

respectively. From the evolution equations (II.5.15)–(II.5.17), it can be shown that

the energy and momentum of the short waves are governed by the equations

$$\frac{\rho}{2}\sum_{n=1}^{3}\omega_n\frac{\omega_n}{k_n}\left(\frac{\partial}{\partial t_1}+\boldsymbol{c}_{g,n}\cdot\nabla_{\boldsymbol{a}_1}\right)|A_n|^2=0, \tag{II.5.26}$$

$$\frac{\rho}{2}\sum_{n=1}^{3}\boldsymbol{k}_n\frac{\omega_n}{k_n}\left(\frac{\partial}{\partial t_1}+\boldsymbol{c}_{g,n}\cdot\nabla_{\boldsymbol{a}_1}\right)|A_n|^2=0. \tag{II.5.27}$$

It follows that the change in total energy and momentum within some region is only due to the flux through the boundary of that region. In particular, there is no exchange of energy or momentum between the long and the short waves.

# II.6 Dynamical system for time evolution

The system of partial differential equations (II.5.15)–(II.5.17) is difficult to analyze. We shall restrict the analysis to the special case where the evolution is uniform in the spatial modulation coordinates $\boldsymbol{a}_1$. Since the particle displacement is dominated by the long-wave motion, $\boldsymbol{a}=\boldsymbol{X}-\epsilon^{-1}\boldsymbol{x}_{-1}+\mathcal{O}(\epsilon)$ is essentially the coordinate drifting with fluid particles moved by the long wave. As far as the short-wave evolution is concerned, all particles drift periodically at uniform velocity. Thus $\nabla_{\boldsymbol{a}_1}=0$ means that in this accelerated coordinate system, the short waves are not modulated in space.

However, to be general, we shall allow for a small detuning from resonance. Detuning can be considered as a special type of slow space modulation. Let $(\boldsymbol{k}_n,\omega_n)$ describe the short waves in perfect resonance,

$$\boldsymbol{k}_1+\boldsymbol{k}_2-\boldsymbol{k}_3=0,\quad \omega_1+\omega_2-\omega_3=0,\quad \omega_n=\omega(\boldsymbol{k}_n), \tag{$II.6.1a,b,c$}$$

while $\boldsymbol{k}_n'$ describes the detuned short-wave wavenumber vectors

$$\boldsymbol{k}_n'=\boldsymbol{k}_n+\epsilon\boldsymbol{\delta}_n. \tag{II.6.2}$$

Detuning can be expressed as envelope modulation by the following substitution:

$$A_n=\bar{A}_n\mathrm{e}^{\mathrm{i}\boldsymbol{\delta}_n\cdot\boldsymbol{a}_1},\qquad n=1,2,3. \tag{II.6.3}$$

After this substitution, we drop the horizontal gradient operator $\nabla_{\boldsymbol{a}_1}$ by assuming that the short-wave field $(\bar{A}_n)$ is uniform with respect to the modulation reference coordinates $\boldsymbol{a}_1=(a_1,b_1)$. For consistency, it is then necessary to assume that the wavenumbers satisfy the resonance condition (II.6.1a) exactly, hence

$$\boldsymbol{\delta}_1+\boldsymbol{\delta}_2-\boldsymbol{\delta}_3=0. \tag{II.6.4}$$

In the following, it is convenient to employ the normalized variables

$$t=-\phi=-(Ka_2-\Omega t_1+\arg B), \tag{II.6.5}$$

$$A'_n = \sqrt{\frac{\omega_n}{k_n}}\bar{A}_n, \qquad \beta'_n = \frac{\beta_n}{\Omega}, \qquad \alpha' = \frac{2\alpha}{\Omega}\sqrt{\frac{k_1k_2k_3}{\omega_1\omega_2\omega_3}}, \qquad \Delta'_n = \frac{\boldsymbol{c}_{g,n}\cdot\boldsymbol{\delta}_n}{\Omega}. \quad \text{(II.6.6)}$$

The evolution equations then become

$$\frac{\partial A'_1}{\partial t} = -\mathrm{i}\frac{\alpha'}{2}A'^*_2A'_3 - \mathrm{i}\beta'_1A'_1\cos t - \mathrm{i}\Delta'_1A'_1, \quad \text{(II.6.7)}$$

$$\frac{\partial A'_2}{\partial t} = -\mathrm{i}\frac{\alpha'}{2}A'^*_1A'_3 - \mathrm{i}\beta'_2A'_2\cos t - \mathrm{i}\Delta'_2A'_2, \quad \text{(II.6.8)}$$

$$\frac{\partial A'_3}{\partial t} = -\mathrm{i}\frac{\alpha'}{2}A'_1A'_2 - \mathrm{i}\beta'_3A'_3\cos t - \mathrm{i}\Delta'_3A'_3. \quad \text{(II.6.9)}$$

We now introduce polar coordinates $A'_n = \sqrt{I_n}\mathrm{e}^{\mathrm{i}\theta_n}$ where $I_n \geq 0$. Note that in physical variables, $I_n = \frac{\omega_n}{k_n}|A_n|^2$ is proportional to the wave action of the $n$th short wave (see Appendix II.E). After separating the real and imaginary parts, we get a system of six real equations.

$$\frac{\partial I_1}{\partial t} = \frac{\partial I_2}{\partial t} = -\frac{\partial I_3}{\partial t} = -\alpha'\sqrt{I_1I_2I_3}\sin(\theta_1+\theta_2-\theta_3), \quad \text{(II.6.10)}$$

$$\frac{\partial}{\partial t}\begin{pmatrix}\theta_1\\ \theta_2\\ \theta_3\end{pmatrix} = -\frac{\alpha'}{2}\begin{pmatrix}\sqrt{\frac{I_2I_3}{I_1}}\\ \sqrt{\frac{I_1I_3}{I_2}}\\ \sqrt{\frac{I_1I_2}{I_3}}\end{pmatrix}\cos(\theta_1+\theta_2-\theta_3) - \begin{pmatrix}\beta'_1\\ \beta'_2\\ \beta'_3\end{pmatrix}\cos t - \begin{pmatrix}\Delta'_1\\ \Delta'_2\\ \Delta'_3\end{pmatrix}. \quad \text{(II.6.11)}$$

Note that

$$J_1 = I_1 + I_3 \qquad \text{and} \qquad J_2 = I_2 + I_3 \quad \text{(II.6.12)}$$

are constant in time. They are the sums of the wave actions of the shortest wave and one of the longer waves.

The dimension of this dynamical system can be reduced from six to two by using the conserved quantities $J_1$ and $J_2$, and the fact that the phase angles appear in only one combination. Let

$$\psi = \theta_1+\theta_2-\theta_3, \qquad \beta = \beta'_3-\beta'_2-\beta'_1, \qquad \Delta = \Delta'_3-\Delta'_2-\Delta'_1 \qquad \text{and} \qquad J = I_3, \quad \text{(II.6.13)}$$

where $J$ is the normalized wave action of the shortest wave. The new equations for $J$ and $\psi$ are

$$\frac{\partial J}{\partial t} = \alpha'\sqrt{J(J_1-J)(J_2-J)}\sin\psi, \quad \text{(II.6.14)}$$

$$\frac{\partial \psi}{\partial t} = -\frac{1}{2}\alpha'\frac{-3J^2+2(J_1+J_2)J-J_1J_2}{\sqrt{J(J_1-J)(J_2-J)}}\cos\psi + \Delta + \beta\cos t. \quad \text{(II.6.15)}$$

The phase angles $\theta_1$ and $\theta_2$ decouple and can be found after $J$ and $\psi$ are solved,

$$\frac{\partial \theta_1}{\partial t} = -\frac{\alpha'}{2}\sqrt{\frac{(J_2-J)J}{J_1-J}}\cos\psi - \beta'_1\cos t - \Delta'_1, \quad \text{(II.6.16)}$$

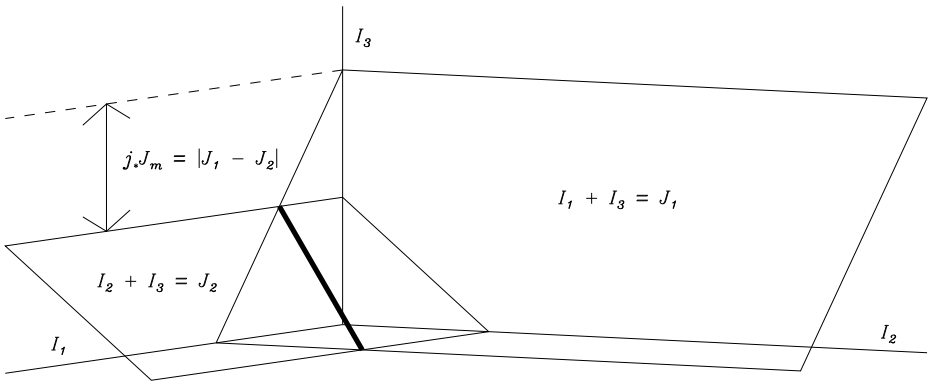


Figure II-3: Intersection between two planes. Each axis represents the wave-action of each short wave. The action conservation laws are indicated as planes. The exchange of action between the three resonating waves must happen along the line of intersection. The asymmetry between the two planes is indicated in terms of $j_*$.

$$\frac{\partial \theta_2}{\partial t} \;=\; -\frac{\alpha'}{2}\sqrt{\frac{(J_1 - J)J}{J_2 - J}}\cos\psi - \beta_2' \cos t - \Delta_2'. \qquad \text{(II.6.17)}$$

Thus the original set of six real equations is reduced to a non-autonomous dynamical system of second order for $J$ and $\psi$.

If $I_1$, $I_2$ and $I_3$ are used to form a rectilinear coordinate system, the conserved quantities $J_1$ and $J_2$ define two planes. The line of intersection between the two planes defines the range of $J$. Since $I_n \geq 0$, only the segment extending from $J = 0$ to $J = \min\{J_1, J_2\}$ is physically meaningful, as sketched in figure II-3. All exchange of action between the short waves is confined to this line segment. As a further simplification, we define $0 \leq j \leq 1$ by

$$J = J_m(1 - j) \qquad \text{where} \qquad J_m = \min\{J_1, J_2\}. \qquad \text{(II.6.18)}$$

Hence $j = 1$ corresponds to $I_3 = 0$ and $j = 0$ corresponds to the maximum $I_3$. Thus $(1 - j)$ is a measure of the action of the shortest wave.

Let us introduce the parameters

$$j_* = \frac{|J_1 - J_2|}{J_m} \geq 0, \qquad r = \alpha'\sqrt{J_m}. \qquad \text{(II.6.19)}$$

The normalized parameter $j_*$ vanishes when the wave actions of the two longer waves are equal, and hence is a measure of the asymmetry in action between the two longer waves, see figure II-3. The parameter $r$ is proportional to the maximum amplitude attainable by the shortest wave.

In figure II-4 we show surface plots of the effective long-wave parameter $\beta$ as a function of the wavenumber $k_1$ and the angle $v_1$ for $u_{12} = 30°$, $u_{12} = 45°$ and $u_{12} = 70°$. In general, when the angle between the resonating waves $u_{12}$ is small, $\beta$ is insensitive to variations in the angle of incidence of the long wave $v_1$. When the

angle between the resonating waves is large, $\beta$ varies significantly with the long-wave angle of incidence. In particular, if $u_{12} > 44^\circ$ (approximately), it is possible to have $\beta = 0$ while the interaction coefficients $\beta_1$, $\beta_2$, $\beta_3$ are individually non-zero. The zero crossings of $\beta$ are plotted as thick contour curves on the surface. When $\beta$ vanishes, the influence of the long wave is not dynamically significant for the triad *at this order*, and will only give a trivial phase shift.

In terms of $j$ and $\psi$ the dynamical system becomes

$$\frac{dj}{dt} = -r\sqrt{(1-j)j(j+j_*)}\sin\psi = \frac{\partial H}{\partial \psi}, \tag{II.6.20}$$

$$\frac{d\psi}{dt} = r\frac{3j^2 - 2j + 2j_*j - j_*}{2\sqrt{(1-j)j(j+j_*)}}\cos\psi + \Delta + \beta\cos t = -\frac{\partial H}{\partial j}, \tag{II.6.21}$$

where $H$ is the time-dependent Hamiltonian defined by

$$H(j,\psi;t) = r\sqrt{(1-j)j(j+j_*)}\cos\psi - (\Delta + \beta\cos t)j. \tag{II.6.22}$$

In the special case of $j_* = 0$ , the equations reduce to a much simpler form

$$\frac{dj}{dt} = -rj\sqrt{1-j}\sin\psi, \tag{II.6.23}$$

$$\frac{d\psi}{dt} = r\frac{3j-2}{2\sqrt{1-j}}\cos\psi + \Delta + \beta\cos t. \tag{II.6.24}$$

This occurs when the two longer waves $\boldsymbol{k}_1$ and $\boldsymbol{k}_2$ have the same wave action. Then $J_1 = J_2$ and $j_* = 0$. A special case is Wilton's ripples for which $\boldsymbol{k}_1 = \boldsymbol{k}_2$.

We remark that laboratory experiments in the literature fall into two categories. They either consider collinear Wilton's ripples, e.g. McGoldrick (1970), Henderson & Hammack (1987), or they correspond to the initial condition that only the shortest wave has finite amplitude, while the two longer waves start out with infinitesimal amplitudes, e.g. Banerjee & Korpel (1982), Henderson & Hammack (1987), Perlin *et al.* (1990). Hence all of these experiments correspond to $j_* = 0$.

# II.7 Analytical solution without the long wave

In the absence of the long wave ($\beta = 0$), the temporal solution of the conservative three-wave equations, with and without detuning, has been discussed before. Bifurcation properties of steady solutions for certain special triads have been discussed by Chen & Saffman (1979) for collinear Wilton's ripples, and independently by Reeder & Shinbrot (1981a) and Ma (1982) for three-dimensional triads where the wavenumber vectors form an isosceles triangle.

In order to facilitate the subsequent analysis of the effect of the long wave, we first summarize the known analytical solution, and illustrate properties of the phase portrait and the bifurcations that may occur due to detuning. In particular we point out that the bifurcation criterion found previously for certain special triad

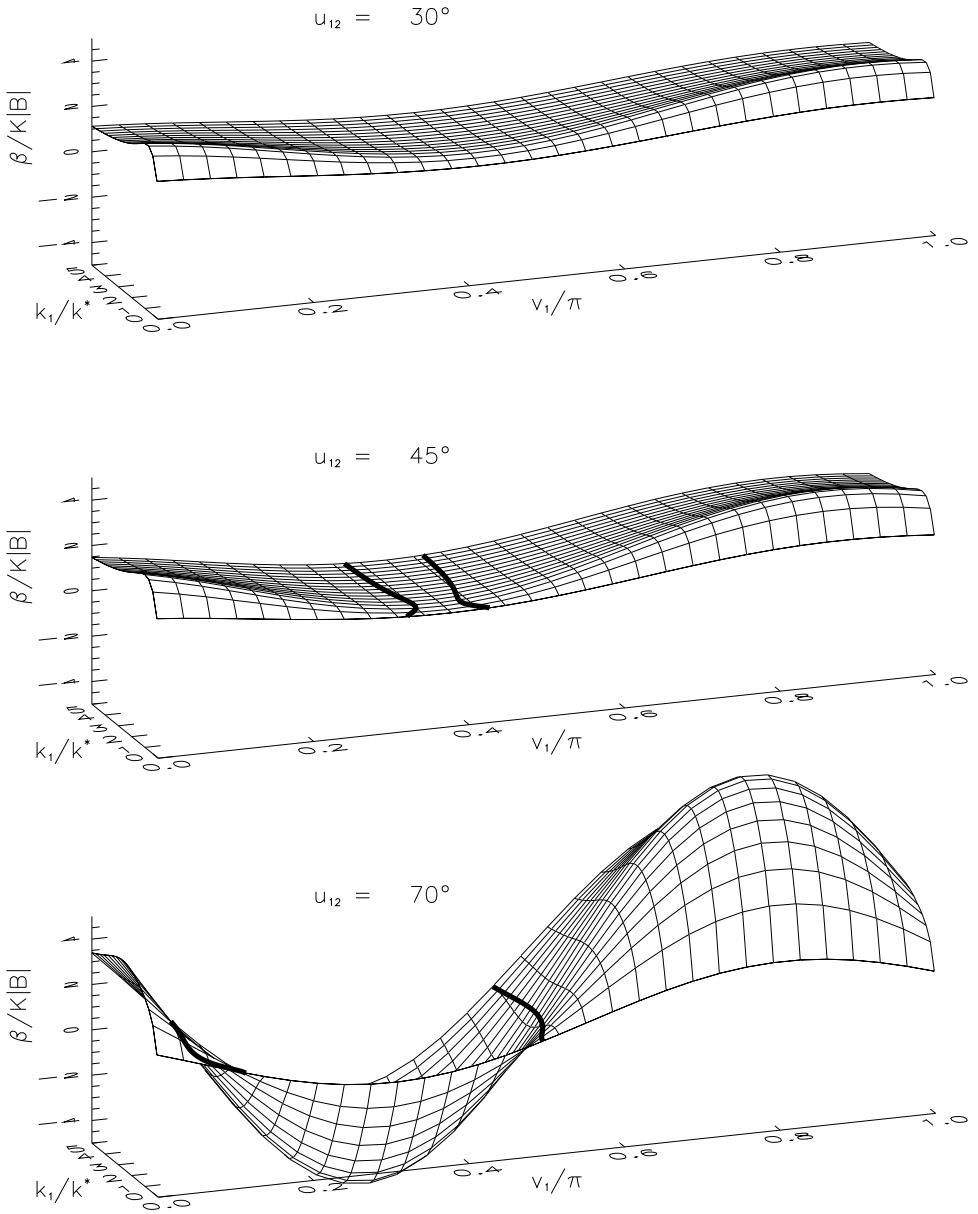


Figure II-4: The effective long-wave/short-wave interaction coefficient $\beta/K|B|$ as a function of the angle of incidence $v_1/\pi$ and the wavenumber $k_1/k^*$ in the range (0.1, 5.0) for three selected angles $u_{12} = 30°$, $u_{12} = 45°$ and $u_{12} = 70°$. The zero-crossings are indicated by thick contour lines.

configurations, can be extended to any resonating triad as long as the wave actions of the two longer waves are equal.

The variable $\psi$ can be eliminated from the system (II.6.20)–(II.6.21) by using the Hamiltonian (II.6.22). The resulting equation for $j$ is

$$\frac{\mathrm{d}j}{\mathrm{d}t} = \pm\sqrt{r^2(1-j)j(j+j_*) - (H+\Delta j)^2} = \pm r\sqrt{(h_2-j)(j-h_1)(j-h_0)}, \quad \text{(II.7.1)}$$

where $h_0$, $h_1$ and $h_2$ are the zeroes of the radicand. We let

$$h_0 \le 0 \le h_1 \le j \le h_2 \le 1, \quad \text{(II.7.2)}$$

such that $h_1$ and $h_2$ are the lower and upper bounds for $j$.

If we take the initial condition $j(0) = h_2$, the negative sign must be taken in (II.7.1), and the solution is

$$j(t) = h_2 - (h_2 - h_1)\,\mathrm{sn}^2(\frac{rt}{2}\sqrt{h_2-h_0}, m). \quad \text{(II.7.3)}$$

Here sn is a Jacobi elliptic function, and the parameter

$$m = \sqrt{\frac{h_2-h_1}{h_2-h_0}} \quad \text{(II.7.4)}$$

is defined according to Gradshteyn & Ryzhik (1980). The period $\mathcal{T}$ of modulational oscillation is given by the complete elliptic integral of the first kind, K,

$$\mathcal{T} = \frac{4}{r\sqrt{h_2-h_0}}\,\mathrm{K}(m). \quad \text{(II.7.5)}$$

These results are well know, see e.g. Craik (1985).

The parameter $m$ is in the range $0 \le m \le 1$. In the limit $m = 0$, we have $h_1 = h_2$ and sn $\to$ sin. The solution reduces to a fixed point of (II.6.20)–(II.6.21) with $\beta = 0$,

$$j = j_c = h_1, \qquad \psi = \psi_c \in \{0, \pi\}. \quad \text{(II.7.6)}$$

The value $j_c$ is the solution of

$$(3j_c^2 - 2j_c + 2j_*j_c - j_*)\cos\psi_c = -\frac{2\Delta}{r}\sqrt{(1-j_c)j_c(j_c+j_*)}. \quad \text{(II.7.7)}$$

Of particular interest is the special case when $j_* = 0$; the solution is then

$$j_c = \frac{6 - 2(\frac{\Delta}{r})^2 \pm 2\sqrt{(\frac{\Delta}{r})^4 + 3(\frac{\Delta}{r})^2}}{9}, \quad \text{(II.7.8)}$$

see figure II-5. In the absence of detuning ($\Delta = 0$), the solution asymptotes to $j_c = \frac{1}{2}$,

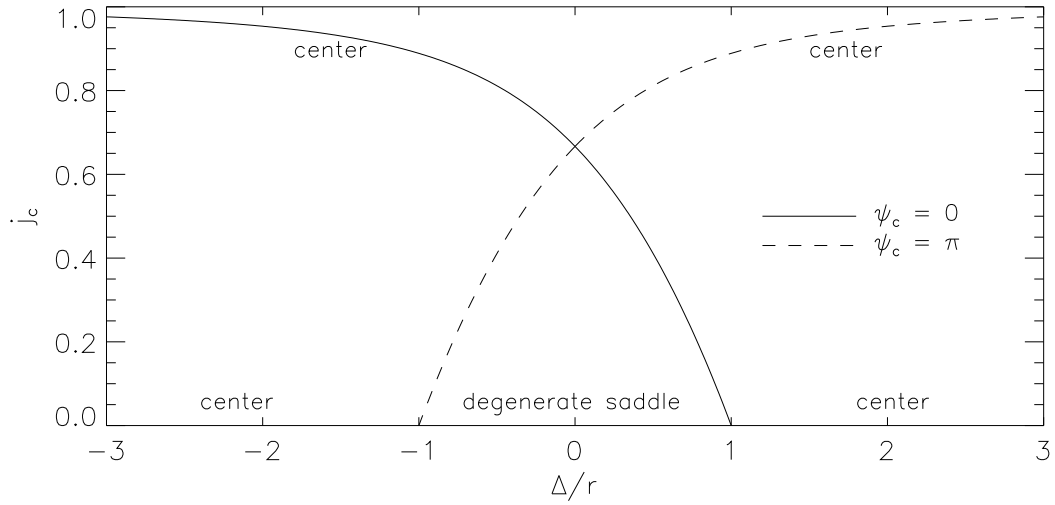


Figure II-5: Bifurcation diagram for the location $j_c$ of centers when $j_* = 0$ and $-3 < \Delta/r < 3$. $j = 0$ is a fixed point for all $\Delta/r$. The generalized bifurcation of Chen & Saffman (1979) is seen at $j = 0$ and $\Delta/r = \pm 1$. Solid line $\psi_c = 0$, dashed line $\psi_c = \pi$.

and is given by

$$j_c = \frac{1 - j_* + \sqrt{1 + j_* + j_*^2}}{3}, \tag{II.7.9}$$

which is shown in figure II-6. The figure indicates that in this case, the range of $j_c$ is between $\frac{1}{2}$ and $\frac{2}{3}$.

By linearization of (II.6.20)–(II.6.21) about $(j_c, \psi_c)$, we get

$$\frac{\mathrm{d}}{\mathrm{d}t}\begin{pmatrix} j - j_c \\ \psi - \psi_c \end{pmatrix} = r\cos\psi_c \begin{pmatrix} 0 & -\sqrt{(1-j_c)j_c(j_c+j_*)} \\ \frac{3j_c - 1 + j_* + (\frac{\Delta}{r})^2}{\sqrt{(1-j_c)j_c(j_c+j_*)}} & 0 \end{pmatrix} \begin{pmatrix} j - j_c \\ \psi - \psi_c \end{pmatrix}, \tag{II.7.10}$$

which shows that $(j_c, \psi_c)$ is a center. The frequency of oscillation around the center is

$$\lambda = r\sqrt{3j_c - 1 + j_* + (\frac{\Delta}{r})^2}, \tag{II.7.11}$$

in accordance with (II.7.5) with $m = 0$.

For further insight into the behavior in terms of the variables $j$ and $\psi$, it is convenient to regard these as coordinates on a sphere, with $j\pi$ being the latitude measured from the south pole, and $\psi$ the longitude. Thus $j = 0$ (only the shortest wave is present) corresponds to the south pole and $j = 1$ (the shortest wave is absent) the north pole. We perform local analyses at the poles to understand the behavior there.

Near the south pole $j = 0$, i.e. when the shortest wave $\boldsymbol{k}_3$ is much bigger than the

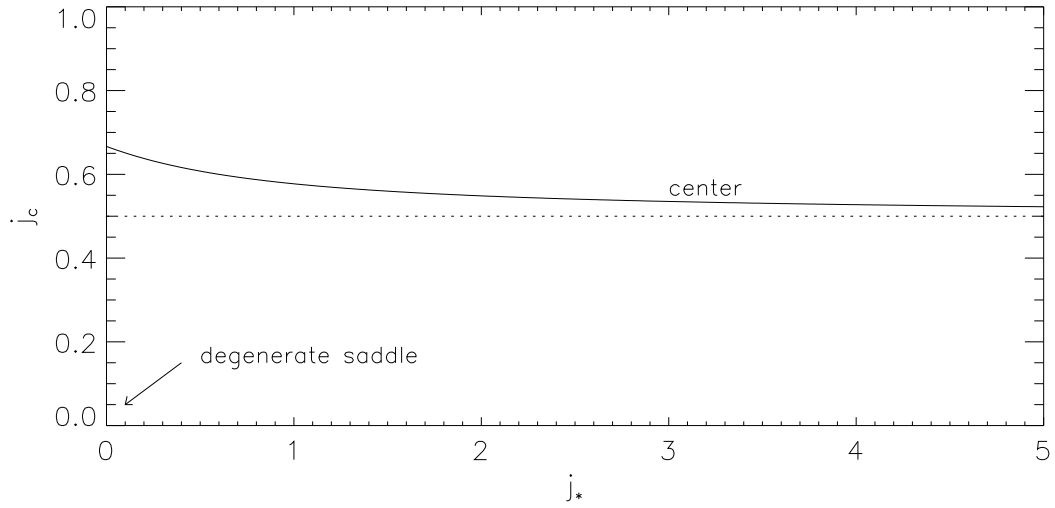


Figure II-6: Diagram for the location $j_c$ of centers when $\Delta = 0$ and $0 \leq j_* \leq 5$.

other two of the triad, let us introduce new coordinates

$$x = \sqrt{j}\cos\psi, \qquad y = \sqrt{j}\sin\psi \tag{II.7.12}$$

in (II.6.20)–(II.6.21). When $j_* > 0$, we get to the zeroth order in $x$ and $y$,

$$\frac{\mathrm{d}x}{\mathrm{d}t} = 0, \qquad \frac{\mathrm{d}y}{\mathrm{d}t} = -\frac{r\sqrt{j_*}}{2}. \tag{II.7.13}$$

Hence the south pole has a finite flow in the negative $y$-direction. For $j_* = 0$, the above approximation is inadequate, and it is more convenient to return to the polar representation. To the zeroth order in $\sqrt{j}$, we have

$$\frac{\mathrm{d}\sqrt{j}}{\mathrm{d}t} = 0, \qquad \frac{\mathrm{d}\psi}{\mathrm{d}t} = -r\cos^3\psi + \Delta. \tag{II.7.14}$$

The south pole is now a fixed point. When $|\Delta/r| > 1$, it is a center. When $|\Delta/r| < 1$, it is a "saddle" point, with invariant stable and unstable directions along the two rays ($\psi$ constant) determined by

$$\cos^3\psi = \frac{\Delta}{r}. \tag{II.7.15}$$

Hence the situation that only the shortest wave $\boldsymbol{k}_3$ is present, is an unstable equilibrium solution. Because there is only one stable and one unstable eigendirection, this fixed point will be called a degenerate saddle.

By a similar analysis it can be shown that the north pole $j = 1$ (i.e. the shortest wave is not present), is never a fixed point.

The stable and unstable eigendirections of the degenerate saddle are part of a homoclinic trajectory. This occurs in the limit $m = 1$ in (II.7.4), and the solution

reduces to

$$j = (1 - (\frac{\Delta}{r})^2)\,\mathrm{sech}^2\,\frac{rt}{2}, \qquad \cos\psi = \frac{\Delta}{r\sqrt{1 - (1 - (\frac{\Delta}{r})^2)\,\mathrm{sech}^2\,\frac{rt}{2}}}. \tag{II.7.16}$$

This happens only when $j_* = 0$ and

$$\left|\frac{\Delta}{r}\right| < 1. \tag{II.7.17}$$

Chen & Saffman (1979) discussed the bifurcations of steady solutions for collinear Wilton's ripples. They gave the criterion that if the height ($h$) of a steady second-harmonic wave (wavenumber $2k$) exceeds

$$h > \frac{4}{3k}\left|\frac{Tk^2}{\rho g} - \frac{1}{2}\right|, \tag{II.7.18}$$

then the second-harmonic wave can bifurcate into a steady sum of the first and second-harmonic waves. To the leading order in detuning, their condition is a special limit of the bifurcation condition (II.7.17) in the special case of Wilton's ripples. The bifurcation can be seen in figure II-5 as the branching of the center curve (II.7.8) away from $j = 0$. At the branch point, $j = 0$ changes from being a center to a saddle.

To see that (II.7.17) reduces to (II.7.18) for Wilton's ripples, we drop the ordering parameter $\epsilon$, and set

$$k_1 = k_2 = \frac{1}{2}k_3 = \sqrt{\frac{g}{2\gamma}} \qquad \text{and} \qquad \delta_1 = \delta_2 = \frac{1}{2}\delta_3 = k - k_1.$$

The following quantities can then be calculated

$$c_{g,1} = c_{g,2} = \frac{5g}{4\omega_1}, \quad c_{g,3} = \frac{7g}{4\omega_1}, \quad \Delta = \frac{g}{\omega_1}(k - k_1), \quad \alpha = \frac{3}{2}\gamma k_1^3, \quad r = \frac{3\gamma k_1^4 h}{\omega_1}.$$

Our condition (II.7.17) then becomes

$$h > \frac{4}{3k}\left|\frac{\gamma k^2}{g} - \frac{1}{2} - \frac{\delta_1}{2k_1}\right|,$$

which is the same as (II.7.18) within the order of the detuning $\mathcal{O}(\delta_1/k_1) = \mathcal{O}(\epsilon)$.

Reeder & Shinbrot (1981a) and Ma (1982) generalized the analysis of Chen & Saffman (1979) to three-dimensional triads for which the amplitudes of the two longer waves are equal and the wavenumber vectors form an isosceles triangle. We have now shown that this bifurcation can occur for any resonating triad, as long as $j_* = 0$, i.e. whenever the wave actions of the two longer waves are equal.

The existence of the degenerate saddle point, which is predicted by the bifurcation condition, will be found to have an important consequence for the onset of chaotic behavior in the presence of a long wave.

The possible phase portraits are simply contours of constant Hamiltonian, and are presented in figure II-7. The two important parameters that determine the qualitative phase space behavior are $j_*$ and $|\Delta/r|$. When $j_* > 0$, there are only two centers, at $\psi = 0$ and $\psi = \pi$, and with $0 < j_c < 1$. When $j_* = 0$ there are two centers, and if $|\Delta/r| < 1$ there is an additional degenerate saddle point. The homoclinic loop of the saddle is highlighted as a thick curve in figure II-7.

In figure II-8 the frequency of the closed orbits, $2\pi/r\mathcal{T}$, is plotted as a function of the value of $j$ where the orbit crosses $\psi = 0$ or $\psi = \pi$, for selected values of $j_*$ and $\Delta/r$. The value along the abscissa ($j$) first increases from 0 to 1 corresponding to $\psi = 0$, and then decreases from 1 back to 0 corresponding to $\psi = \pi$. While the homoclinic orbit is non-periodic with zero frequency, large values of $j_*$ causes all orbits to have approximately the same frequency. This has an important physical consequence in our later analysis of the effect of the long wave: When there is a broad range of natural oscillation frequencies, the triad can be exited more easily by the long wave. The broadest range of natural frequencies happens for $j_* = 0$ and moderate detuning.

## II.8 Effects of a weak long wave

We shall now discuss the effect of the long wave on the triad. In this section we derive approximate analytical results by assuming that the long-wave forcing coefficient $\beta$ is sufficiently small that a perturbation approach can be employed. Numerical confirmation by integration of the original evolution equations will be presented afterward. In the next section we consider a much stronger long-wave disturbance numerically.

Corresponding to the closed orbits, the typical behavior of triad resonance is the periodic modulation of the envelopes, as found analytically in section II.7. If the period of the long wave is on the same timescale, the natural modulation oscillations of the envelope may then be resonated. We denote this *modulational resonance*, to distinguish it from the basic wave resonance between the three short waves.

A natural way to present the dynamics of the disturbed triad is to use the Poincaré map, defined to be either the first, second or third return map, depending on the situation that one wants to study[3]. These maps are defined by sampling the state of the triad periodically with a time interval equal to one, two or three periods of the long-wave oscillation, respectively. For example, the Poincaré first return map corresponds to sampling at times $t = 2\pi n$ for $n = 1, 2, 3, \ldots$.

We first carry out a perturbation analysis for the case of no modulational resonance, and then consider two cases of modulational resonances. Specifically, a small parameter $\mu \ll 1$ will be used to characterize the envelope modulation, and will be distinguished from $\epsilon \ll 1$ in the original perturbation analysis. We use the normalized time coordinate $t$ as defined by (II.6.5), to be the basic time for modulation of the envelope. Within the basic time range of $t = \mathcal{O}(1)$, we allow a cascade of slow times $\mu t, \mu^2 t, \ldots$. In this section, indices always refer to the order in terms of $\mu$.

[3]These are the only three maps that we need to consider.

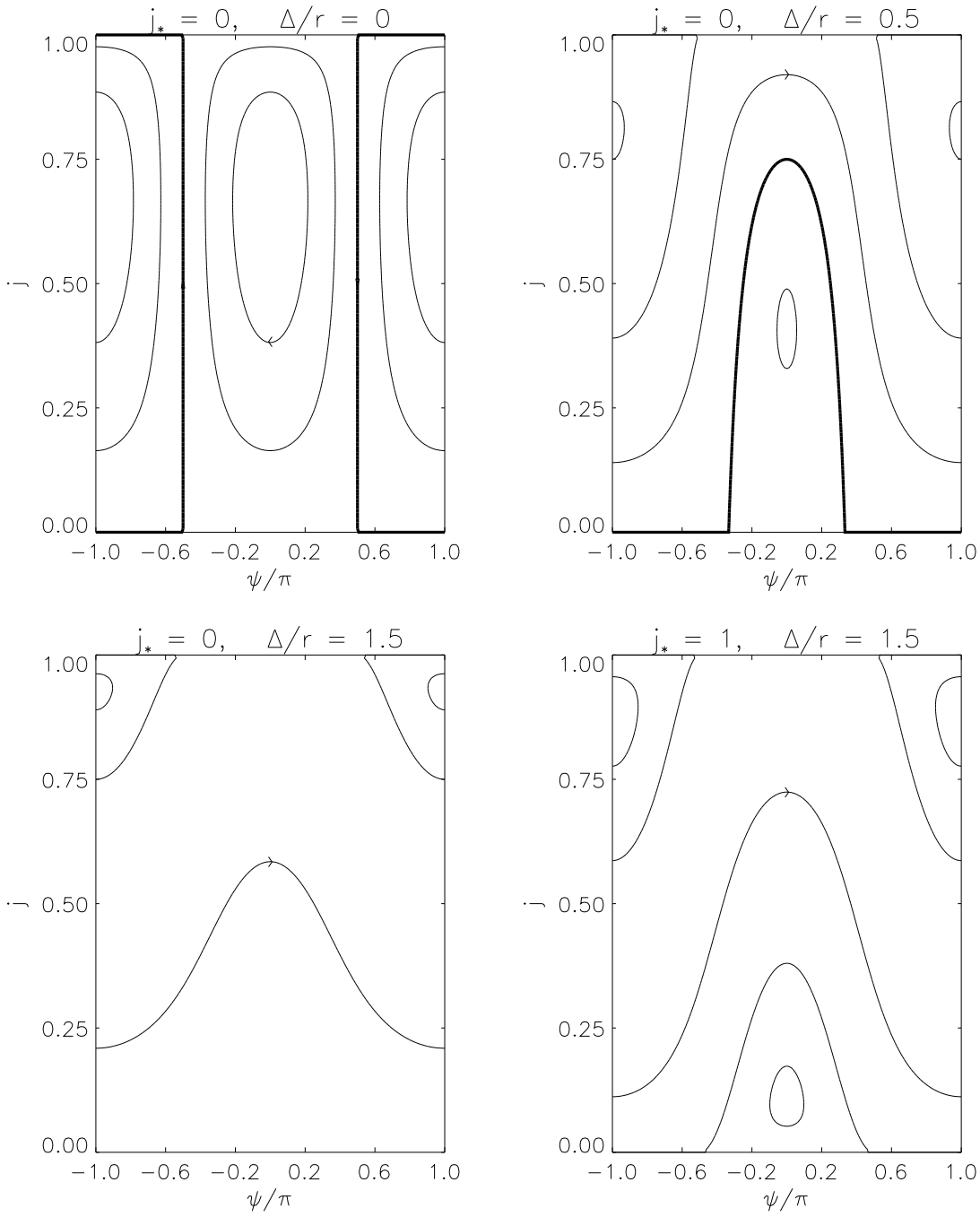


Figure II-7: Phase portraits $(j, \psi)$ for the autonomous system. (a) $j_* = 0$, $\Delta/r = 0$; (b) $j_* = 0$, $\Delta/r = 0.5$; (c) $j_* = 0$, $\Delta/r = 1.5$; (d) $j_* = 1$, $\Delta/r = 1.5$. The homoclinic trajectory is drawn as a thick line in (a) and (b).

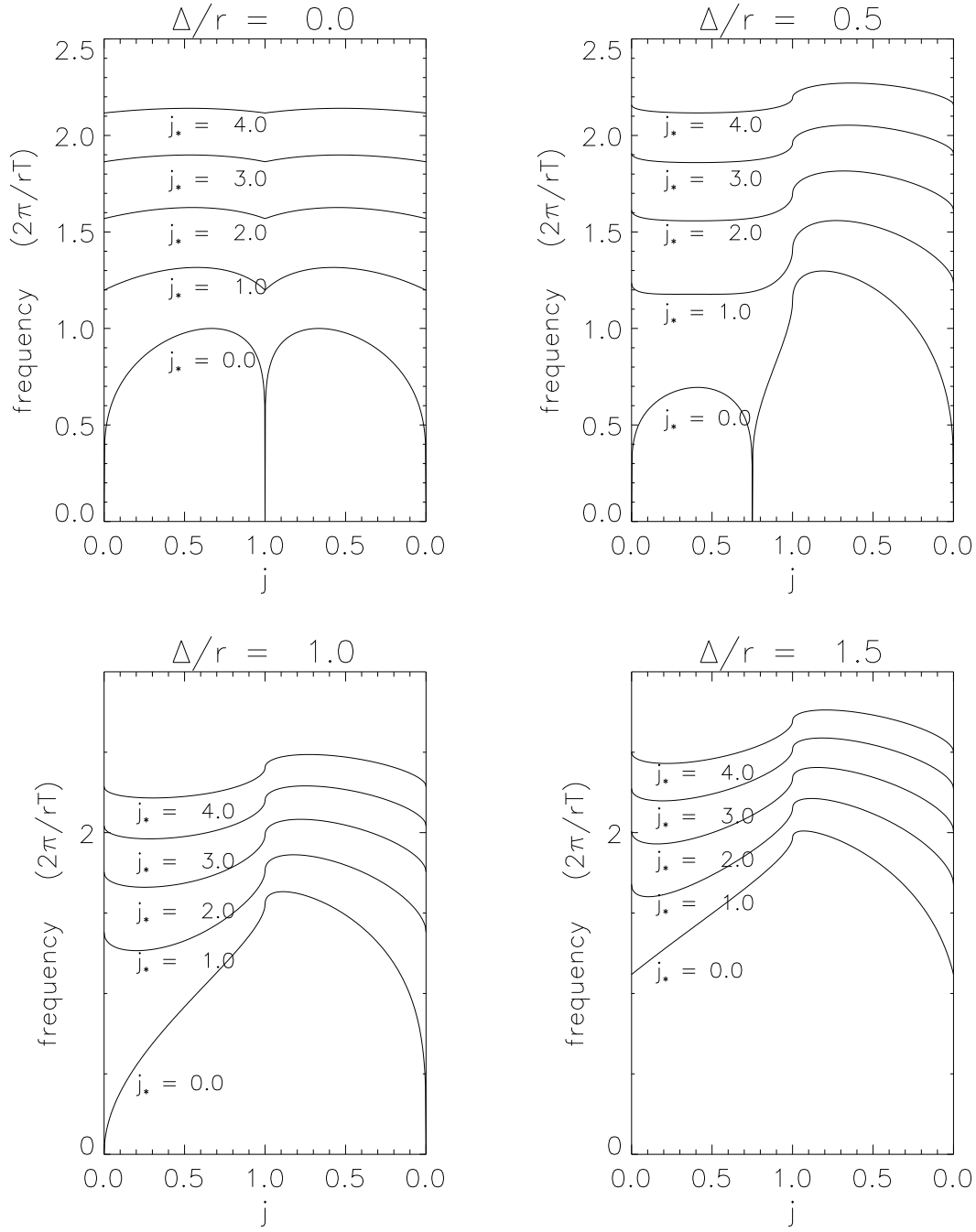


Figure II-8: Frequency of envelope oscillation, $2\pi/r\mathcal{T}$, of the autonomous system. Along the first axis, $j$ first increases from 0 to 1 corresponding to $\psi = 0$, then decreases from 1 to 0 corresponding to $\psi = \pi$. (a) $\Delta/r = 0$, (b) $\Delta/r = 0.5$, (c) $\Delta/r = 1$, (d) $\Delta/r = 1.5$

The starting equations are (II.6.20)–(II.6.21). It suffices to consider only perturbations around the center at $\psi_c = 0$, see equation (II.7.9) and figure II-5. By the symmetry of the governing equations, the solution near $\psi_c = \pi$ can be obtained by translating $\psi \to \pi - \psi$ and changing the signs of $\beta$ and $\Delta$. For simplicity, we consider only $\Delta = 0$, with extensions for $\Delta \neq 0$ being straightforward.

## II.8.1 Non-resonant long wave

Let us assume that the long wave is weak such that $\beta = \mu\beta_1$. We also assume a slow modulational time $\tau = \mu^2 t$. Solutions will be sought in the perturbation expansions

$$j = j_c + \mu j_1 + \mu^2 j_2 + \mu^3 j_3 + \cdots, \tag{II.8.1}$$
$$\psi = \psi_c + \mu\psi_1 + \mu^2\psi_2 + \mu^3\psi_3 + \cdots, \tag{II.8.2}$$

where all $j_n$, $\psi_n$ depend on the fast and the slow times.

We choose to express $j_*$ in terms of $j_c$:

$$j_* = \frac{2j_c - 3j_c^2}{2j_c - 1}. \tag{II.8.3}$$

In order to simplify the equations, we introduce the notation:

$$\mathcal{S} \equiv \sqrt{3j_c^2 - 3j_c + 1}. \tag{II.8.4}$$

At the leading order $\mathcal{O}(\mu)$, we get

$$\frac{\mathrm{d}j_1}{\mathrm{d}t} - \frac{(j_c - 1)j_c r}{\sqrt{2j_c - 1}}\psi_1 = 0, \tag{II.8.5}$$
$$\frac{\mathrm{d}\psi_1}{\mathrm{d}t} + \frac{\mathcal{S}^2 r}{(j_c - 1)j_c\sqrt{2j_c - 1}}j_1 = \beta_1 \cos t. \tag{II.8.6}$$

These are the equations for a linear oscillator with a natural frequency $\lambda$ given by (II.7.11), but forced at the frequency 1. The first-order response must therefore be of the form

$$j_1 = p_1 \mathrm{e}^{\mathrm{i}\lambda t} + q_1 \mathrm{e}^{\mathrm{i}t} + \text{c.c.}, \tag{II.8.7}$$
$$\psi_1 = r_1 \mathrm{e}^{\mathrm{i}\lambda t} + s_1 \mathrm{e}^{\mathrm{i}t} + \text{c.c.}, \tag{II.8.8}$$

where c.c. denotes the complex conjugate. The complex amplitudes of the free oscillation, $p_1$ and $r_1$, are so far arbitrary functions of the slow time, while the amplitudes of the forced oscillation, $q_1$ and $s_1$, are constants. Their detailed forms are not of particular interest, and are omitted here.

Due to nonlinear interactions and the long wave, the following harmonics will be

forced at the higher orders of $\mu$:

$$\left.\begin{array}{rcl} \mathcal{O}(\mu) & : & 1 \\ \mathcal{O}(\mu^2) & : & 2\lambda,\ \lambda+1,\ \lambda-1,\ 2,\ 0 \\ \mathcal{O}(\mu^3) & : & 3\lambda,\ 2\lambda+1,\ 2\lambda-1,\ \lambda+2,\ \lambda-2,\ \lambda,\ 3,\ 1 \\ \text{etc.} & & \end{array}\right\} \tag{II.8.9}$$

In this subsection we assume that all of the harmonics listed above, except $\lambda$ itself, are different from $\lambda$, so that resonant forcing only occurs at $\mathcal{O}(\mu^3)$. We must now allow $p_1$ to vary with $\tau$ in order to avoid secular forcing at frequency $\lambda$.

At the second order in $\mu$, we have

$$\frac{\mathrm{d}j_2}{\mathrm{d}t} - \frac{(j_c-1)j_c r}{\sqrt{2j_c-1}}\psi_2 = 0, \tag{II.8.10}$$

$$\frac{\mathrm{d}\psi_2}{\mathrm{d}t} + \frac{\mathcal{S}^2 r}{(j_c-1)j_c\sqrt{2j_c-1}}j_2 = -\frac{3r\sqrt{2j_c-1}}{2(j_c-1)j_c}j_1^2. \tag{II.8.11}$$

The solution is of the form

$$j_2 = p_{20} + p_{21}\mathrm{e}^{\mathrm{i}\lambda t} + p_{22}\mathrm{e}^{2\mathrm{i}\lambda t} + p_{23}\mathrm{e}^{\mathrm{i}(\lambda+1)t} + p_{24}\mathrm{e}^{\mathrm{i}(\lambda-1)t} + q_{22}\mathrm{e}^{2\mathrm{i}t} + \text{c.c.}, \tag{II.8.12}$$

$$\psi_2 = r_{20} + r_{21}\mathrm{e}^{\mathrm{i}\lambda t} + r_{22}\mathrm{e}^{2\mathrm{i}\lambda t} + r_{23}\mathrm{e}^{\mathrm{i}(\lambda+1)t} + r_{24}\mathrm{e}^{\mathrm{i}(\lambda-1)t} + s_{22}\mathrm{e}^{2\mathrm{i}t} + \text{c.c.} \tag{II.8.13}$$

The solutions of the coefficients are omitted here for brevity.

At the third order, we have

$$\begin{aligned} \frac{\mathrm{d}j_3}{\mathrm{d}t} - \frac{(j_c-1)j_c r}{\sqrt{2j_c-1}}\psi_3 &= -\frac{\mathcal{S}^2 r}{2(j_c-1)j_c\sqrt{2j_c-1}}j_1^2\psi_1 - \frac{(j_c-1)j_c r}{6\sqrt{2j_c-1}}\psi_1^3 \\ &\quad - \frac{\mathrm{d}j_1}{\mathrm{d}\tau} \end{aligned} \tag{II.8.14}$$

$$\begin{aligned} \frac{\mathrm{d}\psi_3}{\mathrm{d}t} + \frac{\mathcal{S}^2 r}{(j_c-1)j_c\sqrt{2j_c-1}}j_3 &= \frac{\mathcal{S}^2 r}{2(j_c-1)j_c\sqrt{2j_c-1}}j_1\psi_1^2 - \frac{\mathcal{S}^2 r}{2(j_c-1)^3 j_c^3\sqrt{2j_c-1}}j_1^3 \\ &\quad - \frac{3r\sqrt{2j_c-1}}{(j_c-1)j_c}j_1 j_2 - \frac{\mathrm{d}\psi_1}{\mathrm{d}\tau} \end{aligned} \tag{II.8.15}$$

The natural oscillation frequency is now forced through the nonlinear terms on the right-hand side. Solvability for $p_{31}$ leads to the following condition for $p_1$,

$$\frac{\mathrm{d}p_1}{\mathrm{d}\tau} + \mathrm{i}C_1 p_1|p_1|^2 + \mathrm{i}C_2 p_1 = 0, \tag{II.8.16}$$

where

$$C_1 = \frac{15(2j_c-1)^2\lambda}{4\mathcal{S}^4}, \tag{II.8.17}$$

$$C_2 = -\beta_1^2\lambda\left\{\frac{(3j_c-2)^2(3j_c-1)^2\lambda^4 + \mathcal{S}^6}{4\mathcal{S}^6(\lambda^2-1)^2(4\lambda^2-1)}\right.$$

$$- \frac{(234j_c^6 - 702j_c^5 + 963j_c^4 - 756j_c^3 + 351j_c^2 - 90j_c + 10)\lambda^2}{8\mathcal{S}^6(\lambda^2-1)^2(4\lambda^2-1)}\Bigg\}. \quad \text{(II.8.18)}$$

The evolution equation (II.8.16) is readily solved, subject to the initial condition $p_1(0) = P$,

$$p_1 = P\mathrm{e}^{-\mathrm{i}(C_1|P|^2+C_2)\tau}. \quad \text{(II.8.19)}$$

The expansion for $j$ becomes

$$j = j_c + 2\mu\,\mathrm{Re}\left\{p_1(\mu^2 t)\mathrm{e}^{\mathrm{i}\lambda t} + q_1\mathrm{e}^{\mathrm{i}t}\right\} + \mathcal{O}(\mu^2), \quad \text{(II.8.20)}$$

with a similar expansion for $\psi$. Physically, the slow modulation due to (II.8.16) gives a small correction to the natural oscillation frequency. The resulting modulation of the wave amplitude is simply a superposition of discrete simple-harmonic oscillations.

The perturbation results have been confirmed with numerical integrations of the full evolution equations. As an example, let us fix $r = 0.7$, $j_* = 2.$, $\beta = 0.1$, $\Delta = 0$, and take the initial condition $(j, \psi) = (0.6, 0)$. Figure II-9 shows the phase-plane trajectory for a duration of 50. Superimposed as a thick curve is the Poincaré first return map, as described above. Figure II-10 shows $10 \cdot \log_{10}$ of the magnitude of the Fourier transform of $j(t)$. An FFT of size 8192 was used with a time step of 0.105. The frequencies and amplitudes of the first and second harmonics, as predicted by this perturbation theory, are indicated by asterisks. The markings are plotted with the corrected frequency, which takes into account the slow modulation predicted by (II.8.16). The approximate analysis gives an accurate prediction of the dominant frequencies and their amplitudes. The approximate analysis works quite well even when the amplitude $|j - j_c|$ is not small.

From the list in (II.8.9) it can be seen that modulational resonance may occur at first order in $\mu$ if $\lambda = 1$, at second order if $\lambda$ is $\frac{1}{2}$ or 2, and at third order if $\lambda$ is $\frac{1}{3}$ or 3. In principle there may be modulational resonance for $\lambda$ equal to any rational number for some order of $\mu$. In the next subsections, we consider in some detail these modulational resonances.

## II.8.2 First-order synchronous modulational resonance $\lambda = 1$

For synchronous modulational resonance we set

$$\lambda = 1 + f, \quad \text{(II.8.21)}$$

where $f$ denotes detuning of the natural frequency from the forcing frequency. We choose to express $r$ in terms of $f$ and $j_c$, see (II.7.11) and (II.8.4),

$$r = (1+f)\frac{\sqrt{2j_c - 1}}{\mathcal{S}}. \quad \text{(II.8.22)}$$

In order to balance slow growth and nonlinearity, let us assume a weak long wave,

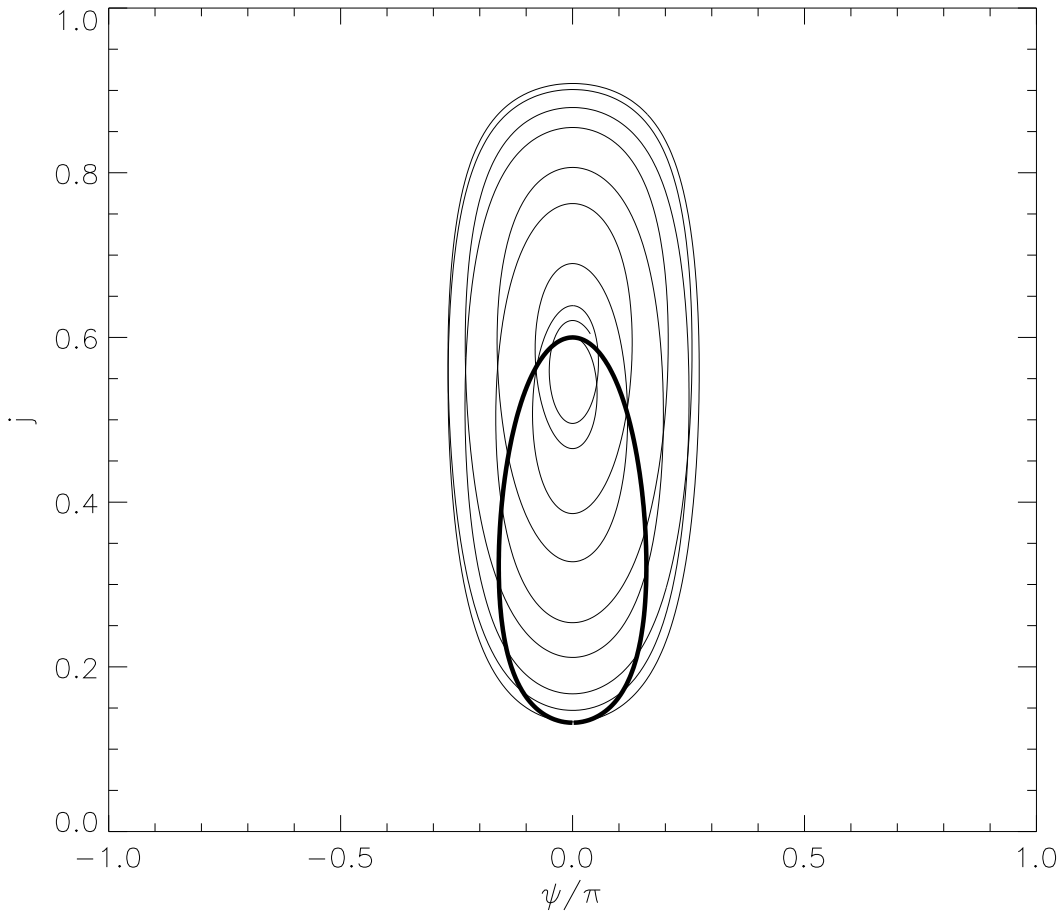


Figure II-9: Numerically computed trajectory $(j, \psi)$ (thin line) for $\beta = 0.1$, $r = 0.7$, $j_* = 2$ and $\Delta = 0$. The system evolved from the initial condition $(j, \psi) = (0.6, 0)$ until time $t = 50$. The Poincaré map, sampling every long-wave period $t = 2\pi n$, is indicated by the thick curve.

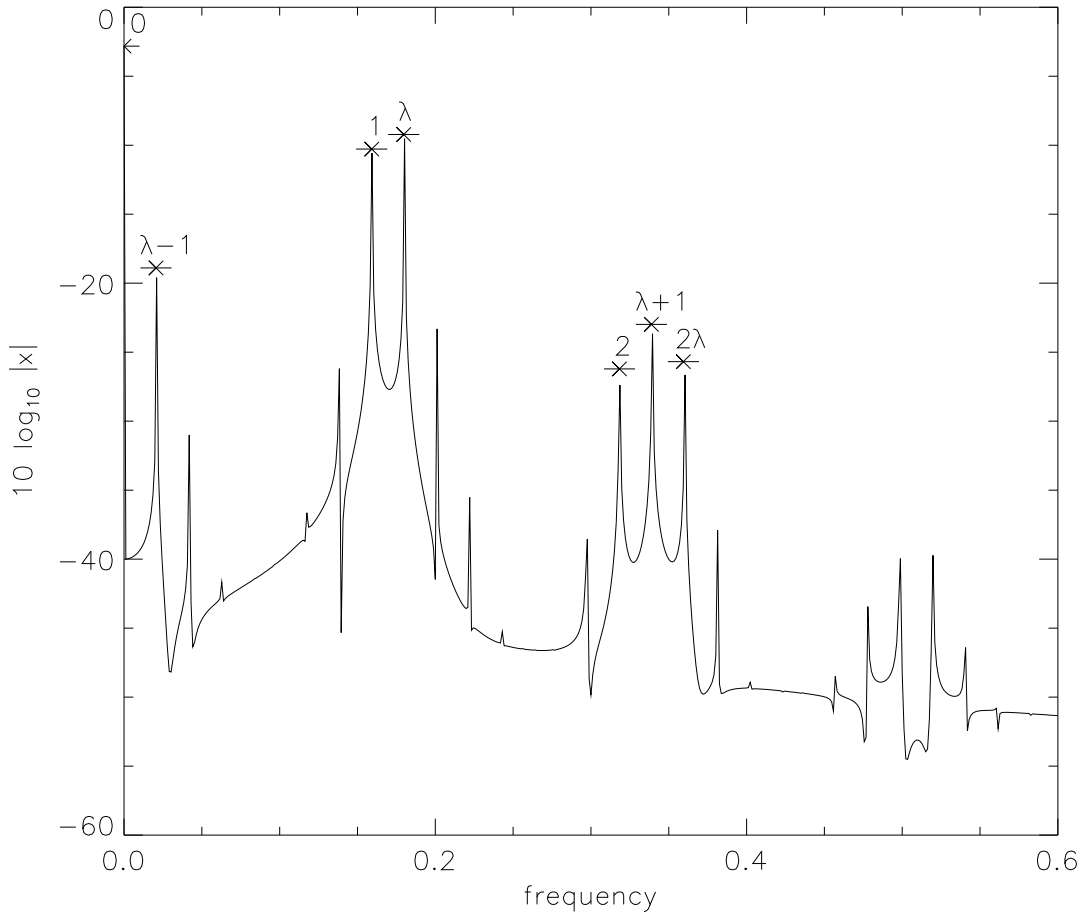


Figure II-10: Fourier spectrum of $j(t)$ for the trajectory shown in figure 8. The continuous curve is the FFT computed with 8192 samples and time step 0.105. The asterisks are the analytically computed Fourier amplitudes according to our perturbation analysis, with the frequencies adjusted to compensate for slow time modulation. The natural modulation frequency is $\lambda$ and the forcing frequency due to the long wave is unity (1). The expressions for the amplitudes are omitted in the text.

small detuning and slow modulational time according to the following scales,

$$\beta = \mu^3 \beta_3, \qquad f = \mu^2 f_2, \qquad \tau = \mu^2 t. \tag{II.8.23}$$

Perturbation expansions of the form (II.8.1) and (II.8.2) with $\psi_c = 0$ are assumed, where all $j_n$ and $\psi_n$ depend on the fast and the slow time.

At the leading order, we get

$$\begin{aligned} \frac{\mathrm{d}j_1}{\mathrm{d}t} - \frac{(j_c-1)j_c}{\mathcal{S}}\psi_1 &= 0, & \text{(II.8.24)} \\ \frac{\mathrm{d}\psi_1}{\mathrm{d}t} + \frac{\mathcal{S}}{(j_c-1)j_c} j_1 &= 0. & \text{(II.8.25)} \end{aligned}$$

This is an oscillator with natural frequency 1. We therefore assume a response

$$j_1 = p_1 \mathrm{e}^{\mathrm{i}t} + \text{c.c.}, \qquad \psi_1 = \frac{\mathrm{i}\mathcal{S}}{(j_c-1)j_c} p_1 \mathrm{e}^{\mathrm{i}t} + \text{c.c.} \tag{II.8.26}$$

The complex amplitude $p_1$ is a function of the slow time $\tau$.

At the second order, we have

$$\begin{aligned} \frac{\mathrm{d}j_2}{\mathrm{d}t} - \frac{(j_c-1)j_c}{\mathcal{S}}\psi_2 &= 0, & \text{(II.8.27)} \\ \frac{\mathrm{d}\psi_2}{\mathrm{d}t} + \frac{\mathcal{S}}{(j_c-1)j_c} j_2 &= -\frac{3(2j_c-1)}{2(j_c-1)j_c\mathcal{S}} j_1^2. & \text{(II.8.28)} \end{aligned}$$

The second-order system is not forced at the natural frequency. We assume the solution

$$\begin{aligned} j_2 &= p_{20} + p_{21}\mathrm{e}^{\mathrm{i}t} + p_{22}\mathrm{e}^{2\mathrm{i}t} + \text{c.c.}, & \text{(II.8.29)} \\ \psi_2 &= r_{20} + r_{21}\mathrm{e}^{\mathrm{i}t} + r_{22}\mathrm{e}^{2\mathrm{i}t} + \text{c.c.} & \text{(II.8.30)} \end{aligned}$$

Again, the complex amplitudes are functions of $\tau$.

At the third order, we have

$$\begin{aligned} \frac{\mathrm{d}j_3}{\mathrm{d}t} - \frac{(j_c-1)j_c}{\mathcal{S}}\psi_3 &= -\frac{(j_c-1)j_c}{6\mathcal{S}}\psi_1^3 + \frac{(j_c-1)j_c}{\mathcal{S}} f_2\psi_1 - \\ &\quad \frac{\mathcal{S}}{2(j_c-1)j_c} j_1^2\psi_1 - \frac{\mathrm{d}j_1}{\mathrm{d}\tau}, & \text{(II.8.31)} \\ \frac{\mathrm{d}\psi_3}{\mathrm{d}t} + \frac{\mathcal{S}}{(j_c-1)j_c} j_3 &= \frac{\mathcal{S}}{2(j_c-1)j_c} j_1\psi_1^2 - \frac{\mathcal{S}}{(j_c-1)j_c} f_2 j_1 + \beta_3 \cos t - \frac{\mathrm{d}\psi_1}{\mathrm{d}\tau} - \\ &\quad \frac{3(2j_c-1)}{(j_c-1)j_c\mathcal{S}} j_1 j_2 - \frac{1}{2}\left[\frac{\mathcal{S}}{(j_c-1)j_c}\right]^3 j_1^3. & \text{(II.8.32)} \end{aligned}$$

The third order problem is forced at its natural frequency. Hence we impose a solvability condition, to avoid secular growth of the first-harmonic response. This

leads to the following slow evolution equation for the complex amplitude $p_1$,

$$\frac{\mathrm{d}p_1}{\mathrm{d}\tau} + \mathrm{i}A_1|p_1|^2 p_1 - \mathrm{i}f_2 p_1 - \mathrm{i}A_2\beta_3 = 0, \tag{II.8.33}$$

where the real and non-negative coefficients $A_1$ and $A_2$ are

$$A_1 = \frac{15(2j_c-1)^2}{4\mathcal{S}^4}, \qquad A_2 = \frac{(1-j_c)j_c}{4\mathcal{S}}. \tag{II.8.34}$$

The complex evolution equation can be written as two coupled real equations, by introducing $p_1 = x + \mathrm{i}y$,

$$\frac{\mathrm{d}}{\mathrm{d}\tau}\begin{pmatrix} x \\ y \end{pmatrix} = \begin{pmatrix} A_1 y(x^2+y^2) - f_2 y \\ -A_1 x(x^2+y^2) + f_2 x + A_2\beta_3 \end{pmatrix} = \begin{pmatrix} \partial h/\partial y \\ -\partial h/\partial x \end{pmatrix} \tag{II.8.35}$$

where $h$ is the Hamiltonian

$$h(x,y) = \frac{1}{4}A_1(x^2+y^2)^2 - \frac{1}{2}f_2(x^2+y^2) - A_2\beta_3 x. \tag{II.8.36}$$

Hence the trajectories of $(x,y)$ are easily plotted as the level curves of $h$.

From the leading-order solution (II.8.26), it is seen that the Poincaré first return map of the original $(j,\psi)$-system is

$$j(2\pi n) = j_c + 2\mu x_n + \mathcal{O}(\mu^2), \tag{II.8.37}$$

$$\psi(2\pi n) = \psi_c - \frac{2\mu\mathcal{S}}{(j_c-1)j_c} y_n + \mathcal{O}(\mu^2), \tag{II.8.38}$$

where

$$\begin{pmatrix} x_n \\ y_n \end{pmatrix} = \begin{pmatrix} x \\ y \end{pmatrix} (t = 2\pi n\mu^2). \tag{II.8.39}$$

Hence the invariant manifolds of the Poincaré map of $(j,\psi)$ are qualitatively similar to and approximated by the level curves of $h(x,y)$ after an appropriate linear transformation.

The bifurcation set of the system (II.8.35), written compactly as

$$\dot{x} = F(x,y,j_c,f,\beta), \quad \dot{y} = G(x,y,j_c,f,\beta), \tag{II.8.40}$$

is the set of parameter values $(j_c,f,\beta)$ where the system changes its qualitative behavior. The bifurcation set is given as the solution of the three equations

$$F = 0, \qquad G = 0, \qquad \frac{\partial(F,G)}{\partial(x,y)} = 0. \tag{II.8.41}$$

The solution is readily found to be the union of the two surfaces

$$\begin{cases} S_1: & f_2 = \left(\frac{27}{4} A_2^2 A_1 \beta_3^2\right)^{1/3}, \\ S_2: & \beta_3 = 0, \quad f_2 \geq 0. \end{cases} \tag{II.8.42}$$

The two surfaces divide the parameter space into three regions, as shown in figure II-11. In region I the map has one center. In regions II and III the map has two centers and one saddle point, with two homoclinic manifolds connecting back to it. In figure II-12 we show typical phase portraits in the $(x, y)$-plane for regions II and III by plotting the level curves of $h(x, y)$. These phase portraits are qualitatively similar to the Poincaré first return map of $(j, \psi)$. The phase portraits in regions II and III are mirror images of each other, corresponding to the symmetries of the Hamiltonian $h(x, y)$.

### II.8.3 Second-order subharmonic modulational resonance $\lambda = 1/2$

We set

$$\lambda = 1/2 + f, \tag{II.8.43}$$

and assume the following scales,

$$\beta = \mu^2 \beta_2, \qquad f = \mu^2 f_2, \qquad \tau = \mu^2 t. \tag{II.8.44}$$

The leading-order natural response is assumed to be

$$j_1 = p_{1,\frac{1}{2}} \mathrm{e}^{\frac{1}{2}\mathrm{i}t} + \text{c.c.}, \qquad \psi_1 = \frac{\mathrm{i}\mathcal{S}}{(j_c - 1) j_c} p_{1,\frac{1}{2}} \mathrm{e}^{\frac{1}{2}\mathrm{i}t} + \text{c.c.}, \tag{II.8.45}$$

where the complex amplitude $p_{1,\frac{1}{2}}$ is a function of the slow time $\tau$.

Removal of secular growth at order $\mathcal{O}(\mu^3)$ gives

$$\frac{\mathrm{d}p_{1,\frac{1}{2}}}{\mathrm{d}\tau} + \mathrm{i}A_1 |p_{1,\frac{1}{2}}|^2 p_{1,\frac{1}{2}} - \mathrm{i}f_2 p_{1,\frac{1}{2}} - \mathrm{i}A_2 \beta_2 p^*_{1,\frac{1}{2}} = 0, \tag{II.8.46}$$

where the real and non-negative coefficients $A_1$ and $A_2$ are

$$A_1 = \frac{15(2j_c - 1)^2}{8\mathcal{S}^4}, \qquad A_2 = \frac{(1 - j_c) j_c (2j_c - 1)}{4\mathcal{S}^3}. \tag{II.8.47}$$

The complex evolution equation can be written as two coupled real equations similar to (II.8.35) by introducing $p_{1,\frac{1}{2}} = x + \mathrm{i}y$. The Hamiltonian is now

$$h(x, y) = \frac{1}{4} A_1 (x^2 + y^2)^2 - \frac{1}{2} f_2 (x^2 + y^2) - \frac{1}{2} A_2 \beta_2 (y^2 - x^2). \tag{II.8.48}$$

The evolution equation (II.8.46) and the associated Hamiltonian (II.8.48) are now

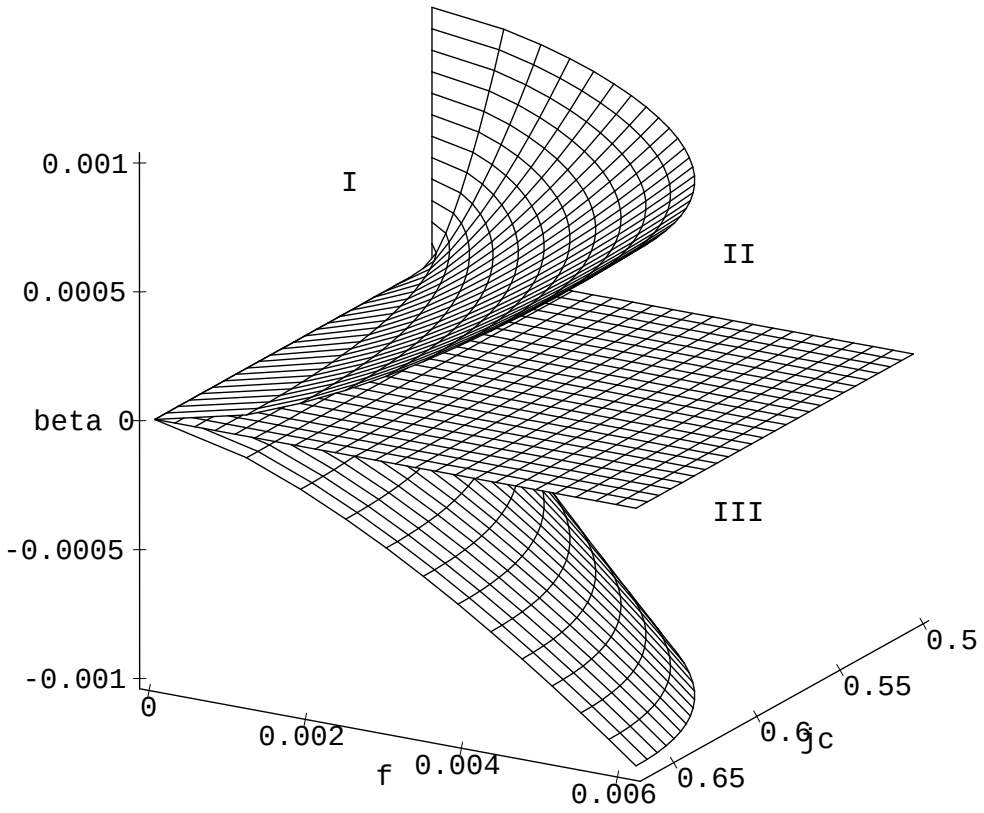


Figure II-11: Bifurcation diagram for synchronous modulational resonance. The bifurcation surfaces are shown in the parameter space of $f$, $j_c$ and $\beta$.

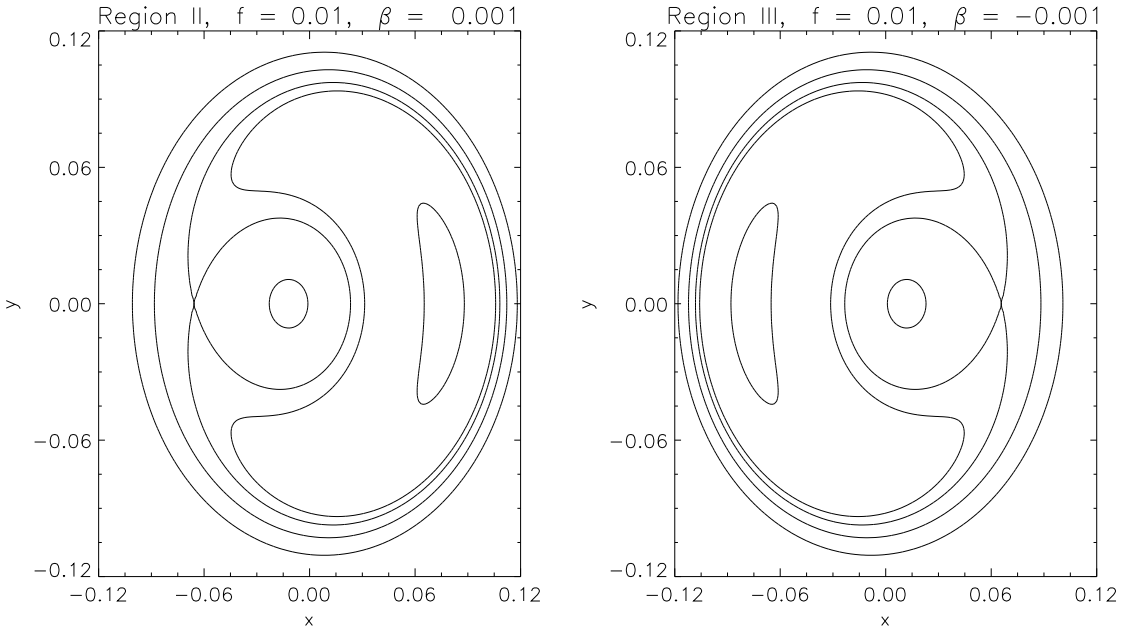


Figure II-12: Invariant manifolds of the Poincaré map for synchronous modulational resonance. Sketch of the level curves of the Hamiltonian $h(x, y)$ indicating the qualitative behavior of the Poincaré map in regions II and III.

qualitatively different from (II.8.33) and (II.8.36), respectively.

It is now convenient to use the Poincaré second return map, by choosing the sampling time equal to twice the period of the long wave, $t = 4\pi n$ for $n = 1, 2, 3, \ldots$. The Poincaré second return map is now given by

$$j(4\pi n) = j_c + 2\mu x_{2n} + \mathcal{O}(\mu^2), \tag{II.8.49}$$

$$\psi(4\pi n) = \psi_c - \frac{2\mu\mathcal{S}}{(j_c - 1)j_c} y_{2n} + \mathcal{O}(\mu^2), \tag{II.8.50}$$

where

$$\begin{pmatrix} x_{2n} \\ y_{2n} \end{pmatrix} = \begin{pmatrix} x \\ y \end{pmatrix} (t = 4\pi n\mu^2). \tag{II.8.51}$$

The manifolds of the Poincaré second return map for $(j, \psi)$ are thus approximated by the level curves of $h(x, y)$ after an appropriate linear transformation.

The bifurcation set is the union of the three surfaces

$$\begin{cases} S_1: & f_2 = -A_2|\beta_2|, \\ S_2: & f_2 = A_2|\beta_2|, \\ S_3: & \beta_2 = 0, \quad f_2 \geq 0. \end{cases} \tag{II.8.52}$$

These three surfaces divide the parameter space into five regions, see figure II-13. In region I the map has one center. In regions II and III the map has two centers and one saddle point, with two homoclinic manifolds connecting back to it. In regions

IV and V the map has three centers and two saddle points, which are connected by four heteroclinic manifolds. In figure II-14 we show typical phase portraits in the $(x, y)$-plane for regions II, III, IV and V by plotting the level curves of $h(x, y)$. These phase portraits are qualitatively similar to the Poincaré second return map for $(j, \psi)$. We notice that the bifurcation surfaces are symmetric with respect to changing the sign of $\beta_2$, while the phase portraits for positive and negative $\beta_2$ can be obtained from each other by a 90° rotation, according to the symmetries of the Hamiltonian $h(x, y)$.

### II.8.4 Second-order superharmonic modulational resonance $\lambda = 2$

We set

$$\lambda = 2 + f, \tag{II.8.53}$$

and assume the following scales in order to balance slow growth and nonlinearity at order $\mu^3$,

$$\beta = \mu^{3/2}\beta_{3/2}, \qquad f = \mu^2 f_2, \qquad \tau = \mu^2 t. \tag{II.8.54}$$

The leading-order natural response is assumed to be

$$j_1 = p_{12}\mathrm{e}^{2\mathrm{i}t} + \text{c.c.}, \qquad \psi_1 = \frac{\mathrm{i}\mathcal{S}}{(j_c - 1)j_c} p_{12}\mathrm{e}^{2\mathrm{i}t} + \text{c.c.}, \tag{II.8.55}$$

where the complex amplitude $p_{12}$ is a function of the slow time $\tau$.

Removal of secular growth at order $\mathcal{O}(\mu^3)$ gives

$$\frac{\mathrm{d}p_{12}}{\mathrm{d}\tau} + \mathrm{i}A_1|p_{12}|^2 p_{12} - \mathrm{i}f_2 p_{12} - \mathrm{i}A_2\beta_{3/2}^2 = 0, \tag{II.8.56}$$

with real and non-negative coefficients $A_1$ and $A_2$

$$A_1 = \frac{15(2j_c - 1)^2}{2\mathcal{S}^4}, \qquad A_2 = \frac{(j_c - 1)^2 j_c^2 (2j_c - 1)}{6\mathcal{S}^4}. \tag{II.8.57}$$

The complex evolution equation can be written as two coupled real equations, by introducing $p_{12} = x + \mathrm{i}y$. The Hamiltonian is now

$$h(x, y) = \frac{1}{4}A_1(x^2 + y^2)^2 - \frac{1}{2}f_2(x^2 + y^2) - A_2\beta_{3/2}^2 x. \tag{II.8.58}$$

When (II.8.56) is compared with (II.8.33), it is revealed that they describe qualitatively the same behavior, except that we now have the symmetry $\beta_{3/2} \to -\beta_{3/2}$.

The bifurcation set is found to be the union of the two surfaces

$$\begin{cases} S_1: & f_2 = \left(\frac{3}{2}\sqrt{3A_1}A_2\right)^{2/3} |\beta_{3/2}|^{4/3}, \\ S_2: & \beta = 0, \quad f \geq 0. \end{cases} \tag{II.8.59}$$

The two surfaces $S_1$ and $S_2$ divide the parameter space into three regions, shown

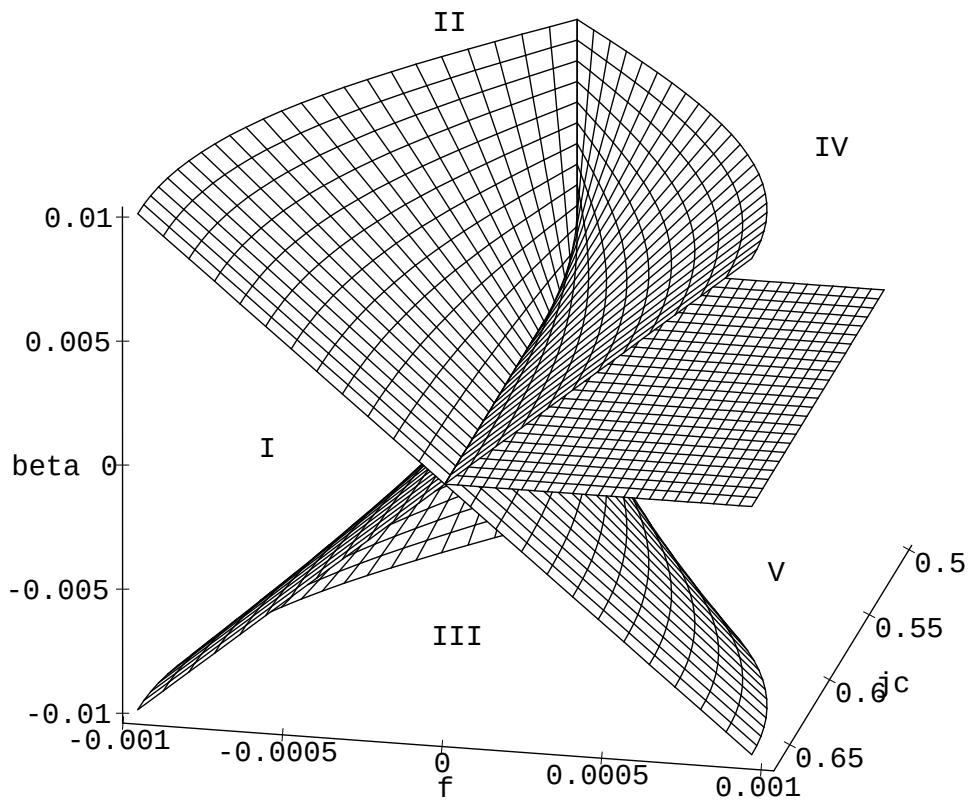


Figure II-13: Bifurcation diagram for subharmonic 1/2 modulational resonance.

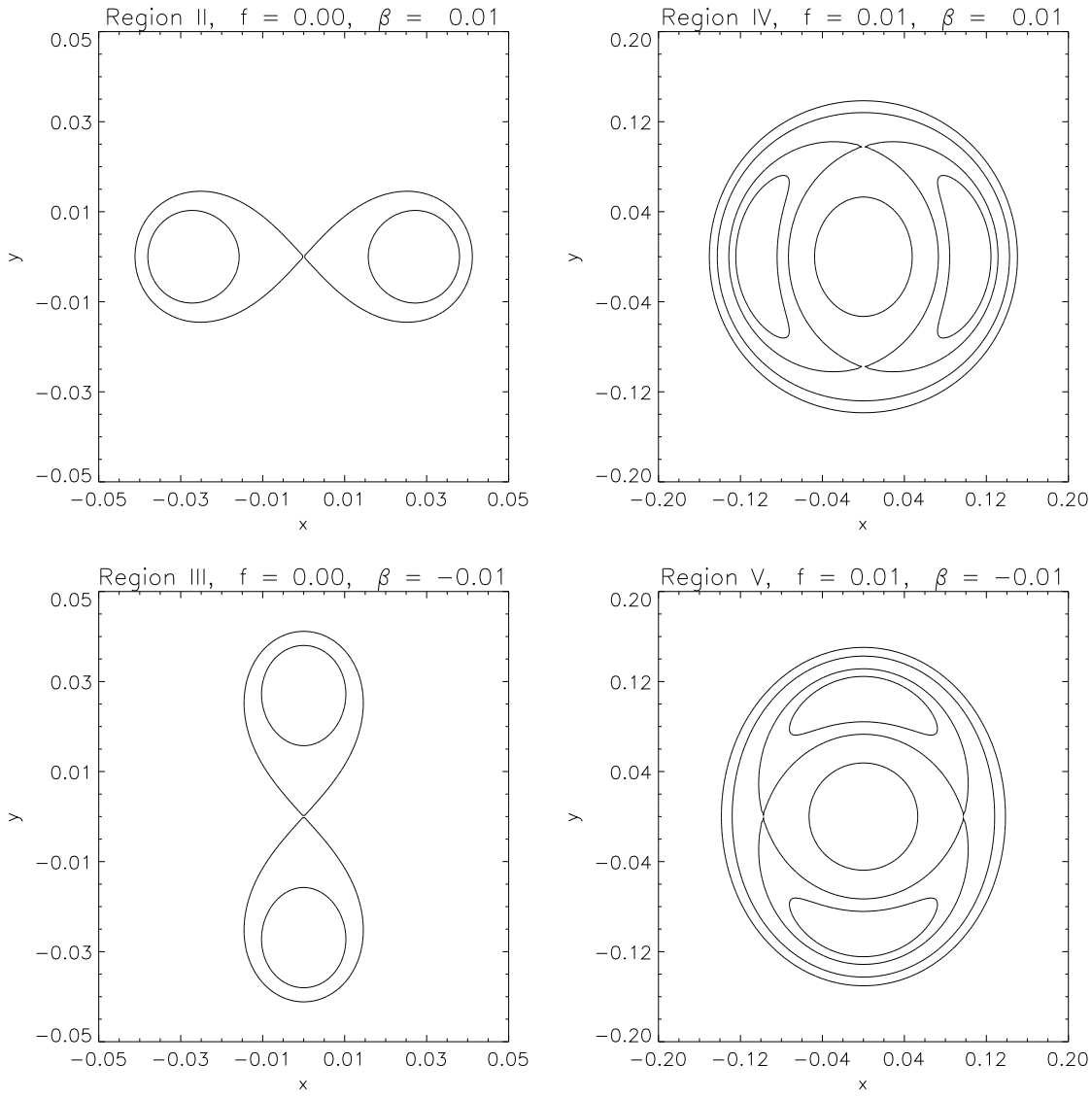


Figure II-14: Phase portraits for subharmonic 1/2 modulational resonance.

in figure II-15. In region I the map has one center. In regions II and III, there are two centers and one saddle point, which has two homoclinic manifolds connecting back to it. Typical phase portraits in regions II and III are shown in figure II-16 by plotting the level curves of $h(x, y)$. These indicate the qualitative properties of the Poincaré first return map.

### II.8.5 Third-order subharmonic modulational resonance $\lambda = 1/3$

We set

$$\lambda = 1/3 + f, \tag{II.8.60}$$

and assume the following scales,

$$\beta = \mu\beta_1, \qquad f = \mu^2 f_2, \qquad \tau = \mu^2 t. \tag{II.8.61}$$

Now the leading-order response is the superposition of the natural and forced frequencies,

$$j_1 = p_{1,\frac{1}{3}} \mathrm{e}^{\frac{1}{3}\mathrm{i}t} + p_{11}\mathrm{e}^{\mathrm{i}t} + \text{c.c.}, \qquad \psi_1 = r_{1,\frac{1}{3}} \mathrm{e}^{\frac{1}{3}\mathrm{i}t} + r_{11}\mathrm{e}^{\mathrm{i}t} + \text{c.c.}, \tag{II.8.62}$$

where the complex amplitudes of the free oscillation $p_{1,\frac{1}{3}}$, $r_{1,\frac{1}{3}}$ are functions of the slow time $\tau$, and the complex amplitudes of the forced oscillation $p_{11}$ and $r_{11}$ are constants.

After removing secular growth at $\mathcal{O}(\mu^3)$, we get

$$\frac{\mathrm{d}p_{1,\frac{1}{3}}}{\mathrm{d}\tau} + \mathrm{i}A_1|p_{1,\frac{1}{3}}|^2 p_{1,\frac{1}{3}} - \mathrm{i}f_2 p_{1,\frac{1}{3}} - \mathrm{i}A_2\beta_1(p^*_{1,\frac{1}{3}})^2 + \mathrm{i}A_3\beta_1^2 p_{1,\frac{1}{3}} = 0, \tag{II.8.63}$$

where the real and non-negative coefficients $A_1$, $A_2$ and $A_3$ are

$$A_1 = \frac{5(2j_c - 1)^2}{4\mathcal{S}^4}, \qquad A_2 = \frac{9(1 - j_c)j_c(2j_c - 1)^2}{64\mathcal{S}^5}, \tag{II.8.64}$$

$$A_3 = \frac{3(2268j_c^6 - 6804j_c^5 + 8991j_c^4 - 6642j_c^3 + 2907j_c^2 - 720j_c + 80)}{2560\mathcal{S}^6}. \tag{II.8.65}$$

The complex evolution equation can be written as two coupled real equations, by introducing $p_{1,\frac{1}{3}} = x + \mathrm{i}y$, and the Hamiltonian

$$h(x, y) = \frac{1}{4}A_1(x^2 + y^2)^2 + \frac{1}{2}(A_3\beta_1^2 - f_2)(x^2 + y^2) + A_2\beta_1 x(y^2 - \frac{1}{3}x^2). \tag{II.8.66}$$

It is now most natural to use the Poincaré third return map, for which we sample every third long wave period, $t = 6\pi n,\ n = 1, 2, 3, \ldots$. The bifurcation set is found

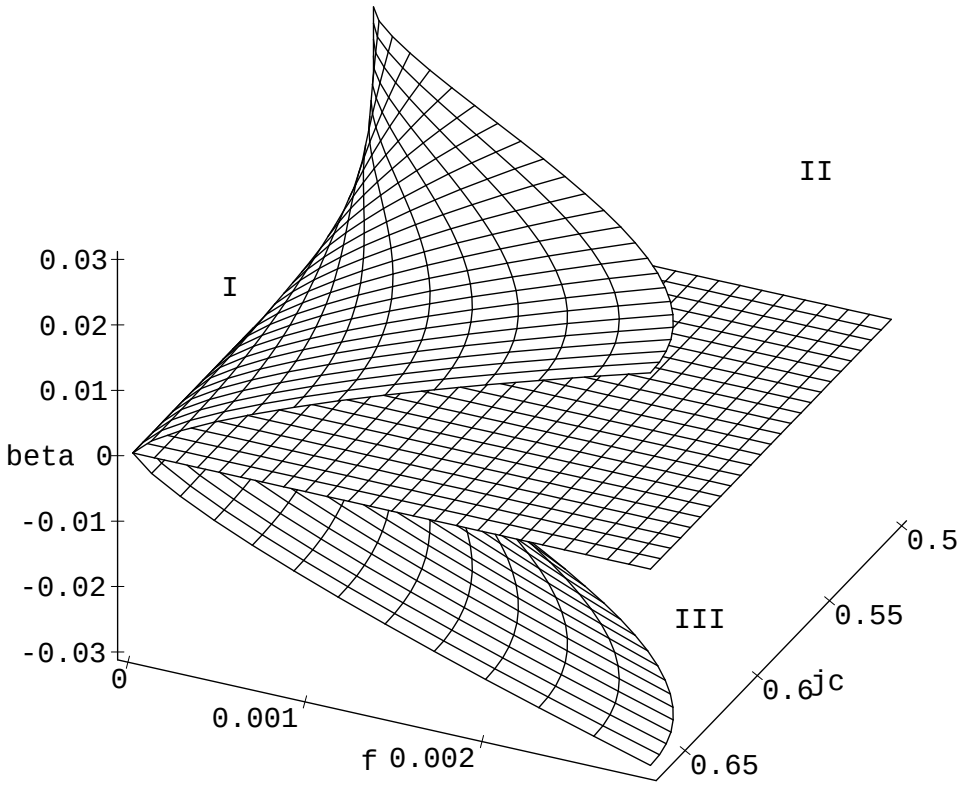


Figure II-15: Bifurcation diagram for superharmonic 2 modulational resonance.

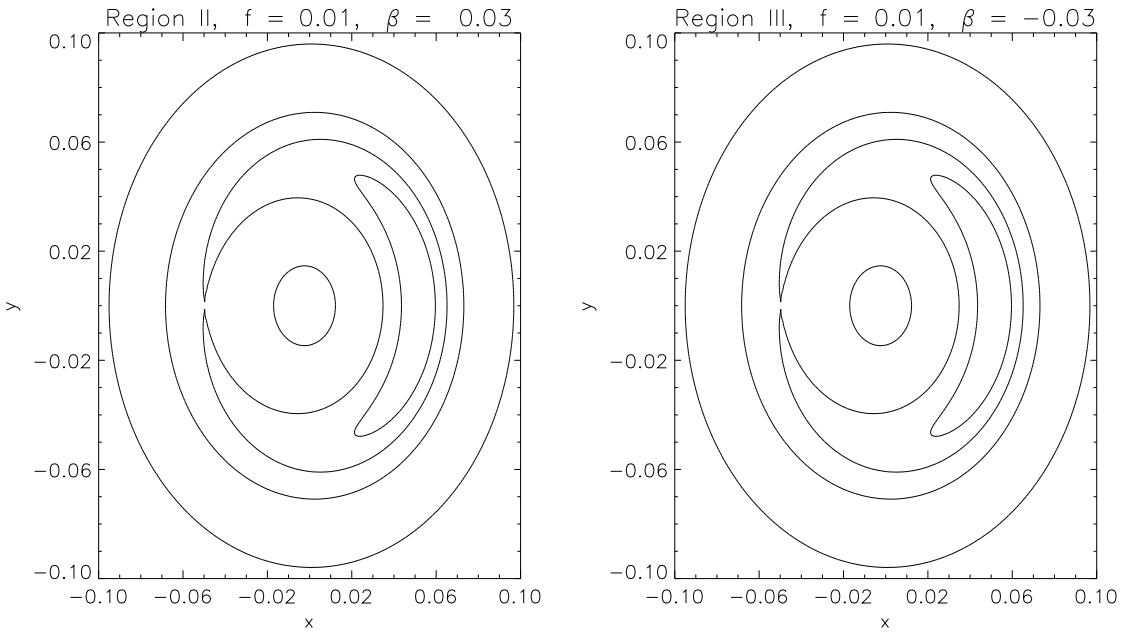


Figure II-16: Phase portraits for superharmonic 2 modulational resonance.

to be the union of three surfaces

$$\begin{cases} S_1: & f_2 = \left(A_3 - \frac{A_2^2}{4A_1}\right)\beta_1^2, \\ S_2: & f_2 = A_3\beta_1^2, \\ S_3: & \beta_1 = 0, \quad f_2 \geq 0. \end{cases} \tag{II.8.67}$$

The three surfaces divide the parameter space into five regions, shown in figure II-17. Note that $S_1$ and $S_2$ are so close together that they cannot be distinguished in the figure, and thus regions II and III, which are between them, are very thin. It can be shown numerically that

$$\max_{\frac{1}{2}<j_c\leq\frac{2}{3}} \frac{A_2^2}{4A_1A_3} \approx 0.005952. \tag{II.8.68}$$

This thin transition region is unlikely to have any physical significance.

In region I the map has one center. In the thin regions II and III there are four centers and three saddle points with three heteroclinic and three homoclinic manifolds. In regions IV and V there are four centers and three saddle points which are connected by six heteroclinic manifolds. The phase portraits in the $(x, y)$-plane for regions II, III, IV and V are shown in figure II-18 by plotting the level curves of $h(x, y)$. These are qualitatively similar to the Poincaré third return map. We notice that by changing $\beta_1 \to -\beta_1$ and $x \to -x$, the Hamiltonian is invariant. Hence phase portraits for $\beta_1 > 0$ and $\beta_1 < 0$ are mirror images of each other.

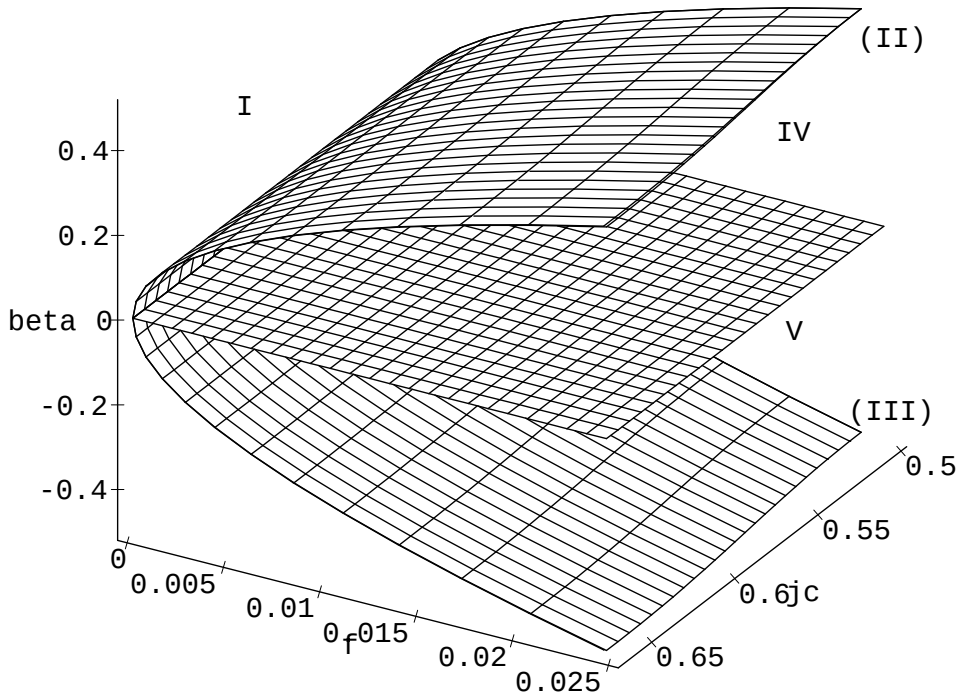


Figure II-17: Bifurcation diagram for subharmonic 1/3 modulational resonance.

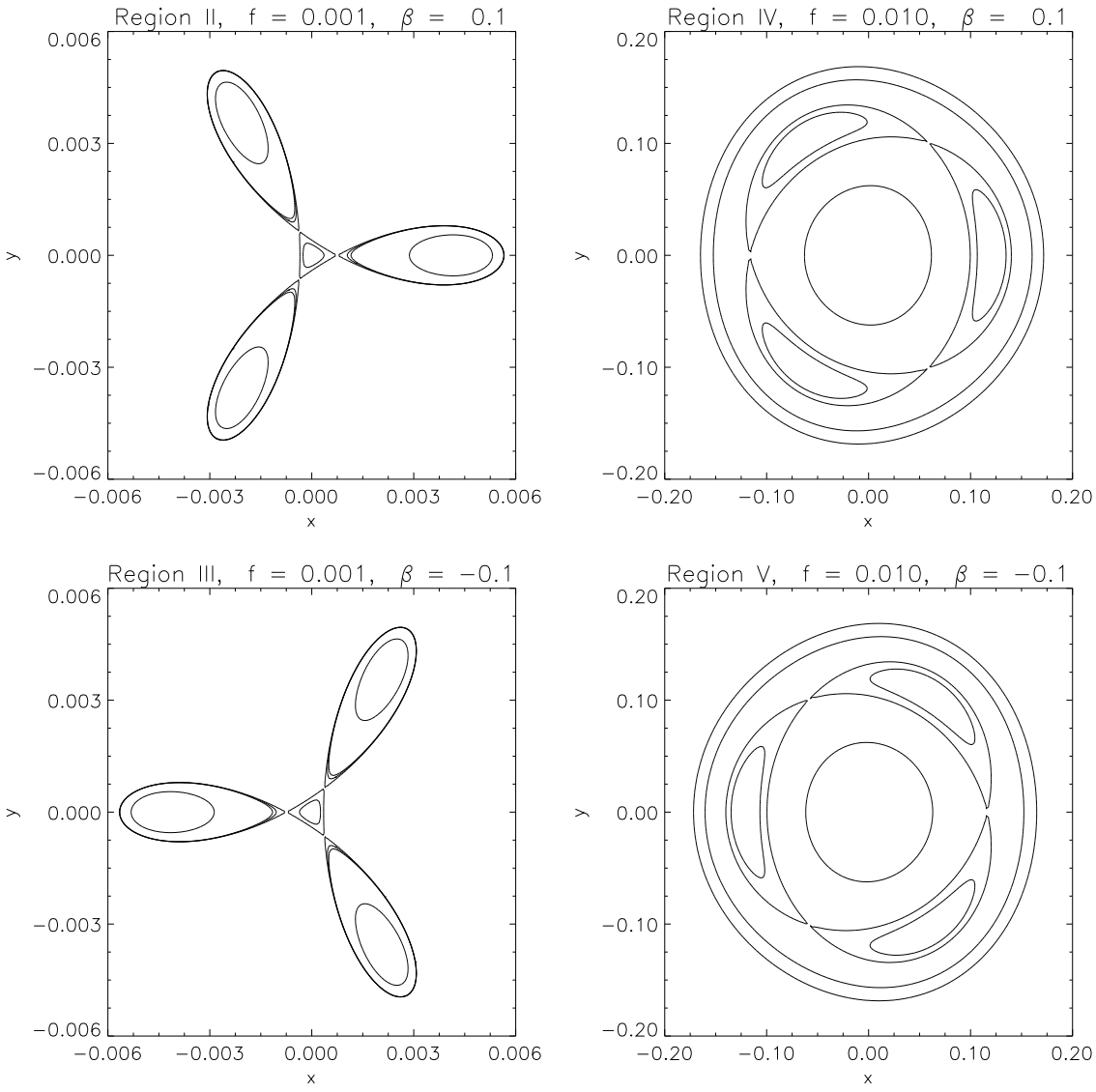


Figure II-18: Phase portraits for subharmonic 1/3 modulational resonance.

### II.8.6 Third-order superharmonic modulational resonance $\lambda = 3$

We set

$$\lambda = 3 + f, \tag{II.8.69}$$

and assume the following scales,

$$\beta = \mu\beta_1, \qquad f = \mu^2 f_2, \qquad \tau = \mu^2 t. \tag{II.8.70}$$

The leading-order natural response is assumed to be

$$j_1 = p_{11}\mathrm{e}^{\mathrm{i}t} + p_{13}\mathrm{e}^{3\mathrm{i}t} + \text{c.c.}, \qquad \psi_1 = r_{11}\mathrm{e}^{\mathrm{i}t} + r_{13}\mathrm{e}^{3\mathrm{i}t} + \text{c.c.}, \tag{II.8.71}$$

where the complex amplitudes of the free oscillation $p_{13}$, $r_{13}$ are functions of the slow time $\tau$, and the complex amplitudes of the forced oscillation $p_{11}$ and $r_{11}$ are constants.

Removal of secular growth at $\mathcal{O}(\mu^3)$ gives

$$\frac{\mathrm{d}p_{13}}{\mathrm{d}\tau} + \mathrm{i}A_1|p_{13}|^2 p_{13} - \mathrm{i}f_2 p_{13} + \mathrm{i}A_2\beta_1^2 p_{13} - \mathrm{i}A_3\beta_1^3 = 0, \tag{II.8.72}$$

where the real coefficients $A_1$, $A_2$ and $A_3$ are

$$A_1 = \frac{45(2j_c - 1)^2}{4\mathcal{S}^4}, \tag{II.8.73}$$

$$A_2 = \frac{3(2052j_c^6 - 6156j_c^5 - 4671j_c^4 + 19602j_c^3 - 15867j_c^2 + 5040j_c - 560)}{17920\mathcal{S}^6}, \tag{II.8.74}$$

$$A_3 = \frac{(1 - j_c)j_c(17604j_c^6 - 52812j_c^5 + 50733j_c^4 - 13446j_c^3 - 4959j_c^2 + 2880j_c - 320)}{81920\mathcal{S}^7}. \tag{II.8.75}$$

The complex evolution equation can be written as two coupled real equations, by introducing $p_{13} = x + \mathrm{i}y$. The Hamiltonian is now

$$h(x, y) = \frac{1}{4}A_1(x^2 + y^2)^2 + \frac{1}{2}(A_2\beta_1^2 - f_2)(x^2 + y^2) - A_3\beta_1^3 x. \tag{II.8.76}$$

When (II.8.72) is compared with (II.8.33), it is revealed that they describe qualitatively the same behavior.

The bifurcation set is found to be the union of two surfaces

$$\begin{cases} S_1: & f_2 = \left\{ A_2 + \left(\frac{3}{2}\sqrt{3A_1}|A_3|\right)^{2/3} \right\} \beta_1^2, \\ S_2: & \beta = 0, \quad f_2 \geq 0. \end{cases} \tag{II.8.77}$$

The two surfaces $S_1$ and $S_2$ divide the parameter space into three regions, shown in figure II-19. In region I the map has one center. In regions II and III there are two centers and one saddle point with two homoclinic manifolds. The phase portraits in the $(x, y)$-plane for regions II and III are shown in figure II-20 by plotting the level

curves of $h(x, y)$. These indicate the properties of the Poincaré first return map.

### II.8.7 Other resonances

We have so far only considered the case of zero detuning $\Delta = 0$. When detuning is present, the resulting modulational resonances and bifurcations can be anticipated with the help of figures II-7 and II-8, which show phase portraits and modulational oscillation frequencies for the autonomous system. In particular, figure II-21 shows a numerically computed Poincaré map for $\beta = 0.1$, $r = 0.7$, $j_* = 0$ and $\Delta = 0.7$. The corresponding frequencies of closed orbits of the unforced system is shown in figure II-8c. The unforced system has no saddle points or homoclinic loops. It has two centers: the first at $j = 0$ with frequency 0 and the second at $(j = \frac{8}{9}, \psi = \pi)$ with frequency $\lambda = 1.4\sqrt{\frac{2}{3}} = 1.143$, according to (II.7.8) and (II.7.11). Since the unforced modulational oscillation frequency decreases monotonically from $\lambda = 1.143$ to 0 from the center at $j = \frac{8}{9}$ to $j = 0$, we expect the occurrence of modulational resonances with frequencies 1, 1/2, 1/3 etc. at some intermediate locations when the forcing is weak. In figure II-21 this can indeed be observed. The first center of the unforced system can be traced at $j = 0$, while the second one is at $\psi = \pi$ and $j = 0.948$. Between these two centers (from north to south), we can see the resonant manifolds for synchronous resonance (a), subharmonic 1/2 resonance (b) and subharmonic 1/3 resonance (c).

In principle, there may be modulational resonance whenever the ratio between the natural modulational oscillation frequency and the forcing frequency is a rational number. A few resonances obtained by numerical integration, are shown in figure II-22, for parameter values $\beta = 0.1$, $r = 0.26$, $j_* = 0$ and $\Delta = 0$. The unforced system now has a degenerate saddle point at $j = 0$ with a homoclinic trajectory at $\psi = \pm\frac{\pi}{2}$. There are two centers at $j = \frac{2}{3}$ and $\psi = 0, \pi$, with frequency $\lambda = 0.26$, according to (II.7.7) and (II.7.11). Since the unforced modulational oscillation frequency decreases monotonically from $\lambda = 0.26$ at the two centers to 0 at the homoclinic trajectory, we expect the occurrence of various modulational resonances at some intermediate locations when the forcing is weak. In figure II-22, we show the characteristic manifolds of four modulational resonances. Starting closest to the centers and going outward, we see a subharmonic 1/4 resonance (a) inside a subharmonic 1/5 resonance (b) inside a subharmonic 1/6 resonance (c) inside a subharmonic 1/7 resonance (d). These resonances are identified numerically as follows. We first locate any center or saddle point of that resonance. Then we count how many iterations of the map are needed to get back to the same point. In doing so, we trace all the other centers or saddle point of the given resonant manifold as well. The plots showing the invariant manifolds of the saddle points, have been generated by first finding the linear eigenspaces of each saddle point, and then taking a few initial conditions along these eigenspaces and iterate a few times forward and backward in time.

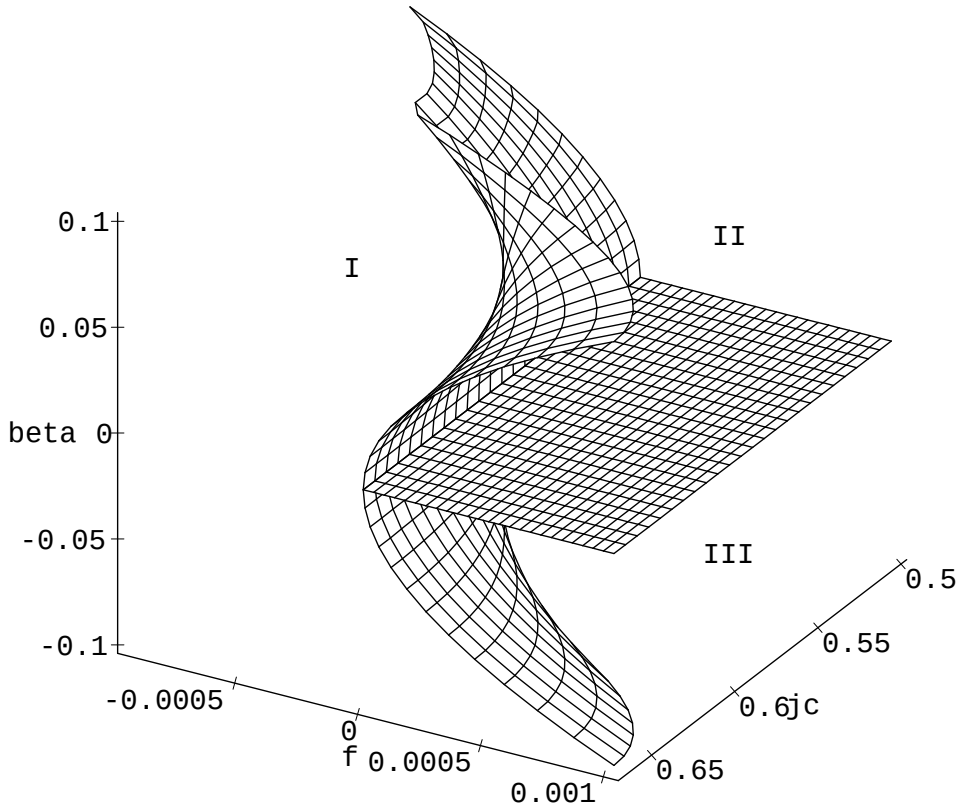


Figure II-19: Bifurcation diagram for superharmonic 3 modulational resonance.

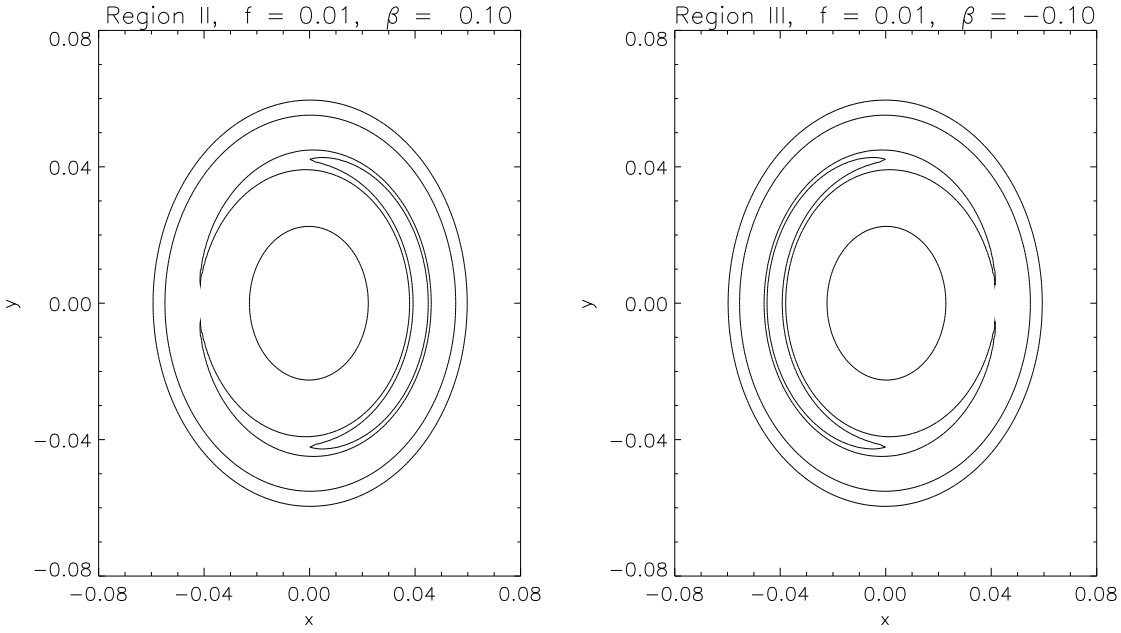


Figure II-20: Phase portraits for superharmonic 3 modulational resonance.

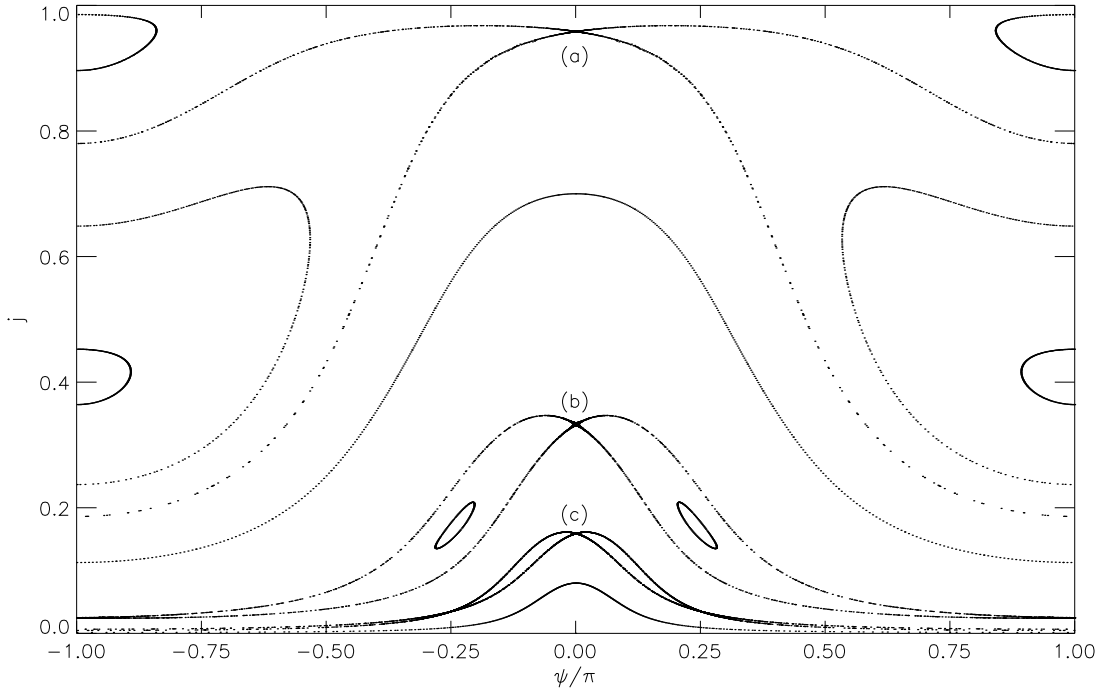


Figure II-21: Poincaré map for $\beta = 0.1$, $r = 0.7$, $j_* = 0$ and $\Delta = 0.7$, showing the characteristic manifolds of synchronous resonance (a), subharmonic 1/2 resonance (b) and subharmonic 1/3 resonance (c).

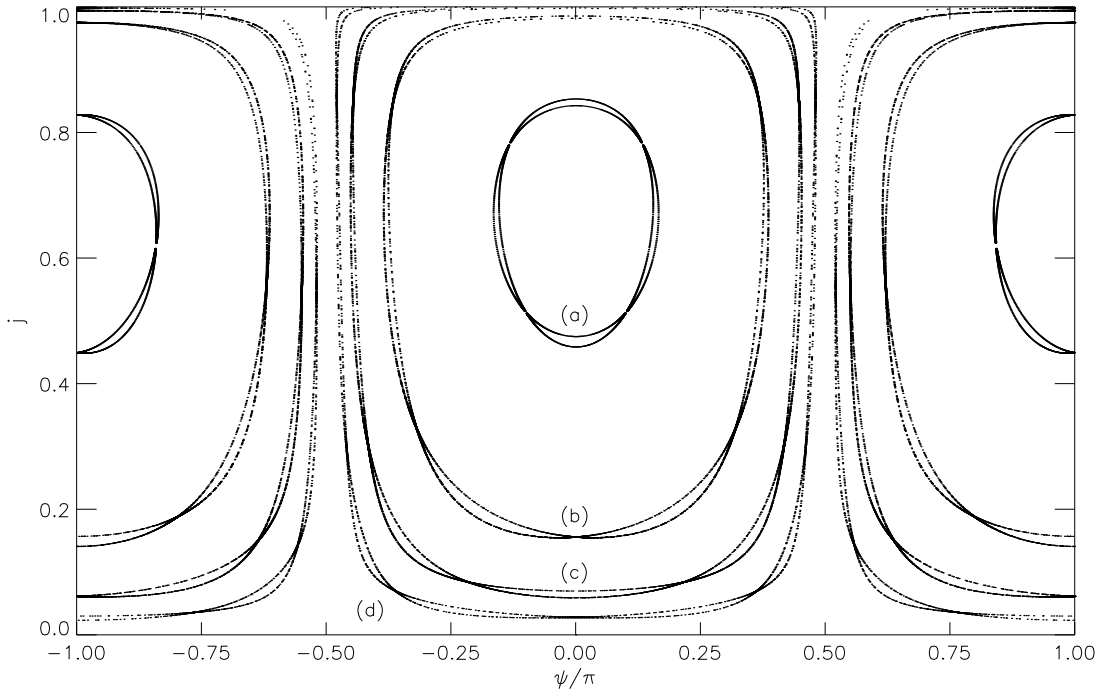


Figure II-22: Poincaré map for $\beta = 0.1$, $r = 0.26$, $j_* = 0$ and $\Delta = 0$, showing the characteristic manifolds of subharmonic 1/4 resonance (a), subharmonic 1/5 resonance (b), subharmonic 1/6 resonance (c) and subharmonic 1/7 resonance (d).

## II.9 Effects of a stronger long-wave disturbance

Guided by the insight gained by the approximate analysis for weak long-wave disturbances, we have performed extensive numerical integration of the evolution equations. Because the reduced representation with $j$ and $\psi$ is singular at the poles of the sphere, we integrate the full six-dimensional system (II.6.7)–(II.6.9), and then transform the results to $j$ and $\psi$ for graphical presentation. Presented below are the Poincaré (first return) maps obtained by sampling the state of the triad every long-wave period $t = 2\pi n$ for $n = 1, 2, 3, \ldots$.

We found in section II.7 that whenever $j_* = 0$ and $|\Delta/r| < 1$, the unforced system has a homoclinic trajectory connecting the degenerate saddle point at $j = 0$ to itself. In Appendix II.F we perform a Melnikov analysis which shows that the homoclinic loop will tangle and thus form a stochastic layer for any small disturbance by the long wave. This is to be expected since our model does not include non-conservative effects. Thus whenever the conditions $j_* = 0$ and $|\Delta/r| < 1$ are satisfied, which is our generalization of the bifurcation condition of Chen & Saffman (1979), there are initial conditions that give rise to chaotic behavior for an arbitrarily small long-wave disturbance.

In section II.8 we found homoclinic and heteroclinic manifolds of the Poincaré map, associated with modulational resonance. According to the analysis of that section, these manifolds should not tangle for a sufficiently weak long-wave disturbance. However, numerical computations show that these manifolds do tangle provided the long-wave disturbance is sufficiently large. Chaotic behavior due to modulational resonance tends therefore to occur at a higher threshold value of the long-wave disturbance.

The Poincaré maps in figures II-23–II-27 illustrate the behavior of the triad subject to successively stronger disturbances by the long wave. We fix $j_* = 0$, $r = 0.55$, $\Delta = 0$ and let $\beta$ take the values 0.01, 0.1, 0.2, 1.2 and 2.0.

The weakest long-wave disturbance, $\beta = 0.01$ (figure II-23) is within the validity of the perturbation theory, although the detuning from modulational resonance is rather large. We can see the characteristic heteroclinic manifolds of a subharmonic 1/2 resonance (a), corresponding to regions IV and V in figures II-13 and II-14. On the outside, we see the manifolds of a subharmonic 1/3 resonance (b), corresponding to regions IV and V in figures II-17 and II-18. The disturbance by the long wave is sufficiently small that the heteroclinic manifolds of the map do not tangle. The homoclinic trajectory of the autonomous system does tangle and gives rise to a stochastic layer, in accordance with the Melnikov analysis in Appendix II.F.

When $\beta = 0.1$ (figure II-24), the stochastic layer of the homoclinic trajectory of the autonomous system has grown in size to cover the area occupied by the subharmonic 1/3 resonant manifold. The subharmonic 1/2 resonant heteroclinic manifolds are now tangling and forming their own stochastic layer, which is separate from the first stochastic layer. The details of how the heteroclinic manifolds of the subharmonic 1/2 modulational resonances are tangling, are shown in figure II-28.

When $\beta = 0.2$ (figure II-25), the subharmonic 1/2 tangle has joined with the tangle of the homoclinic trajectory of the autonomous system. Only small islands of

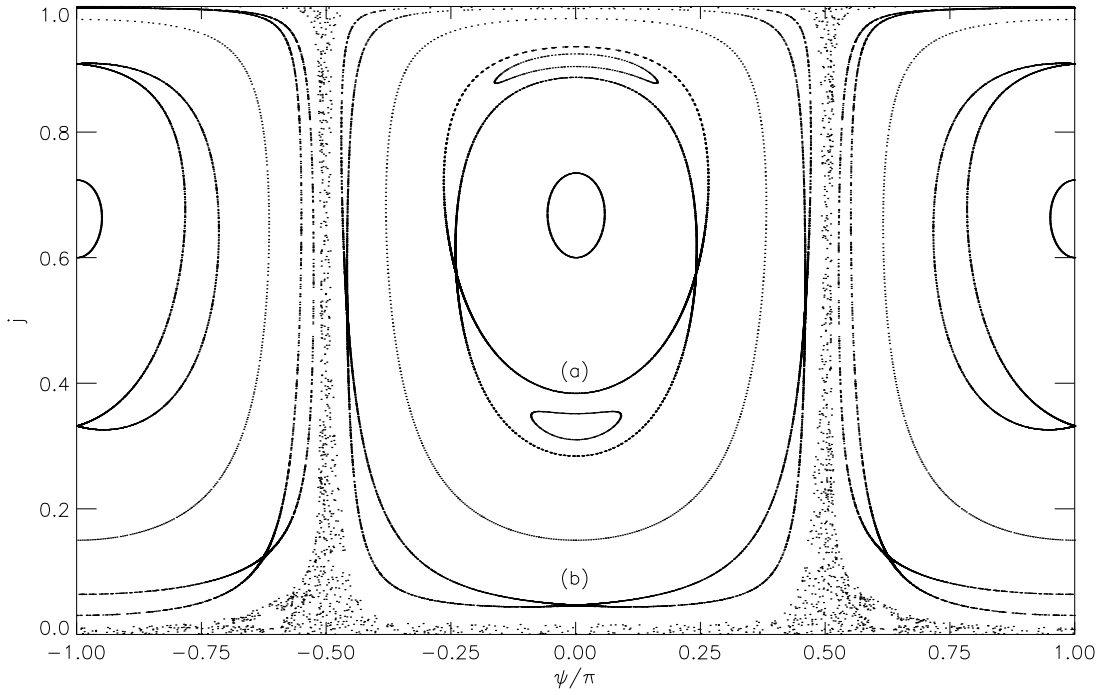


Figure II-23: Poincaré map for $r = 0.55$, $j_* = 0$, $\Delta = 0$, $\beta = 0.01$. We see subharmonic 1/2 resonance (a) and subharmonic 1/3 resonance (b).

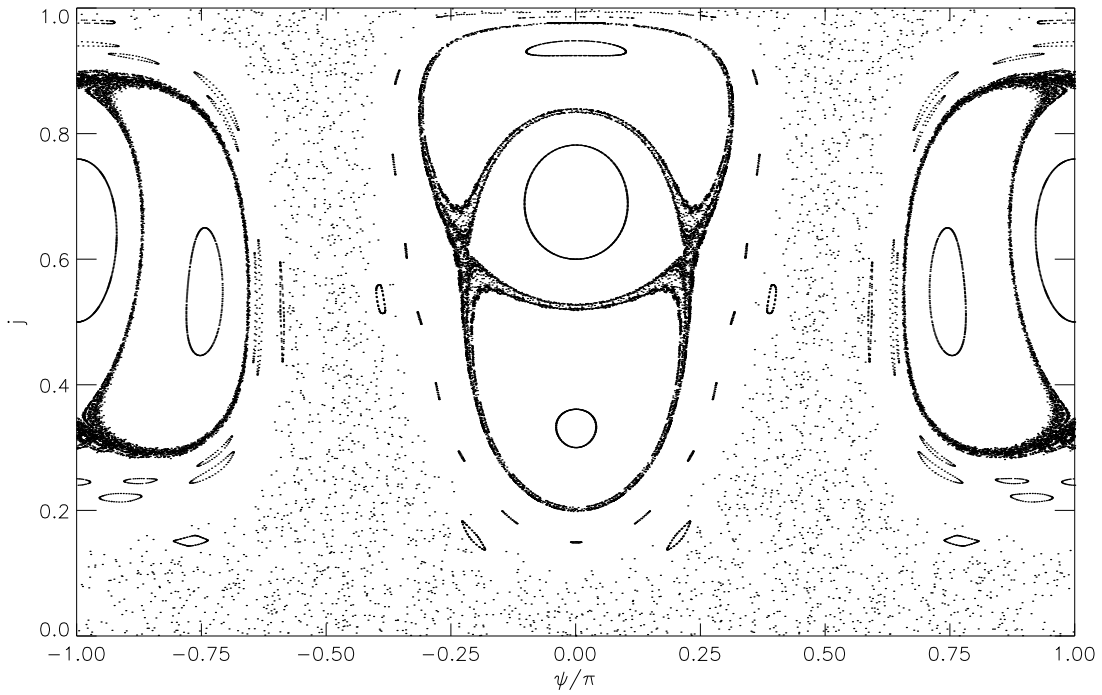


Figure II-24: Poincaré map for $r = 0.55$, $j_* = 0$, $\Delta = 0$, $\beta = 0.1$.

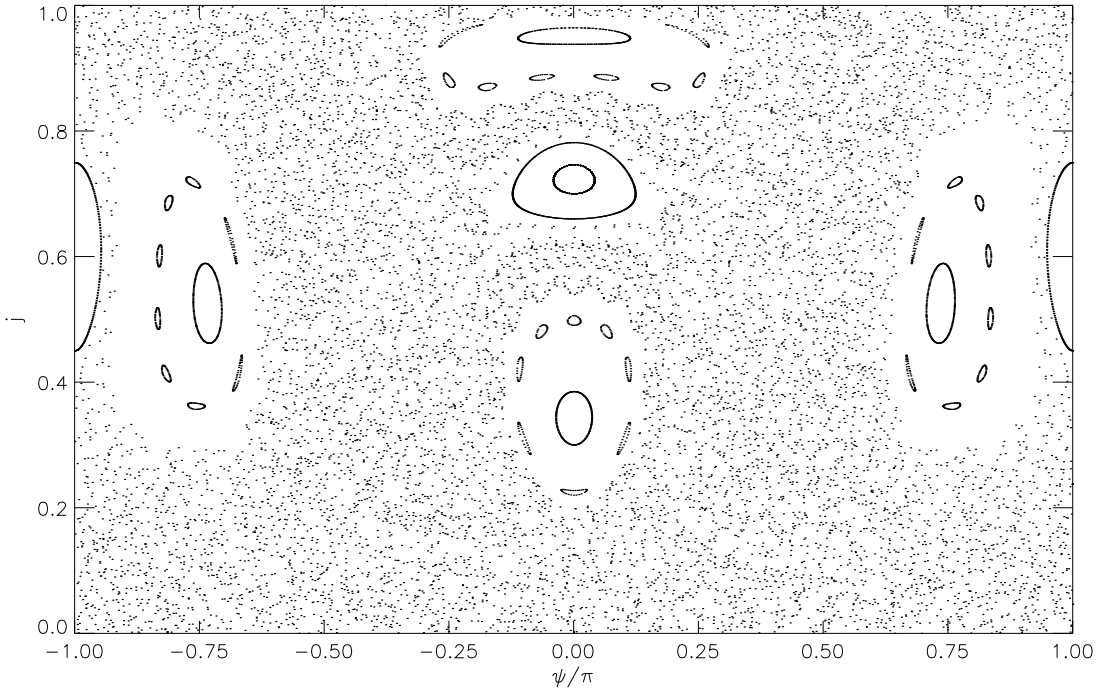


Figure II-25: Poincaré map for $r = 0.55$, $j_* = 0$, $\Delta = 0$, $\beta = 0.2$.

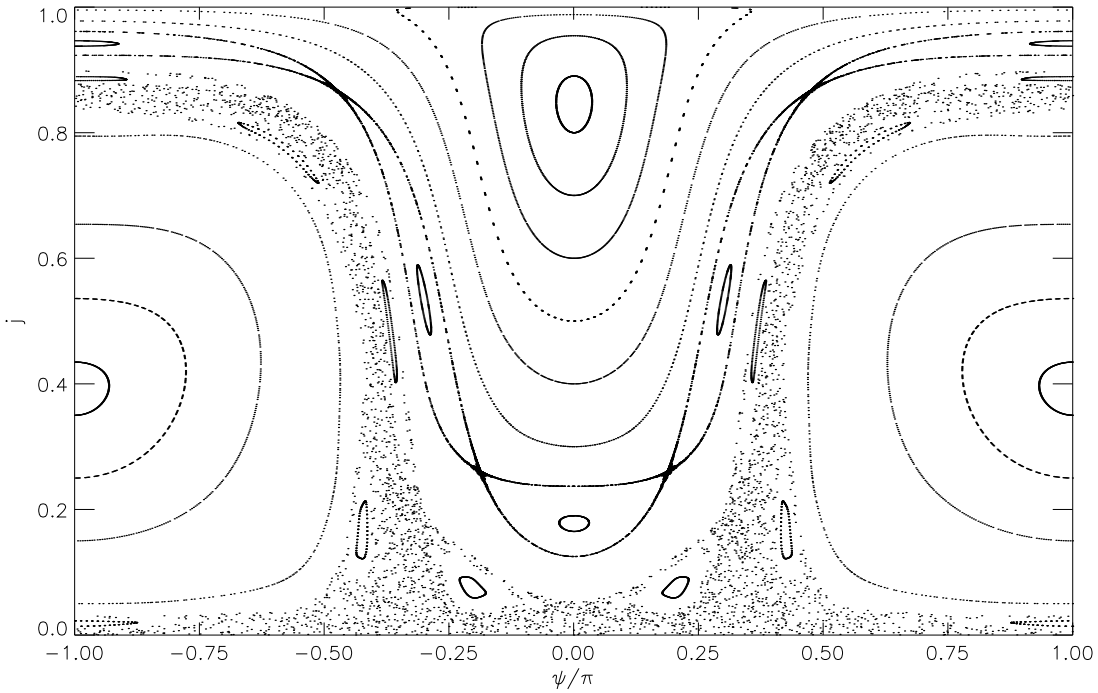


Figure II-26: Poincaré map for $r = 0.55$, $j_* = 0$, $\Delta = 0$, $\beta = 1.2$.

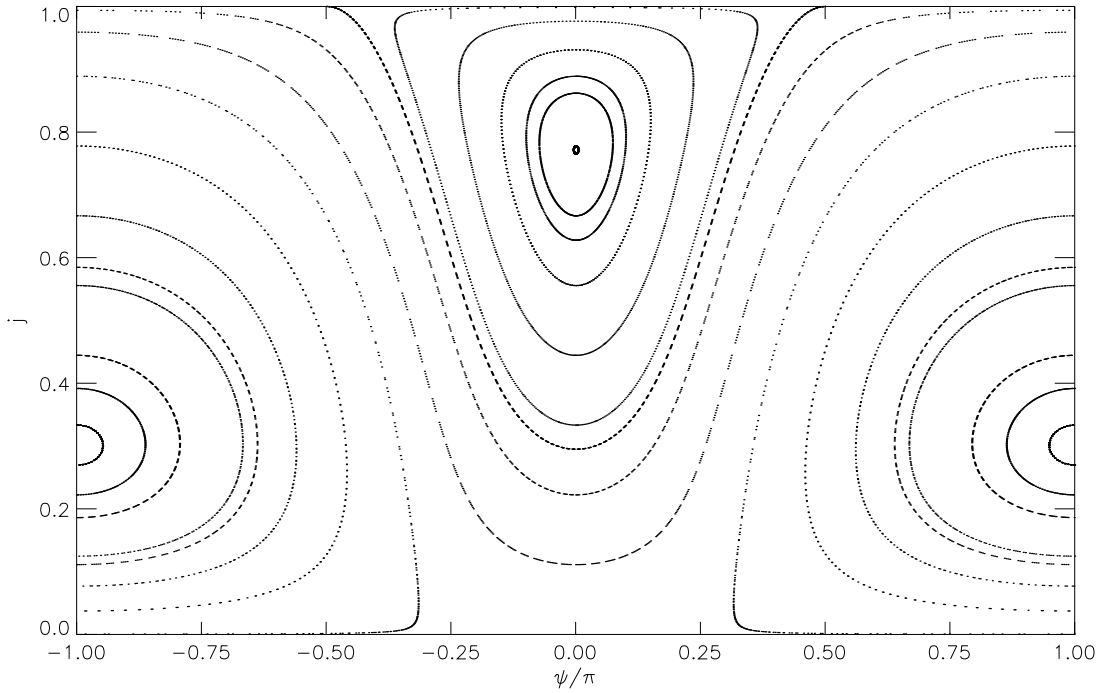


Figure II-27: Poincaré map for $r = 0.55$, $j_* = 0$, $\Delta = 0$, $\beta = 2.0$.

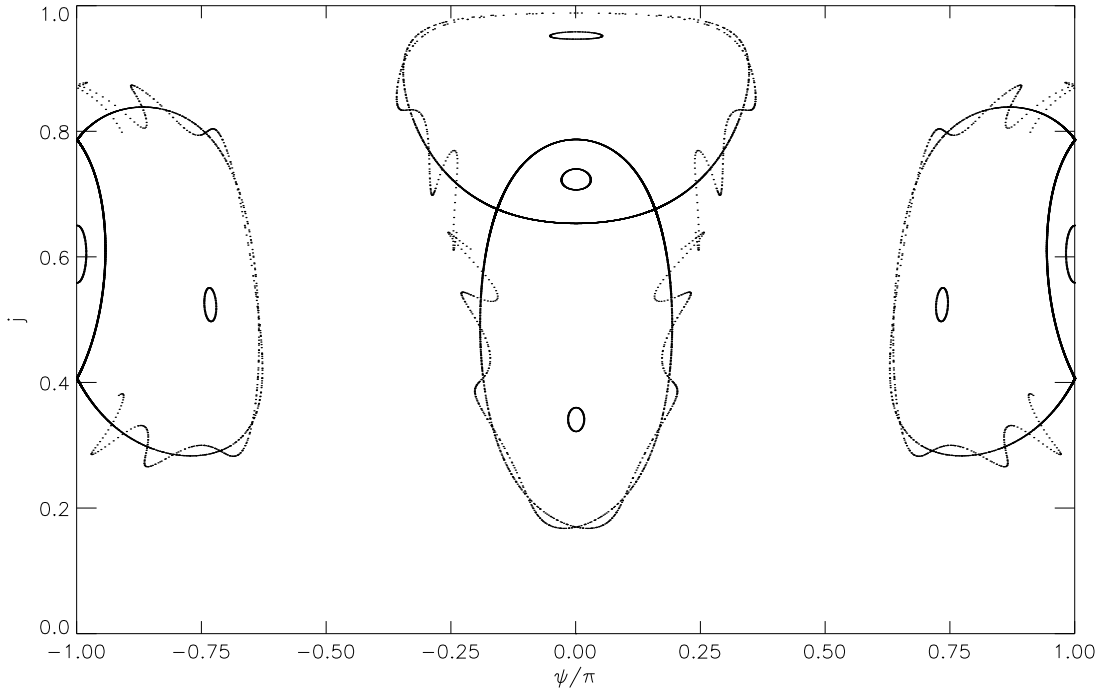


Figure II-28: Poincaré map for $r = 0.55$, $j_* = 0$, $\Delta = 0$, $\beta = 0.1$, showing the tangling of the heteroclinic manifolds of the subharmonic modulational resonance 1/2.

phase space remain, that are not covered by stochastic layers.

In general, as the long-wave disturbance increases, the stochastic layers will grow in size, and will eventually cover the entire phase space. Numerical experience indicates however that when the long-wave disturbance becomes much larger, the chaotic behavior may recede by the shrinking and disappearance of the stochastic layers. This is illustrated in figure II-26 for $\beta = 1.2$. Here we can see that the area of phase space covered with stochastic layers has diminished.

In figure II-27, $\beta = 2.0$ is sufficiently large that the dynamical behavior is non-chaotic throughout phase space.

It is now clear that chaotic behavior tends to develop first near the homoclinic trajectory of the autonomous system, if it exists. For an increasingly strong long wave, chaos may develop near the manifolds of modulational resonances. The greatest likelihood for modulational resonance to occur, is when there is a wide range of natural modulational frequencies available. From figure II-8, which shows the natural modulational frequencies for the autonomous system, it is clear that a wide range is available when $j_*$ is small and $\Delta/r$ is of unit magnitude or smaller. In physical terms, this means that the wave actions of the two longer waves should be approximately equal, and the mismatch in the resonance condition should be small. Then chaotic behavior of a triad is easily excited by a passing long wave.

## II.10 Conclusion

We have studied theoretically the effect of a uniform long wave on a resonant triad of short gravity–capillary waves. To consider cases where the short-wave wavelengths are much smaller than the long-wave amplitude, we employ a Lagrangian formulation to simplify the description of the free surface. Without dissipation the equations governing the slow evolution of the wave envelope are derived for weakly nonlinear short waves on a gentle long wave. To the order of approximation dominated by quadratic interactions among the short waves, the long wave is shown to modify the evolution equation through terms with time-periodic coefficients. The interaction coefficients signifying the coupling between the short waves are found to be the same in both the Lagrangian and the Eulerian formulations. Important features of the nonlinear dynamics can therefore be expected to remain the same in either formulation. Detailed dynamics is then studied for the time evolution of short waves which are spatially unmodulated in a coordinate system moving with the long-wave flow.

From the analytical solution without the long wave, bifurcations due to detuning are examined. The bifurcation criterion of Chen & Saffman (1979) for collinear Wilton's ripples is found to apply to triads with arbitrary wavenumber configurations whenever the two longer waves have the same wave action.

The effect of the long wave is then studied analytically for a weak disturbance. Modulational resonance of the short-wave envelope is studied when the long-wave frequency is a rational multiple of the natural modulational frequency of the triad. Several bifurcations of the Poincaré map are found, and confirmed by direct numerical integration.

Finally, by increasing the amplitude of the long wave, Hamiltonian chaos is found to begin in two different situations. The first one is due to the tangling of the homoclinic trajectory that can exist for a triad that is not disturbed by the long wave. This situation occurs for an arbitrarily small long-wave disturbance, whenever the two longer gravity–capillary waves have nearly the same wave action. The second one is due to the tangling of the homoclinic and heteroclinic manifolds of the Poincaré map associated with modulational resonance of the triad when it is disturbed by the long wave. This occurs for a higher threshold value of the long wave disturbance. Furthermore, we have given reasons for why modulational resonance is most likely to occur when the two longer waves have nearly the same wave action.

We have hence found that when the two longer gravity–capillary waves have nearly the same wave action, then chaos is likely to be excited by the long wave provided the detuning from triad resonance is not large.

This work has been carried out under the assumption that the waves are not affected by wind or viscosity within a second-order approximation. This assumption was shown to hold true for a clean surface without the effects of aging or contamination. In nature, however, gravity–capillary waves are often generated and maintained by wind. Not only will the wind force the short waves, but the wind itself can be modulated by long waves such that the wind-forcing of the short waves is periodic as well. We believe that the conservative second-order theory presented here can provide valuable insight as a leading-order approximation to the more complete problem of non-conservative evolution of resonating short waves on top of a long wave subject to a weak wind that can balance viscous damping over a long time.

It would be an interesting topic for future research to see how the combined modulational effects of wind and viscosity, including long-wave induced modulation of wind stress, can affect the long-time evolution of a resonating triad. The predictions of such an investigation should then be compared to the present inviscid second-order theory. The theoretical treatment of the long-wave induced modulation of wind stress could be pursued along the lines of the recent work by Troitskaya (1994). When these effects have been included, it will also be easier to compare the theoretical predictions to the actual behavior of waves in the ocean.

# II.A The derivatives of the reference positions

Let the Lagrangian particle positions be functions of the Lagrangian reference positions

$$X = X(a,b,c), \qquad Y = Y(a,b,c), \qquad Z = Z(a,b,c), \tag{II.A.1}$$

and let these three equations be invertible

$$a = a(X,Y,Z), \qquad b = b(X,Y,Z), \qquad c = c(X,Y,Z). \tag{II.A.2}$$

Differentiation of (II.A.1) with respect to $X$ gives

$$1 = \frac{\partial a}{\partial X}\frac{\partial X}{\partial a} + \frac{\partial b}{\partial X}\frac{\partial X}{\partial b} + \frac{\partial c}{\partial X}\frac{\partial X}{\partial c}, \tag{II.A.3}$$

$$0 = \frac{\partial a}{\partial X}\frac{\partial Y}{\partial a} + \frac{\partial b}{\partial X}\frac{\partial Y}{\partial b} + \frac{\partial c}{\partial X}\frac{\partial Y}{\partial c}, \tag{II.A.4}$$

$$0 = \frac{\partial a}{\partial X}\frac{\partial Z}{\partial a} + \frac{\partial b}{\partial X}\frac{\partial Z}{\partial b} + \frac{\partial c}{\partial X}\frac{\partial Z}{\partial c}. \tag{II.A.5}$$

When these equations are inverted, we get the derivatives with respect to $X$

$$\frac{\partial a}{\partial X} = \frac{1}{J}\left(-\frac{\partial Y}{\partial c}\frac{\partial Z}{\partial b} + \frac{\partial Y}{\partial b}\frac{\partial Z}{\partial c}\right), \tag{II.A.6}$$

$$\frac{\partial b}{\partial X} = \frac{1}{J}\left(\frac{\partial Y}{\partial c}\frac{\partial Z}{\partial a} - \frac{\partial Y}{\partial a}\frac{\partial Z}{\partial c}\right), \tag{II.A.7}$$

$$\frac{\partial c}{\partial X} = \frac{1}{J}\left(-\frac{\partial Y}{\partial b}\frac{\partial Z}{\partial a} + \frac{\partial Y}{\partial a}\frac{\partial Z}{\partial b}\right). \tag{II.A.8}$$

$J$ is the Jacobian

$$J = \frac{\partial(X,Y,Z)}{\partial(a,b,c)}. \tag{II.A.9}$$

Similarly, by differentiating (II.A.1) with respect to $Y$ and $Z$, we obtain

$$\frac{\partial a}{\partial Y} = \frac{1}{J}\left(\frac{\partial X}{\partial c}\frac{\partial Z}{\partial b} - \frac{\partial X}{\partial b}\frac{\partial Z}{\partial c}\right), \qquad \frac{\partial a}{\partial Z} = \frac{1}{J}\left(-\frac{\partial X}{\partial c}\frac{\partial Y}{\partial b} + \frac{\partial X}{\partial b}\frac{\partial Y}{\partial c}\right),$$

$$\frac{\partial b}{\partial Y} = \frac{1}{J}\left(-\frac{\partial X}{\partial c}\frac{\partial Z}{\partial a} + \frac{\partial X}{\partial a}\frac{\partial Z}{\partial c}\right), \qquad \frac{\partial b}{\partial Z} = \frac{1}{J}\left(\frac{\partial X}{\partial c}\frac{\partial Y}{\partial a} - \frac{\partial X}{\partial a}\frac{\partial Y}{\partial c}\right),$$

$$\frac{\partial c}{\partial Y} = \frac{1}{J}\left(\frac{\partial X}{\partial b}\frac{\partial Z}{\partial a} - \frac{\partial X}{\partial a}\frac{\partial Z}{\partial b}\right), \qquad \frac{\partial c}{\partial Z} = \frac{1}{J}\left(-\frac{\partial X}{\partial b}\frac{\partial Y}{\partial a} + \frac{\partial X}{\partial a}\frac{\partial Y}{\partial b}\right).$$

# II.B Second-order short-wave perturbation equations

We here give the right-hand-side expressions of the second-order perturbation equations for the short waves (II.3.10)–(II.3.14). $J_{(2)}$ denotes the value of the Jacobian at the second order due to the short waves, and is independent of time. These lengthy

expressions have been derived by the symbolic computation program MACSYMA.

$$\mathcal{E}_2 = J_{(2)} - \frac{\partial x_1}{\partial a_1} + \frac{\partial x_1}{\partial b}\frac{\partial y_1}{\partial a} - \frac{\partial x_1}{\partial a}\frac{\partial y_1}{\partial b} - \frac{\partial x_{-1}}{\partial a_2}\frac{\partial y_1}{\partial b} - \frac{\partial y_1}{\partial b_1}$$
$$+ \frac{\partial x_1}{\partial c}\frac{\partial z_1}{\partial a} + \frac{\partial x_{-1}}{\partial c_2}\frac{\partial z_1}{\partial a} + \frac{\partial y_1}{\partial c}\frac{\partial z_1}{\partial b} - \frac{\partial x_1}{\partial a}\frac{\partial z_1}{\partial c} - \frac{\partial x_{-1}}{\partial a_2}\frac{\partial z_1}{\partial c}$$
$$- \frac{\partial y_1}{\partial b}\frac{\partial z_1}{\partial c} - \frac{\partial z_1}{\partial c_1} + \frac{\partial x_1}{\partial c}\frac{\partial z_{-1}}{\partial a_2} - \frac{\partial x_1}{\partial a}\frac{\partial z_{-1}}{\partial c_2} - \frac{\partial y_1}{\partial b}\frac{\partial z_{-1}}{\partial c_2} \qquad \text{(II.B.1)}$$

Irrotationality, $x$-component:

$$\mathcal{F}_2 = \frac{\partial x_1}{\partial c}\frac{\partial^2 y_1}{\partial a \partial t} + \frac{\partial x_{-1}}{\partial c_2}\frac{\partial^2 y_1}{\partial a \partial t} + \frac{\partial^2 y_1}{\partial b \partial t}\frac{\partial y_1}{\partial c} - \frac{\partial x_1}{\partial a}\frac{\partial^2 y_1}{\partial c \partial t} - \frac{\partial x_{-1}}{\partial a_2}\frac{\partial^2 y_1}{\partial c \partial t} - \frac{\partial y_1}{\partial b}\frac{\partial^2 y_1}{\partial c \partial t}$$
$$- \frac{\partial^2 y_1}{\partial c \partial t_1} - \frac{\partial^2 y_1}{\partial c_1 \partial t} - \frac{\partial x_1}{\partial b}\frac{\partial^2 z_1}{\partial a \partial t} + \frac{\partial x_1}{\partial a}\frac{\partial^2 z_1}{\partial b \partial t} + \frac{\partial x_{-1}}{\partial a_2}\frac{\partial^2 z_1}{\partial b \partial t} + \frac{\partial^2 z_1}{\partial b \partial t_1} + \frac{\partial^2 z_1}{\partial b_1 \partial t}$$
$$+ \frac{\partial^2 z_1}{\partial b \partial t}\frac{\partial z_1}{\partial c} - \frac{\partial z_1}{\partial b}\frac{\partial^2 z_1}{\partial c \partial t} + \frac{\partial^2 z_1}{\partial b \partial t}\frac{\partial z_{-1}}{\partial c_2} \qquad \text{(II.B.2)}$$

Irrotationality, $y$-component:

$$\mathcal{G}_2 = \frac{\partial^2 x_1}{\partial a \partial t}\frac{\partial x_1}{\partial c} - \frac{\partial x_1}{\partial a}\frac{\partial^2 x_1}{\partial c \partial t} - \frac{\partial^2 x_1}{\partial c \partial t_1} - \frac{\partial^2 x_1}{\partial c_1 \partial t} - \frac{\partial^2 x_1}{\partial c \partial t}\frac{\partial x_{-1}}{\partial a_2} + \frac{\partial^2 x_1}{\partial a \partial t}\frac{\partial x_{-1}}{\partial c_2}$$
$$- \frac{\partial^2 x_1}{\partial c \partial t}\frac{\partial y_1}{\partial b} + \frac{\partial^2 x_1}{\partial b \partial t}\frac{\partial y_1}{\partial c} + \frac{\partial y_1}{\partial b}\frac{\partial^2 z_1}{\partial a \partial t} + \frac{\partial^2 z_1}{\partial a \partial t_1} + \frac{\partial^2 z_1}{\partial a_1 \partial t} - \frac{\partial y_1}{\partial a}\frac{\partial^2 z_1}{\partial b \partial t}$$
$$+ \frac{\partial^2 z_1}{\partial a \partial t}\frac{\partial z_1}{\partial c} - \frac{\partial z_1}{\partial a}\frac{\partial^2 z_1}{\partial c \partial t} - \frac{\partial^2 z_1}{\partial c \partial t}\frac{\partial z_{-1}}{\partial a_2} + \frac{\partial^2 z_1}{\partial a \partial t}\frac{\partial z_{-1}}{\partial c_2} \qquad \text{(II.B.3)}$$

Free surface condition at $c = 0$, $a$-component:

$$\mathcal{H}_2 = -2\frac{\partial^2 x_1}{\partial t \partial t_1} - \frac{\partial x_1}{\partial a}\frac{\partial^2 x_1}{\partial t^2} - \frac{\partial^2 x_1}{\partial t^2}\frac{\partial x_{-1}}{\partial a_2} - \frac{\partial x_1}{\partial a}\frac{\partial^2 x_{-1}}{\partial t_1^2} - \frac{\partial y_1}{\partial a}\frac{\partial^2 y_1}{\partial t^2} - g\frac{\partial z_1}{\partial a_1} - \frac{\partial z_1}{\partial a}\frac{\partial^2 z_1}{\partial t^2}$$
$$- \frac{\partial^2 z_1}{\partial t^2}\frac{\partial z_{-1}}{\partial a_2} - \frac{\partial z_1}{\partial a}\frac{\partial^2 z_{-1}}{\partial t_1^2} + \gamma\left(-\frac{\partial^3 x_1}{\partial a \partial b^2}\frac{\partial z_1}{\partial a} - \frac{\partial^3 x_1}{\partial a^3}\frac{\partial z_1}{\partial a} - 2\frac{\partial^2 x_1}{\partial a \partial b}\frac{\partial^2 z_1}{\partial a \partial b} - 3\frac{\partial^2 y_1}{\partial a^2}\frac{\partial^2 z_1}{\partial a \partial b}\right.$$
$$- \frac{\partial^2 y_1}{\partial b^2}\frac{\partial^2 z_1}{\partial a \partial b} + 2\frac{\partial^3 z_1}{\partial a \partial b \partial b_1} - 2\frac{\partial y_1}{\partial b}\frac{\partial^3 z_1}{\partial a \partial b^2} - 3\frac{\partial^2 x_1}{\partial a^2}\frac{\partial^2 z_1}{\partial a^2} - \frac{\partial^2 x_1}{\partial b^2}\frac{\partial^2 z_1}{\partial a^2} + 3\frac{\partial^3 z_1}{\partial a^2 \partial a_1}$$
$$- 2\frac{\partial x_1}{\partial b}\frac{\partial^3 z_1}{\partial a^2 \partial b} - 2\frac{\partial y_1}{\partial a}\frac{\partial^3 z_1}{\partial a^2 \partial b} - 2\frac{\partial x_1}{\partial a}\frac{\partial^3 z_1}{\partial a^3} - 2\frac{\partial x_{-1}}{\partial a_2}\frac{\partial^3 z_1}{\partial a^3} + \frac{\partial^3 z_1}{\partial a_1 \partial b^2} - \frac{\partial^3 y_1}{\partial a \partial b^2}\frac{\partial z_1}{\partial b}$$
$$\left. - \frac{\partial^3 y_1}{\partial a^3}\frac{\partial z_1}{\partial b} - 2\frac{\partial^2 y_1}{\partial a \partial b}\frac{\partial^2 z_1}{\partial b^2} - \frac{\partial^3 x_1}{\partial a \partial b^2}\frac{\partial z_{-1}}{\partial a_2} - \frac{\partial^3 x_1}{\partial a^3}\frac{\partial z_{-1}}{\partial a_2}\right) \qquad \text{(II.B.4)}$$

Free surface condition at $c=0$, $b$-component:

$$\mathcal{I}_2 = -\frac{\partial x_1}{\partial b}\frac{\partial^2 x_1}{\partial t^2} - \frac{\partial x_1}{\partial b}\frac{\partial^2 x_{-1}}{\partial t_1^2} - 2\frac{\partial^2 y_1}{\partial t \partial t_1} - \frac{\partial y_1}{\partial b}\frac{\partial^2 y_1}{\partial t^2} - g\frac{\partial z_1}{\partial b_1} - \frac{\partial z_1}{\partial b}\frac{\partial^2 z_1}{\partial t^2} - \frac{\partial z_1}{\partial b}\frac{\partial^2 z_{-1}}{\partial t_1^2}$$
$$+\gamma\left(-\frac{\partial^3 x_1}{\partial a^2 \partial b}\frac{\partial z_1}{\partial a} - \frac{\partial^3 x_1}{\partial b^3}\frac{\partial z_1}{\partial a} + 2\frac{\partial^3 z_1}{\partial a \partial a_1 \partial b} - \frac{\partial^2 x_1}{\partial a^2}\frac{\partial^2 z_1}{\partial a \partial b} - 3\frac{\partial^2 x_1}{\partial b^2}\frac{\partial^2 z_1}{\partial a \partial b}\right.$$
$$-2\frac{\partial^2 y_1}{\partial a \partial b}\frac{\partial^2 z_1}{\partial a \partial b} - 2\frac{\partial x_1}{\partial b}\frac{\partial^3 z_1}{\partial a \partial b^2} - 2\frac{\partial y_1}{\partial a}\frac{\partial^3 z_1}{\partial a \partial b^2} - 2\frac{\partial^2 x_1}{\partial a \partial b}\frac{\partial^2 z_1}{\partial a^2} - 2\frac{\partial x_1}{\partial a}\frac{\partial^3 z_1}{\partial a^2 \partial b}$$
$$-2\frac{\partial x_{-1}}{\partial a_2}\frac{\partial^3 z_1}{\partial a^2 \partial b} + \frac{\partial^3 z_1}{\partial a^2 \partial b_1} - \frac{\partial^3 y_1}{\partial a^2 \partial b}\frac{\partial z_1}{\partial b} - \frac{\partial^3 y_1}{\partial b^3}\frac{\partial z_1}{\partial b} - \frac{\partial^2 y_1}{\partial a^2}\frac{\partial^2 z_1}{\partial b^2} - 3\frac{\partial^2 y_1}{\partial b^2}\frac{\partial^2 z_1}{\partial b^2}$$
$$\left.+3\frac{\partial^3 z_1}{\partial b^2 \partial b_1} - 2\frac{\partial y_1}{\partial b}\frac{\partial^3 z_1}{\partial b^3} - \frac{\partial^3 x_1}{\partial a^2 \partial b}\frac{\partial z_{-1}}{\partial a_2} - \frac{\partial^3 x_1}{\partial b^3}\frac{\partial z_{-1}}{\partial a_2}\right) \qquad \text{(II.B.5)}$$

# II.C Phase relations in the Eulerian frame

In this appendix, we shall derive the phase relations of the short resonating waves in the Eulerian description from the results in the Lagrangian description. Our arguments are similar to Naciri & Mei (1992).

For a leading order theory, it suffices to consider a single short wave. The vertical particle displacement is given by

$$\eta = \epsilon z_1 + \epsilon^2 z_2 + \cdots = \frac{\epsilon}{2}\mathcal{A}\mathrm{e}^{\mathrm{i}S} + \mathcal{O}(\epsilon^2) + \text{c.c.} \quad \text{at} \quad c=0. \qquad \text{(II.C.1)}$$

Here $\mathcal{A}$ is the real, slowly varying amplitude and $S = k_a a + k_b b - \omega t$ is the real, rapidly varying phase of the short wave. We can neglect the complex phase of $\mathcal{A}$ due to dependence on slow variables.

We rewrite (II.2.12) and (II.3.5) to get

$$a = X - \epsilon^{-1}x_{-1} - x_0 - \epsilon x_1 - \epsilon^2 x_2 - \ldots, \qquad \text{(II.C.2)}$$
$$b = Y - \epsilon y_1 - \epsilon^2 y_2 - \ldots. \qquad \text{(II.C.3)}$$

For simplicity, we assume that the long wave amplitude $B$ is real. The expressions for $a$ and $b$ can then be written

$$a = X - \epsilon^{-1}x_{-10} + \epsilon^{-1}B\mathrm{e}^{Kc_2}\sin(Ka_2 - \Omega t_1) + \ldots, \qquad \text{(II.C.4)}$$
$$b = Y + \ldots. \qquad \text{(II.C.5)}$$

The derivatives of the reference positions were found in appendix II.A, but for the present purposes, we only need the leading order contributions. The derivatives at the surface $c=0$, become

$$\frac{\partial a}{\partial t} = -\Omega B\cos(Ka_2 - \Omega t_1), \qquad \frac{\partial a}{\partial X} = 1, \qquad \frac{\partial a}{\partial Y} = 0, \qquad \text{(II.C.6)}$$

$$\frac{\partial b}{\partial t} = 0, \qquad \frac{\partial b}{\partial X} = 0, \qquad \frac{\partial b}{\partial Y} = 1. \tag{II.C.7}$$

Corrections at order $\mathcal{O}(\epsilon)$ depend on the nonlinear interactions between the short waves, and are not considered here.

The leading order Eulerian horizontal wavenumbers and frequency can now be found by the chain rule

$$k_x^E = \frac{\partial S}{\partial X} = k_a \frac{\partial a}{\partial X} + k_b \frac{\partial b}{\partial X} = k_a, \tag{II.C.8}$$

$$k_y^E = \frac{\partial S}{\partial Y} = k_a \frac{\partial a}{\partial Y} + k_b \frac{\partial b}{\partial Y} = k_b, \tag{II.C.9}$$

$$\omega^E = -\frac{\partial S}{\partial t} = -k_a \frac{\partial a}{\partial t} - k_b \frac{\partial b}{\partial t} + \omega = \omega + k_a \Omega B \cos(KX_2 - \Omega t_1). \tag{II.C.10}$$

The Eulerian wavenumber is equal to the Lagrangian wavenumber at the leading order, while the Eulerian frequency experiences a Doppler shift.

Recall that the short wave dispersion relation in the Lagrangian description has the same form as in the Eulerian description, but without a Doppler shift,

$$\omega^2 = gk + \gamma k^3. \tag{II.C.11}$$

We can now find the corresponding dispersion relation in the Eulerian description. It has the anticipated Doppler shift,

$$\left[\omega^E - k_x^E \Omega B \cos(KX_2 - \Omega t_1)\right]^2 = gk^E + \gamma (k^E)^3. \tag{II.C.12}$$

The resonance conditions in the Lagrangian description are

$$\boldsymbol{k}_1 + \boldsymbol{k}_2 = \boldsymbol{k}_3, \qquad \omega_1 + \omega_2 = \omega_3. \tag{II.C.13}$$

It is seen that at the leading order, the resonance conditions in the Eulerian description are not affected by the Doppler shift.

$$\boldsymbol{k}_1^E + \boldsymbol{k}_2^E = \boldsymbol{k}_3^E, \qquad \omega_1^E + \omega_2^E = \omega_3^E. \tag{II.C.14}$$

We conclude that the conditions for resonance in both frames are the same at the leading order.

## II.D Derivation of the long-wave/short-wave interaction coefficient in Eulerian variables

The new terms in the system of evolution equations (II.5.15)–(II.5.17) are those representing interactions between short and long waves. In order to gain physical insight it is instructive to give an alternative derivation. Such an endeavor may also facilitate future studies of the additional effects of wind.

Because the interaction terms are linear in $B$ and $A_n$, it is sufficient to begin from approximate Eulerian equations, linearized with respect to the long wave. It suffices to consider one short wave train. The key to a successful derivation is a nonlinear transformation into a moving coordinate system that follows the the long wave such that the short waves appear to evolve in a stationary medium.

Let the long wave surface displacement and velocity potential be denoted by $\zeta$ and $\Phi$, and the short wave surface displacement and velocity potential be denoted by $\eta$ and $\phi$, respectively. If all quantities are scaled relative to the short wave length and time, we get the exact Eulerian equations

$$\epsilon\frac{\partial^2\Phi}{\partial x_2^2}+\frac{\partial^2\phi}{\partial x^2}+\frac{\partial^2\phi}{\partial y^2}+\epsilon\frac{\partial^2\Phi}{\partial z_2^2}+\frac{\partial^2\phi}{\partial z^2}=0 \qquad \text{for} \quad -\infty<z<\epsilon^{-1}\zeta+\epsilon\eta, \tag{II.D.1}$$

$$\epsilon^{-1}\frac{\partial\zeta}{\partial t_1}+\frac{\partial\eta}{\partial t}+\frac{\partial\Phi}{\partial x_2}\frac{\partial\zeta}{\partial x_2}+\frac{\partial\Phi}{\partial x_2}\frac{\partial\eta}{\partial x}+\epsilon\frac{\partial\zeta}{\partial x_2}\frac{\partial\phi}{\partial x}+\epsilon\frac{\partial\phi}{\partial x}\frac{\partial\eta}{\partial x}+\epsilon\frac{\partial\phi}{\partial y}\frac{\partial\eta}{\partial y}$$
$$-\epsilon^{-1}\frac{\partial\Phi}{\partial z_2}-\frac{\partial\phi}{\partial z}=0 \qquad \text{at} \quad z=\epsilon^{-1}\zeta+\epsilon\eta, \tag{II.D.2}$$

$$\epsilon^{-2}\frac{\partial\Phi}{\partial t_1}+\frac{\partial\phi}{\partial t}+\frac{1}{2}\left(\epsilon^{-\frac{1}{2}}\frac{\partial\Phi}{\partial x_2}+\epsilon^{\frac{1}{2}}\frac{\partial\phi}{\partial x}\right)^2+\frac{1}{2}\epsilon\left(\frac{\partial\phi}{\partial y}\right)^2+\epsilon^{-2}g\zeta+g\eta$$
$$-\gamma\left(\frac{\partial^2\eta}{\partial x^2}+\frac{\partial^2\eta}{\partial y^2}\right)=0 \qquad \text{at} \quad z=\epsilon^{-1}\zeta+\epsilon\eta. \tag{II.D.3}$$

The surface conditions are now Taylor-expanded around the long-wave surface, $z=\epsilon^{-1}\zeta$. The linearized equations for the short waves then become

$$\frac{\partial^2\phi}{\partial x^2}+\frac{\partial^2\phi}{\partial y^2}+\frac{\partial^2\phi}{\partial z^2}=0 \qquad \text{for} \qquad -\infty<z<\epsilon^{-1}\zeta, \tag{II.D.4}$$

$$\frac{\partial\eta}{\partial t}+\frac{\partial\Phi}{\partial x_2}\frac{\partial\eta}{\partial x}+\epsilon\frac{\partial\zeta}{\partial x_2}\frac{\partial\phi}{\partial x}-\frac{\partial\phi}{\partial z}=0 \qquad \text{at} \qquad z=\epsilon^{-1}\zeta, \tag{II.D.5}$$

$$\frac{\partial\phi}{\partial t}+\epsilon\frac{\partial^2\Phi}{\partial t_1\partial z_2}\eta+\frac{\partial\Phi}{\partial x_2}\frac{\partial\phi}{\partial x}+g\eta-\gamma\left(\frac{\partial^2\eta}{\partial x^2}+\frac{\partial^2\eta}{\partial y^2}\right)=0 \qquad \text{at} \qquad z=\epsilon^{-1}\zeta. \tag{II.D.6}$$

These equations will now be subject to a set of moving coordinate transformations. It is important to notice that the changes of coordinates that will be performed subsequently, must be done after evaluation of derivatives at the surface. Hence the surface conditions are not subject to new vertical derivatives. This is because the moving coordinate transformation is independent of the vertical variation of the velocity potentials.

Derivatives of the long-wave quantities are not subject to coordinate transformation, since they are supposed to be known at the surface *a priori*.

Let us introduce a notation for the long-wave surface velocity,

$$U(t_1,x_2)=\frac{\partial\Phi}{\partial x_2}, \qquad W(t_1,x_2)=\frac{\partial\Phi}{\partial z_2} \qquad \text{at} \quad z_2=\epsilon\zeta(t_1,x_2). \tag{II.D.7}$$

Notice that $U$ and $W$ have no $z_2$ dependence since their values are needed only at the surface. We first introduce a new vertical coordinate that follows the vertical displacement of the surface,

$$\bar{z} = z - \epsilon^{-1}\zeta(t_1, x_2). \tag{II.D.8}$$

Then a horizontal transformation moving with the long wave is also introduced, such that the short wave appears to propagate in a stationary medium. If the transformation is of the general form

$$\bar{x} = x - \epsilon^{-1} f(t_1, x_2), \tag{II.D.9}$$

then the advective derivative in the surface conditions becomes

$$\frac{\partial}{\partial t} + U\frac{\partial}{\partial x} = \frac{\partial}{\partial t} + \left(-\frac{\partial f}{\partial t_1} + U - \epsilon U\frac{\partial f}{\partial x_2}\right)\frac{\partial}{\partial \bar{x}}. \tag{II.D.10}$$

For the long wave to appear stationary, we require

$$U - \frac{\partial f}{\partial t_1} - \epsilon U\frac{\partial f}{\partial x_2} = 0. \tag{II.D.11}$$

In terms of the perturbation expansion

$$f = f_0 + \epsilon f_1 + \epsilon^2 f_2 + \ldots, \tag{II.D.12}$$

the solution at any order is

$$f_0 = \int^{t_1} U \,\mathrm{d}t_1', \qquad f_n = -\int^{t_1} U\frac{\partial f_{n-1}}{\partial x_2}\,\mathrm{d}t_1', \quad \text{for } n \geq 1. \tag{II.D.13}$$

The desired horizontal transformation with $\mathcal{O}(\epsilon)$ accuracy is then

$$\bar{x} = x - \epsilon^{-1}\int^{t_1} U \,\mathrm{d}t_1' + \int^{t_1}\left(U\int^{t_1'}\frac{\partial U}{\partial x_2}\,\mathrm{d}t_1''\right)\mathrm{d}t_1'. \tag{II.D.14}$$

Under the two transformations (II.D.8) and (II.D.14), the derivatives are modified to

$$\frac{\partial}{\partial t} = \frac{\partial}{\partial t} - U\frac{\partial}{\partial \bar{x}} + \epsilon U\left(\int^{t_1}\frac{\partial U}{\partial x_2}\,\mathrm{d}t_1'\right)\frac{\partial}{\partial \bar{x}} - \frac{\partial \zeta}{\partial t_1}\frac{\partial}{\partial \bar{z}}, \tag{II.D.15}$$

$$\frac{\partial}{\partial x} = \frac{\partial}{\partial \bar{x}} - \epsilon\left(\int^{t_1}\frac{\partial U}{\partial x_2}\,\mathrm{d}t_1'\right)\frac{\partial}{\partial \bar{x}} - \epsilon\frac{\partial \zeta}{\partial x_2}\frac{\partial}{\partial \bar{z}}, \tag{II.D.16}$$

$$\frac{\partial}{\partial z} = \frac{\partial}{\partial \bar{z}}. \tag{II.D.17}$$

The $z$ derivative remains unchanged since $U$ has been evaluated at the surface before the coordinate transformation, and has no vertical dependence.

The transformed linear equations for the short wave are

$$\frac{\partial^2\phi}{\partial\bar{x}^2} - 2\epsilon\left(\int^{t_1}\frac{\partial U}{\partial x_2}\,\mathrm{d}t_1'\right)\frac{\partial^2\phi}{\partial\bar{x}^2} - 2\epsilon\frac{\partial\zeta}{\partial x_2}\frac{\partial^2\phi}{\partial\bar{x}\partial\bar{z}} + \frac{\partial^2\phi}{\partial y^2} + \frac{\partial^2\phi}{\partial\bar{z}^2} = 0 \qquad \text{for} \quad -\infty < \bar{z} < 0, \tag{II.D.18}$$

$$\frac{\partial\eta}{\partial t} + \epsilon\frac{\partial\zeta}{\partial x_2}\frac{\partial\phi}{\partial\bar{x}} - \frac{\partial\phi}{\partial\bar{z}} = 0 \qquad \text{at} \qquad \bar{z} = 0, \tag{II.D.19}$$

$$\frac{\partial\phi}{\partial t} + \epsilon\frac{\partial W}{\partial t_1}\eta + g\eta - \gamma\left(\frac{\partial^2\eta}{\partial\bar{x}^2} + \frac{\partial^2\eta}{\partial y^2}\right) + 2\epsilon\gamma\left(\int^{t_1}\frac{\partial U}{\partial x_2}\,\mathrm{d}t_1'\right)\frac{\partial^2\eta}{\partial\bar{x}^2} = 0 \qquad \text{at} \qquad \bar{z} = 0. \tag{II.D.20}$$

After introducing the slow coordinates $\bar{x}_1$, $y_1$ and $t_1$ throughout, we assume a WKB solution of the form

$$\eta = (A + \epsilon A_1 + \cdots)\exp\left\{\mathrm{i}\epsilon^{-1}(k_x\bar{x}_1 + k_y y_1 - \omega t_1)\right\}, \tag{II.D.21}$$

$$\phi = (\hat{\phi} + \epsilon\hat{\phi}_1 + \cdots)\exp\left\{\mathrm{i}\epsilon^{-1}(k_x\bar{x}_1 + k_y y_1 - \omega t_1)\right\}, \tag{II.D.22}$$

with $k = \sqrt{k_x^2 + k_y^2}$.

The leading order $\mathcal{O}(1)$ problem is

$$\frac{\partial^2\hat{\phi}}{\partial\bar{z}^2} - k^2\hat{\phi} = 0 \qquad \text{for} \qquad -\infty < \bar{z} < 0, \tag{II.D.23}$$

$$-\mathrm{i}\omega A - \frac{\partial\hat{\phi}}{\partial\bar{z}} = 0 \qquad \text{at} \qquad \bar{z} = 0, \tag{II.D.24}$$

$$-\mathrm{i}\omega\hat{\phi} + (g + \gamma k^2)A = 0 \qquad \text{at} \qquad \bar{z} = 0, \tag{II.D.25}$$

which has the solution

$$\hat{\phi} = -\mathrm{i}\frac{\omega}{k}A\mathrm{e}^{k\bar{z}} \tag{II.D.26}$$

subject to the dispersion relation

$$\omega^2 = gk + \gamma k^3. \tag{II.D.27}$$

In particular, the coordinate transformation has eliminated the Doppler shift in the dispersion relation such that both the wavenumber and the frequency are constants.

The next order $\mathcal{O}(\epsilon)$ problem is

$$\frac{\partial^2\hat{\phi}_1}{\partial\bar{z}^2} - k^2\hat{\phi}_1 = -2\mathrm{i}k_x\frac{\partial\hat{\phi}}{\partial\bar{x}_1} - 2\mathrm{i}k_y\frac{\partial\hat{\phi}}{\partial y_1} - 2k_x^2\left(\int^{t_1}\frac{\partial U}{\partial x_2}\,\mathrm{d}t_1'\right)\hat{\phi} + 2\mathrm{i}k_x k\frac{\partial\zeta}{\partial x_2}\hat{\phi} \qquad \text{for} \qquad -\infty < \bar{z} < 0, \tag{II.D.28}$$

$$-\mathrm{i}\omega A_1 - \frac{\partial\hat{\phi}_1}{\partial\bar{z}} = -\frac{\partial A}{\partial t_1} - \mathrm{i}k_x\frac{\partial\zeta}{\partial x_2}\hat{\phi} \qquad \text{at} \qquad \bar{z} = 0, \tag{II.D.29}$$

$$-\mathrm{i}\omega\hat{\phi}_1 + (g+\gamma k^2)A_1 = -\frac{\partial\hat{\phi}}{\partial t_1} - \frac{\partial W}{\partial t_1}A + 2\mathrm{i}\gamma\left(k_x\frac{\partial A}{\partial\bar{x}_1} + k_y\frac{\partial A}{\partial y_1}\right) + 2\gamma k_x^2\left(\int^{t_1}\frac{\partial U}{\partial x_2}\,\mathrm{d}t_1'\right)A \qquad \text{at} \qquad \bar{z}=0, \tag{II.D.30}$$

The last two surface conditions can be combined to get a condition in terms of $\hat{\phi}_1$ only, and (II.D.26) can be used to eliminate $\hat{\phi}$,

$$\frac{\partial\hat{\phi}_1}{\partial\bar{z}} - k\hat{\phi}_1 = 2\frac{\partial A}{\partial t_1} + k_x\frac{\omega}{k}\frac{\partial\zeta}{\partial x_2}A + \mathrm{i}\frac{k}{\omega}\frac{\partial W}{\partial t_1}A + 2\gamma\frac{k}{\omega}\left(k_x\frac{\partial A}{\partial\bar{x}_1} + k_y\frac{\partial A}{\partial y_1}\right) - 2\mathrm{i}\gamma k_x^2\frac{k}{\omega}\left(\int^{t_1}\frac{\partial U}{\partial x_2}\,\mathrm{d}t_1'\right)A. \tag{II.D.31}$$

The long wave occurs only in the order $\mathcal{O}(\epsilon)$ problem, hence it is sufficient to use the linear solution

$$\zeta = B\cos(Kx_2 - \Omega t_1), \qquad \Phi = \frac{\Omega}{K}B\sin(Kx_2 - \Omega t_1)\mathrm{e}^{Kz_2}, \tag{II.D.32}$$

subject to the dispersion relation

$$\Omega^2 = gK. \tag{II.D.33}$$

Since the second order problem is a inhomogeneous, the following solvability condition must be imposed to avoid secular behavior,

$$\int_{-\infty}^{0}\hat{\phi}\left(\frac{\partial^2\hat{\phi}_1}{\partial\bar{z}^2} - k^2\hat{\phi}_1\right)\mathrm{d}\bar{z} = \hat{\phi}\left(\frac{\partial\hat{\phi}_1}{\partial\bar{z}} - k\hat{\phi}_1\right)\Big|_{\bar{z}=0}. \tag{II.D.34}$$

This gives the following evolution equation for $A$,

$$\frac{\partial A}{\partial t_1} + c_g\left(\frac{k_x}{k}\frac{\partial A}{\partial\bar{x}_1} + \frac{k_y}{k}\frac{\partial A}{\partial y_1}\right) + \mathrm{i}\beta A\cos(Kx_2 - \Omega t_1) = 0. \tag{II.D.35}$$

Here $c_g$ is the group velocity

$$c_g = \frac{g+3\gamma k^2}{2\omega}, \tag{II.D.36}$$

and $\beta$ is the interaction coefficient between the short and the long waves

$$\beta = KB\frac{k}{2\omega}(3\gamma k^2\cos^2 v - g\sin^2 v), \tag{II.D.37}$$

which is identical to (II.5.23).

# II.E Energy, momentum and action

We here derive the expressions for energy, momentum and wave-action for a linear deep-water gravity–capillary wave. Suppose the linear wave is given by

$$\eta = \frac{1}{2}A\mathrm{e}^{\mathrm{i}\theta} + \text{c.c.}, \tag{II.E.1}$$

$$u = \frac{\omega k_a}{2k}A\mathrm{e}^{\mathrm{i}\theta+kc} + \text{c.c.}, \tag{II.E.2}$$

$$v = \frac{\omega k_b}{2k}A\mathrm{e}^{\mathrm{i}\theta+kc} + \text{c.c.}, \tag{II.E.3}$$

$$w = -\frac{i\omega}{2}A\mathrm{e}^{\mathrm{i}\theta+kc} + \text{c.c.}, \tag{II.E.4}$$

were $\theta = k_a a + k_b b - \omega t$ and $k = \sqrt{k_a^2 + k_b^2}$. We let an overline indicate that the rapid oscillation of the phase has been averaged out. Only quadratic nonlinear terms are considered here.

The kinetic energy is

$$K = \int_{-\infty}^{0} \frac{1}{2}\rho\left(\overline{u^2 + v^2 + w^2}\right)\,\mathrm{d}c = \frac{\rho\omega^2}{4k}|A|^2. \tag{II.E.5}$$

The potential gravitational energy is

$$P_g = \overline{\int_0^\eta \rho g c\,\mathrm{d}c} = \frac{1}{4}\rho g|A|^2. \tag{II.E.6}$$

The potential surface energy is

$$P_T = T\left(\overline{\sqrt{1 + \left(\frac{\partial\eta}{\partial a}\right)^2 + \left(\frac{\partial\eta}{\partial b}\right)^2} - 1}\right) = \frac{1}{4}Tk^2|A|^2. \tag{II.E.7}$$

The total potential energy is then, by using the dispersion relation,

$$P = P_g + P_T = \frac{1}{4}\rho\frac{\omega^2}{k}|A|^2, \tag{II.E.8}$$

and the total energy is

$$E = \frac{1}{2}\rho\frac{\omega^2}{k}|A|^2. \tag{II.E.9}$$

We notice that the equipartition theorem holds, i.e. the kinetic and potential energies are equal.

The three components of the linear momentum are

$$M_a = \overline{\int_{-\infty}^{\eta} \rho u\,\mathrm{d}c} = \frac{1}{2}\rho k_a\frac{\omega}{k}|A|^2, \tag{II.E.10}$$

$$M_b = \overline{\int_{-\infty}^{\eta} \rho v \, \mathrm{d}c} = \frac{1}{2}\rho k_b \frac{\omega}{k}|A|^2, \tag{II.E.11}$$

$$M_z = \overline{\int_{-\infty}^{\eta} \rho w \, \mathrm{d}c} = 0. \tag{II.E.12}$$

Finally, the wave-action is given by

$$\frac{E}{\omega} = \frac{1}{2}\rho \frac{\omega}{k}|A|^2. \tag{II.E.13}$$

# II.F Melnikov analysis for the homoclinic trajectory

When $j_* = 0$ and in the absence of a long wave $\beta = 0$, the autonomous system (section II.7) has a homoclinic trajectory connecting the degenerate saddle point back to itself. Because we consider a Hamiltonian system, and the perturbation due to the long wave is conservative and time-dependent, we may expect that an arbitrarily weak disturbance by the long wave will cause the homoclinic trajectory to tangle. This is confirmed by the following Melnikov analysis for $|\beta| \ll 1$.

The perturbed system (II.6.23)–(II.6.24) can be written as

$$\begin{aligned} \frac{\mathrm{d}}{\mathrm{d}t}\begin{pmatrix} j \\ \psi \end{pmatrix} &= f(j,\psi) + \mu g(j,\psi,t) \\ &= \begin{pmatrix} -rj\sqrt{1-j}\sin\psi \\ r\frac{3j-2}{2\sqrt{1-j}}\cos\psi + \Delta \end{pmatrix} + \mu \begin{pmatrix} 0 \\ \beta\cos t \end{pmatrix}. \end{aligned} \tag{II.F.1}$$

where $\mu \ll 1$ is here defined to be the scale of the weak forcing by the long wave.

Without forcing, the homoclinic trajectory associated with the degenerate saddle point at $j = 0$ is given by equation (II.7.16), which we rewrite as

$$j(t) = (1 - (\frac{\Delta}{r})^2)\,\mathrm{sech}^2\,\frac{r(t-t_0)}{2}, \tag{II.F.2}$$

$$\psi(t) = \cos^{-1}\frac{\Delta}{r\sqrt{1 - (1-(\frac{\Delta}{r})^2)\,\mathrm{sech}^2\,\frac{r(t-t_0)}{2}}}, \tag{II.F.3}$$

for the initial condition $j(t_0) = 1 - (\frac{\Delta}{r})^2$,

The Melnikov function is defined by

$$\begin{aligned} M(t_0) &= \int_{-\infty}^{\infty} f(j(t-t_0),\psi(t-t_0)) \wedge g(j(t-t_0),\psi(t-t_0),t)\,\mathrm{d}t \\ &= -r\beta(1-(\frac{\Delta}{r})^2)^{\frac{3}{2}} \int_{-\infty}^{\infty} \mathrm{sech}^2\,\frac{r(t-t_0)}{2}\tanh\frac{r(t-t_0)}{2}\cos t\,\mathrm{d}t \\ &= 2\beta(1-(\frac{\Delta}{r})^2)^{\frac{3}{2}}\sin t_0 \int_{-\infty}^{\infty} \mathrm{sech}^2\,\tau\tanh\tau\sin\frac{2\tau}{r}\,\mathrm{d}\tau. \end{aligned} \tag{II.F.4}$$

By residue calculus, we can show that

$$\int_{-\infty}^{\infty} \operatorname{sech}^2 t \tanh t \sin(wt)\, \mathrm{d}t = \frac{\pi w^2}{2} \operatorname{csch} \frac{\pi w}{2}. \tag{II.F.5}$$

The Melnikov function is then

$$M(t_0) = \frac{4\pi\beta(1 - (\frac{\Delta}{r})^2)^{\frac{3}{2}} \sin t_0}{r^2 \sinh \frac{\pi}{r}}. \tag{II.F.6}$$

Whenever the condition for the existence of the homoclinic trajectory is satisfied, $|\Delta/r| < 1$, the Melnikov function has simple zeroes regardless of $\beta$, $r$ and $\Delta$. Hence the homoclinic loop will always tangle for any small forcing $\beta$.

# Part III: Time evolution of Wilton's ripples forced by wind and damped by viscosity

## Notations for Part III

| | |
|---|---|
| $A$ | Complex amplitude of first-harmonic Wilton's ripple. |
| $\mathcal{A}$ | Complex amplitude of a single gravity–capillary wave. |
| $a$ | Typical wave amplitude. |
| $a_{k,0}, a_{k,1}$ | Coefficients due to wind-induced current at harmonic $k$. |
| $B$ | Complex amplitude of second-harmonic Wilton's ripple. |
| $b_k$ | Coefficient due to wind-induced current at harmonic $k$. |
| $c$ | Coefficient due to wind-induced current. |
| $\bar{c}$ | Dimensional phase speed of first-harmonic Wilton's ripple. |
| c.c. | Complex conjugate terms. |
| $d_k$ | Coefficients for linear growth rate at harmonic $k$. |
| $d_{k,R}, d_{k,I}$ | Real and imaginary parts of $d_k$. |
| $E$ | Energy of Wilton's ripples. |
| $E_0$ | Second-order energy of Wilton's ripples. |
| e | 2.71828182845... |
| $g$ | Acceleration due to gravity. |
| $H$ | Hamiltonian. |
| i | $\sqrt{-1}$. |
| $k$ | Normalized wavenumber. |
| $k_a, k_b$ | Detuned wavenumbers for the first and second harmonic. |
| $k^*$ | Wavenumber of gravity–capillary wave of smallest phase velocity. |
| $\bar{k}$ | Dimensional wavenumber of first-harmonic Wilton's ripple. |
| $M_x$ | Horizontal momentum of Wilton's ripples. |
| $N$ | Normal stress. |
| $N^{(n)}$ | Perturbation normal stress at order $n$. |
| $\hat{N}_k^{(n)}$ | Perturbation normal stress at order $n$ and harmonic $k$. |
| $\hat{N}_{k,R}^{(n)}, \hat{N}_{k,I}^{(n)}$ | Real and imaginary parts of $\hat{N}_k^{(n)}$. |
| $\mathcal{O}(\cdot)$ | Order of. |
| $p$ | Sections III.2 and III.3: Dimensional water pressure. |

| | |
|---|---|
| | Elsewhere: Normalized interior inviscid water pressure. |
| $p'$ | Sections III.2 and III.3: Dimensional air pressure. |
| | Elsewhere: Normalized interior inviscid air pressure. |
| $p_{BL}$ | Normalized boundary-layer water pressure. |
| $p'_{BL}$ | Normalized boundary-layer air pressure. |
| $p_T$ | Normalized total wave-induced water pressure. |
| $p'_T$ | Normalized total wave-induced air pressure. |
| $p^{(n)}$ | Total air pressure at order $n$. |
| $\hat{p}_k^{(n)}$ | Total air pressure at order $n$ and harmonic $k$. |
| $T$ | Tangential stress. |
| $\hat{T}_k$ | Tangential stress at harmonic $k$. |
| $t$ | Time. |
| $t_1, t_2$ | Slow modulation times. |
| $\mathcal{U}$ | Absolute amplitude of first amplitude $A$. |
| $U^S$ | Dimensional (III.2 and III.3) and normalized (elsewhere) horizontal wind velocity in water. |
| $U'^S$ | Dimensional (III.2 and III.3) and normalized (elsewhere) horizontal wind velocity in air. |
| $U_d$ | Dimensional (III.2 and III.3) and normalized (elsewhere) horizontal wind drift velocity at the water surface. |
| $u$ | Dimensional horizontal water velocity (III.2 and III.3), normalized interior inviscid horizontal water velocity (elsewhere). |
| $u'$ | Sections III.2 and III.3: Dimensional horizontal air velocity. |
| | Elsewhere: Normalized interior inviscid horizontal air velocity. |
| $u_{BL}$ | Normalized horizontal boundary-layer water velocity. |
| $u'_{BL}$ | Normalized horizontal boundary-layer air velocity. |
| $u_T$ | Normalized total wave-induced horizontal water velocity. |
| $u'_T$ | Normalized total wave-induced horizontal air velocity. |
| $u_*$ | Friction velocity in water. |
| $u'_*$ | Friction velocity in air. |
| $u'_{*LU}$ | Minimum $u'_*$ above which both harmonics are linearly unstable. |
| $u'_{*TC}$ | Value of $u'_*$ at a transcritical bifurcation. |
| $u'_{*TP}$ | Value of $u'_*$ at a regular turning point. |
| $\mathcal{V}$ | Absolute amplitude of second amplitude $B$. |
| $w$ | Sections III.2 and III.3: Dimensional vertical water velocity. |
| | Elsewhere: Normalized interior inviscid vertical water velocity. |
| $w'$ | Sections III.2 and III.3: Dimensional vertical air velocity. |
| | Elsewhere: Normalized interior inviscid vertical air velocity. |
| $w_{BL}$ | Normalized horizontal boundary-layer water velocity. |
| $w'_{BL}$ | Normalized horizontal boundary-layer air velocity. |
| $w_T$ | Normalized total wave-induced vertical water velocity. |
| $w'_T$ | Normalized total wave-induced vertical air velocity. |
| $X$ | Transformed dynamical variable. |
| $X_c$ | Center of second-order system. |

| | |
|---|---|
| $x$ | Horizontal position. |
| $x_1, x_2$ | Long horizontal modulation scales. |
| $Y$ | Transformed dynamical variable. |
| $Y_c$ | Center of second-order system. |
| $Z$ | Transformed dynamical variable. |
| $Z_c$ | Center of second-order system. |
| $z$ | Vertical position. |
| $z_{BL}$ | Vertical boundary-layer coordinate in water. |
| $z'_{BL}$ | Vertical boundary-layer coordinate in air. |
| $\bar{z}_{BL}$ | Vertical coordinate in water following the surface. |
| $\alpha_1, \alpha_2, \alpha_3$ | Coefficients of dynamical system. |
| $\alpha_{1,0}, \alpha_{2,0}, \alpha_{3,0}$ | Coefficients of dynamical system at second order. |
| $\alpha_{1,1}, \alpha_{2,1}, \alpha_{3,1}$ | Coefficients of dynamical system at third order. |
| $\beta$ | Linear growth rate. |
| $\Gamma$ | Surface tension between water and air. |
| $\delta$ | Detuning. |
| $\delta_a, \delta_b$ | Detuning of first and second harmonic. |
| $\epsilon$ | Small ordering parameter indicating short-wave steepness. |
| $\eta$ | Dimensional (sections III.2 and III.3) and normalized (elsewhere) surface displacement. |
| $\eta_n$ | Surface displacement at order $n$. |
| $\hat{\eta}_{n,k}$ | Surface displacement at order $n$, harmonic $k$. |
| $\theta$ | Detuned phase. |
| $\theta_1, \theta_2$ | Phases of first and second harmonic. |
| $\kappa$ | Kármán's universal constant. |
| $\lambda$ | Eigenvalue. |
| $\mu$ | Viscous shear-layer thickness in air. |
| $\nu$ | Kinematic viscosity of water. |
| $\nu'$ | Kinematic viscosity of air. |
| $\pi$ | 3.1415926535... |
| $\rho$ | Density of water. |
| $\rho'$ | Density of air. |
| $\sigma^2$ | Dimensionless viscosity in water. |
| $\sigma'^2$ | Dimensionless viscosity in air. |
| $\tau^S$ | Shear stress on water surface. |
| $\phi$ | Total phase. |
| $\Psi$ | Wind stream function in water. |
| $\Psi'$ | Wind stream function in air. |
| $\psi$ | Interior inviscid stream function in water. |
| $\psi_n$ | Interior inviscid stream function in water at order $n$. |
| $\hat{\psi}_{n,k}$ | Interior inviscid stream function in water at order $n$, harmonic $k$. |
| $\psi'$ | Interior inviscid stream function in air. |
| $\hat{\psi}_k^{(n)}$ | Total stream function in air at order $n$ and harmonic $k$. |
| $\psi_{BL}$ | Boundary-layer stream function in water. |

| | |
|---|---|
| $\hat{\psi}_{BL,k}$ | Boundary-layer stream function in water at harmonic $k$. |
| $\psi'_{BL}$ | Boundary-layer stream function in air. |
| $\psi'_T$ | Total stream function in air. |
| $\psi^{(n)}$ | Total stream functions in air at order $n$. |
| $\omega$ | Normalized angular frequency. |
| $\omega^*$ | Dimensional frequency of gravity–capillary wave of smallest phase velocity. |
| $\bar{\omega}$ | Dimensional frequency of first-harmonic Wilton's ripple. |

# III.1 Introduction

## III.1.1 Literature review

Interest in the nonlinear evolution of water-surface waves was spurred by the prediction of Lighthill (1965) and subsequent measurements of Feir (1967), that uniform Stokes waves are modulationally unstable. This particular form of modulational instability is now known as Benjamin–Feir instability (Benjamin & Feir 1967).

The leading-order nonlinear modulation of gravity waves was found to be governed by a cubic Schrödinger equation by Benney & Newell (1967), Zakharov (1968), Hasimoto & Ono (1972) and Davey (1972). Lake, Yuen, Rungaldier & Ferguson (1977) investigated both experimentally and numerically the long-time evolution of a uniform gravity wave with sideband disturbances. Theoretically, they found that the upper and lower sidebands initially grow at equal rates, at the expense of the carrier frequency. Then follows a period of strong modulation of the wave, which is in turn followed by a recurrence of the initial state of a uniform wave with small sideband disturbances. In their experiments, however, they found that when an approximate recurrence of the initial uniform wave train occurred, the frequency had sometimes been lowered from the original carrier wave frequency to that of the most unstable lower sideband. It can further be seen from their experimental records that the wave-group envelopes can be asymmetric, suggesting uneven growth of the upper and lower sidebands.

A fourth-order extension of the nonlinear Schrödinger equation for gravity waves was derived by Dysthe (1979). The fourth-order effect on the initial growth rates of the unstable sidebands was found to cause the lower sideband to grow faster than the upper sideband. Lo & Mei (1985) subsequently performed a numerical integration for the long-time evolution of the fourth-order equations. The initial uneven growth of the upper and lower sidebands was shown to give rise to asymmetric wave-groups, in good agreement with experimental data. However, the fourth-order equations still predicted that the recurrence of the initial uniform wave train should occur without a permanent down-shift in frequency.

Experiments indicate that the down-shift does not always happen, but only when the initial steepness of the uniform wave train is sufficiently large. Melville (1982) performed experiments suggesting that the initial steepness should be greater than 0.16. These experiments also suggested that whenever down-shift occurs, there is also wave-breaking. Further experimental work by Melville (1983) showed that spatial separation of the different frequency components occurs during the evolution of the modulational instability. It so happens that the spatial localization of the upper sideband corresponds to the steepest parts of the wave train, where the wave is most likely to break. Following these ideas, Trulsen & Dysthe (1990) extended the work of Lo & Mei (1985) by incorporating an empirical model for dissipation due to wave-breaking into the fourth-order equations of Dysthe (1979), where waves are damped when the steepness exceeds a critical value. A permanent down-shift was indeed found to occur, lasting well beyond the characteristic time of recurrence.

Hara & Mei (1991) studied the long-time evolution of nonlinear gravity waves

subject to forcing by a weak wind and viscous dissipation. The non-conservative effects were balanced at the fourth order such that wind and viscous dissipation balance approximatly over a long time. They showed that down-shift is possible without wave-breaking. Poitevin & Kharif (1991) studied the nonlinear evolution of a uniform wavetrain using a high-order spectral method, including the effects of viscosity and capillarity. Their model also showed a lasting frequency down-shift. Uchiyama & Kawahara (1994) gave further evidence that viscous damping can be responsible for the down-shifting in a model that accounted for viscous boundary-layer effects on the induced mean flow.

Experiments for stronger winds were performed by Bliven, Huang & Long (1986), suggesting that for a sufficiently strong wind, modulational instability may be reduced or even suppressed. Extending their previous work, Trulsen & Dysthe (1992) incorporated an empirical model for the growth-rate due to wind according to Plant (1982), and verified that a stronger wind can indeed reduce or suppress modulational instability.

The nonlinear modulation of gravity–capillary waves was found to obey a cubically nonlinear Schrödinger equation by Djordjevic & Redekopp (1977). They noted that a gravity–capillary wave may resonate with its second harmonic, and in the case of finite depth it may also resonate with its own induced long shallow-water wave. Hogan (1985) extended the analysis to the fourth order in steepness, similar to Dysthe (1979) for a pure gravity wave. Hara & Mei (1994) extended their previous work by considering the long-time evolution of nonlinear gravity–capillary waves subject to forcing by a weak wind and viscous dissipation. The non-conservative effects were again balanced at the fourth order. They showed that down-shift is also possible for gravity–capillary waves, but there may also be up-shift occurring for very short waves.

The above theories for gravity–capillary waves are invalid when there is harmonic resonance, through which two different harmonics of the carrier wave are both free waves that interact nonlinearly. The theoretical study of resonant interactions between gravity–capillary waves was initiated by Harrison (1909) and Wilton (1915). Wilton (1915) solved the steady progressive waves resulting from exact second harmonic resonance. Wilton's solution was generalized to allow for detuning by Pierson & Fife (1961). These waves are now known as steady Wilton's ripples. McGoldrick (1965) and Simmons (1969) later showed that Wilton's ripples are just a special case of general triad resonance.[4] Indeed, McGoldrick (1970b) pointed out that the steady solutions of Wilton (1915) correspond to special initial conditions for the general triad resonance theory. Nayfeh (1973) considered inviscid conservative Wilton's ripples in the presence of a uniform airflow above the water surface.

Jones (1992) derived cubically nonlinear evolution equations for Wilton's ripples in order to investigate their slow time and space modulation. A stability analysis was presented for uniform wave solutions. Christodoulides & Dias (1994) considered cubically nonlinear steady Wilton's ripples on the interface between two fluids of different densities. They let each wave consist of two components propagating in

[4] A more extensive review of general conservative triad resonance is given in part II.

opposite directions, and found that the oppositely propagating waves are coupled at the third nonlinear order. They also found that new and interesting bifurcations arise when the density ratio is varied.

If resonant triads are driven by wind, then the interaction will occur in the wind-induced shear-current in the water. Morland (1994) assumed that the shear-current was of the same order of magnitude as the phase velocity of the waves, and solved the Rayleigh equation for the wave disturbance in water. He also discussed the modifications to the kinematic resonance conditions due to the wind-induced current.

Bifurcations of steady wave trains subject to harmonic resonance were studied by Chen & Saffman (1979). They showed that steady Wilton's ripples are associated with a period-doubling bifurcation, through which a pure steady second-harmonic wave can become a steady combination wave of the first and second harmonics. Janssen (1986) investigated the initial growth of Wilton's ripples subject to wind forcing and viscous damping, and found that the wind can give rise to a sudden period doubling of the waves, i.e. from the second to the first harmonic of a Wilton's ripple. This numerical result is in qualitative agreement with experimental laboratory observations of Choi (1977) and Ramamonjiarisoa, Baldy & Choi (1978) (see figure 2 in the General Introduction). Janssen (1987) later generalized his analysis to a continuous spectrum of waves subject to three-dimensional resonant triad interaction forced by wind. He found that under certain conditions there may be a sudden migration of the peak of the spectrum to lower wavenumbers. In both papers, Janssen (1986, 1987) employed a wind forcing that is much stronger than the damping due to viscosity, and hence the theory is only valid for a limited time until the wave amplitudes become too large. He concluded that nonlinear second-harmonic or three-wave interaction may be important during the generation of the initial wavelets by wind.

In general, non-conservative triad-interaction can be brought about in two ways; either by linear damping or growth of individual waves, or by non-conservative quadratic interaction. Viscous damping and linear wind forcing of water waves gives rise to the first mechanism. The second mechanism can be brought about by triad-interaction in shear flows, and, as we shall see in this study, by nonlinear wind forcing of waves.

Non-conservative long-time evolution of triad resonance in plasma physics was investigated by Vyshkind & Rabinovich (1976). They used generic quadratically nonlinear model equations for which linear non-conservative effects were balanced at the quadratic order. It was shown that the dynamical behavior can be chaotic. Wersinger, Finn & Ott (1980a, 1980b), reconsidered the same problem and found that the system can exhibit a sequence of period doubling followed by apparently chaotic behavior. Hughes & Proctor (1990) studied bifurcation and chaos in a model for triad resonance where one wave is linearly unstable and the other two are more heavily damped, while having energy-preserving quadratic interaction.

McDougall & Craik (1991) considered triad resonance with non-conservative quadratic coupling, and found that the system can "blow up" after a finite time. They hence suggested that cubically nonlinear terms may be necessary for a physically consistent theory. Hughes & Proctor (1992) considered triad interaction with non-conservative quadratic coupling, where two modes are damped and have identical

properties, while the third mode is linearly unstable. They specifically focused their attention on a parameter range that did not lead to unbounded solutions.

Bontozoglou & Hanratty (1990) explained the observation of Choi (1977) by a Kelvin–Helmholtz instability mechanism. However, their theory seems to be most appropriate for strong winds and highly viscous fluids. Jurman, Deutsch & McCready (1992) presented theory and experiments on centimeter range wind-driven surface waves on a shallow and highly viscous fluid (they used a glycerine-water solution with viscosity 10–100 times greater than water). They adjusted the gas flow to be just sufficient to produce measurable waves. They were able to observe that a fundamental wave, corresponding to the highest linear growth rate due to wind, could saturate at a small steepness, while energy was transferred from the fundamental to its second-harmonic which was linearly damped.

Miles (1976) gave an analytical solution for secons-harmonic resonance with damping. Craik (1986) gave analytical solutions for certain special cases of non-conservative triad interaction. Chow, Bers & Ram (1992) showed that non-conservative space-time evolution of the equations for triad resonance may yield spatio-temporal chaos.

It is worthwhile noticing that theories on non-conservative triad interaction generally fall into two categories. In applications with relevance to plasma physics, the high-frequency wave is often unstable while the low-frequency wave is damped, and hence energy is transferred to the low-frequency wave by nonlinearity and then dissipated. The resulting dynamical behavior often leads to chaos through a series of period-doubling bifurcations. In applications with relevance to hydrodynamics, the high-frequency wave is usually damped while the low-frequency wave is unstable, and hence energy is transferred to the high-frequency wave by nonlinearity and then dissipated. In such cases the second-order nonlinear theory often predicts "blow-up" unless the forcing is very weak.

Field observations of three and four-wave resonant interactions on the sea surface have been reported by Strizhkin & Raletnev (1986). They analyzed photographs taken from a platform at 14 m height. Triad interaction was observed for winds in the range 2.7–18 m/s. Four-wave interaction was also observed, but for a larger threshold wind speed, typically greater than 4–6 m/s. They reported that the detection of resonant triads was often made difficult by the presence of much longer gravity waves. When the long gravity waves were taken into account, the discrepancies in the resonance conditions for frequencies and wavenumbers was reportedly reduced.

Wind can cause waves to grow either because of the part of the normal wind stress in phase with the surface slope, or because of the part of the tangential wind stress in phase with the surface elevation.

Modern theories for how wind can force waves, were begun by Phillips (1957) and Miles (1957). The former proposed a wave generation mechanism whereby random turbulent pressure fluctuations in the air would cause waves to grow. In this model, there is no feedback from the waves to the disturbance in the air. This mechanism is likely to be important only at the very initial stage of wave development, and has been shown to be insignificant for wave growth. Miles (1957) proposed that gravity waves may be forced by a shear instability mechanism, by which the waves excite an instability in the air according to the inviscid Orr–Sommerfeld equation. The

resulting inviscid normal pressure exerted from the air on the water will cause waves to grow. The shear-profile in the air was governed by the universal logarithmic law for turbulent flow over a plate, while any induced motion in water was neglected. The rate of energy transfer to the waves was found to be proportional to the curvature of the shear profile at the critical height where the wind velocity is equal to the phase velocity of the wave.

Benjamin (1959) calculated the shear stresses on a wavy boundary due to shear flow. Miles (1959a) reconsidered the growth of gravity waves by solving the problem more accurately. By keeping the leading order viscous term in the Orr–Sommerfeld equation, it was shown that viscous effects are not important for the growth of long gravity waves. On the other hand, Miles (1959b) showed that a Kelvin-Helmholtz instability mechanism is not important for the growth of water waves, since the required wind speed would be unrealistically high due to the small viscosity of water.

Miles (1962) considered the growth of gravity–capillary waves and short gravity waves by using a viscous Orr–Sommerfeld equation and a linear-logarithmic wind profile. He found that for the growth of short waves, viscid stresses are much more important than the inviscid normal stress associated with the curvature of the wind profile (Miles 1957). Indeed for short waves the critical height is often within the linear viscous sublayer of the wind profile, where the curvature vanishes.

Shemdin (1972) investigated experimentally and analytically the effect of wind-generated surface drift on waves, and found that it can significantly modify the dispersion relation. Valenzuela (1976) considered the modifications to the wave growth rates and phase speeds due to a coupled linear-logarithmic shear flow in air and water. He suggested that when the flow in the water is vanishing, Miles (1962) underestimated the growth rates for small wavenumbers and overestimated the growth rates for large wavenumbers. The shear flow in the water was shown to be capable of causing a significant increase in the growth rate. Kawai (1979) presented both theory and experiments on the initial growth rates of waves due to wind. It was demonstrated that there exists waves with maximum growth rates, which are precisely the dominant waves seen in experiments. These waves are short gravity–capillary waves. It was also shown that the initial linear mechanism for growth is only valid for a short time, after which the waves become decidedly nonlinear.

Gastel, Janssen & Komen (1985) reconsidered the wind-induced growth of gravity–capillary waves. They solved the shear flow problem in water and the viscous part of the shear flow problem in air analytically by asymptotic methods, while the inviscid part of the shear flow problem in air was solved numerically. They found that the growth rate is sensitive to the assumed wind profile in air, but is not sensitive to the wind-induced current profile in water.

Short waves riding on long waves can also be modulated indirectly by the long-wave induced modulation of the wind, which will give rise to a periodic wind-forcing of the short waves. Troitskaya (1994) solved the modified Orr–Sommerfeld equation, where the modulational effect of the long wave was accounted for by multiple-scales perturbation.

### III.1.2 Objectives of the present work

In nature, gravity–capillary waves often owe their existence to a gentle wind blowing over water. It is our goal here to develop a model for the non-conservative long-time evolution of Wilton's ripples, by incorporating a gentle wind and viscous dissipation that are of comparable order of magnitude.

Previous studies on non-conservative second-order resonance (Vyshkind & Rabinovich 1976; Wersinger, Finn & Ott 1980a, 1980b; Craik 1986; Janssen 1986, 1987; Hughes & Proctor 1990, 1992; McDougall & Craik 1991; Chow, Bers & Ram 1992; Jurman, Deutsch & McCready 1992) have included the non-conservative effects at the second order. We shall now explain why this may not be appropriate for the long-time evolution of water waves, due to the small viscosity of water and our desire to balance wave growth and damping. Hence the non-conservative effects should instead be included at the third order.

Consider a fresh and clean water surface without the effects of aging or contamination. Because the length-scales are small, it is reasonable to employ a laminar viscosity. At 20°C the following values for surface tension, density, gravitational acceleration and viscosity can be taken:

$$\Gamma = 7.28 \cdot 10^{-2}\,\mathrm{N/m}, \quad \rho = 9.98 \cdot 10^{2}\,\mathrm{kg/m^3}, \quad g = 9.80\,\mathrm{m/s^2}, \quad \nu = 1.00 \cdot 10^{-6}\mathrm{m^2/s}.$$

We define the characteristic wavenumber and frequency by equating the gravity and capillary terms in the dispersion relation, corresponding to the minimum phase velocity, i.e.

$$k^* = \sqrt{\frac{\rho g}{T}} = 367\,\mathrm{m^{-1}}, \quad \omega^* = \sqrt{2gk^*} = 84.8\,\mathrm{s^{-1}}. \tag{III.1.1}$$

This corresponds to wavelength 1.7 cm, frequency 13 Hz and phase velocity 0.23 m/s. For a clean water surface, the ratio of a wave period to the damping time is then

$$\frac{1}{\omega^*} 2\nu (k^*)^2 = 0.0032.$$

The ratio of a wave period to the time for second-order resonant interaction is known to be comparable to the wave steepness. If we let the steepness be in the range $\epsilon = \mathcal{O}(0.03)$–$\mathcal{O}(0.1)$, then internal viscous damping can be scaled at the third order. The typical wave amplitude is then in the range from 80 $\mu$m to 0.3 mm. If viscous effects were scaled at the second order, as in the references cited, then the steepness must be roughly of the order $\epsilon = \mathcal{O}(0.0032)$, and the typical wave amplitude is about 9 $\mu$m. Even though it has been reported that wave amplitudes can be measured with sensitivity down to 0.4 $\mu$m (e.g. Liu, Paul & Gollub 1993), such a small characteristic amplitude is probably not very interesting for practical applications of gravity–capillary waves.

The scales for steepness and amplitude can be made larger by balancing wind forcing and viscous damping at a higher nonlinear order. Hara & Mei (1994) considered a case where there is such a balance at the fourth order. Their characteristic steepness is therefore implied to be of the order $\epsilon = \mathcal{O}(0.0032^{1/3}) = \mathcal{O}(0.15)$. On

the other hand, Janssen (1986) scaled both wind forcing and viscous damping at the second order, but let growth due to wind dominate over viscous damping such that the waves will grow until they eventually violate the weakly nonlinear theory.

If, on the other hand, the surface is contaminated and behaves as an inextensible film, the non-dimensional characteristic damping rate can be found to be

$$\frac{1}{\omega^*}\frac{k^*}{2}\sqrt{\frac{\nu\omega^*}{2}} = 0.014.$$

Viscosity is then more important in the study of the long-time behavior, and the non-conservative effects can be balanced at a lower order.

Based on these estimates, we shall assume that the surface is clean, and balance the effects of viscous dissipation and wave-growth due to a gentle wind at the third order in the evolution equations for Wilton's ripples[5]. It will be shown that for a single monochromatic wave, the leading order nonlinear effects in air are of third order and relatively insignificant. However for Wilton's ripples, nonlinear effects in air are of second order, and are much more important.

Our model has only two independent parameters: (1) the strength of the wind, given in terms of the friction velocity in air $u'_*$, and (2) the detuning parameter $\delta$ measuring imperfect second-harmonic resonance.

In section III.2 we first summarize the governing equations in Eulerian form for small wave disturbances in the presence of a coupled air-water shear flow. In section III.3 we discuss the normalization assumptions. In section III.4, the equations and boundary conditions for the wave disturbance in water and air are expanded in multiple-scales perturbation expansions.

It is found useful for later reference to first derive the evolution equation for a single gravity–capillary wave. This is done in section III.5. Then the coupled evolution equations for second-harmonic resonance (Wilton's ripples) are derived in section III.6. Our results are in correspondence with previous related works by Hara & Mei (1994) and Jones (1992). We discover interaction terms which do not seem to have been reported previously. At the end of section III.6 we summarize expressions for the total energy and momentum of the two Wilton's ripples, and show how these quantities evolve in time. The energy and momentum are derived from first principles in Appendix III.A.

The perturbation problem for the wave disturbance in air is solved in section III.7. We compare our linear growth rates to those of Gastel, Janssen & Komen (1985), and find good agreement for the cases where our two theories apply.

In section III.8, the dynamical system is reduced to three dimensions and transformed into a convenient rectangular representation. The second-order behavior is reviewed, and previous bifurcation results of Chen & Saffman (1979) are recovered. The third-order behavior is investigated by first discussing the existence and stability of fixed points, and then presenting numerical computations.

[5]Ideally, we would have liked to study non-conservative three-dimensional triad resonance, but it proved to be too algebraically intractable to carry out to the third order.

# III.2 Governing equations and steady wind profile

Let us summarize the full governing equations for a short-wave disturbance in water and air, subject to viscous stress and a steady wind and induced shear current.

We use a two-dimensional Eulerian system with $x$ and $z$ denoting the horizontal and vertical coordinates. The steady shear flow due to wind is denoted by $U^S(z)$, and has a component in the $x$-direction only. Those terms that only govern the steady shear flow have been separated out and are not included here. The short-wave disturbance has horizontal and vertical velocity components $u$ and $w$, and pressure component $p$. The resulting surface displacement is denoted by $\eta$. The density is $\rho$, the kinematic viscosity is $\nu$, and the surface tension between water and air is $\Gamma$. We let all quantities in air have primes, while the corresponding quantities in water are unprimed. In water, the governing equations for the wave disturbance are as follows:

Continuity:

$$\frac{\partial u}{\partial x} + \frac{\partial w}{\partial z} = 0. \tag{III.2.1}$$

Momentum conservation:

$$\frac{\partial u}{\partial t} + u\frac{\partial u}{\partial x} + U^S\frac{\partial u}{\partial x} + w\frac{\partial u}{\partial z} + w\frac{\partial U^S}{\partial z} = -\frac{1}{\rho}\frac{\partial p}{\partial x} + \nu\left(\frac{\partial^2}{\partial x^2} + \frac{\partial^2}{\partial z^2}\right)u, \tag{III.2.2}$$

$$\frac{\partial w}{\partial t} + u\frac{\partial w}{\partial x} + U^S\frac{\partial w}{\partial x} + w\frac{\partial w}{\partial z} = -\frac{1}{\rho}\frac{\partial p}{\partial z} + \nu\left(\frac{\partial^2}{\partial x^2} + \frac{\partial^2}{\partial z^2}\right)w. \tag{III.2.3}$$

The air disturbance is described by similar equations with the corresponding quantities distinguished by primed symbols:

Continuity:

$$\frac{\partial u'}{\partial x} + \frac{\partial w'}{\partial z} = 0. \tag{III.2.4}$$

Momentum conservation:

$$\frac{\partial u'}{\partial t} + u'\frac{\partial u'}{\partial x} + U'^S\frac{\partial u'}{\partial x} + w'\frac{\partial u'}{\partial z} + w'\frac{\partial U'^S}{\partial z} = -\frac{1}{\rho'}\frac{\partial p'}{\partial x} + \nu'\left(\frac{\partial^2}{\partial x^2} + \frac{\partial^2}{\partial z^2}\right)u', \tag{III.2.5}$$

$$\frac{\partial w'}{\partial t} + u'\frac{\partial w'}{\partial x} + U'^S\frac{\partial w'}{\partial x} + w'\frac{\partial w'}{\partial z} = -\frac{1}{\rho'}\frac{\partial p'}{\partial z} + \nu'\left(\frac{\partial^2}{\partial x^2} + \frac{\partial^2}{\partial z^2}\right)w'. \tag{III.2.6}$$

At the water surface, the velocity is continuous,

$$u + U^S = u' + U'^S, \qquad w = w' \qquad \text{at} \quad z = \eta. \tag{III.2.7}$$

The kinematic surface condition is

$$\frac{\partial \eta}{\partial t} + u\frac{\partial \eta}{\partial x} + U^S\frac{\partial \eta}{\partial x} = w \qquad \text{at} \quad z = \eta. \tag{III.2.8}$$

The normal stress condition is, keeping only quadratically nonlinear terms for the viscous stress and cubic terms for the surface tension,

$$-\frac{p}{\rho}+g\eta+\nu\left[-2\left(\frac{\partial u}{\partial z}+\frac{\partial w}{\partial x}\right)\frac{\partial \eta}{\partial x}-2\frac{\partial U^S}{\partial z}\frac{\partial \eta}{\partial x}+2\frac{\partial w}{\partial z}\right]-\frac{\Gamma}{\rho}\frac{\partial^2\eta}{\partial x^2}\left(1-\frac{3}{2}\left(\frac{\partial \eta}{\partial x}\right)^2\right)$$

$$=\frac{\rho'}{\rho}\left\{-\frac{p'}{\rho'}+g\eta+\nu'\left[-2\left(\frac{\partial u'}{\partial z}+\frac{\partial w'}{\partial x}\right)\frac{\partial \eta}{\partial x}-2\frac{\partial U'^S}{\partial z}\frac{\partial \eta}{\partial x}+2\frac{\partial w'}{\partial z}\right]\right\}\qquad \text{at}\quad z=\eta. \tag{III.2.9}$$

The tangential stress condition with only quadratic terms is

$$\nu\left[-2\frac{\partial u}{\partial x}\frac{\partial \eta}{\partial x}+\frac{\partial u}{\partial z}+\frac{\partial w}{\partial x}+\frac{\partial U^S}{\partial z}+2\frac{\partial w}{\partial z}\frac{\partial \eta}{\partial x}\right]$$
$$=\frac{\rho'\nu'}{\rho}\left[-2\frac{\partial u'}{\partial x}\frac{\partial \eta}{\partial x}+\frac{\partial u'}{\partial z}+\frac{\partial w'}{\partial x}+\frac{\partial U'^S}{\partial z}+2\frac{\partial w'}{\partial z}\frac{\partial \eta}{\partial x}\right]\qquad \text{at}\quad z=\eta. \tag{III.2.10}$$

We also require that the wave disturbance dies out at large depth and height,

$$u,w,p\to 0\qquad \text{as}\quad z\to-\infty, \tag{III.2.11}$$

$$u',w',p'\to 0\qquad \text{as}\quad z\to\infty. \tag{III.2.12}$$

### III.2.1 The steady wind profile

The friction velocities in air and water, $u'_*$ and $u_*$, are related to the shear stress on the undisturbed water surface $\tau^S$ through the defining relationships

$$u_*=\sqrt{\frac{\tau^S}{\rho}}\qquad\text{and}\qquad u'_*=\sqrt{\frac{\tau^S}{\rho'}}, \tag{III.2.13}$$

and hence we also have the relationship between the friction velocities

$$\frac{u_*}{u'_*}=\sqrt{\frac{\rho'}{\rho}}. \tag{III.2.14}$$

We employ the usual linear-logarithmic shear profile for the wind in the air and for the induced shear current in the water (see e.g. Miles 1962; Valenzuela 1976; Kawai 1979; Gastel *et al.* 1985; Hara & Mei 1991, 1994). In air we have

$$U'^S=\begin{cases} U_d+\frac{u'^2_*}{\nu'}z & z\le 5\frac{\nu'}{u'_*},\\ U_d+5u'_*+\frac{u'_*}{\kappa}(\alpha-\tanh\frac{\alpha}{2}) & z>5\frac{\nu'}{u'_*},\end{cases} \tag{III.2.15}$$

where

$$\sinh\alpha=2\kappa\frac{u'_*}{\nu'}(z-5\frac{\nu'}{u'_*}), \tag{III.2.16}$$

and where $U_d$ is the drift velocity at the water surface and $\kappa = 0.4$ is the universal Kármán constant. The viscous sublayer height of the wind profile is $5\nu'/u'_*$.

In water we have

$$U^S = \begin{cases} U_d + \frac{u_*^2}{\nu} z & z \leq 5\frac{\nu}{u_*}, \\ U_d + 5u_* + \frac{u_*}{\kappa}(\alpha - \tanh\frac{\alpha}{2}) & z > 5\frac{\nu}{u_*}, \end{cases} \tag{III.2.17}$$

where

$$\sinh\alpha = 2\kappa\frac{u_*}{\nu}(z - 5\frac{\nu}{u_*}). \tag{III.2.18}$$

The viscous sublayer depth of the wind-induced current profile is $5\nu/u_*$.

The wind model requires that we know the relationship between the induced drift velocity at the water surface, $U_d$, and the friction velocity in air, $u'_*$. We shall primarily be interested in wind strengths corresponding to an air friction velocity in the range up to 0.15 m/s. In this range, the drift velocity is nearly proportional to the friction velocity. For example, Shemdin (1972) reported that the air friction velocity was 4.95% of the reference wind speed in his experiment. He further noted that several investigators recorded surface drift velocities in the range 2.5–4.0% of the wind speed. We shall adopt the empirical formula

$$U_d = 0.565\, u'_*. \tag{III.2.19}$$

In figure III-1, we compare our empirical formula (III.2.19) with the data used by Gastel *et al.* (1985). Our linear formula agrees well with the data for weak winds.

In figure III-2, we show the linear-logarithmic steady wind profile for water and air, according to (III.2.15)–(III.2.18). We show the profile for the air friction velocity $u'_* = 0.1$ m/s. The viscous sublayer height and depth relative to the water surface, are indicated with dashed lines.

## III.3 Scaling assumptions

It is convenient to let length and time be normalized by the wavenumber and frequency of the first harmonic of a train of Wilton's ripples, i.e.

$$\bar{k} = \sqrt{\frac{\rho g}{2\Gamma}}, \qquad \bar{\omega} = \sqrt{\frac{3}{2} g\bar{k}}. \tag{III.3.1}$$

To characterize the small wave steepness, we introduce the parameter $\epsilon = \bar{k}a \ll 1$, where $a$ is a typical wave amplitude,

$$\eta \sim a. \tag{III.3.2}$$

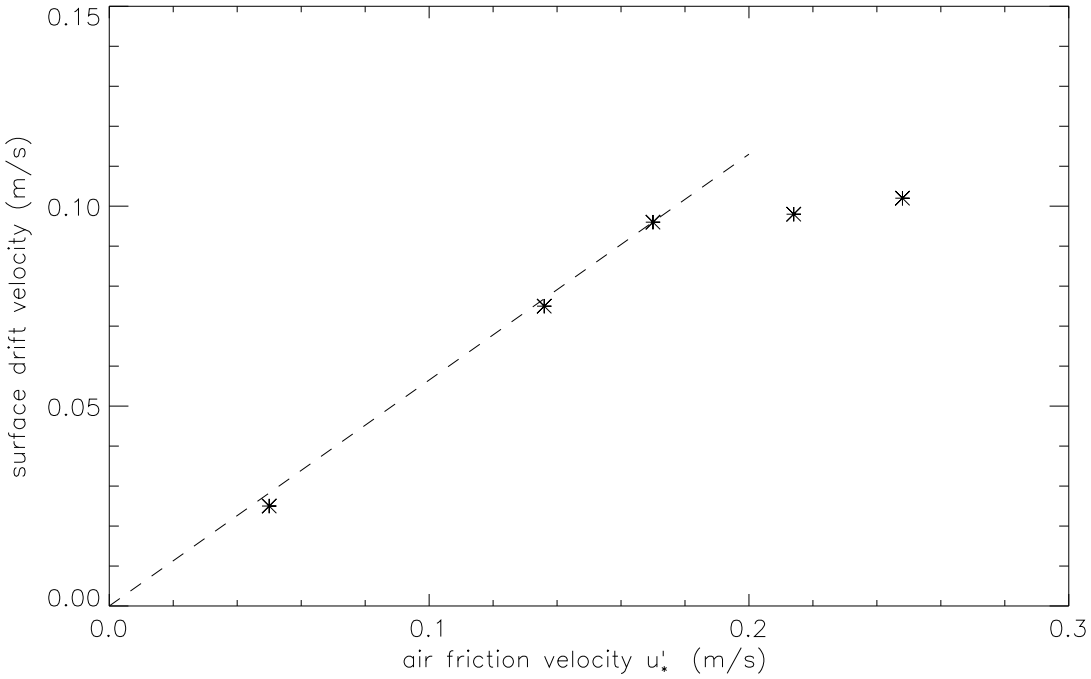


Figure III-1: Comparison of (III.2.19) (- - -) with data used by Gastel *et al.* (1985) (∗).

We assume that the interior inviscid field quantities of the wave-disturbance in water can be normalized by

$$u, w \sim \bar{\omega} a, \qquad \frac{p}{\rho} \sim \frac{\bar{\omega}^2}{\bar{k}} a. \tag{III.3.3}$$

The interior inviscid field quantities of the wave-disturbance in air can be normalized by a similar scheme

$$u', w' \sim \bar{\omega} a, \qquad \frac{p'}{\rho'} \sim \frac{\bar{\omega}^2}{\bar{k}} a. \tag{III.3.4}$$

The following physical quantities are normalized with a view to balancing viscous damping and growth due to wind at the third order in wave steepness. The small ratio between the densities is taken to be $\mathcal{O}(\epsilon^2)$ such that the stress exerted on the water surface balances cubically nonlinear wave interactions in water,

$$\frac{\rho'}{\rho} \sim \epsilon^2. \tag{III.3.5}$$

The necessary strength of the wind to exactly balance viscous damping can be inferred from the results of Gastel *et al.* (1985). We shall limit our consideration to air friction velocities below 0.16 m/s, with the most interesting dynamical behavior occurring for air friction velocities around 0.1 m/s. It is then reasonable to assume that the wind is of leading order importance in air, while the wind-induced shear current in water

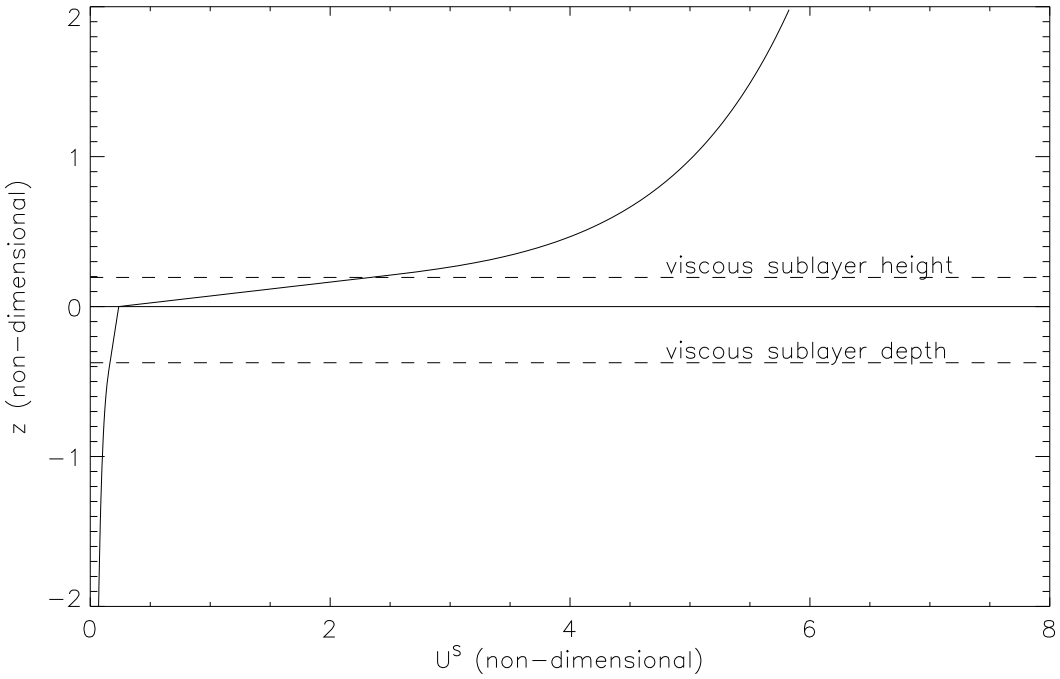


Figure III-2: Linear-logarithmic wind profile in water and air for $u'_* = 0.1$ m/s. The viscous sublayer depth and height are indicated with dashed lines. The height and speed are normalized by the wavenumber $\bar{k}$ and phase speed $\bar{c}$ of a first-harmonic Wilton's ripple.

is $\mathcal{O}(\epsilon)$, see figure III-2. We set

$$U^S \sim \epsilon\frac{\bar{\omega}}{\bar{k}}, \qquad U'^S \sim \frac{\bar{\omega}}{\bar{k}}, \tag{III.3.6}$$

and let the surface drift velocity also be of $\mathcal{O}(\epsilon)$,

$$U_d \sim \epsilon\frac{\bar{\omega}}{\bar{k}}. \tag{III.3.7}$$

The kinematic viscosity in water is normalized such that damping occurs at the third order. We let the dimensionless viscosities be

$$\sigma^2 = \frac{\nu\bar{k}^2}{\bar{\omega}} \sim \epsilon^2, \qquad \sigma'^2 = \frac{\nu'\bar{k}^2}{\bar{\omega}} \sim \epsilon. \tag{III.3.8}$$

Hence the ratios $U^S/U'^S$ and $\sigma^2/\sigma'^2$ are both of $\mathcal{O}(\sqrt{\rho'/\rho}) = \mathcal{O}(\epsilon)$, which is appropriate for the continuity of shear stress for turbulent eddy viscosity in air and water.

Just below the water surface, there is a viscous boundary layer which is essentially governed by the following leading-order balance of terms in (III.2.2):

$$\frac{\partial u}{\partial t} \sim \nu\frac{\partial^2 u}{\partial z^2}. \tag{III.3.9}$$

Hence the viscous boundary layer in water is assumed to have thickness $\mathcal{O}(\sigma) = \mathcal{O}(\epsilon)$. The appropriate vertical boundary-layer coordinate is then

$$z_{BL} = \epsilon^{-1}z, \tag{III.3.10}$$

and the appropriate velocity and pressure scales are

$$u_{BL} \sim \epsilon\bar{\omega}a, \qquad w_{BL} \sim \epsilon^2\bar{\omega}a, \qquad \frac{p_{BL}}{\rho} \sim \epsilon^3\frac{\bar{\omega}^2}{\bar{k}}a. \tag{III.3.11}$$

Just above the water surface, there is a viscous boundary layer, which in the limit of vanishing wind is essentially governed by the following leading-order balance of terms in (III.2.5):

$$\frac{\partial u'}{\partial t} \sim \nu'\frac{\partial^2 u'}{\partial z^2}. \tag{III.3.12}$$

Hence the viscous boundary layer in air is assumed to have thickness $\mathcal{O}(\sigma') = \mathcal{O}(\epsilon^{\frac{1}{2}})$. Higher up in the air, at the critical height where the wind speed is equal to the phase velocity of the wave, there is a viscous shear layer. At the critical height, the first two linear terms in (III.2.5) cancel out,

$$\frac{\partial u'}{\partial t} + U'^S\frac{\partial u'}{\partial x} \approx 0, \tag{III.3.13}$$

and the boundary layer is essentially governed by the leading-order balance of terms:

$$\frac{\partial U'^S}{\partial z} w' \sim \nu' \frac{\partial^2 u'}{\partial z^2}. \tag{III.3.14}$$

After invoking (III.2.4), the viscous shear layer at the critical height is assumed to have thickness $\mathcal{O}(\sigma'^{\frac{2}{3}}) = \mathcal{O}(\epsilon^{\frac{1}{3}})$.

Notice that the scaling assumption for the wind (III.3.6) guarantees that the critical height is always above the water surface. For a sufficiently weak wind these two viscous layers are well separated from each other. For a sufficiently strong wind they overlap, and should be thought of as a single wall boundary layer. To get an estimate of the importance of the partially overlapping viscous shear and wall boundary layers in air, we assume for scaling purposes that an approximate viscous vertical coordinate is

$$z'_{BL} = \mu^{-1} z \tag{III.3.15}$$

where the thickness $\mu$ is

$$\epsilon^{\frac{1}{2}} \leq \mu \leq \epsilon^{\frac{1}{3}}. \tag{III.3.16}$$

Approximate viscous scales are then given by

$$u'_{BL} \sim \bar{\omega} a, \qquad w'_{BL} \sim \mu \bar{\omega} a, \qquad \frac{p'_{BL}}{\rho'} \sim \epsilon \mu \frac{\bar{\omega}^2}{\bar{k}} a. \tag{III.3.17}$$

In figure III-3, the solid curve indicates the critical height for Wilton's ripples, where the wind velocity is equal to the phase velocity (recall that for Wilton's ripples, the phase velocities of the first and the second harmonics are equal). The dotted curve shows the viscous sublayer height of the wind profile, where it changes from linear to logarithmic. The critical and sublayer heights that can be deduced from the data used by Gastel *et al.* (1985) are indicated in the figure by asterisks and diamonds. We also indicate the scaling thicknesses for the viscous wall boundary layer ($\mu = \epsilon^{\frac{1}{2}}$) and the viscous shear layer at the critical height ($\mu = \epsilon^{\frac{1}{3}}$), relative to the water surface at height 0. We have chosen $\epsilon = 0.04$, corresponding to the numerical example given in the the following subsection.

Gastel *et al.* (1985) solved the wave-induced viscous wall boundary layer by an asymptotic method based on two fundamental assumptions: (1) The wave-induced viscous shear layer at the critical height overlaps the viscous wall boundary layer, and (2) the wave-induced viscous shear layer is contained within the viscous sublayer of the wind profile. They could then solve the viscous shear layer analytically by using scales corresponding to $\mu = \epsilon^{\frac{1}{3}}$, and solve the inviscid interior flow separately by a Rayleigh equation.

Figure III-3 demonstrates that for application to Wilton's ripples, their first assumption is appropriate only for a sufficiently strong wind, i.e. for an air friction velocity greater than 0.1 m/s, say. For weaker winds, the critical height is farther away from the water surface, and the boundary layer structure is more complicated. The figure also suggests that their second assumption may never be fully satisfied for Wilton's ripples, and the viscous shear layer may be affected by the curved wind pro-

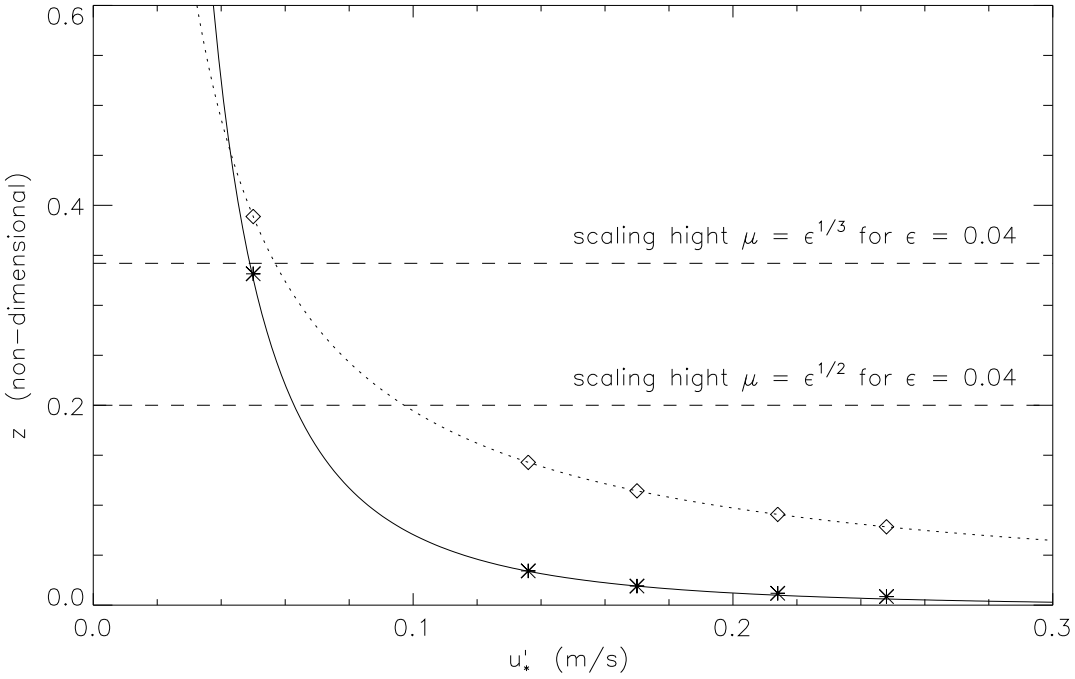


Figure III-3: Critical height (—) for Wilton's ripples and viscous sublayer height $(\cdots)$ for air friction velocities in the range 0–0.3 m/s. Heights that can be inferred from the data used by Gastel *et al.* (1985) ($*$ and $\diamond$). Scaling heights (- - -) above $z = 0$ corresponding to $\mu = \epsilon^{\frac{1}{2}}$ and $\mu = \epsilon^{\frac{1}{3}}$ for $\epsilon = 0.04$.

file. Indeed, for sufficiently weak winds the critical height may be above the viscous sublayer.

Our goal is to allow for grow due to wind that balances viscous damping over a long time. The required air friction velocity will later be shown to be roughly in order of magnitude 0.1 m/s. Based on the above discussion and figure III-3, it is difficult to solve the viscous part of the wave disturbance in air separately by a perturbation approach. We shall hence solve the total wave disturbance in air numerically by lumping together the viscous and inviscid parts of the solution.

### III.3.1 Numerical example — laminar viscosities at 20°C

To have some quantitative idea about the implications of the scaling scheme, let us take the following values for surface tension, gravitational acceleration, densities and laminar viscosities at 20°C:

$$\Gamma = 7.28 \cdot 10^{-2}\,\mathrm{N/m}, \quad g = 9.80\,\mathrm{m/s^2}, \quad \rho = 9.98 \cdot 10^{2}\,\mathrm{kg/m^3}, \quad \rho' = 1.205\,\mathrm{kg/m^3},$$

$$\nu = 1.004 \cdot 10^{-6}\,\mathrm{m^2/s}, \quad \nu' = 1.50 \cdot 10^{-5}\,\mathrm{m^2/s}.$$

The characteristic wavenumber and frequency are given in (III.3.1):

$$\bar{k} = 259\,\mathrm{m^{-1}} = \frac{2\pi}{2.4\,\mathrm{cm}}, \qquad \bar{\omega} = 61.7\,\mathrm{s^{-1}} = 2\pi \cdot 9.8\,\mathrm{Hz}. \tag{III.3.18}$$

The non-dimensional viscosities and density ratio become

$$\sigma^2 = 1.1 \cdot 10^{-3}, \qquad \sigma'^2 = 1.6 \cdot 10^{-2}, \qquad \frac{\rho'}{\rho} = 1.2 \cdot 10^{-3}. \tag{III.3.19}$$

In accordance with the above non-dimensional numbers, the characteristic ordering parameter $\epsilon$ has the rough magnitude

$$\epsilon^2 \sim 1.6 \cdot 10^{-3}, \quad \epsilon \sim 4.0 \cdot 10^{-2}, \quad \epsilon^{\frac{1}{2}} \sim 2.0 \cdot 10^{-1}, \quad \epsilon^{\frac{1}{3}} \sim 3.4 \cdot 10^{-1}. \tag{III.3.20}$$

The implied physical magnitudes for the gravity-capillary wave amplitude and the horizontal wind shear velocities are then

$$a \sim 0.15\mathrm{mm}, \qquad U'^S \sim 24\mathrm{cm/s}, \qquad U^S, U_d \sim 1\mathrm{cm/s}. \tag{III.3.21}$$

The implied boundary-layer thickness in water is $\epsilon\bar{k}^{-1} \sim 0.15$ mm and the thickness of the viscous shear layer in air ($\mu\bar{k}^{-1}$) is in the range from 0.77 mm to 1.3 mm.

## III.4 Multiple-scales perturbation expansions

The dimensional surface displacement $\eta$ is now normalized by

$$\eta \to \bar{k}\epsilon\eta. \tag{III.4.1}$$

The dimensional quantities in water are normalized and expanded into interior and boundary-layer components by

$$u \rightarrow \frac{\bar{\omega}}{\bar{k}}\epsilon u_T = \frac{\bar{\omega}}{\bar{k}}(\epsilon u + \epsilon^2 u_{BL}), \tag{III.4.2}$$

$$w \rightarrow \frac{\bar{\omega}}{\bar{k}}\epsilon w_T = \frac{\bar{\omega}}{\bar{k}}(\epsilon w + \epsilon^3 w_{BL}), \tag{III.4.3}$$

$$\frac{p}{\rho} \rightarrow \frac{\bar{\omega}^2}{\bar{k}}\epsilon p_T = \frac{\bar{\omega}^2}{\bar{k}}(\epsilon p + \epsilon^4 p_{BL}), \tag{III.4.4}$$

where index $T$ indicates total flow field and index $BL$ indicates boundary-layer components that depend on the vertical coordinate $z_{BL} = \epsilon^{-1} z$. The normalized inviscid interior components are unprimed.

In air, the dimensional quantities are normalized by

$$u' \rightarrow \frac{\bar{\omega}}{\bar{k}}\epsilon u'_T = \frac{\bar{\omega}}{\bar{k}}(\epsilon u' + \epsilon u'_{BL}), \tag{III.4.5}$$

$$w' \rightarrow \frac{\bar{\omega}}{\bar{k}}\epsilon w'_T = \frac{\bar{\omega}}{\bar{k}}(\epsilon w' + \epsilon\mu w'_{BL}), \tag{III.4.6}$$

$$\frac{p'}{\rho'} \rightarrow \frac{\bar{\omega}^2}{\bar{k}}\epsilon p'_T = \frac{\bar{\omega}^2}{\bar{k}}(\epsilon p' + \epsilon\mu p'_{BL}), \tag{III.4.7}$$

where the boundary-layer components depend on the vertical coordinate $z'_{BL} = \mu^{-1} z$. Since the wave disturbance in air will be obtained by solving the total flow field numerically, the decomposition into interior and boundary-layer components is only used to indicate the scaling magnitudes.

The wind velocities are normalized similarly:

$$U^S \rightarrow \frac{\bar{\omega}}{\bar{k}}\epsilon U^S, \tag{III.4.8}$$

$$U_d \rightarrow \frac{\bar{\omega}}{\bar{k}}\epsilon U_d, \tag{III.4.9}$$

$$U'^S \rightarrow \frac{\bar{\omega}}{\bar{k}} U'^S. \tag{III.4.10}$$

### III.4.1 Water flow-field equations and boundary conditions

After we substitute the above expansions (III.4.1)–(III.4.10) into the governing equations for the water flow field, we can separate the interior and the boundary-layer components. The resulting normalized equations for the water interior flow field are

$$\frac{\partial u}{\partial x} + \frac{\partial w}{\partial z} = 0, \tag{III.4.11}$$

$$\frac{\partial u}{\partial t} + \epsilon u\frac{\partial u}{\partial x} + \epsilon U^S\frac{\partial u}{\partial x} + \epsilon w\frac{\partial u}{\partial z} + \epsilon w\frac{\partial U^S}{\partial z} + \frac{\partial p}{\partial x} - \epsilon^2\sigma^2\left(\frac{\partial^2}{\partial x^2} + \frac{\partial^2}{\partial z^2}\right)u = 0, \tag{III.4.12}$$

$$\frac{\partial w}{\partial t}+\epsilon u\frac{\partial w}{\partial x}+\epsilon U^S\frac{\partial w}{\partial x}+\epsilon w\frac{\partial w}{\partial z}+\frac{\partial p}{\partial z}-\epsilon^2\sigma^2\left(\frac{\partial^2}{\partial x^2}+\frac{\partial^2}{\partial z^2}\right)w=0. \qquad \text{(III.4.13)}$$

In the water surface boundary layer, the governing equations are

$$\frac{\partial u_{BL}}{\partial x}+\frac{\partial w_{BL}}{\partial z_{BL}}=0, \qquad \text{(III.4.14)}$$

$$\frac{\partial u_{BL}}{\partial t}+w\frac{\partial u_{BL}}{\partial z_{BL}}-\sigma^2\frac{\partial^2 u_{BL}}{\partial z_{BL}^2}=\mathcal{O}(\epsilon), \qquad \text{(III.4.15)}$$

$$\frac{\partial w_{BL}}{\partial t}+u_{BL}\frac{\partial w}{\partial x}+w\frac{\partial w_{BL}}{\partial z_{BL}}+\frac{\partial p_{BL}}{\partial z_{BL}}-\sigma^2\frac{\partial^2 w_{BL}}{\partial z_{BL}^2}=\mathcal{O}(\epsilon). \qquad \text{(III.4.16)}$$

The kinematic surface condition is

$$\frac{\partial \eta}{\partial t}+\epsilon U^S\frac{\partial \eta}{\partial x}+\epsilon u\frac{\partial \eta}{\partial x}+\epsilon^2 u_{BL}\frac{\partial \eta}{\partial x}-w-\epsilon^2 w_{BL}=\mathcal{O}(\epsilon^3)\quad\text{at}\quad z=\epsilon\eta. \qquad \text{(III.4.17)}$$

The normal stress condition is

$$-p+\frac{2}{3}\eta-\frac{1}{3}\frac{\partial^2\eta}{\partial x^2}+\frac{1}{2}\epsilon^2\left(\frac{\partial\eta}{\partial x}\right)^2\frac{\partial^2\eta}{\partial x^2}+2\epsilon^2\sigma^2\frac{\partial w}{\partial z}-\epsilon^2 N=\mathcal{O}(\epsilon^3)\quad\text{at}\quad z=\epsilon\eta, \qquad \text{(III.4.18)}$$

where the normal stress ($N$) due to the wave disturbance in air is denoted by

$$\epsilon^2 N=\epsilon^2\frac{\rho'}{\rho}\left\{-p'_T+\frac{2}{3}\eta+\mathcal{O}(\epsilon)\right\}\quad\text{at}\quad z=\epsilon\eta. \qquad \text{(III.4.19)}$$

The tangential stress condition is

$$\frac{\partial u}{\partial z}+\frac{\partial u_{BL}}{\partial z_{BL}}+\frac{\partial w}{\partial x}-\epsilon\mu^{-1}T=\mathcal{O}(\epsilon)\quad\text{at}\quad z=\epsilon\eta, \qquad \text{(III.4.20)}$$

where the tangential stress ($T$) due to the wave disturbance in air is denoted by

$$\epsilon\mu^{-1}T=\epsilon\frac{\rho'\nu'}{\rho\nu}\left\{\mu^{-1}\frac{\partial u'_T}{\partial z}+\mathcal{O}(1)\right\}\quad\text{at}\quad z=\epsilon\eta. \qquad \text{(III.4.21)}$$

The tangential stress gets its most significant contribution from the vertical derivative of the boundary-layer component of the horizontal velocity in air,

$$\mu^{-1}\frac{\partial u'_T}{\partial z}=\frac{\partial u'}{\partial z}+\mu^{-1}\frac{\partial u'_{BL}}{\partial z'_{BL}}.$$

Therefore the tangential stress is significant within the highest nonlinear order of our approximation.

We note that due to our choice of normalization by $\bar{k}$ and $\bar{\omega}$, the physical constants $g$ and $\frac{\Gamma}{\rho}$ appear as the numbers $\frac{2}{3}$ and $\frac{1}{3}$, respectively.

The pressure can now be eliminated between the two momentum conservation

equations in the water interior and boundary layer, respectively. We then introduce the stream-functions,

$$u = \frac{\partial \psi}{\partial z}, \quad w = -\frac{\partial \psi}{\partial x}, \quad u_{BL} = \frac{\partial \psi_{BL}}{\partial z_{BL}}, \quad w_{BL} = -\frac{\partial \psi_{BL}}{\partial x}, \quad U^S = \frac{\partial \Psi^S}{\partial z}. \tag{III.4.22}$$

The resulting equations for the stream functions are in the interior

$$\frac{\partial}{\partial t}\nabla^2\psi - \epsilon\frac{\partial(\Psi^S + \psi, \nabla^2(\Psi^S + \psi))}{\partial(x,z)} - \epsilon^2\sigma^2\nabla^4\psi = 0, \tag{III.4.23}$$

and in the surface boundary layer

$$\frac{\partial^2\psi_{BL}}{\partial t \partial z_{BL}} - \frac{\partial \psi}{\partial x}\frac{\partial^2\psi_{BL}}{\partial z_{BL}^2} - \sigma^2\frac{\partial^3\psi_{BL}}{\partial z_{BL}^3} = \mathcal{O}(\epsilon). \tag{III.4.24}$$

The kinematic surface condition becomes

$$\frac{\partial \eta}{\partial t} + \frac{\partial \psi}{\partial x} + \epsilon\left(U^S + \frac{\partial \psi}{\partial z}\right)\frac{\partial \eta}{\partial x} + \epsilon^2\frac{\partial \psi_{BL}}{\partial x} = \mathcal{O}(\epsilon^3) \quad \text{at} \quad z = \epsilon\eta. \tag{III.4.25}$$

The normal stress condition becomes

$$\frac{\partial^2\psi}{\partial t\partial z} + \frac{2}{3}\frac{\partial \eta}{\partial x} - \frac{1}{3}\frac{\partial^3\eta}{\partial x^3} + \epsilon\frac{\partial}{\partial z}(\Psi^S + \psi)\frac{\partial^2\psi}{\partial x\partial z} + \epsilon\frac{\partial \psi}{\partial x}\frac{\partial^2}{\partial z^2}(\Psi^S + \psi)$$

$$+\epsilon\left(-\frac{\partial^2\psi}{\partial t\partial x} - \epsilon\frac{\partial}{\partial z}(\Psi^S + \psi)\frac{\partial^2\psi}{\partial x^2} + \epsilon\frac{\partial \psi}{\partial x}\frac{\partial^2\psi}{\partial x\partial z}\right)\frac{\partial \eta}{\partial x} + \epsilon^2\frac{\partial \eta}{\partial x}\left(\frac{\partial^2\eta}{\partial x^2}\right)^2 + \frac{1}{2}\epsilon^2\left(\frac{\partial \eta}{\partial x}\right)^2\frac{\partial^3\eta}{\partial x^3}$$

$$-\epsilon^2\sigma^2\frac{\partial^3\psi}{\partial z^3} - 3\epsilon^2\sigma^2\frac{\partial^3\psi}{\partial x^2\partial z} - \epsilon^2\frac{\partial N}{\partial x} = \mathcal{O}(\epsilon^3) \quad \text{at} \quad z = \epsilon\eta. \tag{III.4.26}$$

The tangential stress condition becomes

$$\frac{\partial^2\psi_{BL}}{\partial z_{BL}^2} + \frac{\partial^2\psi}{\partial z^2} - \frac{\partial^2\psi}{\partial x^2} - \epsilon\mu^{-1}T = \mathcal{O}(\epsilon) \quad \text{at} \quad z = \epsilon\eta. \tag{III.4.27}$$

The water surface boundary-layer thickness is of the same order as the wave amplitude. It is therefore natural to introduce a vertical boundary-layer coordinate which follows the actual position of the free surface. Let us introduce the coordinate

$$\bar{z}_{BL} = z_{BL} - \eta(t,x). \tag{III.4.28}$$

Then the time and space derivatives will be transformed as follows:

$$\left.\begin{array}{lcl} \frac{\partial}{\partial t} & \rightarrow & \frac{\partial}{\partial t} - \frac{\partial \eta}{\partial t}\frac{\partial}{\partial \bar{z}_{BL}}, \\ \frac{\partial}{\partial x} & \rightarrow & \frac{\partial}{\partial x} - \frac{\partial \eta}{\partial x}\frac{\partial}{\partial \bar{z}_{BL}}, \\ \frac{\partial}{\partial z_{BL}} & \rightarrow & \frac{\partial}{\partial \bar{z}_{BL}}. \end{array}\right\} \tag{III.4.29}$$

The surface boundary-layer equation now becomes

$$\frac{\partial^2 \psi_{BL}}{\partial t \partial \bar{z}_{BL}} - \left( \frac{\partial \eta}{\partial t} + \frac{\partial \psi}{\partial x} \right) \frac{\partial^2 \psi_{BL}}{\partial \bar{z}_{BL}^2} - \sigma^2 \frac{\partial^3 \psi_{BL}}{\partial \bar{z}_{BL}^3} = \mathcal{O}(\epsilon). \tag{III.4.30}$$

In the free-surface boundary conditions, the inviscid interior variables are evaluated at $z = \epsilon\eta$ while the viscid boundary-layer variables are evaluated at $\bar{z}_{BL} = 0$. The kinematic surface condition becomes

$$\frac{\partial \eta}{\partial t} + \frac{\partial \psi}{\partial x} + \epsilon U^S \frac{\partial \eta}{\partial x} + \epsilon \frac{\partial \eta}{\partial x} \frac{\partial \psi}{\partial z} + \epsilon^2 \frac{\partial \psi_{BL}}{\partial x} = \mathcal{O}(\epsilon^3) \quad \text{at} \quad \left\{ \begin{array}{l} z = \epsilon\eta, \\ \bar{z}_{BL} = 0, \end{array} \right. \tag{III.4.31}$$

and the tangential stress condition becomes

$$\frac{\partial^2 \psi_{BL}}{\partial \bar{z}_{BL}^2} + \frac{\partial^2 \psi}{\partial z^2} - \frac{\partial^2 \psi}{\partial x^2} - \epsilon \mu^{-1} T = \mathcal{O}(\epsilon) \quad \text{at} \quad \left\{ \begin{array}{l} z = \epsilon\eta, \\ \bar{z}_{BL} = 0. \end{array} \right. \tag{III.4.32}$$

The normal stress condition does not change subject to the coordinate transformation (III.4.28) since it does not involve any boundary-layer variables in water at the present order of accuracy.

In the surface conditions we can now let the boundary-layer variables remain evaluated at the true surface $\bar{z}_{BL} = 0$, while the inviscid interior variables can be Taylor-expanded around the equilibrium surface position $z = 0$. The kinematic surface condition then becomes

$$\begin{aligned} &\frac{\partial \eta}{\partial t} + \frac{\partial \psi}{\partial x} + \epsilon \left( U^S \frac{\partial \eta}{\partial x} + \frac{\partial \eta}{\partial x} \frac{\partial \psi}{\partial z} + \eta \frac{\partial^2 \psi}{\partial x \partial z} \right) \\ &+ \epsilon^2 \left( \frac{\partial U^S}{\partial z} \eta \frac{\partial \eta}{\partial x} + \frac{\partial \psi_{BL}}{\partial x} + \eta \frac{\partial \eta}{\partial x} \frac{\partial^2 \psi}{\partial z^2} + \frac{1}{2} \eta^2 \frac{\partial^3 \psi}{\partial x \partial z^2} \right) = \mathcal{O}(\epsilon^3) \quad \text{at} \quad \left\{ \begin{array}{l} z = 0, \\ \bar{z}_{BL} = 0. \end{array} \right. \end{aligned} \tag{III.4.33}$$

The normal stress condition becomes

$$\begin{aligned} &\frac{\partial^2 \psi}{\partial t \partial z} + \frac{2}{3} \frac{\partial \eta}{\partial x} - \frac{1}{3} \frac{\partial^3 \eta}{\partial x^3} + \epsilon \left( -\frac{\partial \psi}{\partial x} \frac{\partial U^S}{\partial z} + \frac{\partial^2 \psi}{\partial x \partial z} U^S - \frac{\partial \psi}{\partial x} \frac{\partial^2 \psi}{\partial z^2} + \frac{\partial^2 \psi}{\partial x \partial z} \frac{\partial \psi}{\partial z} + \eta \frac{\partial^3 \psi}{\partial t \partial z^2} \right. \\ &\left. - \frac{\partial \eta}{\partial x} \frac{\partial^2 \psi}{\partial t \partial x} \right) + \epsilon^2 \left( -\eta \frac{\partial \psi}{\partial x} \frac{\partial^2 U^S}{\partial z^2} + \frac{\partial \eta}{\partial x} \frac{\partial^2 \psi}{\partial x^2} U^S - \eta \frac{\partial^3 \psi}{\partial x \partial z^2} U^S + \eta \frac{\partial \psi}{\partial x} \frac{\partial^3 \psi}{\partial z^3} + \sigma^2 \frac{\partial^3 \psi}{\partial z^3} \right. \\ &+ \frac{\partial \eta}{\partial x} \frac{\partial^2 \psi}{\partial x^2} \frac{\partial \psi}{\partial z} - \eta \frac{\partial^3 \psi}{\partial x \partial z^2} \frac{\partial \psi}{\partial z} + 3\sigma^2 \frac{\partial^3 \psi}{\partial x^2 \partial z} - \frac{\partial \eta}{\partial x} \frac{\partial \psi}{\partial x} \frac{\partial^2 \psi}{\partial x \partial z} - \frac{1}{2} \eta^2 \frac{\partial^4 \psi}{\partial t \partial z^3} + \eta \frac{\partial \eta}{\partial x} \frac{\partial^3 \psi}{\partial t \partial x \partial z} \\ &\left. + \eta \frac{\partial \eta}{\partial x} \frac{\partial^3 \psi}{\partial t \partial x \partial z} - \frac{1}{2} \left( \frac{\partial \eta}{\partial x} \right)^2 \frac{\partial^3 \eta}{\partial x^3} - \frac{\partial \eta}{\partial x} \left( \frac{\partial^2 \eta}{\partial x^2} \right)^2 + \frac{\partial N}{\partial x} \right) = \mathcal{O}(\epsilon^3) \quad \text{at} \quad \left\{ \begin{array}{l} z = 0, \\ \bar{z}_{BL} = 0. \end{array} \right. \end{aligned} \tag{III.4.34}$$

The tangential stress condition becomes

$$\frac{\partial^2 \psi_{BL}}{\partial \bar{z}_{BL}^2} + \frac{\partial^2 \psi}{\partial z^2} - \frac{\partial^2 \psi}{\partial x^2} - \epsilon \mu^{-1} T = \mathcal{O}(\epsilon) \quad \text{at} \quad \begin{cases} z = 0, \\ \bar{z}_{BL} = 0. \end{cases} \tag{III.4.35}$$

In the boundary-layer equation (III.4.30) the inviscid interior variables must be evaluated within the boundary layer $z = \epsilon(\eta + \bar{z}_{BL})$, and hence it becomes

$$\frac{\partial^2 \psi_{BL}}{\partial t \partial \bar{z}_{BL}} - \left( \frac{\partial \eta}{\partial t} + \left. \frac{\partial \psi}{\partial x} \right|_{z=0} \right) \frac{\partial^2 \psi_{BL}}{\partial \bar{z}_{BL}^2} - \sigma^2 \frac{\partial^3 \psi_{BL}}{\partial \bar{z}_{BL}^3} = \mathcal{O}(\epsilon). \tag{III.4.36}$$

By using the kinematic surface condition (III.4.33), the boundary-layer equation simplifies to

$$\frac{\partial^2 \psi_{BL}}{\partial t \partial \bar{z}_{BL}} - \sigma^2 \frac{\partial^3 \psi_{BL}}{\partial \bar{z}_{BL}^3} = \mathcal{O}(\epsilon). \tag{III.4.37}$$

The decaying boundary condition at large depth is

$$\psi \to 0 \quad \text{as} \quad z \to -\infty. \tag{III.4.38}$$

We now expand the unknown water disturbance field variables in perturbation expansions. The appropriate expansions are

$$\eta = \eta_1 + \epsilon \eta_2 + \epsilon^2 \eta_3 + \ldots, \tag{III.4.39}$$

$$\psi = \psi_1 + \epsilon \psi_2 + \epsilon^3 \psi_3 + \ldots, \tag{III.4.40}$$

where all the perturbed quantities depend on the fast coordinates $(t, x)$ and the slow modulation coordinates

$$(t_j, x_j) = \epsilon^j (t, x) \quad \text{for} \quad j = 1, 2. \tag{III.4.41}$$

These perturbation expansions have been carried out by the symbolic computation system MACSYMA. The perturbation equations at each order are given later, when their solutions are discussed.

## III.4.2 Air flow-field equations and boundary conditions

After we substitute the expansions (III.4.1)–(III.4.10) into the governing equations for the air flow field, we get the leading-order equations

$$\frac{\partial u_T'}{\partial x} + \frac{\partial w_T'}{\partial z} = 0, \tag{III.4.42}$$

$$\frac{\partial u_T'}{\partial t} + U'^S \frac{\partial u_T'}{\partial x} + w_T' \frac{\partial U'^S}{\partial z} + \frac{\partial p_T'}{\partial x} - \epsilon \mu^{-2} \sigma'^2 \nabla^2 u_T' = -\epsilon \mu^{-1} w_T' \frac{\partial u_T'}{\partial z} + \mathcal{O}(\epsilon), \tag{III.4.43}$$

$$\frac{\partial w_T'}{\partial t} + U'^S \frac{\partial w_T'}{\partial x} + \frac{\partial p_T'}{\partial z} - \epsilon \mu^{-1} \sigma'^2 \nabla^2 w_T' = \mathcal{O}(\epsilon). \tag{III.4.44}$$

In the linear part on the left-hand sides of (III.4.43) and (III.4.44), the viscous shear derivatives contribute to leading order

$$\mu^{-2}\nabla^2 u'_T = \frac{\partial^2 u'}{\partial x^2} + \frac{\partial^2 u'}{\partial z^2} + \frac{\partial^2 u'_{BL}}{\partial x^2} + \mu^{-2}\frac{\partial^2 u'_{BL}}{\partial z'^2_{BL}}$$

and

$$\mu^{-1}\nabla^2 w'_T = \frac{\partial^2 w'}{\partial x^2} + \frac{\partial^2 w'}{\partial z^2} + \mu\frac{\partial^2 w'_{BL}}{\partial x^2} + \mu^{-1}\frac{\partial^2 w'_{BL}}{\partial z'^2_{BL}}.$$

On the other hand, the leading-order nonlinearity on the right-hand side of (III.4.43) contributes

$$\epsilon\mu^{-1}w'_T\frac{\partial u'_T}{\partial z} = \epsilon w'\frac{\partial u'}{\partial z} + \epsilon\mu^{-1}w'\frac{\partial u'_{BL}}{\partial z'_{BL}} + \epsilon\mu w'_{BL}\frac{\partial u'}{\partial z} + \epsilon w'_{BL}\frac{\partial u'_{BL}}{\partial z'_{BL}}.$$

We have written out the scaling factor $\mu$ explicitly to indicate the importance of the boundary layer.

For a single wave, the nonlinearity in (III.4.43) give rise to second and zeroth harmonics at the leading nonlinear order, which will then in turn give feedback to the first harmonic at the next higher order in nonlinearity. It can therefore be anticipated that the resulting correction to the growth rate will be of order $\mathcal{O}(\epsilon^2\mu^{-1})$, which can be neglected here. However, for Wilton's ripples, the first and the second harmonics have equal magnitudes, and the above nonlinearity will give a correction to the growth rate of relative order $\mathcal{O}(\epsilon\mu^{-1})$, which is of the same order as the correction due to the tangential stress, and is within the highest nonlinear order of our theory. From the results of Hara & Mei (1994) (their figure 1) and later from our figure III-6 it can be inferred that the tangential stress can contribute roughly 20–30% of the total growth rate. We shall therefore compute the nonlinear correction to the growth rate and assess its importance.

The no-slip surface boundary conditions are

$$u'_T + \epsilon^{-1}U'^S = u + U^S + \mathcal{O}(\epsilon) \qquad \text{at} \quad z = \epsilon\eta, \tag{III.4.45}$$

$$w'_T = w + \mathcal{O}(\epsilon^2) \qquad \text{at} \quad z = \epsilon\eta. \tag{III.4.46}$$

The boundary-layer components of the flow-field in water are too small to be accounted for here. Note that we can Taylor-expand both the interior and the boundary-layer components of the air variables around the equilibrium surface position because the boundary-layer thickness in air is greater than the surface displacement. After the boundary conditions are Taylor-expanded about the equilibrium surface position, and the terms that only govern the shear current are eliminated, we get

$$u'_T = u - \frac{\partial U'^S}{\partial z}\eta - \epsilon\mu^{-1}\frac{\partial u'_T}{\partial z}\eta + \mathcal{O}(\epsilon) \qquad \text{at} \quad z = 0, \tag{III.4.47}$$

$$w'_T = w + \mathcal{O}(\epsilon) \qquad \text{at} \quad z = 0. \tag{III.4.48}$$

The pressure is now eliminated between the two momentum conservation equa-

tions (III.4.43) and (III.4.44). We then use the stream function introduced for the interior flow field in water (III.4.22), and also introduce a stream-function in air,

$$u'_T = \frac{\partial \psi'_T}{\partial z}, \qquad w'_T = -\frac{\partial \psi'_T}{\partial x}. \tag{III.4.49}$$

It is implied that the interior and boundary-layer components are $\psi'_T = \psi' + \mu\psi'_{BL}$. The resulting equation for the stream function then becomes

$$\frac{\partial}{\partial t}\nabla^2\psi'_T + U'^S\frac{\partial}{\partial x}\nabla^2\psi'_T - \mu\frac{\partial^2 U'^S}{\partial z^2}\frac{\partial \psi'_T}{\partial x} - \epsilon\mu^{-2}\sigma'^2\nabla^4\psi'_T = \epsilon\mu^{-1}\frac{\partial \psi'_T}{\partial x}\frac{\partial^3\psi'_T}{\partial z^3} + \mathcal{O}(\epsilon). \tag{III.4.50}$$

The no-slip surface boundary conditions become

$$\frac{\partial \psi'_T}{\partial z} = \frac{\partial \psi}{\partial z} - \frac{\partial U'^S}{\partial z}\eta - \epsilon\mu^{-1}\frac{\partial^2\psi'_T}{\partial z^2}\eta + \mathcal{O}(\epsilon) \qquad \text{at} \quad z = 0, \tag{III.4.51}$$

$$\frac{\partial \psi'_T}{\partial x} = \frac{\partial \psi}{\partial x} + \mathcal{O}(\epsilon) \qquad \text{at} \quad z = 0. \tag{III.4.52}$$

We also require that the wave disturbance vanishes at great height,

$$\psi'_T \to 0 \quad \text{as} \quad z \to \infty. \tag{III.4.53}$$

After the stream-function has been solved, the pressure can be found from the $x$-component of the momentum equation

$$\frac{\partial p'_T}{\partial x} = -\frac{\partial^2\psi'_T}{\partial t\partial z} - U'^S\frac{\partial^2\psi'_T}{\partial x\partial z} + \frac{\partial U'^S}{\partial z}\frac{\partial \psi'_T}{\partial x} + \epsilon\mu^{-2}\sigma'^2\frac{\partial}{\partial z}\nabla^2\psi'_T + \epsilon\mu^{-1}\frac{\partial \psi'_T}{\partial x}\frac{\partial^2\psi'_T}{\partial z^2} + \mathcal{O}(\epsilon). \tag{III.4.54}$$

In the equations for the wave disturbance in air (III.4.50)–(III.4.54) there are several small parameters. The linear terms are multiplied by $\mu$ and $\epsilon\mu^{-2}$ which are in the ranges $\epsilon^{\frac{1}{2}} \le \mu \le \epsilon^{\frac{1}{3}}$ and $\epsilon^{\frac{1}{3}} \le \epsilon\mu^{-2} \le 1$. The nonlinear terms are multiplied by $\epsilon\mu^{-1}$ which is in the range $\epsilon^{\frac{2}{3}} \le \epsilon\mu^{-1} \le \epsilon^{\frac{1}{2}}$. Hence it is seen that the leading-order contributions from all the linear terms are more significant than the leading-order contributions from the nonlinear terms. It is then natural to solve the problem by a perturbation method, in which we make use of the small parameter $\epsilon\mu^{-1}$ multiplying the nonlinear terms. For simplicity, we let the entire linear expression on the left-hand side of (III.4.50) be denoted by $L(\psi'_T)$ and the nonlinear right-hand side be denoted by $NL(\psi'_T)$, such that

$$L(\psi'_T) = \epsilon\mu^{-1}NL(\psi'_T). \tag{III.4.55}$$

We then expand

$$\psi'_T = \psi^{(1)} + \epsilon\mu^{-1}\psi^{(2)} + \ldots, \tag{III.4.56}$$

$$p'_T = p^{(1)} + \epsilon\mu^{-1}p^{(2)} + \ldots, \tag{III.4.57}$$

$$N = N^{(1)} + \epsilon\mu^{-1}N^{(2)} + \ldots, \tag{III.4.58}$$

such that the full linear response is accounted for at the leading order and the quadratic nonlinear correction is accounted for at the second order. We use upper indices in parentheses to denote the order to avoid confusion with the scaling scheme of the water-problem, which is in terms of a different ordering parameter. We also invoke the expansions in water (III.4.39) and (III.4.40).

At the leading order we have the linear homogeneous equation

$$L(\psi^{(1)}) = 0 \tag{III.4.59}$$

which is forced by the boundary conditions

$$\frac{\partial \psi^{(1)}}{\partial z} = \frac{\partial \psi_1}{\partial z} - \frac{\partial U'^S}{\partial z}\eta_1 \qquad \text{and} \qquad \frac{\partial \psi^{(1)}}{\partial x} = \frac{\partial \psi_1}{\partial x} \qquad \text{at} \quad z = 0. \tag{III.4.60}$$

At the second order $\mathcal{O}(\epsilon\mu^{-1})$ the governing equation is forced by a nonlinear inhomogeneity

$$L(\psi^{(2)}) = NL(\psi^{(1)}) \tag{III.4.61}$$

and subject to nonlinear forcing through the boundary conditions

$$\frac{\partial \psi^{(2)}}{\partial z} = -\frac{\partial^2 \psi^{(1)}}{\partial z^2}\eta_1 \qquad \text{and} \qquad \frac{\partial \psi^{(2)}}{\partial x} = 0 \qquad \text{at} \quad z = 0. \tag{III.4.62}$$

# III.5 Evolution equation for a single gravity-capillary wave

Hara & Mei (1994) derived an evolution equation for a single gravity-capillary wave, where the effects of wind forcing and viscous damping were scaled at the fourth order. We find it useful to revisit this problem using our present scaling scheme, in order to facilitate parts of our later discussion. Specifically, we want to obtain a general expression for the linear growth rate due to wind and viscosity valid for any wavenumber.

In this section we solve the problem for a single wave with arbitrary wavenumber and frequency $k$ and $\omega$ (non-dimensional) with general slow space and time modulation. In section III.6 we shall solve the problem for second-harmonic resonance (Wilton's ripples with $k = 1$ and $k = 2$) with general slow time modulation, but with slow space modulation limited to a small detuning from second-order resonance.

## III.5.1 First-order water interior problem

After the scales (III.4.41) and the perturbation expansions (III.4.39) and (III.4.40) have been substituted into the governing equation (III.4.23) and the boundary conditions (III.4.33) and (III.4.34), we can separate the perturbation problems at each order of $\epsilon$.

The leading order water interior problem is

$$\frac{\partial}{\partial t}\nabla^2\psi_1 = 0, \tag{III.5.1}$$

with surface boundary conditions at $z = 0$

$$\frac{\partial \eta_1}{\partial t} + \frac{\partial \psi_1}{\partial x} = 0, \tag{III.5.2}$$

$$\frac{\partial^2 \psi_1}{\partial t \partial z} + \frac{2}{3}\frac{\partial \eta_1}{\partial x} - \frac{1}{3}\frac{\partial^3 \eta_1}{\partial x^3} = 0. \tag{III.5.3}$$

These equations allow for basic solutions of the form

$$\eta_1 = \mathcal{A}(t_1, t_2, x_1, x_2)\mathrm{e}^{\mathrm{i}(kx-\omega t)} + \text{c.c.}, \tag{III.5.4}$$

$$\psi_1 = \frac{\omega}{k}\mathcal{A}(t_1, t_2, x_1, x_2)\mathrm{e}^{\mathrm{i}(kx-\omega t)+kz} + \text{c.c.}, \tag{III.5.5}$$

subject to the dispersion relation

$$\omega^2 = \frac{2}{3}k + \frac{1}{3}k^3. \tag{III.5.6}$$

We let the complex amplitude $\mathcal{A}$ depend on both the slow time and space modulation coordinates $t_1, t_2, x_1, x_2$, as indicated.

## III.5.2 Second-order water interior problem

At the second order, $\mathcal{O}(\epsilon)$, the water interior problem is governed by

$$\begin{aligned}\frac{\partial}{\partial t}\nabla^2\psi_2 = {} & \frac{\partial \psi_1}{\partial x}\frac{\partial^2 U^S}{\partial z^2} - U^S\frac{\partial}{\partial x}\nabla^2\psi_1 + \frac{\partial \psi_1}{\partial x}\frac{\partial^3 \psi_1}{\partial z^3} - \frac{\partial^3 \psi_1}{\partial x^3}\frac{\partial \psi_1}{\partial z} - \frac{\partial^3 \psi_1}{\partial x \partial z^2}\frac{\partial \psi_1}{\partial z} \\ & + \frac{\partial \psi_1}{\partial x}\frac{\partial^3 \psi_1}{\partial x^2 \partial z} - \frac{\partial}{\partial t_1}\nabla^2\psi_1 - 2\frac{\partial^3 \psi_1}{\partial t \partial x \partial x_1},\end{aligned} \tag{III.5.7}$$

with boundary conditions at $z = 0$

$$\frac{\partial \eta_2}{\partial t} + \frac{\partial \psi_2}{\partial x} = -\frac{\partial \eta_1}{\partial x}U^S - \frac{\partial \eta_1}{\partial x}\frac{\partial \psi_1}{\partial z} - \frac{\partial \psi_1}{\partial x_1} - \eta_1\frac{\partial^2 \psi_1}{\partial x \partial z} - \frac{\partial \eta_1}{\partial t_1}, \tag{III.5.8}$$

$$\begin{aligned}\frac{\partial^2 \psi_2}{\partial t \partial z} + \frac{2}{3}\frac{\partial \eta_2}{\partial x} - \frac{1}{3}\frac{\partial^3 \eta_2}{\partial x^3} = {} & \frac{\partial \psi_1}{\partial x}\frac{\partial U^S}{\partial z} - \frac{\partial^2 \psi_1}{\partial x \partial z}U^S + \frac{\partial \psi_1}{\partial x}\frac{\partial^2 \psi_1}{\partial z^2} - \frac{\partial^2 \psi_1}{\partial x \partial z}\frac{\partial \psi_1}{\partial z} - \frac{\partial^2 \psi_1}{\partial t_1 \partial z} \\ & - \eta_1\frac{\partial^3 \psi_1}{\partial t \partial z^2} + \frac{\partial \eta_1}{\partial x}\frac{\partial^2 \psi_1}{\partial t \partial x} - \frac{2}{3}\frac{\partial \eta_1}{\partial x_1} + \frac{\partial^3 \eta_1}{\partial x^2 \partial x_1}.\end{aligned} \tag{III.5.9}$$

Due to quadratically nonlinear interaction, we assume a solution of the form

$$\eta_2 = \hat{\eta}_{2,0} + \hat{\eta}_{2,k}\mathrm{e}^{\mathrm{i}(kx-\omega t)} + \hat{\eta}_{2,2k}\mathrm{e}^{2\mathrm{i}(kx-\omega t)} + \text{c.c.}, \tag{III.5.10}$$

$$\psi_2 \;=\; \hat{\psi}_{2,0} + \hat{\psi}_{2,k}\mathrm{e}^{\mathrm{i}(kx-\omega t)} + \hat{\psi}_{2,2k}\mathrm{e}^{2\mathrm{i}(kx-\omega t)} + \text{c.c.} \tag{III.5.11}$$

The governing equations at the second order give no zeroth-harmonic contribution, and hence

$$\hat{\eta}_{2,0}(t_1,t_2,x_1,x_2) \qquad \text{and} \qquad \hat{\psi}_{2,0}(t_1,t_2,x_1,x_2,z) \tag{III.5.12}$$

remain undetermined. The first and second-harmonic problems have the general form

$$\frac{\partial^2\hat{\psi}_{2,nk}}{\partial z^2} - n^2k^2\hat{\psi}_{2,nk} = E_{2,nk}\mathrm{e}^{nkz}, \tag{III.5.13}$$

with surface boundary conditions at $z=0$

$$\hat{\eta}_{2,nk} - \frac{k}{\omega}\hat{\psi}_{2,nk} = F_{2,nk}, \tag{III.5.14}$$

$$\frac{\partial\hat{\psi}_{2,nk}}{\partial z} - \frac{k(n^2k^2+2)}{3\omega}\hat{\eta}_{2,nk} = G_{2,nk}, \tag{III.5.15}$$

for $n=1$ and $n=2$.

The first-harmonic problem is defined by

$$E_{2,k} \;=\; -2\mathrm{i}\omega\frac{\partial\mathcal{A}}{\partial x_1} - \frac{\partial^2 U^S}{\partial z^2}(z)\mathcal{A}, \tag{III.5.16}$$

$$F_{2,k} \;=\; \frac{k}{\omega}U^S(0)\mathcal{A} - \frac{\mathrm{i}}{\omega}\frac{\partial\mathcal{A}}{\partial t_1} - \frac{\mathrm{i}}{k}\frac{\partial\mathcal{A}}{\partial x_1}, \tag{III.5.17}$$

$$G_{2,k} \;=\; -\frac{\partial U^S}{\partial z}(0)\mathcal{A} + kU^S(0)\mathcal{A} - \mathrm{i}\frac{(3k^2+2)}{3\omega}\frac{\partial\mathcal{A}}{\partial x_1} - \mathrm{i}\frac{\partial\mathcal{A}}{\partial t_1}. \tag{III.5.18}$$

Because the second-order first-harmonic problem is forced by its own homogeneous solution, it must be subjected to a solvability condition to avoid secular behavior. This solvability condition follows conveniently from Green's formula

$$\int_{-\infty}^{0}\hat{\psi}_{1,1}\frac{\partial^2\hat{\psi}_{2,1}}{\partial z^2} - \hat{\psi}_{2,1}\frac{\partial^2\hat{\psi}_{1,1}}{\partial z^2}\,\mathrm{d}z = \left[\hat{\psi}_{1,1}\frac{\partial\hat{\psi}_{2,1}}{\partial z} - \hat{\psi}_{2,1}\frac{\partial\hat{\psi}_{1,1}}{\partial z}\right]_{-\infty}^{0}, \tag{III.5.19}$$

where $\hat{\psi}_{1,1}$ is the homogeneous solution. The solvability condition yields the slow evolution equation

$$\frac{\partial\mathcal{A}}{\partial t_1} + \frac{3k^2+2}{6\omega}\frac{\partial\mathcal{A}}{\partial x_1} + 2\mathrm{i}k^2\int_{-\infty}^{0}\mathrm{e}^{2k\xi}U^S(\xi)\,\mathrm{d}\xi\;\mathcal{A} = 0. \tag{III.5.20}$$

The particular solution is

$$\begin{aligned}\hat{\psi}_{2,k} \;=\; &\left(2k\mathrm{e}^{-kz}\int_{-\infty}^{0}\mathrm{e}^{2k\xi}U^S(\xi)\,d\xi - U^S(z)\mathrm{e}^{kz}\right)\mathcal{A} - \mathrm{i}\left(\frac{\omega}{k}z + \frac{k^2-2}{6k\omega}\right)\frac{\partial\mathcal{A}}{\partial x_1}\mathrm{e}^{kz}\\ &+ \frac{k^2+2}{3\omega}\hat{\eta}_{2,k}\mathrm{e}^{kz},\end{aligned} \tag{III.5.21}$$

where $\hat{\eta}_{2,k}$ is so far undetermined. Hara & Mei (1994) set it equal to zero, while Jones (1992) kept it as a parameter in his equations for Wilton's ripples. We shall keep it as a parameter to facilitate comparison with both of the previous works.

The second-harmonic problem for $\hat{\psi}_{2,2}$ is defined by

$$E_{2,2k} = 0, \qquad F_{2,2k} = k\mathcal{A}^2, \qquad G_{2,2k} = -k\omega\mathcal{A}^2. \tag{III.5.22}$$

The particular solution is

$$\hat{\psi}_{2,2k} = -\frac{3k^2\omega}{2(k^2-1)}\mathcal{A}^2 \mathrm{e}^{2kz}, \qquad \hat{\eta}_{2,2k} = -\frac{3\omega^2}{2(k^2-1)}\mathcal{A}^2. \tag{III.5.23}$$

We notice that the solution for the second harmonic breaks down when $k = 1$, corresponding to second-harmonic resonance (Wilton's ripples). The integral terms give phase shifts corresponding to the Doppler shift induced by the shear current in the water.

The slow evolution equation for $\mathcal{A}$ corresponds to the leading order of equation (4.7) in Hara & Mei (1994). The integral term in our slow evolution equation corresponds to their coefficient $\kappa_{00}$, which is defined through their equations (A6), (A22) and (A27). Their result agrees with our result provided either the sign is corrected on the right-hand side of their (A22), or the sign is corrected in front of the right-most term in their (A6). This correction in sign does not affect their resulting evolution equation.

### III.5.3 Surface boundary-layer correction in water

The boundary-layer correction is governed by (III.4.37) and the tangential stress boundary condition (III.4.35). Their leading order contributions are

$$\frac{\partial^2 \psi_{BL}}{\partial t \partial \bar{z}_{BL}} - \sigma^2 \frac{\partial^3 \psi_{BL}}{\partial \bar{z}_{BL}^3} = 0 \tag{III.5.24}$$

and

$$\frac{\partial^2 \psi_{BL}}{\partial \bar{z}_{BL}^2} = \frac{\partial^2 \psi_1}{\partial x^2} - \frac{\partial^2 \psi}{\partial z^2} + \epsilon\mu^{-1}T \quad \text{at} \quad \begin{cases} z = 0, \\ \bar{z}_{BL} = 0. \end{cases} \tag{III.5.25}$$

The interior component of the stream function is evaluated at $z = 0$.

The leading order boundary-layer problem is linear, and hence we assume a solution of the form

$$\psi_{BL} = \hat{\psi}_{BL,k} \mathrm{e}^{\mathrm{i}(kx-\omega t)} + \text{c.c.} \tag{III.5.26}$$

We also define a harmonic expansion for the tangential stress exerted due to the wave-disturbance in the air

$$T = \hat{T}_k \mathcal{A} \mathrm{e}^{\mathrm{i}(kx-\omega t)} + \text{c.c.} \tag{III.5.27}$$

The boundary-layer correction is then governed by

$$\frac{\partial \hat{\psi}_{BL,k}}{\partial \bar{z}_{BL}} - \mathrm{i}\frac{\sigma^2}{\omega}\frac{\partial^3 \hat{\psi}_{BL,k}}{\partial \bar{z}_{BL}^3} = 0, \tag{III.5.28}$$

with surface boundary condition

$$\frac{\partial^2 \hat{\psi}_{BL,k}}{\partial \bar{z}_{BL}^2} = (\epsilon\mu^{-1}\hat{T}_k - 2k\omega)\mathcal{A}. \tag{III.5.29}$$

The solution is

$$\hat{\psi}_{BL,k} = \mathrm{i}\sigma^2(\epsilon\mu^{-1}\frac{1}{\omega}\hat{T}_k - 2k)\mathcal{A}\mathrm{e}^{-\sigma^{-1}\mathrm{e}^{-\frac{\mathrm{i}\pi}{4}}\bar{z}_{BL}}. \tag{III.5.30}$$

### III.5.4 Third-order water interior problem

At the third order, $\mathcal{O}(\epsilon^2)$, the water interior problem is governed by

$$\frac{\partial}{\partial t}\nabla^2\psi_3 = \mathcal{E}_3, \tag{III.5.31}$$

with boundary conditions at $z = 0$

$$\frac{\partial \eta_3}{\partial t} + \frac{\partial \psi_3}{\partial x} = \mathcal{F}_3, \tag{III.5.32}$$

$$\frac{\partial^2 \psi_3}{\partial t \partial z} + \frac{2}{3}\frac{\partial \eta_3}{\partial x} - \frac{1}{3}\frac{\partial^3 \eta_3}{\partial x^3} = \mathcal{G}_3. \tag{III.5.33}$$

The right-hand-side expressions $\mathcal{E}_3$, $\mathcal{F}_3$ and $\mathcal{G}_3$ are lengthy functions of $\psi_1$, $\psi_2$, $\eta_1$ and $\eta_2$, and are not given here.

We only need to consider the zeroth-harmonic quantities introduced for the second-order problem and the first-harmonic solvability condition of the third-order problem. Since the perturbation problems are always linear in the highest-order variables, it suffices to consider only the first-harmonic contribution to the solution,

$$\eta_3 = \hat{\eta}_{3,k}\mathrm{e}^{\mathrm{i}(kx-\omega t)} + \ldots + \text{c.c.}, \tag{III.5.34}$$

$$\psi_3 = \hat{\psi}_{3,k}\mathrm{e}^{\mathrm{i}(kx-\omega t)} + \ldots + \text{c.c.} \tag{III.5.35}$$

We also define the harmonic expansion of the normal stress exerted due to the wave-disturbance in the air

$$N = \hat{N}_k^{(1)}\mathcal{A}\mathrm{e}^{\mathrm{i}(kx-\omega t)} + \text{c.c.} \tag{III.5.36}$$

The zeroth-harmonic problem at the third order gives the leading-order governing equations for the zeroth-harmonic quantities introduced at the second order. The second-order slow drift is governed by

$$\frac{\partial^3 \hat{\psi}_{2,0}}{\partial t_1 \partial z^2} = 0, \tag{III.5.37}$$

with surface boundary conditions

$$\frac{\partial\hat{\psi}_{2,0}}{\partial x_1}+\frac{\partial\hat{\eta}_{2,0}}{\partial t_1}=-2\omega\frac{\partial}{\partial x_1}|\mathcal{A}|^2, \tag{III.5.38}$$

$$\frac{\partial^2\hat{\psi}_{2,0}}{\partial t_1\partial z}+\frac{2}{3}\frac{\partial\hat{\eta}_{2,0}}{\partial x_1}=0. \tag{III.5.39}$$

The second-order slow drift is forced through the surface conditions. From the governing equation we conclude that $\hat{\psi}_{2,0}$ is independent of $z$. It is indeed well known (Djordjevic & Redekopp 1977; Hara & Mei 1994) that $\hat{\psi}_{2,0}$ depends on the much longer vertical coordinate $z_1$. It follows that the second-order zeroth-harmonic solution is not needed here for our present purposes.

The problem for the first harmonic has the form

$$\frac{\partial^2\hat{\psi}_{3,k}}{\partial z^2}-k^2\hat{\psi}_{3,k}=E_{3,k}\mathrm{e}^{kz}, \tag{III.5.40}$$

with surface boundary conditions

$$\hat{\eta}_{3,k}-\frac{k}{\omega}\hat{\psi}_{3,k}=F_{3,k}, \tag{III.5.41}$$

$$\frac{\partial\hat{\psi}_{3,k}}{\partial z}-\omega\hat{\eta}_{3,k}=G_{3,k}. \tag{III.5.42}$$

The expressions for $E_{3,k}$, $F_{3,k}$ and $G_{3,k}$ are long, and are not given here.

Since the first-harmonic problem is forced by its homogeneous solution, we must impose a solvability condition to avoid secular behavior (see equation (III.5.19)). After using the second-order solvability condition to eliminate derivatives with respect to $t_1$, the third-order solvability condition requires

$$\frac{\partial\mathcal{A}}{\partial t_2}+\frac{3k^2+2}{6\omega}\frac{\partial\mathcal{A}}{\partial x_2}+b_k\frac{\partial\mathcal{A}}{\partial x_1}+(d_k+\mathrm{i}a_{k,1})\,\mathcal{A}-\mathrm{i}\frac{3k^4+12k^2-4}{72\omega^3}\frac{\partial^2\mathcal{A}}{\partial x_1^2}$$

$$-\mathrm{i}\frac{k^3(k^4+k^2+16)}{12\omega(k^2-1)}\mathcal{A}|\mathcal{A}|^2+\frac{\partial\hat{\eta}_{2,k}}{\partial t_1}+\frac{3k^2+2}{6\omega}\frac{\partial\hat{\eta}_{2,k}}{\partial x_1}+\mathrm{i}a_{k,0}\hat{\eta}_{2,k}=0. \tag{III.5.43}$$

The coefficients $a_{k,0}$, $a_{k,1}$ and $b_k$ depend on the shear current in the water, $d_k$ depends on viscous shear in water and the wave disturbance in air; they are all summarized in the next subsection.

The third-order solvability condition breaks down for $k=1$, corresponding to second-order resonance (Wilton's ripples).

The third-order solvability condition for $\mathcal{A}$ corresponds to the $\mathcal{O}(\epsilon)$ contribution to equation (4.7) in Hara & Mei (1994) provided we set $\hat{\eta}_{2,k}=0$. However, they did not have wind forcing or viscous damping occurring at this order, such that our coefficient $d_k$ has no counterpart in their equation at this order. Our coefficient $a_{k,1}$ corresponds to their coefficient $\kappa_{01}+\kappa_{20}$, while our coefficient $b_k$ corresponds to their

$\kappa_{10}$. While we have given our coefficients explicitly as integrals of the shear current, they gave their coefficients implicitly as solutions of auxiliary differential equations. To obtain analytical solutions of these auxiliary differential equations is a lengthy task.

### III.5.5 Summary of the slow evolution equation for a single wave

We can now combine the slow evolution equations from the second and third-order problems to get a combined evolution equation valid over time and space $t_1, x_1 \sim \mathcal{O}(\epsilon^{-1})$. This combined solvability condition is

$$\begin{aligned}\frac{\partial \mathcal{A}}{\partial t_1} + \left(\frac{3k^2+2}{6\omega} + \epsilon b_k\right)\frac{\partial \mathcal{A}}{\partial x_1} + \left\{\epsilon d_k + \mathrm{i}\left(a_{k,0} + \epsilon a_{k,1}\right)\right\}\mathcal{A} \\ - \mathrm{i}\epsilon\frac{3k^4+12k^2-4}{72\omega^3}\frac{\partial^2 \mathcal{A}}{\partial x_1^2} - \mathrm{i}\epsilon\frac{k^3(k^4+k^2+16)}{12\omega(k^2-1)}\mathcal{A}|\mathcal{A}|^2 \\ + \epsilon\left(\frac{\partial \hat{\eta}_{2,k}}{\partial t_1} + \frac{3k^2+2}{6\omega}\frac{\partial \hat{\eta}_{2,k}}{\partial x_1} + \mathrm{i}a_{k,0}\hat{\eta}_{2,k}\right) &= 0. \quad \text{(III.5.44)}\end{aligned}$$

The coefficients that depend on the shear current in water are given by

$$a_{k,0} = 2k^2\int_{-\infty}^{0} \mathrm{e}^{2kz}U^S(z)\,\mathrm{d}z, \quad \text{(III.5.45)}$$

$$a_{k,1} = \frac{k^3}{\omega}\int_{-\infty}^{0} \mathrm{e}^{2kz}\left(U^S(z)\right)^2\,\mathrm{d}z - 2\frac{k^4}{\omega}\left(\int_{-\infty}^{0} \mathrm{e}^{2kz}U^S(z)\,\mathrm{d}z\right)^2, \quad \text{(III.5.46)}$$

$$b_k = 4k^2\int_{-\infty}^{0} z\mathrm{e}^{2kz}U^S(z)\,\mathrm{d}z + 4k\int_{-\infty}^{0} \mathrm{e}^{2kz}U^S(z)\,\mathrm{d}z. \quad \text{(III.5.47)}$$

The coefficient that accounts for viscous damping and linear normal and tangential stress from air on the water surface is

$$d_k = 2k^2\sigma^2 - \frac{\mathrm{i}k}{2\omega}\hat{N}_k^{(1)} - \frac{k\sigma^2}{2\omega}\hat{T}_k. \quad \text{(III.5.48)}$$

The complex coefficients $\hat{N}_k^{(1)}$ and $\hat{T}_k$, which depend on the wave-disturbance in air, will be derived later in section III.7.

The important result from this section is the fact that the linear growth rate (on timescale $t_2$) due to linear normal and tangential stress and viscosity, is given by the expression

$$\beta = \mathrm{Re}\left\{2k^2\sigma^2 - \frac{\mathrm{i}k}{2\omega}\hat{N}_k^{(1)} - \frac{k\sigma^2}{2\omega}\hat{T}_k\right\}. \quad \text{(III.5.49)}$$

This result will be used after the linear wave disturbance in air has been solved in section III.7.

# III.6 Evolution equations for Wilton's ripples

The evolution equation for a single wave (III.5.44) has nonlinear interaction coefficients that become singular for $k = 1$. This is because the second harmonic $k = 2$ is a free wave, and must be scaled at the leading order together with the first harmonic. Coupled evolution equations for Wilton's ripples correct to third order were derived by Jones (1992), but without accounting for non-conservative effects.

We here derive the coupled evolution equations for Wilton's ripples to the third order, with the effects of wind forcing and viscous damping scaled at the third order. We limit our consideration to general slow modulation in time only, but allow for a special type of slow modulation in space corresponding to small detuning from exact second-harmonic resonance.

## III.6.1 First-order water interior problem

The first-order problem is identical to that given for the single wave, (III.5.1)–(III.5.3).

We assume that the leading-order solution is a superposition of a first and a second-harmonic wave with wavenumbers $k = 1$ and $k = 2$. To account for a small detuning from exact second-harmonic resonance, we suppose that the actual wavenumbers of the two waves are

$$k_a = 1 + \epsilon\delta_a \qquad \text{and} \qquad k_b = 2 + \epsilon\delta_b. \tag{III.6.1}$$

Since we do not want any slow space modulation other than the detuning, we must then require that these wavenumbers satisfy the resonance condition exactly,

$$2k_a = k_b, \tag{III.6.2}$$

and hence

$$\delta_a = \frac{1}{2}\delta_b = \delta. \tag{III.6.3}$$

It is convenient to introduce a notation for the detuned phase

$$\theta = x + \delta x_1 - t. \tag{III.6.4}$$

The leading-order solution for second-harmonic resonance with detuning is now taken to be

$$\eta_1 = A(t_1, t_2)\mathrm{e}^{\mathrm{i}\theta} + B(t_1, t_2)\mathrm{e}^{2\mathrm{i}\theta} + \text{c.c.}, \tag{III.6.5}$$

$$\psi_1 = A(t_1, t_2)\mathrm{e}^{\mathrm{i}\theta+z} + B(t_1, t_2)\mathrm{e}^{2\mathrm{i}\theta+2z} + \text{c.c.} \tag{III.6.6}$$

## III.6.2 Second-order water-interior problem

The second-order problem is identical to that given for the single wave, (III.5.7)–(III.5.9).

Due to quadratically nonlinear interaction, we assume a solution of the form

$$\eta_2 = \hat{\eta}_{2,0} + \hat{\eta}_{2,1}\mathrm{e}^{\mathrm{i}\theta} + \hat{\eta}_{2,2}\mathrm{e}^{2\mathrm{i}\theta} + \hat{\eta}_{2,3}\mathrm{e}^{3\mathrm{i}\theta} + \hat{\eta}_{2,4}\mathrm{e}^{4\mathrm{i}\theta} + \text{c.c.}, \tag{III.6.7}$$

$$\psi_2 = \hat{\psi}_{2,0} + \hat{\psi}_{2,1}\mathrm{e}^{\mathrm{i}\theta} + \hat{\psi}_{2,2}\mathrm{e}^{2\mathrm{i}\theta} + \hat{\psi}_{2,3}\mathrm{e}^{3\mathrm{i}\theta} + \hat{\psi}_{2,4}\mathrm{e}^{4\mathrm{i}\theta} + \text{c.c.} \tag{III.6.8}$$

The governing equations at the second order give no zeroth-harmonic terms, and hence

$$\hat{\eta}_{2,0}(t_1, t_2) \qquad \text{and} \qquad \hat{\psi}_{2,0}(t_1, t_2, z) \tag{III.6.9}$$

remain undetermined. The problems for each of the $n$th harmonics have the general form

$$\frac{\partial^2 \hat{\psi}_{2,n}}{\partial z^2} - n^2 \hat{\psi}_{2,n} = E_{2,n}\mathrm{e}^{nz}, \tag{III.6.10}$$

with surface boundary conditions at $z = 0$

$$\hat{\eta}_{2,n} - \hat{\psi}_{2,n} = F_{2,n}, \tag{III.6.11}$$

$$\frac{\partial \hat{\psi}_{2,n}}{\partial z} - \frac{n^2 + 2}{3}\hat{\eta}_{2,n} = G_{2,n}. \tag{III.6.12}$$

The first-harmonic problem is given by

$$E_{2,1} = \left(2\delta - \frac{\partial^2 U^S}{\partial z^2}(z)\right) A, \tag{III.6.13}$$

$$F_{2,1} = U^S(0)A + \delta A + 3A^*B - \mathrm{i}\frac{\partial A}{\partial t_1}, \tag{III.6.14}$$

$$G_{2,1} = -\frac{\partial U^S}{\partial z}(0)A + U^S(0)A + \frac{5}{3}\delta A - A^*B - \mathrm{i}\frac{\partial A}{\partial t_1}. \tag{III.6.15}$$

The first-harmonic problem is forced by its homogeneous solution. The solvability condition yields the slow evolution equation

$$\frac{\partial A}{\partial t_1} + \frac{5}{6}\mathrm{i}\delta A + 2\mathrm{i}\int_{-\infty}^{0} \mathrm{e}^{2\xi} U^S(\xi)\,\mathrm{d}\xi\; A + \mathrm{i}A^*B = 0. \tag{III.6.16}$$

The particular solution is

$$\hat{\psi}_{2,1} = \left(2\mathrm{e}^{-z}\int_{-\infty}^{0} \mathrm{e}^{2\xi} U^S(\xi)\,\mathrm{d}\xi - U^S(z)\mathrm{e}^{z} + \delta z\mathrm{e}^{z} - \frac{1}{6}\delta\mathrm{e}^{z}\right) A - 2A^*B\mathrm{e}^{z} + \hat{\eta}_{2,1}\mathrm{e}^{z}, \tag{III.6.17}$$

where $\hat{\eta}_{2,1}$ is so far undetermined.

The second-harmonic problem is

$$E_{2,2} = \left(8\delta - \frac{\partial^2 U^S}{\partial z^2}(z)\right) B, \tag{III.6.18}$$

$$F_{2,2} = U^S(0)B + \delta B + A^2 - \mathrm{i}\frac{\partial B}{\partial t_1}, \tag{III.6.19}$$

$$G_{2,2} = -\frac{\partial U^S}{\partial z}(0)B + 2U^S(0)B + \frac{14}{3}\delta B - A^2 - \mathrm{i}\frac{\partial B}{\partial t_1}. \tag{III.6.20}$$

The second-harmonic problem is also forced by its homogeneous solution. The solvability condition yields the slow evolution equation

$$\frac{\partial B}{\partial t_1} + \frac{7}{3}\mathrm{i}\delta B + 8\mathrm{i}\int_{-\infty}^{0} \mathrm{e}^{4\xi}U^S(\xi)\,\mathrm{d}\xi\; B + \frac{\mathrm{i}}{2}A^2 = 0. \tag{III.6.21}$$

The particular solution is

$$\hat{\psi}_{2,2} = \left(4\mathrm{e}^{-2z}\int_{-\infty}^{0} \mathrm{e}^{4\xi}U^S(\xi)\,\mathrm{d}\xi - U^S(z)\mathrm{e}^{2z} + 2\delta z\mathrm{e}^{2z} + \frac{1}{6}\delta\mathrm{e}^{2z}\right)B - \frac{3}{4}A^2\mathrm{e}^{2z} + \hat{\eta}_{2,2}\mathrm{e}^{2z}, \tag{III.6.22}$$

where $\hat{\eta}_{2,2}$ is so far undetermined.

The third and fourth-harmonic problems are given by

$$E_{2,3} = 0, \qquad F_{2,3} = 3AB, \qquad G_{2,3} = -5AB, \tag{III.6.23}$$

and

$$E_{2,4} = 0, \qquad F_{2,4} = 2B^2, \qquad G_{2,4} = -4B^2. \tag{III.6.24}$$

Their solutions are

$$\hat{\psi}_{2,3} = -9AB\mathrm{e}^{3z}, \qquad \hat{\eta}_{2,3} = -6AB, \tag{III.6.25}$$

$$\hat{\psi}_{2,4} = -4B^2\mathrm{e}^{4z}, \qquad \hat{\eta}_{2,4} = -2B^2. \tag{III.6.26}$$

In the two solvability conditions, we notice that the fractions $\frac{5}{6}$ and $\frac{7}{3}$ in the slow evolution equations are precisely the group velocities of the first and the second-harmonic waves, respectively. The integral terms give phase shifts corresponding to the Doppler shifts induced by the shear current in water.

## III.6.3 Surface boundary-layer correction in water

The second-order problem is identical to that given for the single wave, (III.5.24) and (III.5.25).

The leading order boundary-layer problem is linear, and hence we assume a solution of the form

$$\psi_{BL} = \hat{\psi}_{BL,1}\mathrm{e}^{\mathrm{i}\theta} + \hat{\psi}_{BL,2}\mathrm{e}^{2\mathrm{i}\theta} + \text{c.c.} \tag{III.6.27}$$

We also define a harmonic expansion for the tangential stress exerted by the air flow field

$$T = \hat{T}_1 A\mathrm{e}^{\mathrm{i}\theta} + \hat{T}_2 B\mathrm{e}^{2\mathrm{i}\theta} + \text{c.c.} \tag{III.6.28}$$

The first-harmonic boundary-layer correction is governed by

$$\frac{\partial\hat{\psi}_{BL,1}}{\partial\bar{z}_{BL}} - \mathrm{i}\sigma^2\frac{\partial^3\hat{\psi}_{BL,1}}{\partial\bar{z}_{BL}^3} = 0, \tag{III.6.29}$$

with surface boundary condition

$$\frac{\partial^2\hat{\psi}_{BL,1}}{\partial\bar{z}_{BL}^2} = (\epsilon\mu^{-1}\hat{T}_1 - 2)A, \tag{III.6.30}$$

and has the solution

$$\hat{\psi}_{BL,1} = \mathrm{i}\sigma^2(\epsilon\mu^{-1}\hat{T}_1 - 2)A\mathrm{e}^{-\sigma^{-1}\mathrm{e}^{-\frac{\mathrm{i}\pi}{4}}\bar{z}_{BL}}. \tag{III.6.31}$$

The second-harmonic boundary-layer correction is governed by

$$2\frac{\partial\hat{\psi}_{BL,2}}{\partial\bar{z}_{BL}} - \mathrm{i}\sigma^2\frac{\partial^3\hat{\psi}_{BL,2}}{\partial\bar{z}_{BL}^3} = 0, \tag{III.6.32}$$

with surface boundary condition

$$\frac{\partial^2\hat{\psi}_{BL,2}}{\partial\bar{z}_{BL}^2} = (\epsilon\mu^{-1}\hat{T}_2 - 8)B, \tag{III.6.33}$$

and has the solution

$$\hat{\psi}_{BL,2} = \frac{\mathrm{i}}{2}\sigma^2(\epsilon\mu^{-1}\hat{T}_2 - 8)B\mathrm{e}^{-\sqrt{2}\sigma^{-1}\mathrm{e}^{-\frac{\mathrm{i}\pi}{4}}\bar{z}_{BL}}. \tag{III.6.34}$$

### III.6.4 Third-order water-interior problem

The third-order problem is identical to that given for the single wave, (III.5.31)–(III.5.33).

We only need to consider the zeroth-harmonic quantities introduced for the second-order problem and the first and second-harmonic solvability conditions of the third-order problem. Since the perturbation problems are always linear in the highest order variables, it suffices to consider only the first and second harmonic contributions to the solution,

$$\eta_3 = \hat{\eta}_{3,1}\mathrm{e}^{\mathrm{i}\theta} + \hat{\eta}_{3,2}\mathrm{e}^{2\mathrm{i}\theta} + \ldots + \text{c.c.}, \tag{III.6.35}$$

$$\psi_3 = \hat{\psi}_{3,1}\mathrm{e}^{\mathrm{i}\theta} + \hat{\psi}_{3,2}\mathrm{e}^{2\mathrm{i}\theta} + \ldots + \text{c.c.} \tag{III.6.36}$$

We also define the harmonic expansion of the normal stress exerted by the air flow field

$$N = (\hat{N}_1^{(1)}A + \hat{N}_1^{(2)}A^*B)\mathrm{e}^{\mathrm{i}\theta} + (\hat{N}_2^{(1)}B + \hat{N}_2^{(2)}A^2)\mathrm{e}^{2\mathrm{i}\theta} + \text{c.c.} \tag{III.6.37}$$

Notice that $\hat{N}_k^{(1)}$ denotes linear normal stress from air, while $\hat{N}_k^{(2)}$ denotes nonlinear normal stress due to quadratically nonlinear interactions in air.

The zeroth-harmonic problem gives the leading-order governing equations for the zeroth-harmonic quantities introduced at the second order. The slow drift is governed by

$$\frac{\partial^3 \hat{\psi}_{2,0}}{\partial t_1 \partial z^2} = 0, \tag{III.6.38}$$

with surface boundary conditions at $z = 0$

$$\frac{\partial \hat{\eta}_{2,0}}{\partial t_1} = 0, \tag{III.6.39}$$

$$\frac{\partial^2 \hat{\psi}_{2,0}}{\partial t_1 \partial z} = 0. \tag{III.6.40}$$

The second-order slow drift is not forced through the surface conditions, since we have limited our theory to slow space modulation corresponding to a small detuning from resonance. We may therefore for the present purposes simply set $\hat{\psi}_{2,0} = \hat{\eta}_{2,0} = 0$.

The problem for the remaining $n$th harmonics all have the general form

$$\frac{\partial^2 \hat{\psi}_{3,n}}{\partial z^2} - n^2 \hat{\psi}_{3,n} = E_{3,n} \mathrm{e}^{nz}, \tag{III.6.41}$$

with surface conditions at $z = 0$

$$\hat{\eta}_{3,n} - \hat{\psi}_{3,n} = F_{3,n}, \tag{III.6.42}$$

$$\frac{\partial \hat{\psi}_{3,n}}{\partial z} - \frac{n^2 + 2}{3} \hat{\eta}_{3,n} = G_{3,n}. \tag{III.6.43}$$

The expressions for $E_{3,n}$, $F_{3,n}$ and $G_{3,n}$ are long, and are not given here.

The first and second-harmonic problems are forced by their homogeneous solutions, and must be subjected to solvability conditions. After the second-order solvability conditions have been used to get rid of derivatives with respect to $t_1$, the third-order solvability conditions become

$$\frac{\partial A}{\partial t_2} + \left\{ d_1 + \mathrm{i} \left( a_{1,1} + \frac{11}{72}\delta^2 + b_1 \delta \right) \right\} A + \mathrm{i} \left\{ 10c + \frac{13}{6}\delta - \frac{1}{2}\hat{N}_1^{(2)} \right\} A^* B + \mathrm{i} A |A|^2 - \frac{21}{2} \mathrm{i} A |B|^2$$
$$+ \frac{\partial \hat{\eta}_{2,1}}{\partial t_1} + \mathrm{i} \left( \frac{5}{6}\delta + a_{1,0} \right) \hat{\eta}_{2,1} + \mathrm{i} B \hat{\eta}_{2,1}^* + \mathrm{i} A^* \hat{\eta}_{2,2} \; = \; 0 \tag{III.6.44}$$

and

$$\frac{\partial B}{\partial t_2} + \left\{ d_2 + \mathrm{i} \left( a_{2,1} + \frac{23}{36}\delta^2 + 2 b_2 \delta \right) \right\} B + \mathrm{i} \left\{ \frac{9}{2}c + \frac{5}{6}\delta - \frac{1}{2}\hat{N}_2^{(2)} \right\} A^2 - \frac{41}{4} \mathrm{i} B |A|^2 - 4 \mathrm{i} B |B|^2$$
$$+ \frac{\partial \hat{\eta}_{2,2}}{\partial t_1} + \mathrm{i} \left( \frac{7}{3}\delta + a_{2,0} \right) \hat{\eta}_{2,2} + \mathrm{i} A \hat{\eta}_{2,1} \; = \; 0. \tag{III.6.45}$$

The coefficients $a_{n,1}$, $b_n$, $c$ depend on the shear current in the water, while the coefficients $d_n$ depend on viscous shear in water and the wave disturbance in air; they are

all summarized in the next subsection.

### III.6.5 Summary of the slow evolution equations for Wilton's ripples

We can now combine the slow evolution equations from the second and third-order problems to get combined evolution equations valid for time $t_1 = \mathcal{O}(\epsilon^{-1})$. These combined solvability conditions are

$$\begin{aligned}
&\frac{\partial A}{\partial t_1} + \left\{\epsilon d_1 + \mathrm{i}\left(a_{1,0} + \epsilon a_{1,1} + \frac{5}{6}\delta + \epsilon b_1 \delta + \frac{11}{72}\epsilon\delta^2\right)\right\} A \\
&+ \mathrm{i}\left\{1 + 10\epsilon c + \frac{13}{6}\epsilon\delta - \frac{1}{2}\epsilon\hat{N}_1^{(2)}\right\} A^* B + \mathrm{i}\epsilon A|A|^2 - \frac{21}{2}\mathrm{i}\epsilon A|B|^2 \\
&+ \epsilon\left\{\frac{\partial\hat{\eta}_{2,1}}{\partial t_1} + \mathrm{i}\left(\frac{5}{6}\delta + a_{1,0}\right)\hat{\eta}_{2,1} + \mathrm{i}B\hat{\eta}_{2,1}^* + \mathrm{i}A^*\hat{\eta}_{2,2}\right\} = 0 \qquad \text{(III.6.46)}
\end{aligned}$$

and

$$\begin{aligned}
&\frac{\partial B}{\partial t_1} + \left\{\epsilon d_2 + \mathrm{i}\left(a_{2,0} + \epsilon a_{2,1} + \frac{7}{3}\delta + 2\epsilon b_2 \delta + \frac{23}{36}\epsilon\delta^2\right)\right\} B \\
&+ \mathrm{i}\left\{\frac{1}{2} + \frac{9}{2}\epsilon c + \frac{5}{6}\epsilon\delta - \frac{1}{2}\epsilon\hat{N}_2^{(2)}\right\} A^2 - \frac{41}{4}\mathrm{i}\epsilon B|A|^2 - 4\mathrm{i}\epsilon B|B|^2 \\
&+ \epsilon\left\{\frac{\partial\hat{\eta}_{2,2}}{\partial t_1} + \mathrm{i}\left(\frac{7}{3}\delta + a_{2,0}\right)\hat{\eta}_{2,2} + \mathrm{i}A\hat{\eta}_{2,1}\right\} = 0. \qquad \text{(III.6.47)}
\end{aligned}$$

The coefficients that depend on the shear current in water are given by

$$a_{1,0} = 2\int_{-\infty}^{0} \mathrm{e}^{2z} U^S(z)\,\mathrm{d}z, \qquad \text{(III.6.48)}$$

$$a_{2,0} = 8\int_{-\infty}^{0} \mathrm{e}^{4z} U^S(z)\,\mathrm{d}z, \qquad \text{(III.6.49)}$$

$$a_{1,1} = \int_{-\infty}^{0} \mathrm{e}^{2z}\left(U^S(z)\right)^2\,\mathrm{d}z - 2\left(\int_{-\infty}^{0} \mathrm{e}^{2z} U^S(z)\,\mathrm{d}z\right)^2, \qquad \text{(III.6.50)}$$

$$a_{2,1} = 4\int_{-\infty}^{0} \mathrm{e}^{4z}\left(U^S(z)\right)^2\,\mathrm{d}z - 16\left(\int_{-\infty}^{0} \mathrm{e}^{4z} U^S(z)\,\mathrm{d}z\right)^2, \qquad \text{(III.6.51)}$$

$$b_1 = 4\int_{-\infty}^{0} z\mathrm{e}^{2z} U^S(z)\,\mathrm{d}z + 4\int_{-\infty}^{0} \mathrm{e}^{2z} U^S(z)\,\mathrm{d}z, \qquad \text{(III.6.52)}$$

$$b_2 = 16\int_{-\infty}^{0} z\mathrm{e}^{4z} U^S(z)\,\mathrm{d}z + 8\int_{-\infty}^{0} \mathrm{e}^{4z} U^S(z)\,\mathrm{d}z, \qquad \text{(III.6.53)}$$

$$c = 2\int_{-\infty}^{0} \mathrm{e}^{4z} U^S(z)\,\mathrm{d}z - \int_{-\infty}^{0} \mathrm{e}^{2z} U^S(z)\,\mathrm{d}z. \qquad \text{(III.6.54)}$$

In figure III-4 we show the coefficients that are linear functions of the shear current ($a_{1,0}$, $a_{2,0}$, $b_1$, $b_2$, $c$), and in figure III-5 we show the coefficients that are quadratically nonlinear in the shear current ($a_{1,1}$, $a_{2,1}$). Recall that the shear current was defined

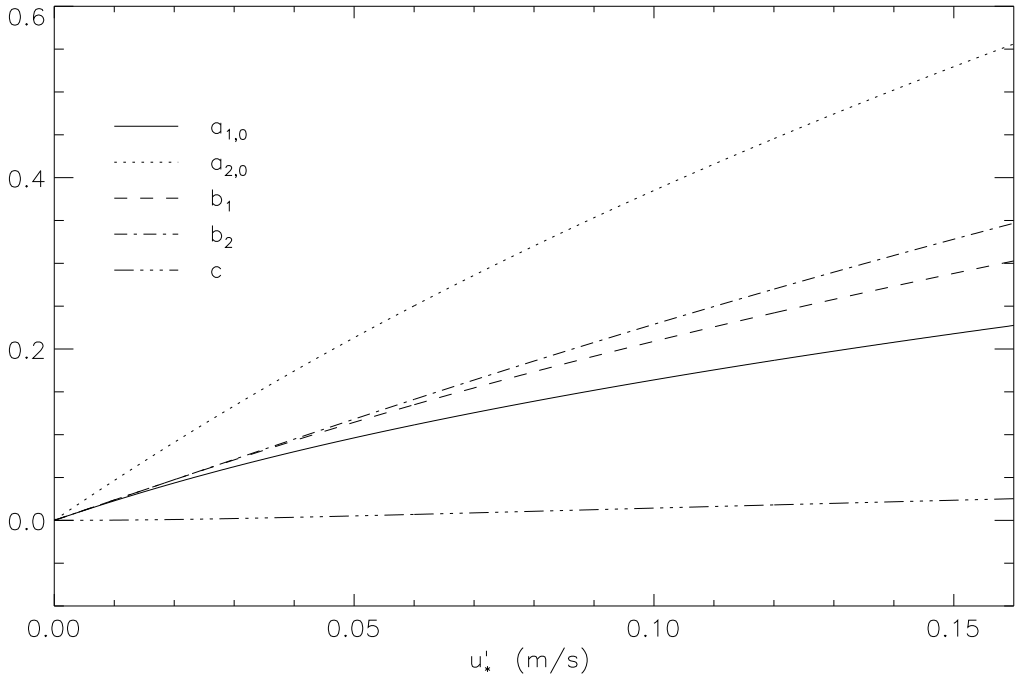


Figure III-4: Linear integral coefficients in water.

by equation (III.2.17). The air friction velocity is allowed to vary in the range 0–0.16 m/s.

The coefficients that account for viscous damping and linear normal and tangential stress from air on the water surface, are

$$d_1 = 2\sigma^2 - \frac{\mathrm{i}}{2}\hat{N}_1^{(1)} - \frac{1}{2}\sigma^2\hat{T}_1, \tag{III.6.55}$$

$$d_2 = 8\sigma^2 - \frac{\mathrm{i}}{2}\hat{N}_2^{(1)} - \frac{1}{2}\sigma^2\hat{T}_2. \tag{III.6.56}$$

Recall that the coefficients $\hat{N}_n^{(2)}$ account for nonlinear normal stress from air on the water surface. The complex coefficients $\hat{N}_n^{(m)}$ and $\hat{T}_n$, which depend on the wave-disturbance in air, will be derived later in section III.7. Numerical computations of these coefficients will be given in that section.

Jones (1992) derived an analogous system of two coupled cubically nonlinear Schrödinger equations for the case of no wind, shear current or viscosity, but included general spatial modulation on scales $x_1$ and $y_1$. To compare our slow evolution equations with his/her corresponding equations (2.28)–(2.31), we first set

$$\hat{\eta}_{2,1} = 2A^*B + \frac{1}{6}\delta A + A^{(2)}, \qquad \hat{\eta}_{2,2} = \frac{3}{4}A^2 - \frac{1}{6}\delta B + B^{(2)}, \tag{III.6.57}$$

where $A^{(2)}$ and $B^{(2)}$ are new and so far unspecified variables, and then perform obvious

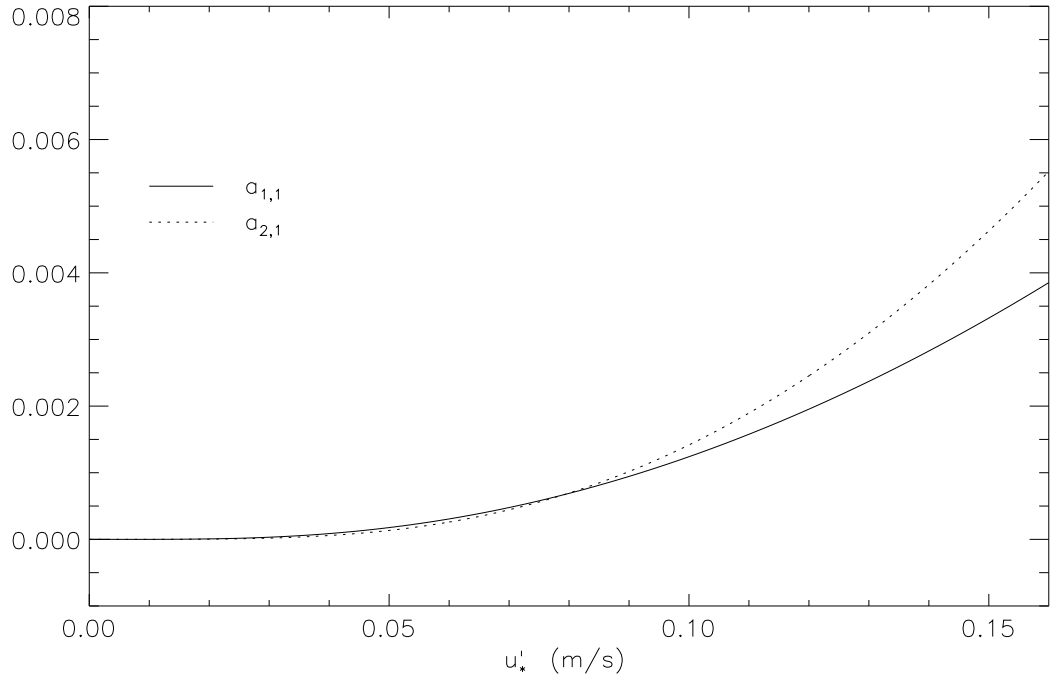


Figure III-5: Nonlinear integral coefficients in water.

changes in notation.

All of our coefficients that are not associated with wind, induced shear current or viscosity, are in exact agreement with Jones (1992), except for the coefficient in the first equation multiplying $\delta A^* B$. To resolve this problem, we rederived the evolution equations of Jones (1992). On the left hand side of their equation (2.22), there should be an extra term $-4\mathrm{i}ka_{2X}a_1^*$. In their equation (2.23), the second last term on the left side should not be there. In their equation (2.24), the second last term on the left side should read $-4\mathrm{i}a_{2X}a_1^*$. In their equation (2.25), the last term on the left side should be $-\frac{\mathrm{i}k}{2}a_{2X}a_1^*$. And finally in their equations (2.30), the last term on the left side should be $-\frac{\mathrm{i}}{2}a_{2X}a_1^*$. When these corrections have been accounted for, our results agree with Jones (1992).

The coefficient $c$ (III.6.54) for the quadratic terms does not appear to have been derived in previous literature.

This model has only two independent parameters: (1) the strength of the wind, given in terms of the friction velocity in air $u'_*$, and (2) the detuning parameter $\delta$.

In the following we set $\hat{\eta}_{2,1} = \hat{\eta}_{2,2} = 0$ without loss of generality, in order to simplify the notation. We can do this because these quantities are simply the coefficients of the homogeneous part of the solution of the second-order perturbation problem.

### III.6.6 Energy and momentum of Wilton's ripples

It is useful to derive expressions for the energy and momentum of the two interacting Wilton's ripples, in order to see how the non-conservative effects affect these quantities. A derivation is given in Appendix III.A. The total energy is

$$E = 2(|A|^2 + 2|B|^2)$$
$$+ \epsilon \left( \frac{4}{3}\delta(|A|^2 + 4|B|^2) + 2(a_{1,0}|A|^2 + a_{2,0}|B|^2) + \mathrm{Re}(A^2 B^*) \right). \tag{III.6.58}$$

Upon taking the time derivative of the total energy, we find

$$\dot{E} = \frac{\partial E}{\partial t_1} + \epsilon \frac{\partial E}{\partial t_2}$$
$$= \epsilon \left( -4(d_{1,R}|A|^2 + 2d_{2,R}|B|^2) + 2\,\mathrm{Im}\left\{ A^2 B^* \left( \hat{N}_1^{(2)*} - 2\hat{N}_2^{(2)} \right) \right\} \right). \tag{III.6.59}$$

The change in energy is due to viscous dissipation and work done by linear and nonlinear stress on the surface. Although only the imaginary part of the linear normal stress $\hat{N}_k^{(1)}$ is involved (through the real part of $d_k$), we see that both the real and imaginary parts of the nonlinear stress $\hat{N}_k^{(2)}$ affect the total energy.

The total horizontal momentum due to the wave disturbance is

$$\begin{aligned} M_x &= 2(|A|^2 + 2|B|^2) + \epsilon \left( \frac{1}{3}\delta(5|A|^2 + 14|B|^2) + 2U^S(0)(|A|^2 + 2|B|^2) \right. \\ &\quad - \frac{\partial U^S}{\partial z}(0)(|A|^2 + |B|^2) - 2(a_{1,0}|A|^2 + a_{2,0}|B|^2) \\ &\quad \left. - \mathrm{Re}(A^2 B^*) \right). \end{aligned} \tag{III.6.60}$$

Upon taking the time derivative of the momentum, we find

$$\begin{aligned} \dot{M}_x &= \frac{\partial M_x}{\partial t_1} + \epsilon \frac{\partial M_x}{\partial t_2} \\ &= \epsilon \left( -4(d_{1,R}|A|^2 + 2d_{2,R}|B|^2) + 2\,\mathrm{Im}\left\{ A^2 B^* \left( \hat{N}_1^{(2)*} - 2\hat{N}_2^{(2)} \right) \right\} \right. \\ &\quad \left. + 2\,\mathrm{Im}\left\{ A^2 B^* \left( 2a_{1,0} - a_{2,0} + \frac{1}{2}\frac{\partial U^S}{\partial z}(0) \right) \right\} \right). \end{aligned} \tag{III.6.61}$$

The change in momentum is due to viscosity in the water, linear and nonlinear stress on the surface, as well as the induced shear current in water.

We notice that the momentum and the energy are identical to leading order.

## III.7 The wave-disturbance in air

The leading-order linear perturbation problem in air is generic for simple-harmonic waves. We first solve the linear problem using the formalism of section III.5 for the evolution of a single wave. The second-order nonlinear perturbation problem

is specific to the case of Wilton's ripples, and does not appear to have been solved previously. Hara & Mei (1994) reported that nonlinear self-interaction in the air was of leading order importance in their model for a single wave. For our purposes, nonlinear self-interaction occurs at the next higher nonlinear order, and is not important here.

### III.7.1 First-order problem in air for a single wave

The wave-disturbance in water is given by the leading-order solution in section III.5, equations (III.5.4) and (III.5.5),

$$\eta_1 = \mathcal{A}\mathrm{e}^{\mathrm{i}(kx-\omega t)} + \text{c.c.}, \tag{III.7.1}$$

$$\psi_1 = \frac{\omega}{k}\mathcal{A}\mathrm{e}^{\mathrm{i}(kx-\omega t)+kz} + \text{c.c.} \tag{III.7.2}$$

We may then assume the following expressions for the air disturbance field

$$\psi^{(1)} = \hat{\psi}_k^{(1)}(z)\mathcal{A}\mathrm{e}^{\mathrm{i}(kx-\omega t)} + \text{c.c.}, \tag{III.7.3}$$

$$p^{(1)} = \hat{p}_k^{(1)}(z)\mathcal{A}\mathrm{e}^{\mathrm{i}(kx-\omega t)} + \text{c.c.}, \tag{III.7.4}$$

$$N^{(1)} = \hat{N}_k^{(1)}\mathcal{A}\mathrm{e}^{\mathrm{i}(kx-\omega t)} + \text{c.c.}, \tag{III.7.5}$$

$$T = \hat{T}_k\mathcal{A}\mathrm{e}^{\mathrm{i}(kx-\omega t)} + \text{c.c.} \tag{III.7.6}$$

The governing equation for $\hat{\psi}_k^{(1)}$ now becomes an Orr–Sommerfeld equation

$$\left[\omega - kU'^S - \mathrm{i}\sigma'^2\left(\frac{\partial^2}{\partial z^2} - k^2\right)\right]\left(\frac{\partial^2}{\partial z^2} - k^2\right)\hat{\psi}_k^{(1)} + k\frac{\partial^2 U'^S}{\partial z^2}\hat{\psi}_k^{(1)} = 0 \tag{III.7.7}$$

with boundary conditions

$$\hat{\psi}_k^{(1)} = \frac{\omega}{k} \qquad \text{and} \qquad \frac{\partial\hat{\psi}_k^{(1)}}{\partial z} = \omega - \frac{\partial U'^S}{\partial z} \qquad \text{at} \quad z = 0. \tag{III.7.8}$$

The pressure then becomes

$$\hat{p}_k^{(1)} = \frac{\partial U'^S}{\partial z}\hat{\psi}_k^{(1)} + \left(\frac{\omega}{k} - U'^S + \mathrm{i}k\sigma'^2\right)\frac{\partial\hat{\psi}_k^{(1)}}{\partial z} - \frac{\mathrm{i}\sigma'^2}{k}\frac{\partial^3\hat{\psi}_k^{(1)}}{\partial z^3}. \tag{III.7.9}$$

The evolution of the wave (III.7.1) is governed by the cubic evolution equation (III.5.44). In particular, recall that the linear growth rate for the amplitude on timescale $t_2$ is given by (III.5.49):

$$\beta = \mathrm{Re}\left\{-2k^2\sigma^2 + \frac{\mathrm{i}k}{2\omega}\hat{N}_k^{(1)} + \frac{k\sigma^2}{2\omega}\hat{T}_k\right\}, \tag{III.7.10}$$

were

$$\hat{N}_k^{(1)} = \frac{\rho'}{\rho}\left\{-\hat{p}_k^{(1)} + \frac{2}{3}\right\} \qquad \text{and} \qquad \hat{T}_k = \frac{\rho'\nu'}{\rho\nu}\frac{\partial^2\hat{\psi}_k^{(1)}}{\partial z^2}. \tag{III.7.11}$$

Numerical computations of growth-rates are shown later in this section.

## III.7.2 Second-order problem in air

The water-surface wave-disturbance for Wilton's ripples is given by the leading-order solution in section III.6, equations (III.6.5) and (III.6.6). In terms of the phase (III.6.4), $\theta = x + \delta x_1 - t$, the leading order flow-field in water is

$$\eta_1 = A\mathrm{e}^{\mathrm{i}\theta} + B\mathrm{e}^{2\mathrm{i}\theta} + \text{c.c.}, \tag{III.7.12}$$

$$\psi_1 = A\mathrm{e}^{\mathrm{i}\theta+z} + B\mathrm{e}^{2\mathrm{i}\theta+2z} + \text{c.c.} \tag{III.7.13}$$

The leading order $\mathcal{O}(1)$ response in the air is

$$\psi^{(1)} = \hat{\psi}_1^{(1)} A\mathrm{e}^{\mathrm{i}\theta} + \hat{\psi}_2^{(1)} B\mathrm{e}^{2\mathrm{i}\theta} + \text{c.c.}, \tag{III.7.14}$$

$$p^{(1)} = \hat{p}_1^{(1)} A\mathrm{e}^{\mathrm{i}\theta} + \hat{p}_2^{(1)} B\mathrm{e}^{2\mathrm{i}\theta} + \text{c.c.}, \tag{III.7.15}$$

$$N^{(1)} = \hat{N}_1^{(1)} A\mathrm{e}^{\mathrm{i}\theta} + \hat{N}_2^{(1)} B\mathrm{e}^{2\mathrm{i}\theta} + \text{c.c.}, \tag{III.7.16}$$

$$T = \hat{T}_1 A\mathrm{e}^{\mathrm{i}\theta} + \hat{T}_2 B\mathrm{e}^{2\mathrm{i}\theta} + \text{c.c.}, \tag{III.7.17}$$

where $\hat{\psi}_k^{(1)}$, $\hat{p}_k^{(1)}$, $\hat{N}_k^{(1)}$ and $\hat{T}_k$ can be obtained from the results of the previous subsection by setting $k$ equal to either 1 or 2, respectively.

At the second order $\mathcal{O}(\epsilon\mu^{-1})$ we need only account for the first and second harmonics

$$\psi^{(2)} = \hat{\psi}_1^{(2)} A^* B\mathrm{e}^{\mathrm{i}\theta} + \hat{\psi}_2^{(2)} A^2\mathrm{e}^{2\mathrm{i}\theta} + \text{c.c.}, \tag{III.7.18}$$

$$p^{(2)} = \hat{p}_1^{(2)} A^* B\mathrm{e}^{\mathrm{i}\theta} + \hat{p}_2^{(2)} A^2\mathrm{e}^{2\mathrm{i}\theta} + \text{c.c.}, \tag{III.7.19}$$

$$N^{(2)} = \hat{N}_1^{(2)} A^* B\mathrm{e}^{\mathrm{i}\theta} + \hat{N}_2^{(2)} A^2\mathrm{e}^{2\mathrm{i}\theta} + \text{c.c.} \tag{III.7.20}$$

The governing equations for $\hat{\psi}_k^{(2)}$ are the inhomogeneous Orr–Sommerfeld equations

$$\left[1 - U'^S - \mathrm{i}\sigma' {}^2 \left(\frac{\partial^2}{\partial z^2} - 1\right)\right] \left(\frac{\partial^2}{\partial z^2} - 1\right) \hat{\psi}_1^{(2)} + \frac{\partial^2 U'^S}{\partial z^2} \hat{\psi}_1^{(2)}$$
$$= -\mathrm{i}\hat{\psi}_1^{(1)*} \frac{\partial^3 \hat{\psi}_2^{(1)}}{\partial z^3} + 2\mathrm{i}\hat{\psi}_2^{(1)} \frac{\partial^3 \hat{\psi}_1^{(1)*}}{\partial z^3} \tag{III.7.21}$$

and

$$\left[2 - 2U'^S - \mathrm{i}\sigma' {}^2 \left(\frac{\partial^2}{\partial z^2} - 4\right)\right] \left(\frac{\partial^2}{\partial z^2} - 4\right) \hat{\psi}_2^{(2)} + 2\frac{\partial^2 U'^S}{\partial z^2} \hat{\psi}_2^{(2)} = \mathrm{i}\hat{\psi}_1^{(1)} \frac{\partial^3 \hat{\psi}_1^{(1)}}{\partial z^3} \tag{III.7.22}$$

with boundary conditions

$$\hat{\psi}_1^{(2)} = 0, \qquad \frac{\partial \hat{\psi}_1^{(2)}}{\partial z} = -\frac{\partial^2 \hat{\psi}_2^{(1)}}{\partial z^2} - \frac{\partial^2 \hat{\psi}_1^{(1)*}}{\partial z^2} \qquad \text{at} \quad z = 0 \tag{III.7.23}$$

and

$$\hat{\psi}_2^{(2)} = 0 \qquad \frac{\partial \hat{\psi}_2^{(2)}}{\partial z} = -\frac{\partial^2 \hat{\psi}_1^{(1)}}{\partial z^2} \qquad \text{at} \quad z = 0. \tag{III.7.24}$$

The first and second harmonics of the pressure then become

$$\hat{p}_1^{(2)} = \frac{\partial U'^S}{\partial z}\hat{\psi}_1^{(2)} + \left(1 - U'^S + \mathrm{i}\sigma'^2\right)\frac{\partial \hat{\psi}_1^{(2)}}{\partial z} - \mathrm{i}\sigma'^2\frac{\partial^3 \hat{\psi}_1^{(2)}}{\partial z^3} - \hat{\psi}_1^{(1)*}\frac{\partial^2 \hat{\psi}_2^{(1)}}{\partial z^2} + 2\hat{\psi}_2^{(1)}\frac{\partial^2 \hat{\psi}_1^{(1)*}}{\partial z^2}, \tag{III.7.25}$$

$$\hat{p}_2^{(2)} = \frac{\partial U'^S}{\partial z}\hat{\psi}_2^{(2)} + \left(1 - U'^S + 2\mathrm{i}\sigma'^2\right)\frac{\partial \hat{\psi}_2^{(2)}}{\partial z} - \frac{\mathrm{i}}{2}\sigma'^2\frac{\partial^3 \hat{\psi}_2^{(2)}}{\partial z^3} + \frac{1}{2}\hat{\psi}_1^{(1)}\frac{\partial^2 \hat{\psi}_1^{(1)}}{\partial z^2}. \tag{III.7.26}$$

The second-order quadratically nonlinear normal stresses are

$$\hat{N}_k^{(2)} = -\frac{\rho'}{\rho}\hat{p}_k^{(2)} \qquad \text{for} \quad k = 1, 2. \tag{III.7.27}$$

There is no significant quadratically nonlinear contribution to the tangential stress within our level of approximation.

Numerical computations of growth-rates are given later in this section.

## III.7.3 Numerical solution of the Orr–Sommerfeld equation

We use the relaxation method as described by Press *et al.* (1992), pp. 762–772. The Orr–Sommerfeld equation is first written as a system of eight real and coupled first-order equations by introducing the real variables $y_{k,n}^{(m)}$ as follows:

$$\hat{\psi}_k^{(m)} = y_{k,1}^{(m)} + \mathrm{i}y_{k,2}^{(m)}, \quad \frac{\partial \hat{\psi}_k^{(m)}}{\partial z} = y_{k,3}^{(m)} + \mathrm{i}y_{k,4}^{(m)},$$

$$\frac{\partial^2 \hat{\psi}_k^{(m)}}{\partial z^2} = y_{k,5}^{(m)} + \mathrm{i}y_{k,6}^{(m)}, \quad \frac{\partial^3 \hat{\psi}_k^{(m)}}{\partial z^3} = y_{k,7}^{(m)} + \mathrm{i}y_{k,8}^{(m)}.$$

The system then becomes

$$\frac{\partial}{\partial z}\begin{pmatrix} y_{k,1}^{(m)} \\ y_{k,2}^{(m)} \\ y_{k,3}^{(m)} \\ y_{k,4}^{(m)} \\ y_{k,5}^{(m)} \\ y_{k,6}^{(m)} \\ y_{k,7}^{(m)} \\ \\ y_{k,8}^{(m)} \end{pmatrix} = \begin{pmatrix} y_{k,3}^{(m)} \\ y_{k,4}^{(m)} \\ y_{k,5}^{(m)} \\ y_{k,6}^{(m)} \\ y_{k,7}^{(m)} \\ y_{k,8}^{(m)} \\ 2k^2 y_{k,5}^{(m)} - k^4 y_{k,1}^{(m)} \\ -\frac{1}{\sigma'^2}\left[(kU'^S-\omega)(y_{k,6}^{(m)} - k^2 y_{k,2}^{(m)}) - k\frac{\partial^2 U'^S}{\partial z^2} y_{k,2}^{(m)} + \operatorname{Im} F_k^{(m)}\right] \\ 2k^2 y_{k,6}^{(m)} - k^4 y_{k,2}^{(m)} \\ +\frac{1}{\sigma'^2}\left[(kU'^S-\omega)(y_{k,5}^{(m)} - k^2 y_{k,1}^{(m)}) - k\frac{\partial^2 U'^S}{\partial z^2} y_{k,1}^{(m)} + \operatorname{Re} F_k^{(m)}\right] \end{pmatrix}. \tag{III.7.28}$$

We let $F_k^{(m)}$ denote the inhomogeneity on the right-hand side of the Orr–Sommerfeld equation. Hence

$$F_k^{(1)} = 0, \qquad \text{for} \quad k = 1, 2, \tag{III.7.29}$$

and

$$F_1^{(2)} = -\mathrm{i}\hat{\psi}_1^{(1)*}\frac{\partial^3 \hat{\psi}_2^{(1)}}{\partial z^3} + 2\mathrm{i}\hat{\psi}_2^{(1)}\frac{\partial^3 \hat{\psi}_1^{(1)*}}{\partial z^3}, \qquad F_2^{(2)} = \mathrm{i}\hat{\psi}_1^{(1)}\frac{\partial^3 \hat{\psi}_1^{(1)}}{\partial z^3} \tag{III.7.30}$$

The boundary conditions at the surface $z = 0$ for the leading-order problem are

$$y_{k,1}^{(1)} = \frac{\omega}{k}, \qquad y_{k,2}^{(1)} = 0, \qquad y_{k,3}^{(1)} = \omega - \frac{\partial U'^S}{\partial z}, \qquad y_{k,4}^{(1)} = 0, \tag{III.7.31}$$

while for the second-order problem, they are

$$y_{k,1}^{(2)} = y_{k,2}^{(2)} = 0, \qquad y_{k,3}^{(2)} = \operatorname{Re} G_k, \qquad y_{k,4}^{(2)} = \operatorname{Im} G_k, \tag{III.7.32}$$

where

$$G_1 = -\frac{\partial^2 \hat{\psi}_2^{(1)}}{\partial z^2} - \frac{\partial^2 \hat{\psi}_1^{(1)*}}{\partial z^2}, \qquad G_2 = -\frac{\partial^2 \hat{\psi}_1^{(1)}}{\partial z^2}. \tag{III.7.33}$$

At great height, we impose the boundary conditions

$$\frac{\partial \hat{\psi}_k^{(m)}}{\partial z} + k\hat{\psi}_k^{(m)} = 0, \tag{III.7.34}$$

$$\frac{\partial^2 \hat{\psi}_k^{(m)}}{\partial z^2} + k\frac{\partial \hat{\psi}_k^{(m)}}{\partial z} = 0, \tag{III.7.35}$$

in order to ensure that the solution decays exponentially and the viscous boundary-layer component is absent high above the water surface. These conditions then become

$$y_{k,3}^{(m)} + k y_{k,1}^{(m)} = 0, \qquad y_{k,4}^{(m)} + k y_{k,2}^{(m)} = 0, \qquad y_{k,5}^{(m)} + k y_{k,3}^{(m)} = 0, \qquad y_{k,6}^{(m)} + k y_{k,4}^{(m)} = 0. \tag{III.7.36}$$

We use a fixed but non-uniform mesh that gives a finer resolution near the water surface than high up in the air. We define the mesh by

$$z_l = \begin{cases} 0 & \text{for} \quad l = 1 \\ z_{l-1} + h & \text{for} \quad 2 \le l \le L^* \\ z_{l-1} + (l - L^*)h & \text{for} \quad L^* < l \le L \end{cases} \tag{III.7.37}$$

for some choice of $h$, $L^*$ and $L$. We have taken $L = 1000$, $L^* = 800$ and $L^* h = 1.0$.

## III.7.4 Numerical values for linear and nonlinear growth-rates

In figure III-6 we compare our linear growth rates (III.7.10) to the asymptotic growth rates inferred from Gastel *et al.* (1985). We also show the influence of the tangential stress $\hat{T}_k$ on the total growth rate. It should be noted that we present the growth rate of the amplitude, while they presented the growth rate of the energy, which is twice the growth rate of the amplitude.

The tangential stress is seen to contribute to a larger growth rate for air friction velocities larger than 0.050 m/s, while it contributes to a larger damping rate for smaller air friction velocities. Our numerical results agree rather well with the asymptotic results of Gastel *et al.* (1985) for all but their weakest wind. This is because the assumptions for their asymptotic analysis are violated for weak winds, as discussed in section III.3.

In figure III-7 we show the real and imaginary parts of the linear coefficients $d_1 = d_{1,R} + \mathrm{i} d_{1,I}$ and $d_2 = d_{2,R} + \mathrm{i} d_{2,I}$, (III.6.55) and (III.6.56), for air friction velocities in the range 0–0.16 m/s. The linear growth rates for the first and second harmonics of Wilton's ripples are of course given by the real parts of the coefficients, $d_{1,R}$ and $d_{2,R}$.

For the long-time evolution of Wilton's ripples, we are interested in situations where damping and growth balance approximately over a long time. If nonlinear growth can be neglected, we can anticipate from figure III-7 that the appropriate range of air friction velocities is roughly 0.09–0.14 m/s.

In figure III-8 we show the real and imaginary parts of the nonlinear normal-stress coefficients $\hat{N}_1^{(2)} = \hat{N}_{1,R}^{(2)} + \mathrm{i}\hat{N}_{1,I}^{(2)}$ and $\hat{N}_2^{(2)} = \hat{N}_{2,R}^{(2)} + \mathrm{i}\hat{N}_{2,I}^{(2)}$, equation (III.7.27), for air friction velocities in the range 0–0.16 m/s.

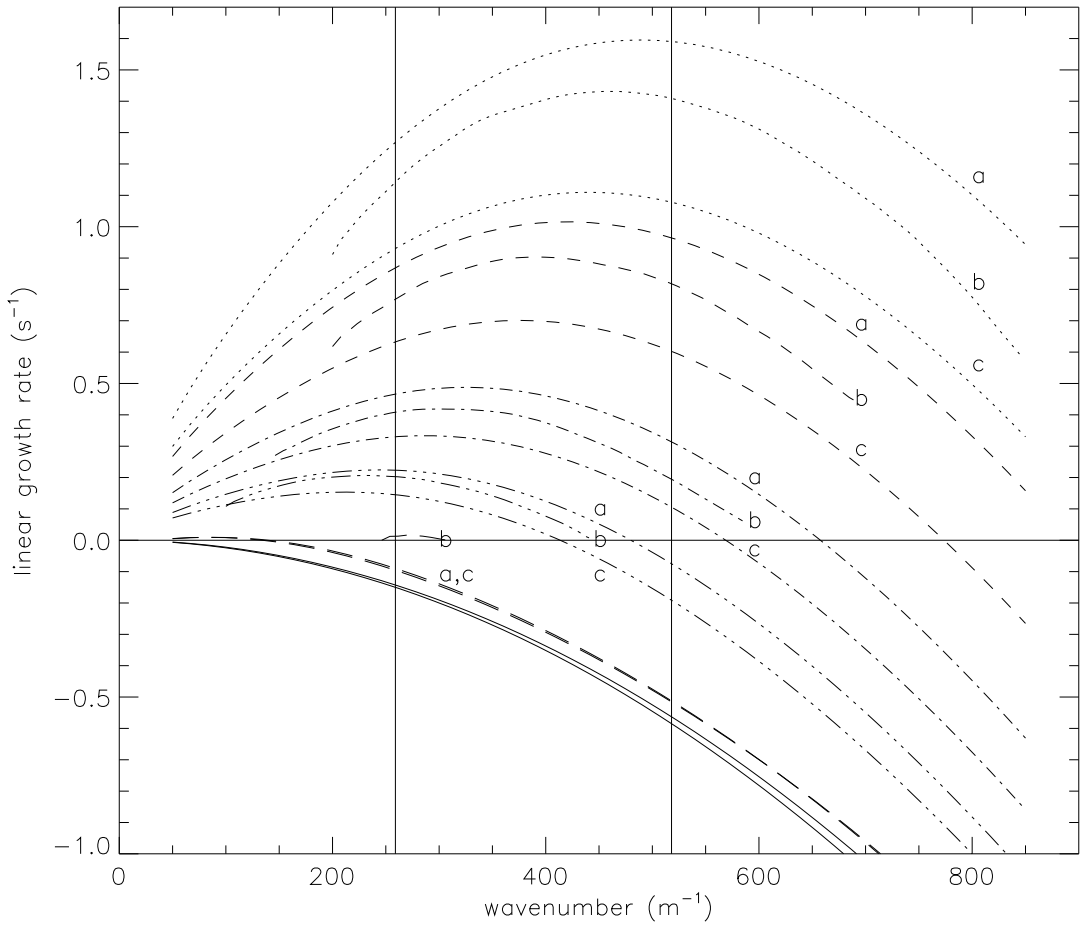


Figure III-6: Our linear growth rates with tangential stress (a) and without tangential stress (c), asymptotic result of Gastel, Janssen & Komen (1985) (b). Air friction velocity $u'_*$: 0.248 m/s ($\cdots$), 0.214 m/s (- - -), 0.170 m/s (- $\cdot$ - $\cdot$), 0.136 m/s (- $\cdots$), 0.050 m/s (— — —), and no wind (solid line). The tangential stress contributes to larger growth for $u'_* > 0.050$ m/s, and stronger damping for $u'_* < 0.050$ m/s.

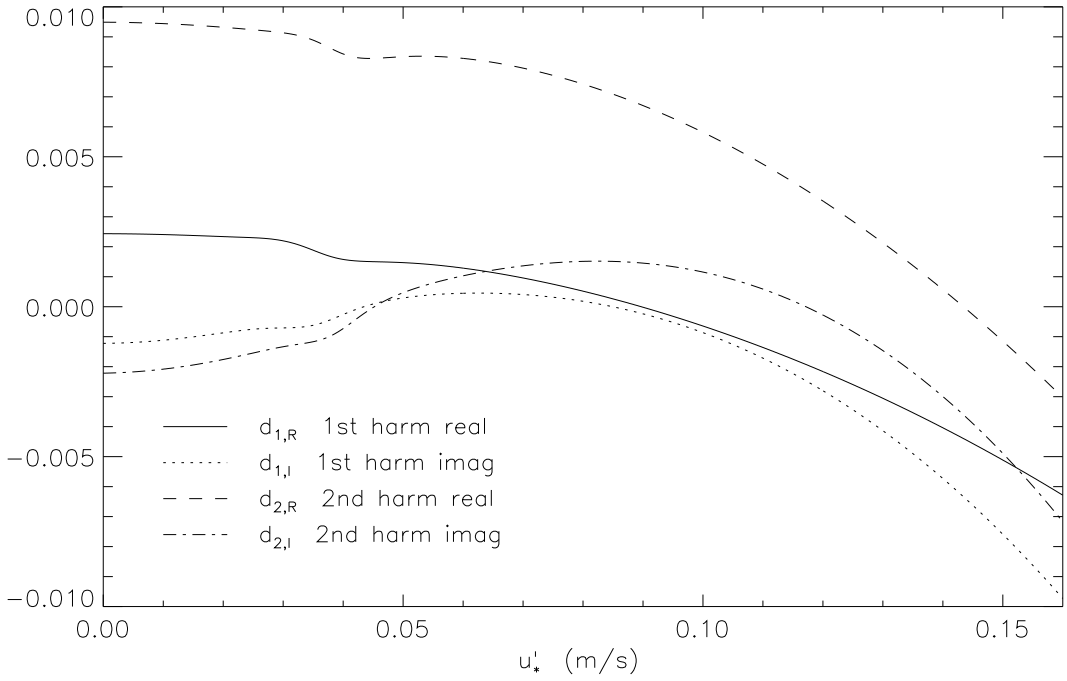


Figure III-7: Linear coefficients $d_k$, equations (III.6.55) and (III.6.56).

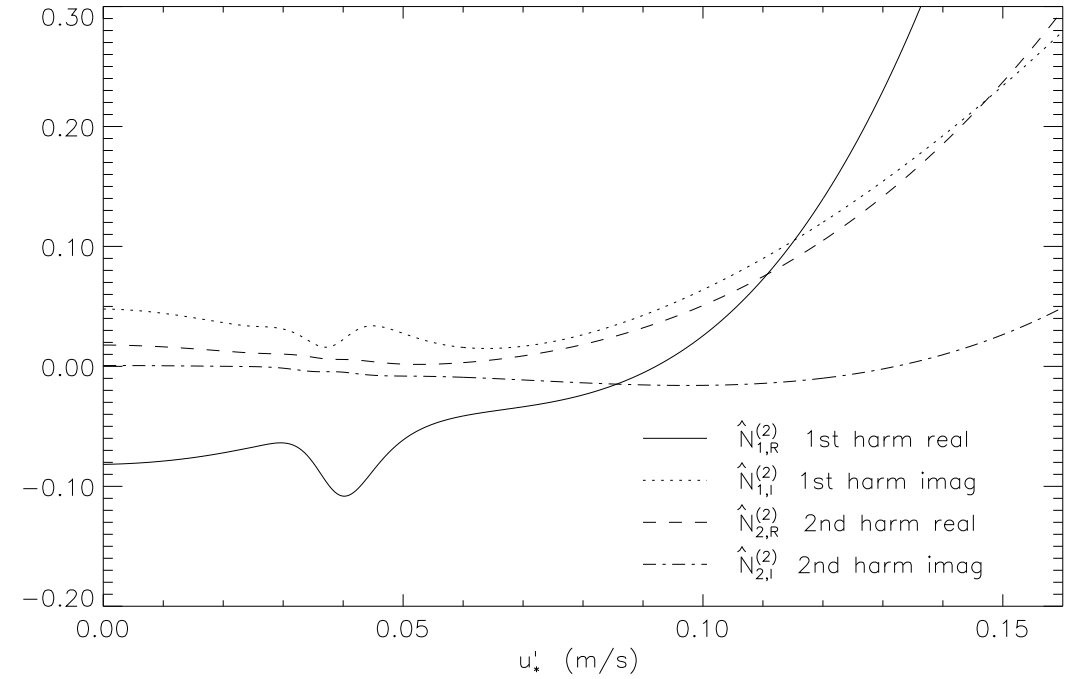


Figure III-8: Nonlinear coefficients $\hat{N}_k^{(2)}$, equation (III.7.27).

# III.8 Dynamical system for time-evolution

Recall that the original dynamical system for the complex coefficients $A$ and $B$ is four-dimensional when it is written out in real form. Here $A$ is the amplitude of the first harmonic and $B$ is the amplitude of the second harmonic of Wilton's ripples. This system can be reduced to three dimensions due to the fact that the phase angles appear in only one dynamically significant combination.

Let us rewrite the complex amplitudes into polar form

$$A = \mathcal{U}\mathrm{e}^{\mathrm{i}\theta_1}, \qquad B = \mathcal{V}\mathrm{e}^{\mathrm{i}\theta_2}, \qquad \phi = 2\theta_1 - \theta_2. \tag{III.8.1}$$

Hence the absolute amplitudes of the first and second harmonics, $\mathcal{U}$ and $\mathcal{V}$, are non-negative, and $\phi$ is the total phase angle. We also split the linear complex forcing coefficients $d_k$ and the nonlinear normal stress $\hat{N}_k^{(2)}$ into real and imaginary parts

$$d_k = d_{k,R} + \mathrm{i}d_{k,I} \qquad \hat{N}_k^{(2)} = \hat{N}_{k,R}^{(2)} + \mathrm{i}\hat{N}_{k,I}^{(2)}. \tag{III.8.2}$$

The reduced system in polar form is

$$\frac{\mathrm{d}\mathcal{U}}{\mathrm{d}t_1} = -\epsilon d_{1,R}\mathcal{U} - \frac{1}{2}\epsilon\hat{N}_{1,I}^{(2)}\mathcal{U}\mathcal{V}\cos\phi + \alpha_1\mathcal{U}\mathcal{V}\sin\phi, \tag{III.8.3}$$

$$\frac{\mathrm{d}\mathcal{V}}{\mathrm{d}t_1} = -\epsilon d_{2,R}\mathcal{V} - \frac{1}{2}\epsilon\hat{N}_{2,I}^{(2)}\mathcal{U}^2\cos\phi + \alpha_2\mathcal{U}^2\sin\phi, \tag{III.8.4}$$

$$\begin{aligned}\frac{\mathrm{d}\phi}{\mathrm{d}t_1} &= \alpha_3 + \left(2\alpha_1\mathcal{V} + \alpha_2\frac{\mathcal{U}^2}{\mathcal{V}}\right)\cos\phi + \epsilon\left(\hat{N}_{1,I}^{(2)}\mathcal{V} + \frac{1}{2}\hat{N}_{2,I}^{(2)}\frac{\mathcal{U}^2}{\mathcal{V}}\right)\sin\phi \\ &\quad - \frac{49}{4}\epsilon\mathcal{U}^2 + 17\epsilon\mathcal{V}^2.\end{aligned} \tag{III.8.5}$$

The coefficients $\alpha_n$ are given by

$$\alpha_1 = \alpha_{1,0} + \epsilon\alpha_{1,1} = -1 + \epsilon\left(-\frac{13}{6}\delta - 10c + \frac{1}{2}\hat{N}_{1,R}^{(2)}\right), \tag{III.8.6}$$

$$\alpha_2 = \alpha_{2,0} + \epsilon\alpha_{2,1} = \frac{1}{2} + \epsilon\left(\frac{5}{6}\delta + \frac{9}{2}c - \frac{1}{2}\hat{N}_{2,R}^{(2)}\right), \tag{III.8.7}$$

$$\begin{aligned}\alpha_3 &= \alpha_{3,0} + \epsilon\alpha_{3,1} \\ &= -2a_{10} + a_{20} + \frac{2}{3}\delta \\ &\quad + \epsilon\left(-2a_{11} + a_{21} + 2(-b_1 + b_2)\delta + \frac{1}{3}\delta^2 - 2d_{1,I} + d_{2,I}\right).\end{aligned} \tag{III.8.8}$$

This representation is well defined for $\mathcal{U} > 0$, $\mathcal{V} > 0$ and is $2\pi$-periodic in $\phi$. The representation is singular for $\mathcal{U} = 0$ or $\mathcal{V} = 0$.

Following Vyshkind & Rabinovich (1976), we next introduce the transformed variables

$$X = \mathcal{V}\cos\phi, \qquad Y = \mathcal{V}\sin\phi, \qquad Z = \mathcal{U}^2. \tag{III.8.9}$$

Hence $Z$ is non-negative and measures the square of the amplitude of the first harmonic. The radial distance from the $Z$-axis, $\sqrt{X^2+Y^2}$, is a measure of the second-harmonic amplitude. The dynamics is confined to the upper half of the $XYZ$-space. The angular position in the $XY$-plane relative to the $Z$-axis gives the total phase angle $\phi$.

The dynamical system now becomes

$$\begin{aligned}
\frac{\mathrm{d}X}{\mathrm{d}t_1} &= -\epsilon d_{2,R}X - \alpha_3 Y - \frac{1}{2}\epsilon\hat{N}^{(2)}_{2,I}Z - 2\alpha_1 XY - \epsilon\hat{N}^{(2)}_{1,I}Y^2 + \frac{49}{4}\epsilon YZ \\
&\quad - 17\epsilon(X^2+Y^2)Y, \qquad \text{(III.8.10)} \\
\frac{\mathrm{d}Y}{\mathrm{d}t_1} &= \alpha_3 X - \epsilon d_{2,R}Y + \alpha_2 Z + 2\alpha_1 X^2 + \epsilon\hat{N}^{(2)}_{1,I}XY - \frac{49}{4}\epsilon XZ \\
&\quad + 17\epsilon X(X^2+Y^2), \qquad \text{(III.8.11)} \\
\frac{\mathrm{d}Z}{\mathrm{d}t_1} &= -2\epsilon d_{1,R}Z - \epsilon\hat{N}^{(2)}_{1,I}XZ + 2\alpha_1 YZ. \qquad \text{(III.8.12)}
\end{aligned}$$

This representation is well defined for $Z$ non-negative. For $Z=0$ the representation is still mathematically well defined, but the physical interpretation is that of a pure second-harmonic wave, and hence the notion of a total phase angle $\phi$ becomes ill-defined.

The energy (III.6.58) and horizontal momentum (III.6.60) are now expressed by

$$E = 4(X^2+Y^2)+2Z+\epsilon XZ+\epsilon\left(\frac{16}{3}\delta+2a_{2,0}\right)(X^2+Y^2)+\epsilon\left(\frac{4}{3}\delta+2a_{1,0}\right)Z, \quad \text{(III.8.13)}$$

and

$$\begin{aligned}
M_x &= 4(X^2+Y^2)+2Z-\epsilon XZ+\epsilon\left(\frac{14}{3}\delta-2a_{2,0}+4U^S(0)-\frac{\partial U^S}{\partial z}(0)\right)(X^2+Y^2) \\
&\quad +\epsilon\left(\frac{5}{3}\delta-2a_{1,0}+2U^S(0)-\frac{\partial U^S}{\partial z}(0)\right)Z. \qquad \text{(III.8.14)}
\end{aligned}$$

The time evolution of the energy and momentum is governed by

$$\frac{\mathrm{d}E}{\mathrm{d}t_1} = -8\epsilon d_{2,R}(X^2+Y^2)-4\epsilon d_{1,R}Z-\epsilon\left(2\hat{N}^{(2)}_{1,I}+4\hat{N}^{(2)}_{2,I}\right)XZ+\epsilon\left(2\hat{N}^{(2)}_{1,R}-4\hat{N}^{(2)}_{2,R}\right)YZ, \quad \text{(III.8.15)}$$

and

$$\begin{aligned}
\frac{\mathrm{d}M_x}{\mathrm{d}t_1} &= -8\epsilon d_{2,R}(X^2+Y^2)-4\epsilon d_{1,R}Z-\epsilon\left(2\hat{N}^{(2)}_{1,I}+4\hat{N}^{(2)}_{2,I}\right)XZ \\
&\quad +\epsilon\left(2\hat{N}^{(2)}_{1,R}-4\hat{N}^{(2)}_{2,R}-8c+\frac{\partial U^S}{\partial z}(0)\right)YZ. \qquad \text{(III.8.16)}
\end{aligned}$$

These time derivatives can be obtained either by differentiation of (III.8.13) and

(III.8.14) and using the dynamical system for $X$, $Y$ and $Z$, (III.8.10)–(III.8.12), or they can be obtained by transforming the previous results (III.6.59) and (III.6.61) into the reduced $XYZ$-notation. The same result is of course obtained either way.

The divergence of the flow-field of (III.8.10)–(III.8.12) in phase-space takes a particularly simple form,

$$\frac{\partial \dot{X}}{\partial X} + \frac{\partial \dot{Y}}{\partial Y} + \frac{\partial \dot{Z}}{\partial Z} = -2\epsilon(d_{1,R} + d_{2,R}). \tag{III.8.17}$$

Hence we have global conservation of volumes in phase-space when $d_{1,R} + d_{2,R} = 0$. Note that only the linear non-conservative forcing coefficients are present in the expression for the divergence of the flow-field in phase-space. The physical interpretation of volumes in phase space is not readily obvious since $X$ and $Y$ are both proportional to the amplitude of the second-harmonic wave, while $Z$ is proportional to the square of the amplitude of the first-harmonic wave.

## III.8.1 Second-order behavior

It is instructive to first consider the second-order behavior in the $XYZ$-notation. To this end, we set $\epsilon = 0$ in equations (III.8.10)–(III.8.12). The dynamical system then becomes

$$\dot{X} = -\alpha_{3,0} Y + 2XY, \tag{III.8.18}$$

$$\dot{Y} = \alpha_{3,0} X + \frac{1}{2} Z - 2X^2, \tag{III.8.19}$$

$$\dot{Z} = -2YZ. \tag{III.8.20}$$

The second-order energy or momentum is conserved, and is given by

$$E_0 = 4(X^2 + Y^2) + 2Z = \text{constant}, \tag{III.8.21}$$

The constancy of energy confines the dynamical behavior to the portion of an upside-down elliptic paraboloid that is above the $XY$-plane. For a given energy $E_0$, we must require that

$$X^2 + Y^2 \leq \frac{1}{4} E_0 \tag{III.8.22}$$

in order to be within the domain of the elliptic paraboloid for non-negative $Z$. Upon eliminating $Z$, we get the Hamiltonian system

$$\dot{X} = -\alpha_{3,0} Y + 2XY = \frac{\partial H}{\partial Y}, \tag{III.8.23}$$

$$\dot{Y} = \alpha_{3,0} X - 3X^2 - Y^2 + \frac{1}{4} E_0 = -\frac{\partial H}{\partial X}, \tag{III.8.24}$$

with

$$H(X,Y) = -\frac{1}{2}\alpha_{3,0}(X^2+Y^2) + X(X^2+Y^2-\frac{1}{4}E_0). \qquad \text{(III.8.25)}$$

The trajectories on the elliptic paraboloid can hence be obtained by computing the level-curves of $H$.

We now look for fixed points of the second-order system. For $Z=0$ initially, then $Z=0$ for all time. This implies that a pure second-harmonic wave is a steady-state solution. For $Z>0$ there are at most two fixed points $(X_c, Y_c, Z_c)$ defined by

$$3X_c^2 - \alpha_{3,0}X_c - \frac{1}{4}E_0 = 0, \qquad Y_c = 0, \qquad Z_c = 4X_c^2 - 2\alpha_{3,0}X_c. \quad (III.8.26a,b,c)$$

At the fixed points, the linearized system for $X$ and $Y$ is

$$\frac{\mathrm{d}}{\mathrm{d}t_1}\begin{pmatrix} X-X_c \\ Y-Y_c \end{pmatrix} = \begin{pmatrix} 0 & -\alpha_{3,0}+2X_c \\ \alpha_{3,0}-6X_c & 0 \end{pmatrix}\begin{pmatrix} X-X_c \\ Y-Y_c \end{pmatrix}. \qquad \text{(III.8.27)}$$

This system has eigenvalues

$$\lambda = \pm\mathrm{i}\sqrt{(\alpha_{3,0}-2X_c)(\alpha_{3,0}-6X_c)} = \pm\mathrm{i}\sqrt{\alpha_{3,0}^2 - 4\alpha_{3,0}X_c + E_0}, \qquad \text{(III.8.28)}$$

where we have made use of (III.8.26a). To see that the radicand is non-negative, we may calculate its minimum value with respect to $\alpha_{3,0}$ while keeping $X_c$ constant as a parameter. We then have $\alpha_{3,0}^2 - 4\alpha_{3,0}X_c + E_0 \geq E_0 - 4X_c^2$ which is non-negative by the constraint (III.8.22). We have therefore established that the fixed points are centers on the surface of the elliptic paraboloid.

The second-order conservative system has in fact a continuum of centers along the parts of the parabola (III.8.26c) that is above the $XY$-plane. From (III.8.26c) and (III.8.22) we see that the part of the parabola that emerges from the $XY$-plane at $X_c = 0$, gives rise to fixed points at all energy levels $E_0$. The part of the parabola that emerges from the $XY$-plane at $X_c = \frac{1}{2}\alpha_{3,0}$ gives rise to fixed points at energies $E_0 \geq \alpha_{3,0}^2$. Hence there are two centers when $E_0 > \alpha_{3,0}^2$ and one center when $E_0 < \alpha_{3,0}^2$. For $E_0 = \alpha_{3,0}^2$ the steady state solution $Z=0$ (the pure second-harmonic wave) bifurcates into a new center with $Z>0$, which represents a steady progressive combination wave of the first and the second harmonics. This bifurcation was first discovered by Chen & Saffman (1979), and has recently been discussed in a more general form for arbitrary three-dimensional resonating triads of gravity-capillary waves by Trulsen & Mei (1995)[6].

In figure III-9 we show a bifurcation diagram indicating the regions of one and two centers in the parameter plane $(\alpha_{3,0}, E_0)$. We also show some sample phase portraits projected onto the $XY$-plane for energy $E_0 = 0.01$. The phase portraits are confined to the region $X^2+Y^2 \leq \frac{1}{4}E_0$.

In figure III-10 we show three-dimensional trajectories of the second-order system by solid curves for one specific energy level $E_0 = 0.01$ and for $u_*' = 0.1$ m/s and $\delta = 0$.

[6]See section II.7.

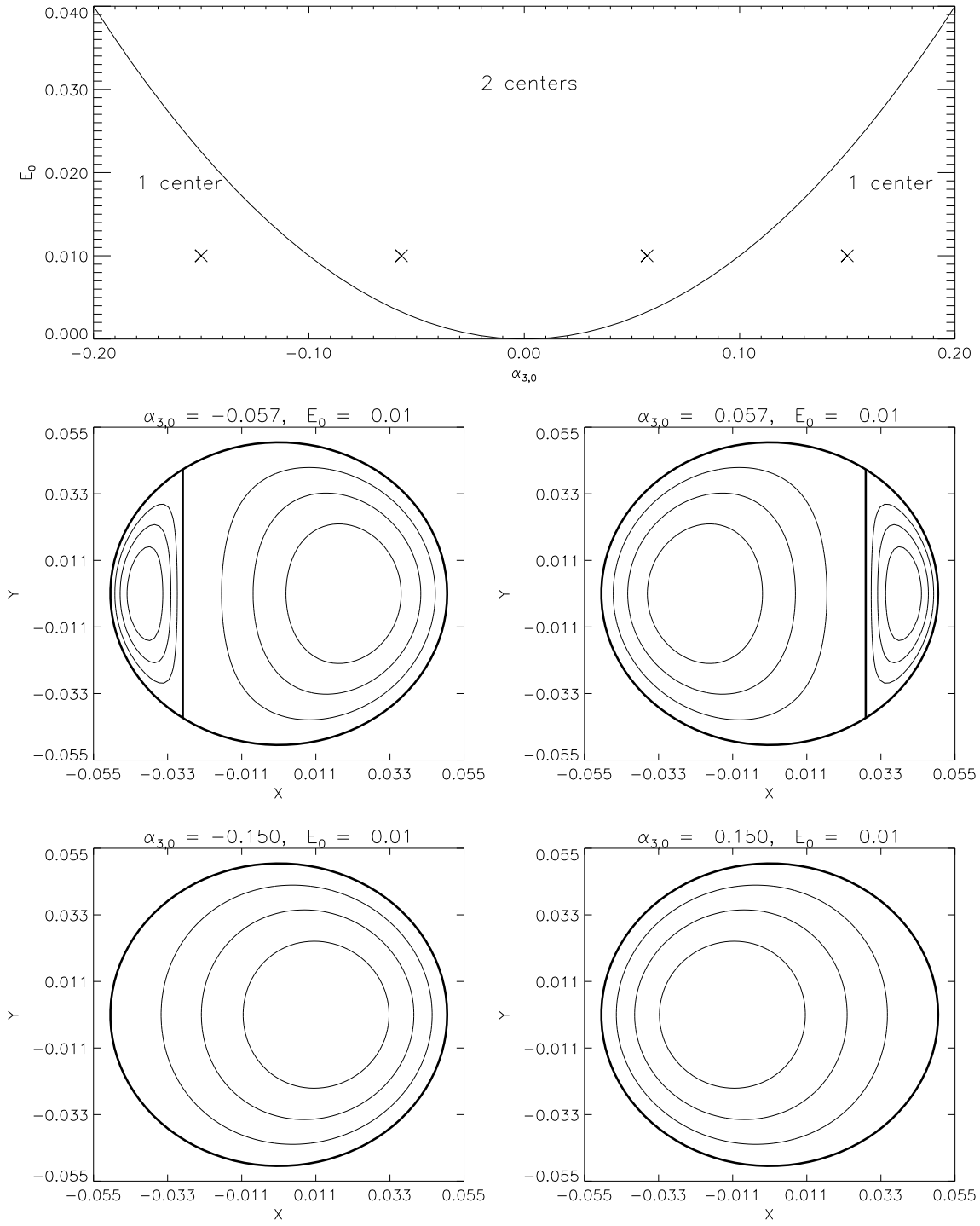


Figure III-9: Second-order behavior. Bifurcation diagram showing regions of one and two centers in the parameter plane $(\alpha_{3,0}, E_0)$. Sample phase portraits projected onto the $XY$-plane for parameter values indicated by $\times$.

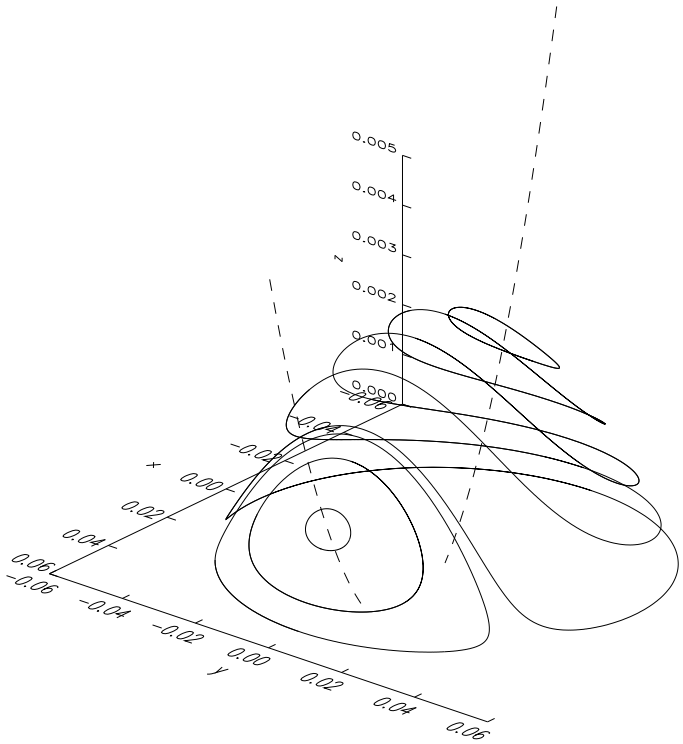


Figure III-10: Trajectories of second-order system for $u'_* = 0.1$ m/s, $\delta = 0$ ($\alpha_{3,0} = 0.0572$) and $E_0 = 0.01$ (—). The parabola of fixed points indicates the locations of the centers (- - -).

This implies that $\alpha_{3,0} = 0.0572$ according to (III.8.8), and corresponds to one of the phase portraits plotted in figure III-9. The parabola of fixed points is shown with a dashed curve for $Z > 0$. The orbits are seen to be located on an elliptic paraboloid.

In figure III-11 we show the surface elevation $\eta = \eta_1$ (equation (III.6.5)) for one wave period ($0 < \theta < 2\pi$) corresponding to the steady-state solutions at the two centers. We have again set $E_0 = 0.01$, $u'_* = 0.1$ m/s, $\delta = 0$ and hence $\alpha_{3,0} = 0.0572$. We have arbitrarily set the phase angle $\theta_1 = 0$; the exact choice is immaterial since it only affects a trivial phase shift and not the shape of the wave. Following the terminology that is commonly used, we may call one of the profiles gravity-like, for which most of the phase is spent below the equilibrium water level (due to its similarity to a Stokes wave). We call the other profile capillary-like, for which most of the phase is spent above the equilibrium level (see e.g. the exact solution for capillary waves by Crapper 1957).

## III.8.2 Third-order behavior

To investigate the full dynamical system (III.8.10)–(III.8.12), proper care must be taken of the small ordering parameter $\epsilon$. We shall formally set $\epsilon = 1$ wherever it occurs in the equations, while letting the dynamical variables themselves have magnitudes indicative of their scales. Recall that the complex amplitudes $A$ and $B$ where assumed to be of $\mathcal{O}(\epsilon)$ magnitude. This implies that $X, Y = \mathcal{O}(\epsilon)$ while $Z = \mathcal{O}(\epsilon^2)$. It also follows that the energy $E = \mathcal{O}(\epsilon^2)$. In the following we therefore limit our numerical

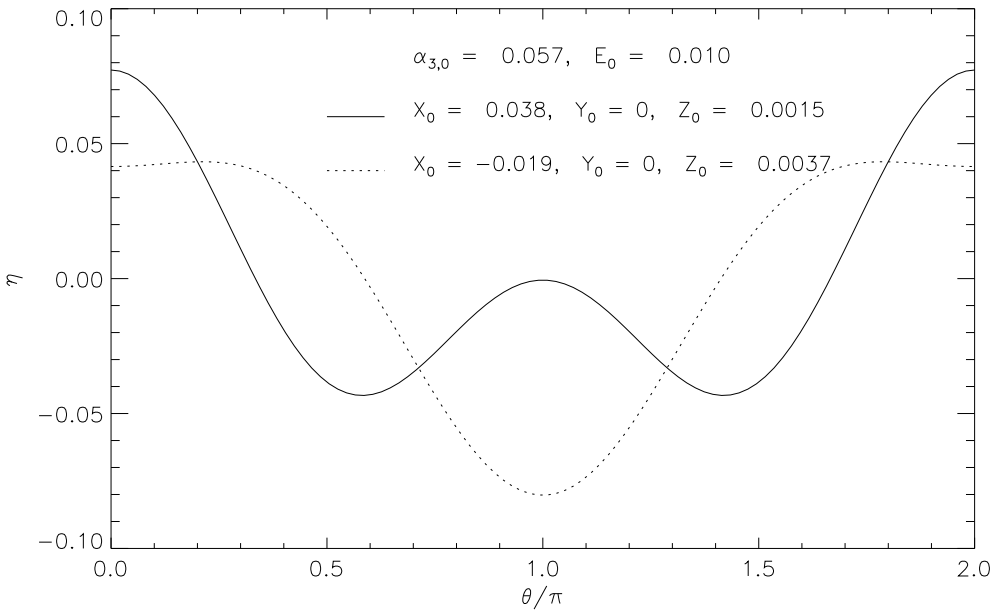


Figure III-11: Wave profiles for the steady-state solutions at the centers for $u'_* = 0.1$ m/s, $\delta = 0$ ($\alpha_{3,0} = 0.0572$) and $E_0 = 0.01$; gravity-like (—), capillary-like ($\cdots$).

discussion to $X, Y = \mathcal{O}(0.1)$ and $Z, E = \mathcal{O}(0.01)$.

### III.8.3 Fixed points

We now discuss the fixed points of the full dynamical system (III.8.10)–(III.8.12). First we note that if $Z = 0$ initially, then $Z = 0$ for all time. This implies that a pure second-harmonic wave is a steady-state solution. In fact, the only fixed point in the $XY$-plane is the origin

$$X = Y = Z = 0. \tag{III.8.29}$$

This can be seen directly from the derivative of the energy (III.8.15), which requires that $X^2 + Y^2 = 0$, and hence $X = Y = 0$ is then the only real solution.

The stability of the fixed point at the origin can easily be analyzed by considering the linearized system

$$\frac{\mathrm{d}}{\mathrm{d}t_1}\begin{pmatrix} X \\ Y \\ Z \end{pmatrix} = \begin{pmatrix} -\epsilon d_{2,R} & -\alpha_3 & -\frac{1}{2}\epsilon \hat{N}^{(2)}_{2,I} \\ \alpha_3 & -\epsilon d_{2,R} & \alpha_2 \\ 0 & 0 & -2\epsilon d_{1,R} \end{pmatrix}\begin{pmatrix} X \\ Y \\ Z \end{pmatrix}. \tag{III.8.30}$$

It follows that the $XY$-plane is an eigenspace with two complex conjugate eigenvalues $\lambda = -\epsilon d_{2,R} \pm \mathrm{i}\alpha_3$. The motion in the $XY$-plane is hence spiraling either into or away from the origin. There is also an eigenvector with eigenvalue $\lambda = -2\epsilon d_{1,R}$ along the

line defined by

$$Y = \epsilon \left( \frac{2d_{1,R} - d_{2,R}}{\alpha_3} + \frac{\hat{N}_{2,I}^{(2)}}{2\alpha_2} \right) X + \mathcal{O}(\epsilon^2), \qquad Z = -\frac{\alpha_3}{\alpha_2} X + \mathcal{O}(\epsilon^2). \tag{III.8.31}$$

Hence the stability of the fixed point at the origin is independent of the detuning parameter $\delta$, but depends on the two linear wind-forcing parameters $d_{1,R}$ and $d_{2,R}$. From figure III-7 we see that $d_{1,R}$ is zero for $u'_* = u'_{*TC} \approx 0.090$ m/s, while $d_{2,R}$ is zero for $u'_* = u'_{*LU} \approx 0.143$ m/s. Hence for $u'_* < u'_{*TC}$ the origin is a stable fixed point with inward spiraling motion in the $XY$-plane. It will later be seen that there is a transcritical bifurcation at $u'_* = u'_{*TC}$, by which a stable fixed point emerges for $Z > 0$ while the origin becomes unstable. For $u'_{*TC} < u'_* < u'_{*LU}$ the origin is unstable along the eigendirection out from the $XY$-plane, but stable with inward spiraling motion in the $XY$-plane. For $u'_* > u'_{*LU}$ both the first and the second-harmonic waves are linearly unstable. The origin is then unstable in all directions, with outward spiraling motion in the $XY$-plane.

Next we consider $Z > 0$. Then $Z$ can be eliminated between the first two equations, (III.8.10) and (III.8.11), while $Y$ can be eliminated by the third equation (III.8.12). This yields a cubic equation for $X$,

$$\epsilon c_3 X^3 + c_2 X^2 + c_1 X + c_0 = 0, \tag{III.8.32}$$

where

$$\begin{aligned}
c_0 &= -16 d_{1,R} \alpha_1^2 \alpha_2 \alpha_3 + \mathcal{O}(\epsilon^2), && \text{(III.8.33)} \\
c_1 &= 8\alpha_1^2 \alpha_3 \left( \alpha_1 \hat{N}_{2,I}^{(2)} - \alpha_2 \hat{N}_{1,I}^{(2)} \right) - 16 \alpha_1^3 \alpha_2 \left( d_{2,R} + 2 d_{1,R} \right) + \mathcal{O}(\epsilon^2), && \text{(III.8.34)} \\
c_2 &= 16\alpha_1^3 \left( \alpha_1 \hat{N}_{2,I}^{(2)} - \alpha_2 \hat{N}_{1,I}^{(2)} \right) + 196 \epsilon \alpha_1^3 d_{2,R} + \mathcal{O}(\epsilon^2), && \text{(III.8.35)} \\
c_3 &= 34 \left( \alpha_1 \hat{N}_{2,I}^{(2)} - \alpha_2 \hat{N}_{1,I}^{(2)} \right) \left( 4\alpha_1^2 + \mathcal{O}(\epsilon^2) \right). && \text{(III.8.36)}
\end{aligned}$$

Then $Y$ is found from

$$Y = \epsilon \frac{\hat{N}_{1,I}^{(2)} X + 2 d_{1,R}}{2\alpha_1}, \tag{III.8.37}$$

and $Z$ is found from

$$Z = 4 \frac{\alpha_3 X - \epsilon d_{2,R} Y + 2\alpha_1 X^2 + \epsilon \hat{N}_{1,I}^{(2)} XY + 17 \epsilon X (X^2 + Y^2)}{49 \epsilon X - 4\alpha_2}. \tag{III.8.38}$$

The cubic equation for $X$ can give three real solutions or one real and two complex conjugate solutions. For a solution to be feasible, it must be real and the resulting value of $Z$ must be non-negative. The magnitude of the solution $(X, Y, Z)$ must also be within the theoretical bounds of our theory. Since the highest-degree term in (III.8.32) is multiplied by the small parameter $\epsilon$, there may be mathematical solutions that are too large to be of any physical significance, and which violate the scaling assumptions.

Recall the discussion in the previous subsection on the scaling magnitudes of $X$, $Y$, $Z$ and $E$.

It is in principle possible to solve (III.8.32) by perturbation. Two of the solutions of (III.8.32) can be found by a regular perturbation expansion

$$X = X_0 + \epsilon X_1 + \mathcal{O}(\epsilon^2). \tag{III.8.39}$$

The leading-order problem is

$$c_2 X_0^2 + c_1 X_0 + c_0 = 0, \tag{III.8.40}$$

while the contributions from (III.8.37) and (III.8.38) are

$$Y = \mathcal{O}(\epsilon), \qquad Z = 4X_0^2 - 2\alpha_{3,0} X_0 + \mathcal{O}(\epsilon). \tag{III.8.41}$$

It is therefore evident that these fixed points are located approximately on the parabola of centers found for the second-order conservative system, (III.8.26b,c).

The third solution of (III.8.32) can be found by the singular perturbation expansion

$$X = \epsilon^{-1} X_{-1} + X_0 + \mathcal{O}(\epsilon), \tag{III.8.42}$$

which has the leading-order solution

$$X_{-1} = -\frac{c_2}{c_3}. \tag{III.8.43}$$

However, this solution has a magnitude much bigger than we can allow in our theory, and must therefore be rejected. In conclusion, the third-order non-conservative system has between one and four fixed points. The feasible solutions are located near the parabola of centers of the second-order conservative system.

In figures III-12–III-16 we show numerically computed bifurcation diagrams where the energy levels of the fixed points are shown as a function of the air friction velocity $u'_*$ when the detuning parameter $\delta$ takes the values $-0.2$, $-0.1$, 0, 0.1 and 0.2. Because the mathematical solutions for the fixed points give widely varying magnitudes of the energy, we show the bifurcation diagrams on both logarithmic and linear scales. However one must keep in mind that we are primarily interested in energies of order $E = \mathcal{O}(\epsilon^2)$. We indicate the stability of the fixed points by using different linestyles depending on the number of stable eigenvalues, as explained in the bifurcation diagrams.

For all values of the detuning $\delta$, there is a stable non-trivial fixed point that emerges at a transcritical bifurcation point $u'_* = u'_{*TC}$. This stable fixed point vanishes at a regular turning point at $u'_* = u'_{*TP}$. The value of $u'_{*TP}$ depends on the detuning parameter $\delta$.

Our analysis suggests that there are three ranges of air friction velocities giving rise to qualitatively different behavior. (1): For weak winds $u'_* < u'_{*TC}$ the trivial fixed point at the origin is stable, and is the only fixed point. Physically, this means that viscous damping dominates over forcing by wind, and any wave disturbance will be

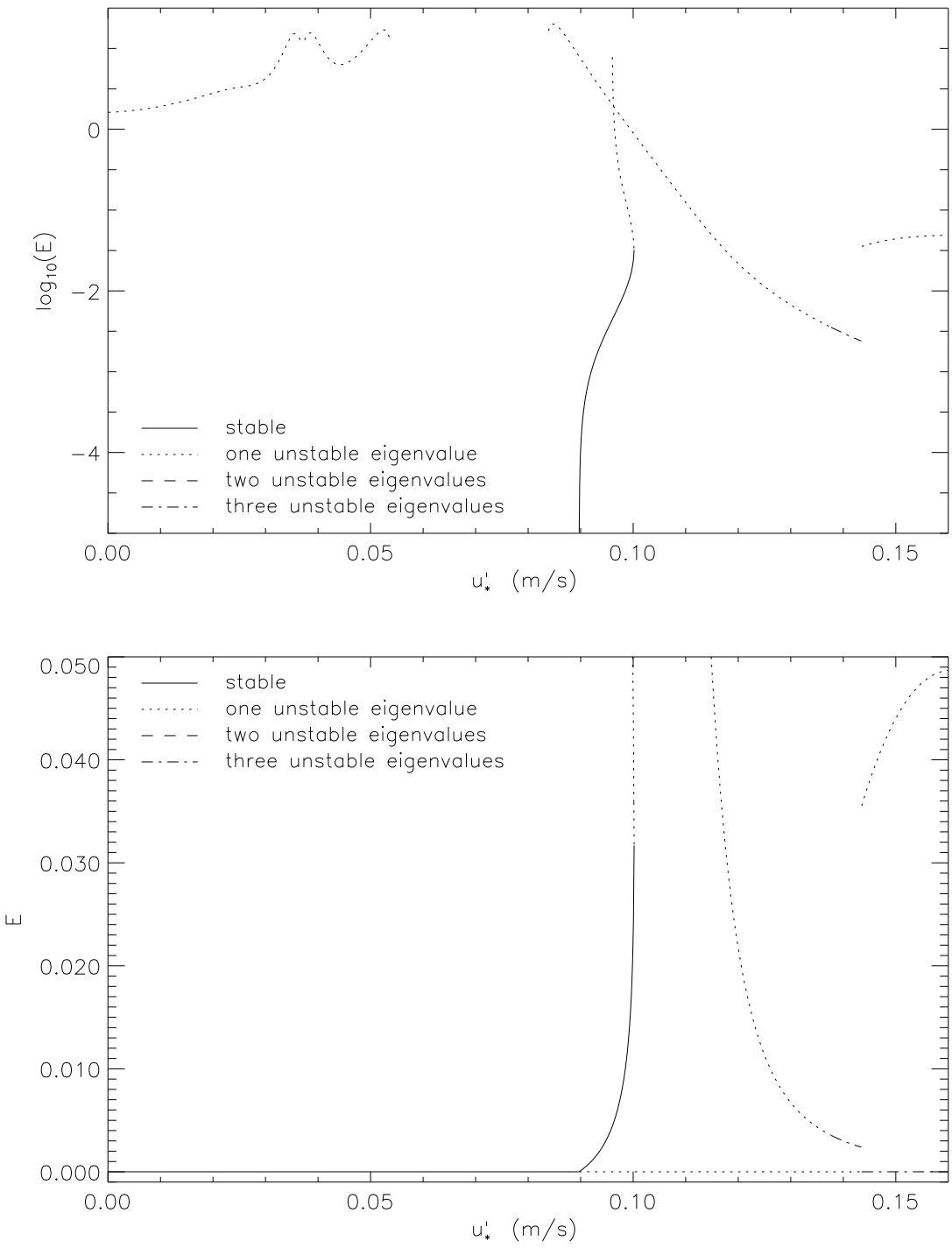


Figure III-12: Bifurcation diagram for $\delta = -0.2$.

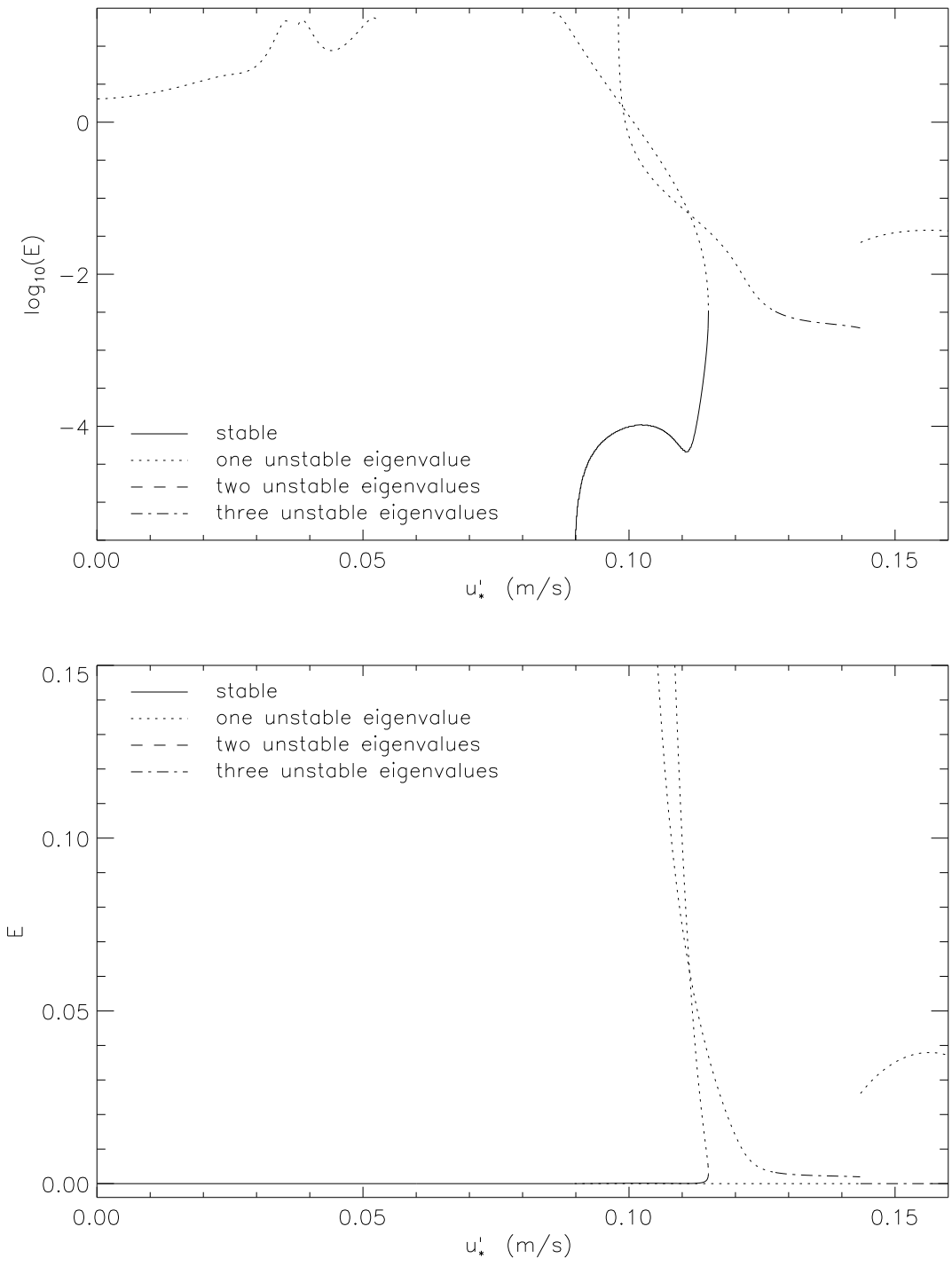


Figure III-13: Bifurcation diagram for $\delta = -0.1$.

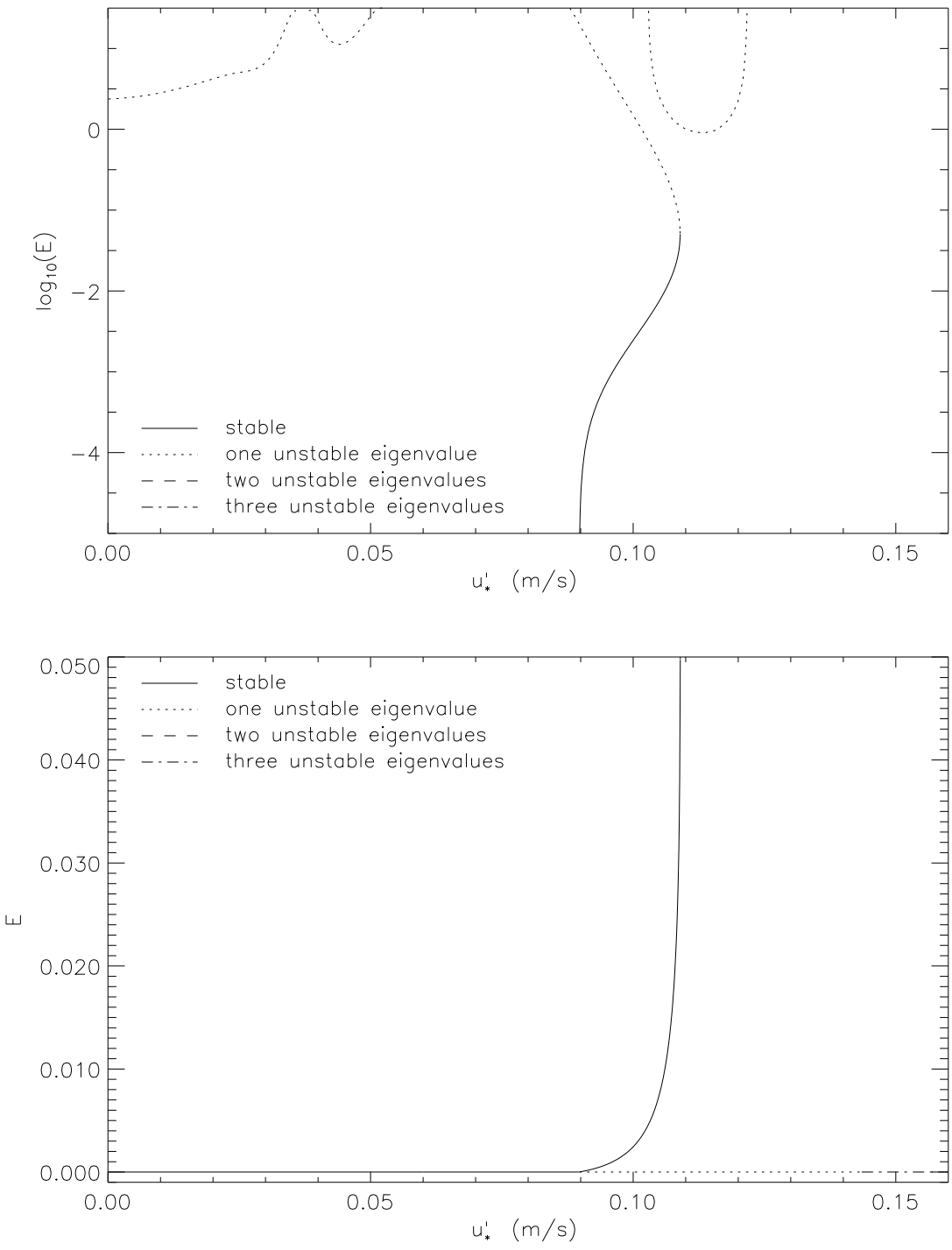


Figure III-14: Bifurcation diagram for $\delta = 0$.

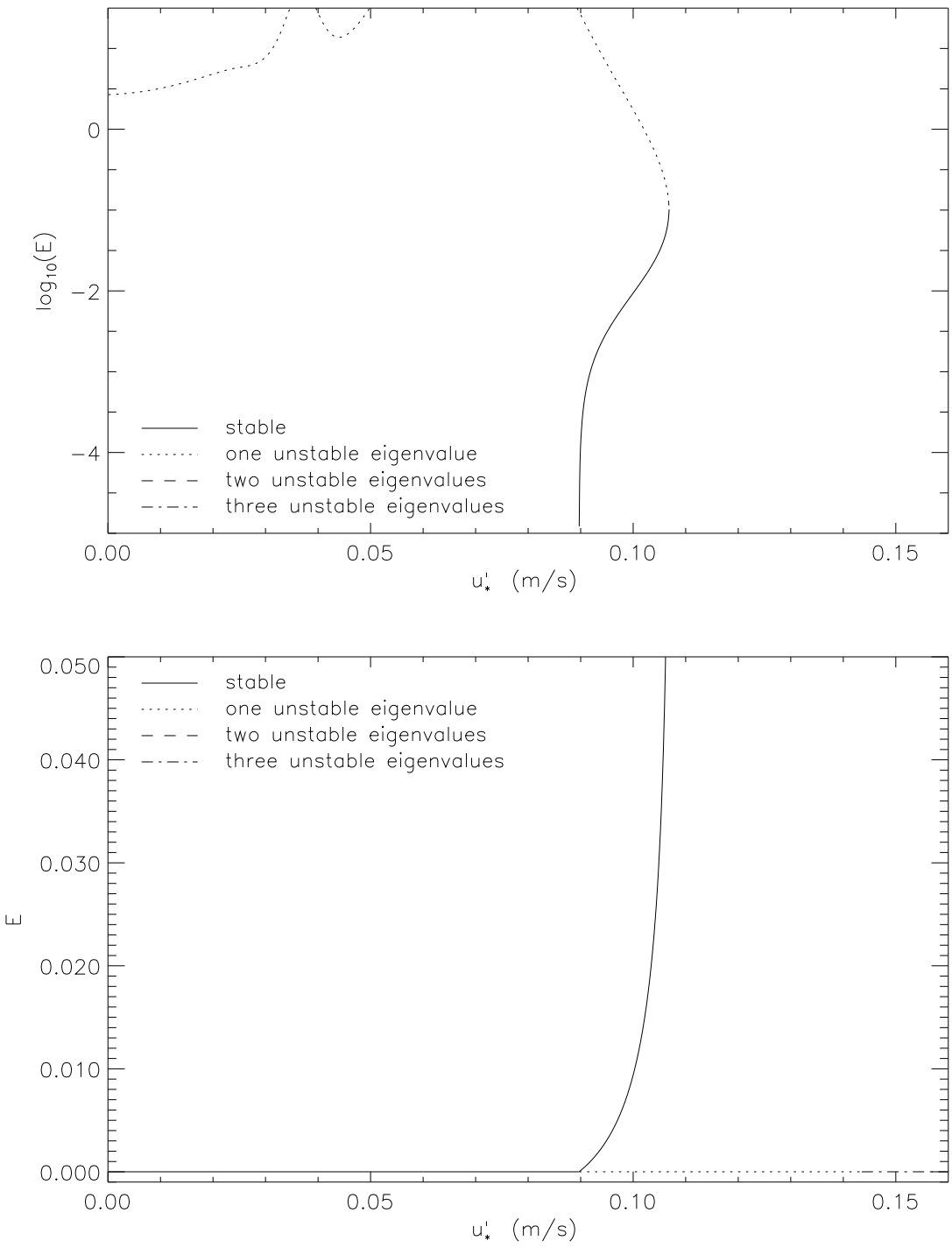


Figure III-15: Bifurcation diagram for $\delta = 0.1$.

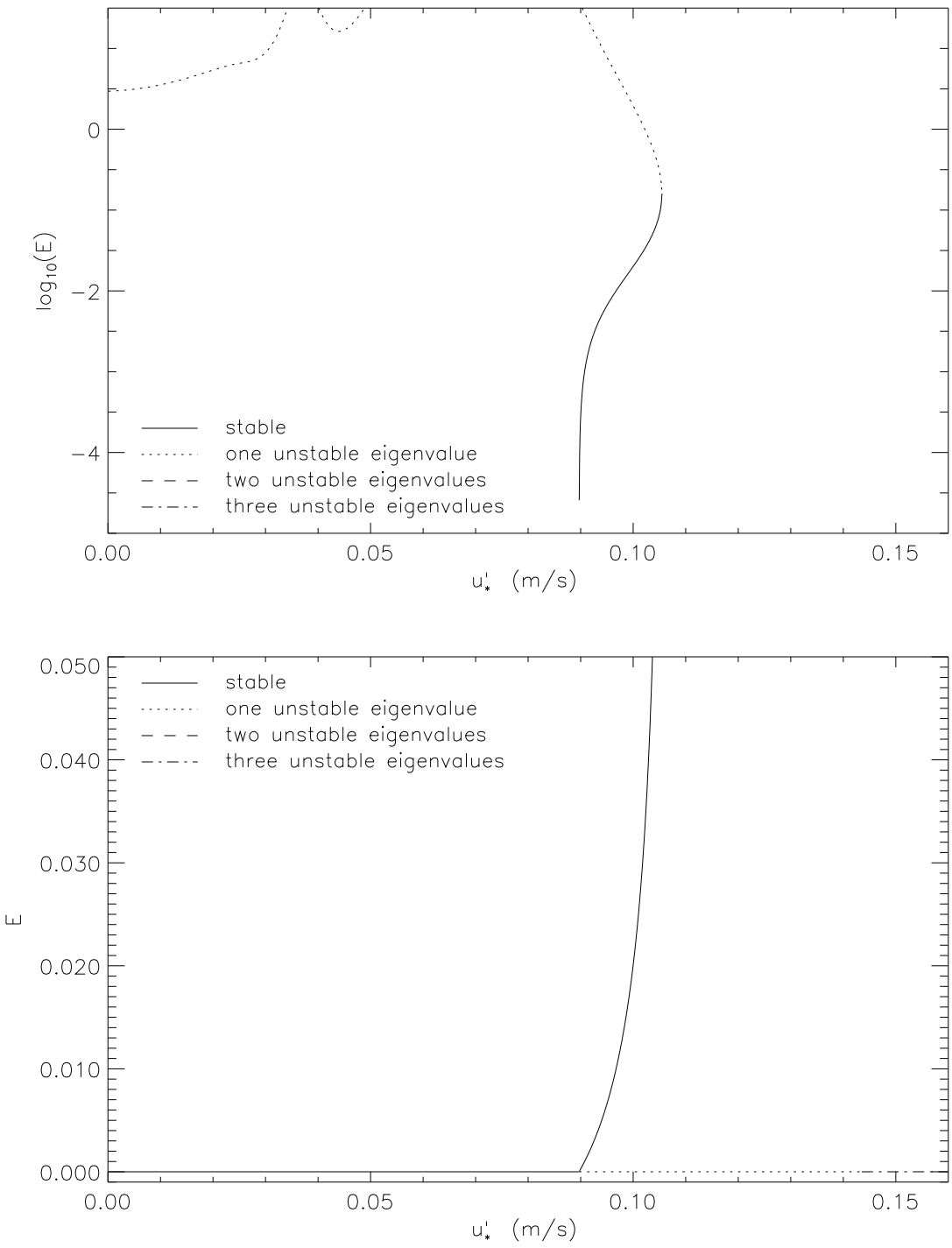


Figure III-16: Bifurcation diagram for $\delta = 0.2$.

damped out. (2): For a gentle wind in the range $u'_{*TC} < u'_* < u'_{*TP}$, there exists one stable non-trivial fixed point while the origin is unstable. Physically, this means that a gentle wind can exactly balance viscous damping and give rise to a stable steady progressive wave. This wave is further discussed in the next subsection. (3): For stronger winds $u'_* > u'_{*TP}$ there are no stable fixed points. Numerical experience for these wind speeds suggests that the solution of the dynamical system always becomes unbounded, and our theory becomes invalid after some time. Numerical computations of trajectories in phase-space are presented later.

In figure III-17 we show the regions of qualitatively different behavior in the parameter plane $(\delta, u'_*)$. In the region where the system blows up (3), we can further distinguish between the regions where volumes in phase-space contract (3a), volumes in phase-space expand (3b and 3c), the first-harmonic wave has positive linear growth-rate while the second-harmonic wave has negative linear growth-rate (3a and 3b), both the first and the second-harmonic waves have positive linear growth-rates (3c). The expansion-rate of volumes in phase-space is calculated according to (III.8.17).

### III.8.4 The stable steady progressive Wilton's ripple

It is a rather narrow interval of air friction velocities $u'_{*TC} < u'_* < u'_{*TP}$ that gives rise to a stable non-trivial fixed point. The lower bound $u'_{*TC} \approx 0.090$ m/s is independent of the detuning, while the upper bound has a maximum of $u'_{*TP,\max} \approx 0.119$ m/s for $\delta \approx -0.108$.

We recall that Wilton (1915) solved the steady progressive inviscid waves resulting from exact second-harmonic resonance, while Pierson & Fife (1961) generalized Wilton's solutions by allowing for slight detuning from exact resonance. They however did not account for viscosity or wind, and hence their steady progressive waves cannot really exist in nature.

Because the stable non-trivial fixed point in region (2) in figure III-17 lies close to the parabola of centers of the second-order system, it is approximately a special case of the steady progressive waves found by Wilton (1915) and Pierson & Fife (1961). We have therefore shown that a finely tuned gentle wind can balance viscosity and give rise to stable steady progressive waves that are rather similar to the classical inviscid steady progressive Wilton's ripples.

In figure III-18 we show the surface elevation $\eta = \eta_1 + \epsilon\eta_2$ (equations (III.6.5) and (III.6.7)) for one wave period ($0 < \theta < 2\pi$) of the stable steady progressive wave. We have fixed the air friction velocity $u'_* = 0.095$ m/s and let the detuning $\delta$ take the values $\pm 0.3$, $\pm 0.2$, $\pm 0.1$, $\pm 0.05$ and 0. We have again arbitrarily set the phase angle $\theta_1 = 0$, since this choice only affects a trivial phase shift and not the shape of the wave. The amplitude is minimum for $\delta \approx -0.1$. For more negative $\delta$, the profile is slightly gravity-like, while for positive $\delta$, the profile is slightly capillary-like.

### III.8.5 Numerical results of phase trajectories

In the following we show trajectories (solid curves) illustrating some typical types of behavior of the third-order dynamical system. The second-order parabola of centers

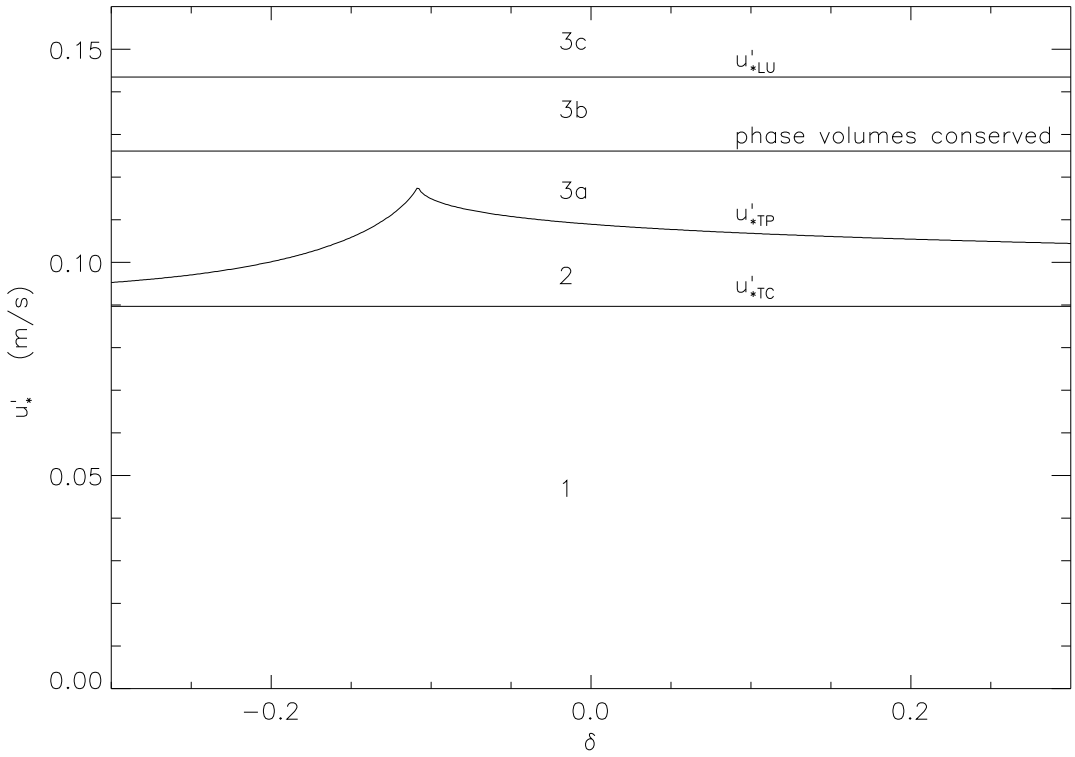


Figure III-17: Regions of qualitatively different behavior in the parameter plane $(\delta, u'_*)$. (1): The origin is a stable fixed point. (2): There exists a stable non-trivial fixed point and the origin is unstable. (3): The system blows up. In the region where the system blows up, we further distinguish between the regions where volumes in phase-space contract (3a), volumes in phase-space expand (3b and 3c), the first-harmonic wave has positive linear growth-rate and the second-harmonic wave has negative linear growth-rate (3a and 3b), both the first and second-harmonic waves have positive linear growth-rates (3c).

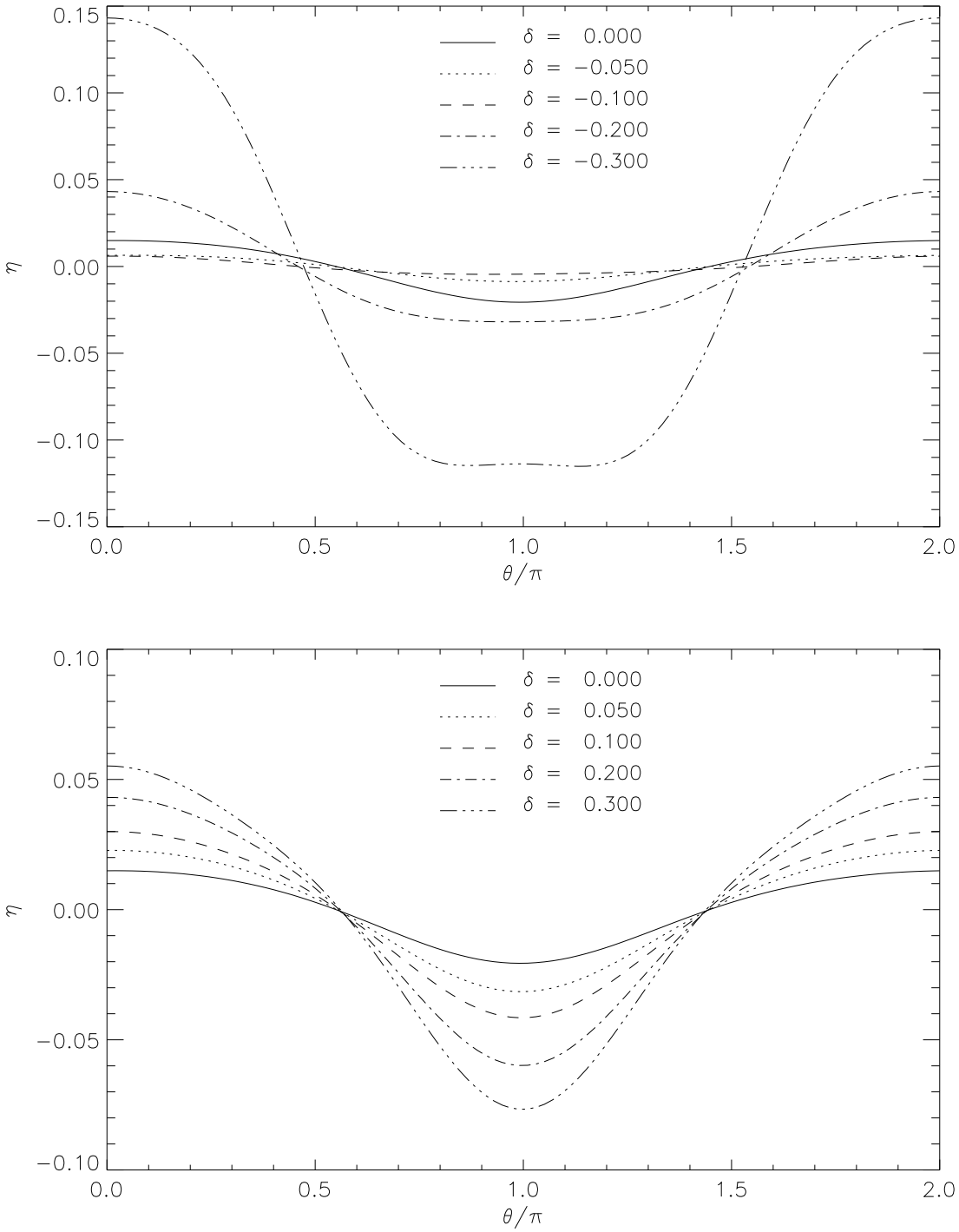


Figure III-18: Wave profiles for the stable steady-state solution for a fixed wind $u'_* = 0.095$ m/s and selected values of detuning $\delta$.

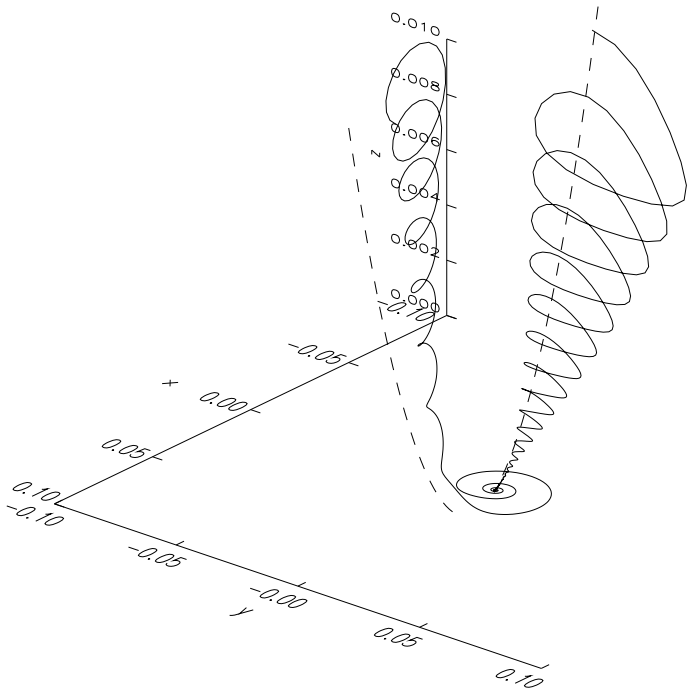


Figure III-19: Two trajectories for $u'_* = 0.08$ m/s, $\delta = 0$. Stable fixed point at the origin $(0, 0, 0)$. Initial conditions $(-0.05, 0, 0.015)$ and $(0.05, 0, 0.015)$.

(III.8.26b,c) is always shown with a dashed curve.

In figure III-19 we show two trajectories for $u'_* = 0.08$ m/s and $\delta = 0$ (region (1) in figure III-17). The origin is the only stable fixed point. From the initial condition (−0.05, 0, 0.015) the trajectory spirals down along the branch of the parabola (III.8.26b,c) with negative $X$, and approaches the origin. From the initial condition (0.05, 0, 0.015) the trajectory first spirals down along the branch of the parabola (III.8.26b,c) with positive $X$. As it approaches the $XY$-plane, it gets caught in the inward spiraling motion toward the origin.

In figure III-20 we show two trajectories for $u'_* = 0.1$ m/s and $\delta = 0$ (region (2) in figure III-17). There is a stable fixed point at $(-0.0076, 0.00079, 0.00094)$. From the initial condition $(-0.05, 0, 0.015)$ the trajectory spirals down along the branch of the parabola (III.8.26b,c) with negative $X$, and approaches the fixed point. From the initial condition $(0.05, 0, 0.015)$ the trajectory first spirals down along the branch of the parabola (III.8.26b,c) with positive $X$. As it approaches the $XY$-plane, it gets caught in the inward spiraling motion toward the origin, but is then ejected up toward the fixed point.

In figure III-21 we show one trajectory for $u'_* = 0.12$ m/s and $\delta = 0$ (region (3a) in figure III-17). The origin is a fixed point, and is stable in the $XY$-plane, but is unstable up toward positive $Z$. From the initial condition (0.055, 0, 0.015) the trajectory first spirals down along the branch of the parabola (III.8.26b,c) with positive $X$. It then gets caught in the inward spiraling motion toward the origin, and

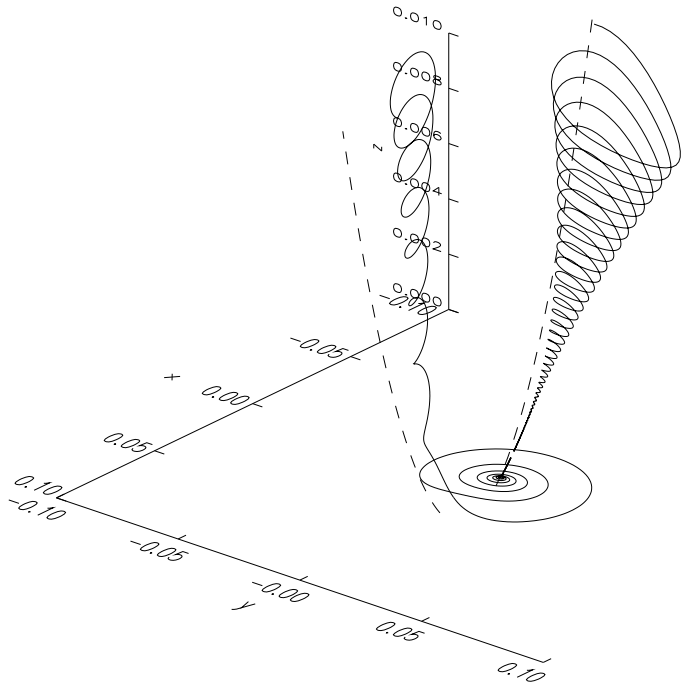


Figure III-20: Two trajectories for $u'_* = 0.1$ m/s, $\delta = 0$. Stable fixed point at $(-0.0076, 0.00079, 0.00094)$. Initial conditions $(-0.05, 0, 0.015)$ and $(0.05, 0, 0.015)$.

is ejected up into a spiraling motion along the branch of the parabola (III.8.26b,c) with negative $X$. The growth along this branch of the parabola is unbounded.

In figure III-22 we show one trajectory for $u'_* = 0.15$ m/s and $\delta = 0$ (region (3c) in figure III-17). The origin is a fixed point, and is unstable in all directions. From the initial condition $(0.03, 0, 0.000001)$ the trajectory first spirals away from the origin close to the $XY$-plane. It is then suddenly ejected away from the $XY$-plane, and becomes unbounded in $Z$.

# III.9 Remarks on existing experiments

Our theoretical predictions require air friction velocities in the range 0.09 to 0.12 m/s. The relationship between the air friction velocity $u'_*$ and the reference wind speed is not completely understood, and is complicated by the uncertainty about the shape of the wind profile, the unknown relationship between surface drift velocity and wind velocity, the arbitrariness in choosing a reference height, the fact that the wind profile changes with time and fetch, and finally the possible influence of wave disturbances on the water surface. Shemdin (1972) reported that the friction velocity was 4.95% of the reference wind speed in his wind-wave facility. Janssen (1986) used the corresponding percentages 4.0% and 4.28% for application to the experiment of Choi (1977). Klinke & Jähne (1992) reported that the air friction velocity was 4.90% of the reference wind speed at one experimental facility. At a second facility, the

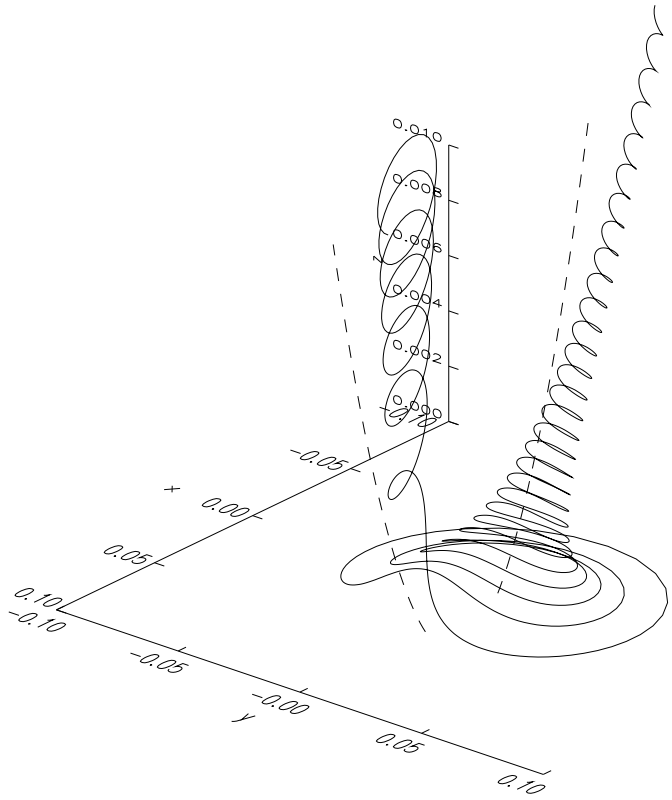


Figure III-21: One trajectory for $u'_* = 0.12$ m/s, $\delta = 0$. One initial condition $(0.055, 0, 0.015)$

friction velocity was a nonlinear function of the reference velocity, while at a third facility the friction velocity could not be determined from the wind velocity since a logarithmic profile was not established.

Based on the above discussion, we can anticipate that the reference wind speeds for application to our theory must be in the range 1.8–3.0 m/s, which is within the range of light breeze on the Beaufort scale.

Strizhkin & Raletnev (1986) observed resonating triads for reference wind speeds from 2.7 m/s (light breeze) to 18 m/s (gale) from an observation platform 14 m above the water surface. The lower threshold wind speed is clearly within our theoretical limits, and should be close to the boundary between regions (2) and (3) of figure III-17. We therefore have some quantitative agreement between their lower threshold wind speed and our bifurcation wind speeds for the emergence of resonant waves.

To verify experimentally our predictions in region (2) of figure III-17, it is necessary to have narrow peaks in the wind-wave frequency and wavenumber spectra for waves that can be in approximate second-order resonance. While comparison between several experiments (e.g. Klinke & Jähne 1992) have shown that the occurrence of discrete spectral peaks in general depends sensitively on the experimental facility itself, the experiment of Choi (1977) described in Ramamonjiarisoa, Baldy & Choi (1978) did indeed show peaks in the spectrum strongly suggesting second-harmonic resonance.

In the experiment of Choi (1977) described in Ramamonjiarisoa, Baldy & Choi

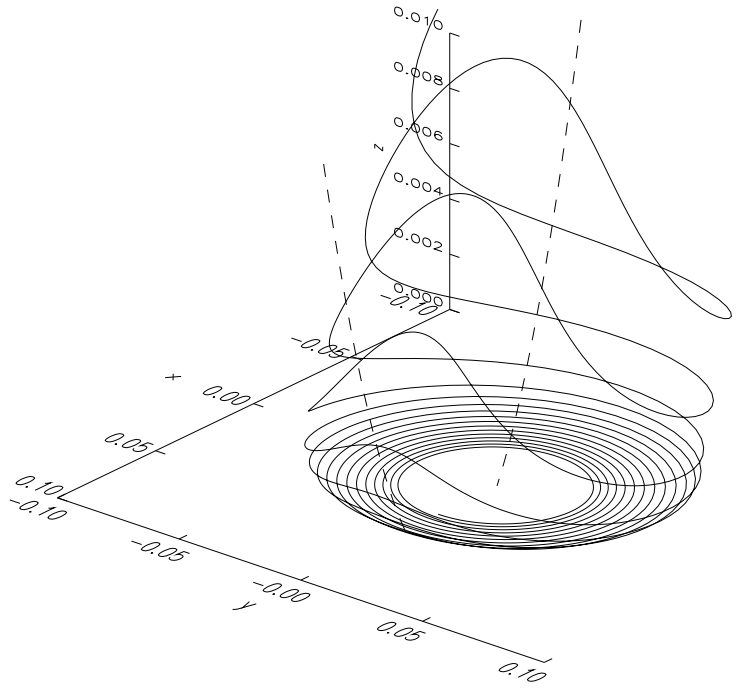


Figure III-22: One trajectory for $u'_* = 0.15$ m/s, $\delta = 0$. One initial condition $(0.03, 0, 0.000001)$.

(1978), a fully turbulent wind with velocity 5 m/s was blown over an initially calm water surface. At 70 cm fetch the first wavelets appeared with a narrow spectral peak at about 16.7 Hz. These initial waves grew according to linear theory up to 100 cm fetch. Then the spectrum broadened up to 150 cm fetch. From 150 to 220 cm fetch there was a definite down-shift in the spectral peak to half its initial value, while the spectral distribution was rendered rather flat. See figure 2. Janssen (1986, 1987) explained this experiment with a second-order weakly nonlinear model in which wind forcing was much stronger than viscous damping. He showed that starting from an initial state of a second-harmonic wave disturbance, a first-harmonic wave can suddenly appear and then grow.

The wind velocity in their experiment is stronger than what we have considered here. The behavior shown in figure III-22 is however qualitatively similar to their observations: At first there exists a second-harmonic wave ($Z \approx 0$). This wave grows slowly due to wind, seen by the outward spiral in the $XY$-plane. Then a first-harmonic wave suddenly appears ($Z > 0$), and grows rapidly beyond the limitations of our weakly nonlinear theory.

Jurman, Deutsch & McCready (1992) performed experiments on centimeter-range wind-driven surface waves on a shallow and highly viscous fluid (a glycerine-water solution 10–100 times more viscid than water). They adjusted the gas flow to be just sufficient to produce measurable waves. They observed that a fundamental wave, corresponding to the highest linear growth rate due to wind, could saturate at a small

steepness, while energy was transferred from the fundamental to its second-harmonic which was linearly damped. Their experimental observation is qualitatively similar to the behavior predicted in region (2) of figure III-17. However since their liquid had large viscosity, the proper balance of wind and damping is at a lower order than in our theory.

## III.10 Conclusion

We have developed a model for second-harmonic resonance of gravity–capillary waves (Wilton's ripples) where non-conservative effects due to viscosity and wind are balanced at the third order in wave steepness. Due to the small viscosity of water, it is necessary to balance these non-conservative effects at the third or higher nonlinear order for the purpose of describing waves that are steep enough to have physical and experimental significance.

This is the first model to incorporate nonlinear stress on the water surface due to second-order nonlinear interaction in air. The second-order nonlinear surface stress is found to be as important as the linear tangential stress on the surface. We explain why nonlinear interaction in air is much more important for waves subject to second-order resonance than for non-resonant monochromatic waves.

For weak winds, such that both the first and the second-harmonic waves are linearly damped, the only limiting state is the trivial state with waves being completely damped out by viscosity.

For winds just stronger than the threshold value where the first-harmonic wave becomes linearly growing while the second-harmonic wave is linearly damped, there exists a narrow range of air friction velocities giving rise to a stable steady-state solution. Our model thus predicts that a finely tuned gentle wind can balance viscous damping and give rise to a stable steady progressive second-harmonic resonant wave. In fact, Wilton (1915) and Pierson & Fife (1961) showed the existence of two types of steady progressive second-harmonic resonant waves with either gravity-like or capillary-like profiles. They did however not account for non-conservative effects and could therefore not discuss the stability of their solutions. We have shown that the combination of a finely tuned wind and viscosity can in fact stabilize one of their solutions at a certain energy level.

For winds stronger than the narrow range that gives rise to the stable steady progressive waves, but not necessarily so strong that the second-harmonic wave has a positive linear growth-rate, our model predicts that the wave amplitudes will grow without bounds. "Blow-up" is known to occur for non-conservative second-order resonant systems that have been truncated at the second nonlinear order (e.g. McDougall & Craik 1991). However, it has been suggested that such singular behavior could be arrested by including third-order nonlinear interactions. We show that "blow-up" can also occur even when third-order nonlinear interactions are included, even though the wind is sufficiently weak that the second-harmonic wave is linearly damped. From numerical experience, we believe that the combined effect of third-order nonlinear and non-conservative interactions is to inhibit the exchange of energy between the

the first and the second-harmonic waves. Instead, the system will approach certain asymptotic states for which the linearly unstable first-harmonic wave is preferred, and hence the energy can grow outside the bounds of our theory. We thus predict the same tendency as in the period doubling mechanism of Janssen (1986), that the dynamical system will eventually give preference to the first-harmonic wave.

The most important prediction of this part is that a gentle wind can balance viscosity and give rise to a stable steady progressive wave. We predict that this can happen for a narrow range of wind speeds that is weaker than what has usually been employed in previous experiments for wind-generation of water waves. It is therefore likely that new experiments are needed to verify this prediction. Experimental verification further requires that second-harmonic resonant waves can be selectively generated.

Three future theoretical extensions of this work seem natural. First, the analysis should be generalized to three-dimensional second-harmonic resonant triads with both space and time modulation. This generalization was initially attempted by us, but was abandoned due to excessive algebraic complexity. Second, since field observations of triad resonance (Strizhkin & Raletnev 1986) are often complicated by the presence of longer gravity waves, it seems appropriate to reconsider the problem of triad-resonance on top of a long wave (Part II) subject to a gentle wind and viscosity. This problem will then be further complicated by the fact that the wind itself is modulated by the long wave (Troitskaya 1994). Third, our model breaks down after some finite time in the cases when it predicts "blow-up" of wave amplitudes. We have shown that third-order nonlinear interaction is not sufficient to arrest this "blowing-up" behavior, contrary to previous beliefs (McDougall & Craik 1991). A theoretical resolution of this problem is still wanting. Indeed, the experimental observations of Choi (1977) and theoretical model of Janssen (1987) may suggest that the spectrum transitions from discrete to broad-banded, and hence the assumption that we can limit our consideration to only discrete harmonic waves may break down.

# III.A Energy and momentum of Wilton's ripples

We now derive expressions for the total energy and horizontal momentum of the two interacting Wilton's ripples correct to the third order, and find how these quantities evolve in time.

In dimensional variables, the wave kinetic energy is

$$\begin{aligned} E_k &= \overline{\epsilon^2 \int_{-\infty}^{\epsilon\eta} \frac{\rho}{2} \left\{ \left(\frac{\partial\psi}{\partial x}\right)^2 + \left(\frac{\partial\psi}{\partial z}\right)^2 + 2\frac{\partial\Psi^S}{\partial z}\frac{\partial\psi}{\partial z} \right\} \mathrm{d}z} \\ &= \epsilon^2 \frac{\rho}{2} \int_{-\infty}^{0} \overline{\left\{ \left(\frac{\partial\psi}{\partial x}\right)^2 + \left(\frac{\partial\psi}{\partial z}\right)^2 + 2\frac{\partial\Psi^S}{\partial z}\frac{\partial\psi}{\partial z} \right\}} \mathrm{d}z \\ &\quad + \epsilon^3 \frac{\rho}{2}\eta \overline{\left\{ \left(\frac{\partial\psi}{\partial x}\right)^2 + \left(\frac{\partial\psi}{\partial z}\right)^2 + 2\frac{\partial\Psi^S}{\partial z}\frac{\partial\psi}{\partial z} \right\}_{z=0}} + \mathcal{O}(\epsilon^4), \end{aligned} \tag{III.A.1}$$

the wave gravitational potential energy is

$$E_g = \overline{\int_{-\infty}^{\epsilon\eta} \rho g z \, \mathrm{d}z} = \frac{1}{2}\epsilon^2 \rho g \overline{\eta^2}, \tag{III.A.2}$$

the wave surface potential energy is

$$E_\Gamma = \overline{\Gamma \left\{ \sqrt{1 + \epsilon^2 \left(\frac{\partial\eta}{\partial x}\right)^2} - 1 \right\}} = \frac{1}{2}\epsilon^2 \Gamma \overline{\left(\frac{\partial\eta}{\partial x}\right)^2} + \mathcal{O}(\epsilon^4), \tag{III.A.3}$$

and the total horizontal momentum of the waves and current is

$$\begin{aligned} M_x &= \overline{\epsilon \int_{-\infty}^{\epsilon\eta} \rho \left( \frac{\partial\psi}{\partial z} + \frac{\partial\Psi^S}{\partial z} \right) \mathrm{d}z} \\ &= \epsilon\rho \overline{(\psi(0) + \Psi^S(0))} + \epsilon^2 \rho\eta \overline{\left( \frac{\partial\psi}{\partial z}(0) + \frac{\partial\Psi^S}{\partial z}(0) \right)} \\ &\quad + \frac{1}{2}\epsilon^3 \rho\eta^2 \overline{\left( \frac{\partial^2\psi}{\partial z^2}(0) + \frac{\partial^2\Psi^S}{\partial z^2}(0) \right)} + \mathcal{O}(\epsilon^4). \end{aligned} \tag{III.A.4}$$

In the non-dimensional normalized variables, making use of the perturbation results in section III.6, the kinetic energy becomes

$$\begin{aligned} E_k &= \frac{1}{2} \int_{-\infty}^{0} \overline{\left\{ \left(\frac{\partial\psi}{\partial x}\right)^2 + \left(\frac{\partial\psi}{\partial z}\right)^2 \right\}} \mathrm{d}z + \epsilon \frac{1}{2} \overline{\eta \left\{ \left(\frac{\partial\psi}{\partial x}\right)^2 + \left(\frac{\partial\psi}{\partial z}\right)^2 \right\}_{z=0}} \\ &= |A|^2 + 2|B|^2 + \frac{2}{3}\epsilon\delta(|A|^2 + 4|B|^2) + 2\epsilon(a_{1,0}|A|^2 + a_{2,0}|B|^2) \\ &\quad + \epsilon \,\mathrm{Re}(A^2 B^*), \end{aligned} \tag{III.A.5}$$

while the total potential energy becomes

$$\begin{aligned} E_p &= E_g + E_\Gamma \\ &= \frac{1}{3}\overline{\eta^2} + \frac{1}{6}\overline{\left(\frac{\partial \eta}{\partial x}\right)^2} \\ &= |A|^2 + 2|B|^2 + \frac{2}{3}\epsilon\delta(|A|^2 + 4|B|^2). \end{aligned} \tag{III.A.6}$$

Hence the total energy is

$$\begin{aligned} E &= E_k + E_p \\ &= 2(|A|^2 + 2|B|^2) + \frac{4}{3}\epsilon\delta(|A|^2 + 4|B|^2) + 2\epsilon(a_{1,0}|A|^2 + a_{2,0}|B|^2) \\ &\quad + \epsilon\,\mathrm{Re}(A^2B^*). \end{aligned} \tag{III.A.7}$$

It is now seen that the equipartition theorem is violated at the second order due to second-order nonlinear resonance and the influence of the induced shear current in the water.

We do not take into account the component of the horizontal momentum that is only due to the steady wind and shear flow. The non-dimensional normalized horizontal momentum due to the wave disturbance becomes

$$\begin{aligned} M_x &= \epsilon^{-1}\overline{\psi(0)} + \overline{\eta\left(\frac{\partial \psi}{\partial z}(0) + \frac{\partial \Psi^S}{\partial z}(0)\right)} + \frac{1}{2}\overline{\epsilon\eta^2\left(\frac{\partial^2 \psi}{\partial z^2}(0) + \frac{\partial^2 \Psi^S}{\partial z^2}(0)\right)} \\ &= 2(|A|^2 + 2|B|^2) + \frac{1}{3}\epsilon\delta(5|A|^2 + 14|B|^2) + 2\epsilon U^S(0)(|A|^2 + 2|B|^2) \\ &\quad - \epsilon\frac{\partial U^S}{\partial z}(0)(|A|^2 + |B|^2) - 2\epsilon(a_{1,0}|A|^2 + a_{2,0}|B|^2) - \epsilon\,\mathrm{Re}(A^2B^*). \end{aligned} \tag{III.A.8}$$

We notice that the momentum and the energy are identical to leading order.

# BIBLIOGRAPHY


Badulin, S. I., Pokazeyev, K. V. & Rozenberg, A. D. 1983 A laboratory study of the transformation of regular gravity–capillary waves in inhomogeneous flows. *Izv. Atmos. Ocean. Phys.* **19**(10), 782–787.

Banerjee, P. P. & Korpel, A. 1982 Subharmonic generation by resonant three-wave interaction of deep-water capillary waves. *Phys. Fluids* **25**, 1938–1943.

Basovich, A. J. & Bahanov, V. V. 1984 Surface wave kinematics in the field of an internal wave. *Izv. Atmos. Ocean. Phys.* **20**(1), 50–54.

Basovich, A. Y. & Talanov, V. I. 1977 Transformation of short surface waves on inhomogeneous currents. *Izv. Atmos. Ocean. Phys.* **13**(7), 514–519.

Benjamin, T. B. 1959 Shearing flow over a wavy boundary. *J. Fluid Mech.* **6**, 161–205.

Benjamin, T. B. & Feir, J. E. 1967 The disintegration of wave trains on deep water. Part 1. Theory. *J. Fluid Mech.* **27**, 417–430.

Benney, D. J. 1976 Significant interactions between small and large scale surface waves. *Stud. Appl. Math.* **55**, 93–106.

Benney, D. J. & Newell, A. C. 1967 The propagation of nonlinear wave envelopes. *J. Math. Phys.* **46**, 133–.

Bliven, L. F., Huang, N. E. & Long, S. R. 1986 Experimental study of the influence of wind on Benjamin–Feir sideband instability. *J. Fluid Mech.* **162**, 273–260.

Bontozoglou, V. & Hanratty, T. J. 1990 Capillary–gravity Kelvin–Helmholtz waves close to resonance. *J. Fluid Mech.* **217**, 71–91.

Bretherton, F. P. & Garrett, C. J. R. 1969 Wavetrains in inhomogeneous moving media. *Proc. R. Soc. Lond. A* **302**, 529–554.

Case, K. M. & Chiu, S. C. 1977 Three-wave resonant interactions of gravity–capillary waves. *Phys. Fluids* **20**, 742–745.

Chen, B. & Saffman, P. G. 1979 Steady gravity–capillary waves in deep water — I. Weakly nonlinear waves. *Stud. Appl. Math.* **60**, 183–210.

Choi, I. 1977 Contributions a l'étude des mecanismes physiques de la génération des ondes de capillarité-gravité à une interface air-eau. Thesis, Université d'Aix Marseille.

Chow, C. C., Bers. A. & Ram, A. K. 1992 The three wave interaction and spatiotemporal chaos. In *Physics of Space Plasmas* (Ed. T. Chang, G. B. Crew & J. R. Jasperse), SPI Conference Proceedings and Reprint Series, Number 11, pp. 179–195. Scientific Publishers Inc. Cambridge MA.

Christodoulides, P. & Dias, F. 1994 Resonant capillary–gravity interfacial waves. *J. Fluid Mech.* **265**, 303–343.

Craik, A. D. D. 1985 *Wave Interactions and Fluid Flows.* Cambridge University Press.

Craik, A. D. D. 1986 Exact solutions of non-conservative equations for three-wave and second-harmonic resonance. *Proc. R. Soc. Lond. A* **406**, 1–12.

Craik, A. D. D. 1988 Interaction of a short-wave field with a dominant long wave in deep water: Derivation from Zakharov's spectral formulation. *J. Austral. Math. Soc. Ser. B* **29**, 430–439.

Crapper, G. D. 1957 An exact solution for progressive capillary waves of arbitrary amplitude. *J. Fluid Mech.* **2**, 532–540.

Davey, A. 1972 The propagation of a weak nonlinear wave. *J. Fluid Mech.* **53**, 769–.

Djordjevic, V. D. & Redekopp, L. G. 1977 On two-dimensional packets of capillary–gravity waves. *J. Fluid Mech.* **79**, 703–714.

Dysthe, K. B. 1979 Note on a modification to the nonlinear Schrödinger equation for application to deep water waves. *Proc. R. Soc. Lond. A* **369**, 105–114.

Feir, J. E. 1967 Discussion: some results from wave pulse experiments. *Proc. R. Soc. Lond. A* **299**, 54–58.

Gastel, K. van, Janssen, P. A. E. M. & Komen, G. J. 1985 On phase velocity and growth rate of wind-induced gravity–capillary waves. *J. Fluid Mech.* **161**, 199–216.

Gradshteyn & Ryzhik 1980 *Table of Integrals, Series and Products.* Academic Press.

Grimshaw, R. 1988 The modulation of short gravity waves by long waves or currents. *J. Austral. Math. Soc. Ser. B* **29**, 410–429.

Hara, T. & Mei, C. C. 1991 Frequency downshift in narrowbanded surface waves under the influence of wind. *J. Fluid Mech.* **230**, 429–477.

Hara, T. & Mei, C. C. 1994 Wind effects on the nonlinear evolution of slowly varying gravity–capillary waves. *J. Fluid Mech.* **267**, 221–250.

Harrison, W. J. 1909 The influence of viscosity and capillarity on waves of finite amplitude. *Proc. Lond. Math. Soc.* **7**, 107–121.

Hasimoto, H. & Ono, H. 1972 Nonlinear modulation of gravity waves. *J. Phys. Soc. Japan* **33**, 805–.

Hasselmann, K. 1967 A criterion for nonlinear wave stability. *J. Fluid Mech.* **30**, 737–739.

Henderson, D. M. & Hammack, J. L. 1987 Experiments on ripple instabilities. Part 1. Resonant Triads. *J. Fluid Mech.* **184**, 15–41.

Henderson, D. M. & Hammack, J. L. 1993 Resonant interactions among surface water waves. *Ann. Rev. Fluid Mech.* **25**, 55–97.

Henyey, F. S., Creamer, D. B., Dysthe, K. B. Schult, R. L. & Wright, J. A. 1988 The energy and action of small waves riding on large waves. *J. Fluid Mech.* **189**, 443–462.

Hogan, S. J. 1985 The fourth-order evolution equation for deep-water gravity–capillary waves. *Proc. R. Soc. Lond. A* **402**, 359–372.

Holliday, D. 1973 Nonlinear gravity–capillary surface waves in a slowly varying current. *J. Fluid Mech.* **57**, 797–802.

Hughes, D. W. & Proctor, M. R. E. 1990 Chaos and the effect of noise in a model of three-wave mode coupling. *Physica D* **46**, 163–176.

Hughes, D. W. & Proctor, M. R. E. 1992 Nonlinear three-wave interaction with non-conservative coupling. *J. Fluid Mech.* **244**, 583–604.

Janssen, P. A. E. M. 1986 The period-doubling of gravity–capillary waves. *J. Fluid Mech.* **172**, 531–546.

Janssen, P. A. E. M. 1987 The initial evolution of gravity–capillary waves. *J. Fluid Mech.* **184**, 581–597.

Jones, M. C. W. 1992 Nonlinear stability of resonant capillary–gravity waves. *Wave Motion* **15**, 267–283.

Jones, M. & Toland, J. 1986 Symmetry and the bifurcation of capillary–gravity waves. *Arch. Rational Mech. Anal.* **96**, 29–53.

Jurman, L. A., Deutsch, S. E. & McCready, M. J. 1992 Interfacial mode interactions in horizontal gas-liquid flows. *J. Fluid Mech.* **238**, 187–219.

Kaup, D. J. 1981 The solution of the general initial value problem for the full three

dimensional three-wave resonant interaction. *Physica D*, **3**, 374–395.

Kawai, S. 1979 Generation of initial wavelets by instability of a coupled shear flow and their evolution to wind waves. *J. Fluid Mech.* **93**, 661–703.

Klinke, J. & Jähne, B. 1992 2D wave number spectra of short wind waves — results from wind wave facilities and extrapolation to the ocean. In *Optics of the Air-Sea Interface: Theory and Measurements* (Ed. L. Estep), SPIE **1749**, pp. 245–257.

Lai, R. J., Long, S. R. & Huang, N. E. 1989 Laboratory studies of wave-current interaction: Kinematics of the strong interaction. *J. Geophys. Res.* **94**, 16201–16214.

Lake, B. M., Yuen, H. C., Rungaldier, H. & Ferguson, W. E. 1977 Nonlinear deep-water waves: theory and experiment. Part 2. Evolution of a continuous wave train. *J. Fluid Mech.* **83**, 49–74.

Lavrenov, I. V. 1987 The theory of rips. *Izv. Atmos. Ocean. Phys.* **23**, 789–796.

Leykin, I. A. 1987 Study of the spectra of ocean waves on a horizontally inhomogeneous current in a rip zone. *Izv. Atmos. Ocean. Phys.* **23**(1), 38–42.

Lighthill, M. J. 1965 Contributions to the theory of waves in nonlinear dispersive systems. *J. Inst. Math. Appl.* **1**, 269–306.

Liu, J., Paul, J. D. & Gollub, J. P. 1993 Measurements of the primary instabilities of film flows. *J. Fluid Mech.* **250**, 69–101.

Lo, E. & Mei, C. C. 1985 A numerical study of water-wave modulation based on a higher-order nonlinear Schrödinger equation. *J. Fluid Mech.* **150**, 395–416.

Longuet-Higgins, M. S. 1987 The propagation of short surface waves on longer gravity waves. *J. Fluid Mech.* **177**, 293–306.

Longuet-Higgins, M. S. & Stewart, R. W. 1960 Changes in the form of short gravity waves on long waves and tidal currents. *J. Fluid Mech.* **8**, 565–583.

Longuet-Higgins, M. S. & Stewart, R. W. 1961 The changes in amplitude of short gravity waves on steady non-uniform currents. *J. Fluid Mech.* **10**, 529–549.

Ma, Y.-C. 1982 Weakly nonlinear steady gravity–capillary waves. *Phys. Fluids* **25**, 945–948.

McDougall, S. R. & Craik, A. D. D. 1991 Blow-up in non-conservative second-harmonic resonance. *Wave Motion* **13**, 155–165.

McGoldrick, L. F. 1965 Resonant interactions among capillary–gravity waves. *J. Fluid Mech.* **21**, 305–331.

McGoldrick, L. F. 1970a An experiment on second-order capillary gravity resonant wave interactions. *J. Fluid Mech.* **40**, 251–271.

McGoldrick, L. F. 1970b On Wilton's ripples: a special case of resonant interactions. *J. Fluid Mech.* **42**, 193–200.

Meiss, J. D. & Watson, K. M. 1978 Discussion of some weakly nonlinear systems in continuum mechanics. In *Topics in Nonlinear Dynamics* (Ed. S. Jorna), **46**, pp. 296–323. American Institute of Physics.

Melville, W. K. 1982 The instability and breaking of deep-water waves. *J. Fluid Mech.* **115**, 165–185.

Melville, W. K. 1983 Wave modulation and breakdown. *J. Fluid Mech.* **128**, 489–506.

Miles, J. W. 1957 On the generation of surface waves by shear flows. *J. Fluid Mech.* **3**, 185–204.

Miles, J. W. 1959a On the generation of surface waves by shear flows. Part 2. *J. Fluid Mech.* **6**, 568–582.

Miles, J. W. 1959b On the generation of surface waves by shear flows. Part 3. Kelvin-Helmholtz instablility. *J. Fluid Mech.* **6**, 583–598.

Miles, J. W. 1962 On the generation of surface waves by shear flows. Part 4. *J. Fluid Mech.* **13**, 433–448.

Miles, J. W. 1976 On internal resonance of two damped oscillators. *Stud. Appl. Math.* **55**, 351–359.

Morland, L. C. 1994 Resonant triads of capillary–gravity waves in the presence of a current. *Phys. Fluids* **6**, 588–594.

Naciri, M. 1992 *On wave-wave interactions on the ocean surface.* Ph.D. thesis. Massachusetts Institute of Technology.

Naciri, M. & Mei, C. C. 1992 Evolution of a short surface wave on a very long surface wave of finite amplitude. *J. Fluid Mech.* **235**, 415–452.

Nayfeh, A. H. 1973 Second-harmonic resonance in the interaction of an air stream with capillary–gravity waves. *J. Fluid Mech.* **59**, 803–816.

Paris, R. B. 1991 The asymptotic behaviour of Pearcey's integral for complex variables. *Proc. R. Soc. Lond. A* **432**, 391–426.

Pearcey, T. 1946 The structure of an electromagnetic field in the neighbourhood of a cusp of a caustic. *Phil. Mag.* **37**, 311–317.

Peregrine, D. H. 1976 Interaction of water waves and currents. *Adv. Appl. Mech.* **16**, 9–117.

Peregrine, D. H. & Smith, R. 1979 Nonlinear effects upon waves near caustics. *Phil. Trans. R. Soc. Lond. A* **292**, 341–370.

Perlin, M. & Hammack, J. L. 1991 Experiments on ripple instabilities. Part 3. Resonant quartets of the Benjamin–Feir type. *J. Fluid Mech.* **229**, 229–268.

Perlin, M., Henderson, D. M. & Hammack, J. L. 1990 Experiments on ripple instabilities. Part 2. Selective amplification of resonant triads. *J. Fluid Mech.* **219**, 51–80.

Perlin, M. & Ting, C.-L. 1992 Steep gravity–capillary waves within the internal resonance regime. *Phys. Fluids A* **4**, 2466–2478.

Phillips, O. M. 1957 On the generation of waves by turbulent wind. *J. Fluid Mech.* **2**, 417–445.

Phillips, O. M. 1960 On the dynamics of unsteady gravity waves of finite amplitude. Part 1. The elementary interactions. *J. Fluid Mech.* **9**, 193–217.

Phillips, O. M. 1981 The dispersion of short wavelets in the presence of a dominant long wave. *J. Fluid Mech.* **107**, 465–485.

Phillips, O. M. 1988 Remote sensing of the sea surface. *Ann. Rev. Fluid Mech.* **20**, 89–109.

Pierson, W. J. & Fife, P. 1961 Some nonlinear properties of long-crested periodic waves with lengths near 2.44 centimeters. *J. Geophys. Res.* **66**, 163–179.

Plant, W. J. 1982 A relationship between wind stress and wave slope. *J. Geophys. Res.* **87**, 1961–1967.

Poitevin, J. & Kharif, C. 1991 Subharmonic transition of a nonlinear wave train on deep water. In *Mathematical and numerical aspects of wave propagation phenomena* (Ed. G. Cohen, L. Halpern & P. Joly), pp. 567–576. SIAM, Philadelphia.

Pokazeyev, K. V. & Rozenberg, A. D. 1983 Laboratory studies of regular gravity–capillary waves in currents. *Oceanology* **23**(4), 429–435.

Press, W. H., Teukolsky, S. A., Vetterling W. T. & Flannery, B. P. 1992 *Numerical recipes in C. Second Edition.* Cambridge University Press.

Ramamonjiarisoa, A., Baldy, S. & Choi, I. 1978 Laboratory studies on wind-wave generation, amplification and evolution. In *Turbulent Fluxes through the Sea Surface, Wave Dynamics, and Prediction* (Ed. A. Favre & K. Hasselmann), pp. 403–420. Plenum.

Reeder, J. & Shinbrot, M. 1981a On Wilton ripples, I: Formal derivation of the phenomenon. *Wave Motion* **3**, 115–135.

Reeder, J. & Shinbrot, M. 1981b On Wilton ripples, II: Rigorous results. *Arch. Rational Mech. Anal.* **77**, 321–348.

Sammarco, P., Mei, C. C. & Trulsen, K. 1994 Nonlinear resonance of free surface waves in a current over a sinusoidal bottom: a numerical study. *J. Fluid Mech.* **279**, 377–405.

Saunders, P. T. 1980 *An introduction to catastrophe theory.* Cambridge University Press.

Shemdin, O. H 1972 Wind-generated current and phase speed of wind waves. *J. Phys. Oceanogr.* **2**, 411–419.

Shyu, J.-H. & Phillips, O. M. 1990 The blockage of gravity and capillary waves by longer waves and currents. *J. Fluid Mech.* **217**, 115–141.

Simmons, W. F. 1969 A variational method for weak resonant wave interactions. *Proc. R. Soc. Lond. A* **309**, 551–575.

Smith, R. 1975 The reflection of short gravity waves on a non-uniform current. *Math. Proc. Camb. Phil. Soc.* **78**, 517–525.

Smith, R. 1976a Giant waves. *J. Fluid Mech.* **77**, 417–431.

Smith, R. 1976b Triple roots and cusped caustics for surface gravity waves. In *Waves on water of variable depth* (Ed. D. G. Provis & R. Radok), pp. 154–164. Springer Verlag.

Stamnes, J. J. 1986 *Waves in Focal Regions.* Adam Hilger.

Stiassnie, M. & Dagan, G. 1979 Partial reflexion of water waves by non-uniform adverse currents. *J. Fluid Mech.* **92**, 119–129.

Strizhkin, I. I. & Raletnev, V. I. 1986 Experimental studies of three- and four-wave resonant interactions of surface sea waves. *Izv. Atmos. Ocean. Phys.* **22**(4), 311–314.

Thomson, J. A. & West, B. J. 1975 Interaction of small-amplitude surface gravity waves with surface currents. *J. Phys. Oceanogr.* **5**, 736–749.

Troitskaya, Y. I. 1994 Modulation of the growth rate of short surface capillary–gravity wind waves by a long wave. *J. Fluid Mech.* **273**, 169–187.

Trulsen, G. N., Dysthe, K. B. & Trulsen, J. K. 1990 Evolution of a gravity wave spectrum through a current gradient. *J. Geophys. Res.* **95**, 22141–22151.

Trulsen, K. & Dysthe, K. B. 1990 Frequency down-shift through self modulation and breaking. In *Water Wave Kinematics* (Ed. A. Tørum & O. T. Gudmestad), pp. 561–572. Kluwer Academic Publishers. The Netherlands.

Trulsen, K. & Dysthe, K. B. 1992 Action of windstress and breaking on the evolution of a wavetrain. In *Breaking Waves* (Ed. M. L. Banner & R. H. J. Grimshaw), pp. 243–249. Springer-Verlag.

Trulsen, K. & Mei, C. C. 1993 Double reflection of capillary/gravity waves by a non-uniform current: a boundary-layer theory. *J. Fluid Mech.* **251**, 239–271.

Trulsen, K. & Mei, C. C. 1995 Modulation of three resonating gravity–capillary waves by a long gravity wave. *J. Fluid Mech.* (In the press.)

Uchiyama, Y. & Kawahara, T. 1994 A possible mechanism for frequency down-shift in nonlinear wave modulation. *Wave Motion* **20**, 99–110.

Valenzuela, G. R. 1976 The growth of gravity–capillary waves in a coupled shear flow.

*J. Fluid Mech.* **76**, 229–250.

Valenzuela, G. R., Chen, D. T., Garrett, W. D. & Kaiser, J. A. C. 1983 Shallow water bottom topography from radar imagery. *Nature* **303**, 687–689.

Vyshkind, S. Y. & Rabinovich, M. I. 1976 The phase stochastization mechanism and the structure of wave turbulence in dissipative media. *Sov. Phys. JETP* **44**, 292–299.

Wersinger, J.-M., Finn, J. M. & Ott, E. 1980a Bifurcations and strange behavior in instability saturation by nonlinear mode coupling. *Phys. Rev. Lett.* **44**, 453–456.

Wersinger, J.-M., Finn, J. M. & Ott, E. 1980b Bifurcation and "strange" behavior in instability saturation by nonlinear three-wave mode coupling. *Phys. Fluids* **23**, 1142–1154.

Wilton, J. R. 1915 On ripples. *Phil. Mag.* **29**, 688–700.

Woodruff, S. L. & Messiter, A. F. 1994 A perturbation analysis of an interaction between long and short surface waves. *Stud. Appl. Math.* **92**, 159–189.

Yermakov, S. A. & Salashin, S. G. 1984 Modulation of gravity–capillary waves in the internal-wave field. *Izv. Atmos. Ocean. Phys.* **20**(5), 394–402.

Zakharov, V. E. 1968 Stability of periodic waves of finite amplitude on the surface of a deep fluid. *Sov. Phys. J. Appl. Mech. Tech. Phys.* **4**, 86–.

Zhang, J. & Melville, W. K. 1990 Evolution of weakly nonlinear short waves riding on long gravity waves. *J. Fluid Mech.* **214**, 321–346.

Zhang, J. & Melville, W. K. 1992 On the stability of weakly nonlinear short waves on finite-amplitude long gravity waves. *J. Fluid Mech.* **243**, 51–72.

Zhang, Y. & Phillips, O. M. 1991 (Private communication)